Causality of the Link between Autumn Arctic Sea Ice and the Winter Extratropical Atmosphere

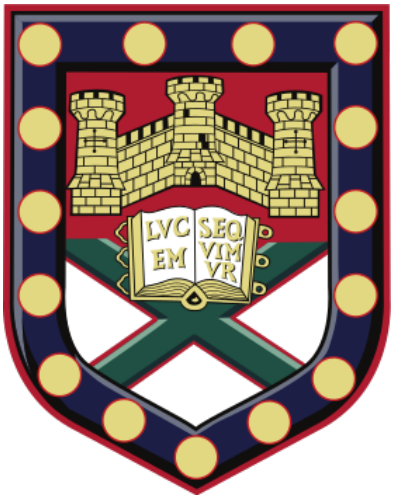

Submitted by James Lewis Warner to the University of Exeter as a thesis for the degree of Doctor of Philosophy in Mathematics in February, 2020.

Abstract

Changes in Arctic sea ice have been proposed to affect the mid-latitude winter atmospheric circulation, often based on observed variability. However, causality of this relationship remains unclear. This thesis investigates the link between autumn sea ice and the extratropical winter atmosphere, clarifying the role of internal variability and demonstrating a role for tropical variability.

Single model experiments can simulate an apparent link between autumn sea ice and the winter North Atlantic Oscillation (NAO) through unforced internal variability, but the ensemble average relationship is weak, suggesting a large role for internal variability. Additionally, longer, free-running simulations also indicate this link is highly non-stationary in time. These results question the robustness of proposed sea ice-NAO links based solely on short observational reanalysis.

Multiple linear regression and causal effect network analysis indicate that the tropical west Pacific plays a role in the link between sea ice and the NAO. This is supported by multi-model simulations containing large ensembles, which demonstrate minimal causal influence of sea ice variability on the winter NAO, and that winter extratropical patterns connected with sea ice variability partly originate in the tropical Pacific.

Tropical nudging experiments in autumn reveal that while tropical information is not sufficient to directly recreate interannual BK ice variability, tropical information can reproduce the autumn stratospheric polar vortex and NAO variability, which are strongly linked to the winter NAO and autumn Barents-Kara sea ice respectively. The signal-to-noise issue present throughout dynamic model simulations may lead to overly weak extratropical teleconnections, which may inhibit the detection any direct tropical to Arctic link. These results provide new evidence of a non-causal link between sea ice and the extratropical circulation, stemming from tropical sources, and further clarify the role of internal variability.

Acknowledgements

First and foremost, I would like to thank my supervisors James Screen and Adam Scaife, who have provided invaluable guidance and support throughout my PhD. Many interesting conversations have laid the foundation for much of the work in this thesis. I would also like to extend my thanks to Anna Maidens and Jeff Knight, who hosted me at the Met Office to undertake the tropical nudging simulations; particularly Anna who supported me with the (many!) error messages that the UM threw at me. Additionally, useful discussions with Nick Dunstone and Doug Smith helped shape the research.

More widely, I would like to thank the climate group at Exeter University for creating a vibrant research culture, and the postgraduate society which I spent many, many hours involved with, and all those in my office who will no doubt go on to change the world in amazing ways.

I am also very grateful of NERC funding (NE/L002434/1), where the generous research budget allocated to me allowed me to partake in some incredible conferences and schools, both nationally and internationally.

On a more personal (and cheesy!) note, I would especially like to thank my mum, who has supported me throughout the PhD program, and has always encouraged and given me strength to keep going. My late grandfather Trevor, whose interest in the weather left a strong impression, further motivated me to pursue meteorology as a career. Last, but certainly by no means least, Emma's support, and being a continual source of happiness, helped me push through some of the most challenging final months of my PhD.

List of Publications

- **Warner, J.L.**, Screen, J.A., Scaife, A.A., 2020. Links between Barents-Kara sea ice and the Extratropical Atmospheric Circulation explained by internal variability and tropical forcing. *Geophysical Research Letters*, **44**, 085679.
- **Warner, J.L.**, 2018. Arctic sea ice; a driver of the winter NAO? *Weather*, **73**, pp.307-310. doi:10.1002/wea.3399

Contents

List of Figures

List of Tables

Abbreviations

Acronym	Definition
AGCM	Atmospheric Global Climate Model
AMIP	Atmospheric Model Intercomparison Project
AO	Arctic Oscillation
BK	Barents-Kara
CESM	Community Earth System Model
CFS	Climate Forecast System
DePreSys3	Decadal Prediction System 3
DJF	December, January, February
ENSO	El Niño Southern Oscillation
EOF	Empirical Orthogonal Function
GCM	Global Climate Model
KDE	Kernel Density Estimate
LOO	Leave One Out (Cross Validation)
MJO	Madden Julian Oscillation
NAO	North Atlantic Oscillation
PC	Principal Component
PNA	Pacific North America
QBO	Quasi-Biennal Oscillation
RPC	Ratio of Predictable Components
SST	Sea Surface Temperature
UM	Unified Model
WRF	Weather and Research Forecast

Chapter 1

Introduction

Accurate seasonal climate prediction is important for adaptation and societal resilience to climate variability and change. European winter weather is strongly influenced by the winter North Atlantic Oscillation (NAO), the leading mode of atmospheric variability over the Atlantic sector [*Hurrell,* 1995]. Both dynamical and empirical models demonstrate skill in predicting interannual variability of the winter NAO [*Scaife et al.,* 2014; *Wang et al.,* 2017; *Hall et al.,* 2017; *Baker et al.,* 2018], up to a year ahead [*Dunstone et al.,* 2016], and beyond [*Smith et al.,* 2019]. NAO predictions are used across society, such as in the transport sector [*Palin et al.,* 2015], river management and flood risk [*Svensson et al.,* 2015], and energy [*Clark et al.,* 2017], among others. Recent NAO extremes are reflected in the exceptionally cold winter of 2009/10 over Europe [*Jung et al.,* 2011], and the stormy winter of 2013/14 in the UK [*Knight et al.,* 2017]. Skilful NAO predictions at a useful lead time support better preparedness for extreme weather.

Despite recent advances in NAO prediction skill, what physically controls interannual variability in the winter NAO is still disputed and components of the climate system may be related to NAO variability, but not have a casual effect on the NAO. While there is general consensus on how tropical modes of variability interact with the extratropical circulation, such as the El Niño Southern Oscillation (ENSO) [*Pozo-Vázquez et al.,* 2001b] and the Madden Julian Oscillation (MJO) [*Cassou,* 2008], how polar variability such as Arctic sea ice influences the extratropics is much less certain [*Smith et al.,* 2017]. Additionally, both ENSO and the MJO have also been shown to affect the Arctic climate [*Lee et al.,* 2011; *Yoo et al.,* 2011], which may imply a non-causal and incidental relationship between Arctic sea ice and the winter NAO, due to tropical variability. This thesis aims

to reconcile the causality of the relationship between Arctic sea ice and the extratropical circulation (particularly the NAO), through a systematic analysis of observational reanalysis, skilful hindcast datasets, and model experiments. While the wider mid-latitude winter circulation is also considered in its links with Arctic sea ice, the primary focus is the NAO, given this mode explains a large degree of variability over the UK during winter and can describe high-impact weather regimes.

Interannual variability in Arctic sea ice is dwarfed by a strong downward trend in recent decades [*Collins et al.,* 2012], attributable to both anthropogenic climate change and internal variability [*Ding et al.,* 2019]. Model projections suggest September sea ice will be lost by the middle of the century [*Collins et al.,* 2012]. This sea ice loss, both concentration and thickness, is non-uniform spatially [*Kwok and Rothrock,* 2009], and the spatial pattern of sea ice loss is proposed to have differing effects on the extratropical circulation through tropospheric [*Orsolini et al.,* 2012] and stratospheric [*McKenna et al., 2017*] pathways. Studies investigating extratropical links with Arctic sea ice vary in model set-up, how sea ice is prescribed, amongst others differences [*Smith et al.,* 2017]. Discrepancies in the extratropical response within model simulations may therefore be due to different experimental configurations, large internal variability masking forced signals [*Screen et al.,* 2017; *Kolstad and Screen,*, 2019], or differing background states of the climate models and their representation of mediating teleconnections [*Smith et al.,* 2017].

- **Is the observed relationship between Arctic sea ice and the extratropical circulation reproducible in a coupled model simulation?**

The first results chapter explores this key question and identifies whether a skilful hindcast model can reproduce the strong link between autumn sea ice and the winter NAO found in observations. Additionally, how autumn sea ice affects the wider extratropical circulation is examined. The stationarity of the relationship between sea ice and the NAO is also assessed using longer reanalyses and a free running coupled model simulation, akin to *Kolstad and Screen* [2019].

Recent literature suggests that variability in the tropics has an impact on Arctic sea-ice variability through poleward heat fluxes and changes in the radiation budget [*Lee et al.,* 2011; *Lee,* 2012], modulated by either ENSO [*Lee,* 2012], the MJO [*Henderson et al.,* 2014], or a combination of the two [*Moon et al.,* 2011]. Potential co-variability of the relationship between Arctic sea ice and the extratropical circulation with tropical rainfall

variability is explored. Tropical rainfall serves as a useful proxy for tropical convection, upper tropospheric divergence/convergence, and thus Rossby wave sources [*Hoskins and Karoly,* 1981; *Trenberth et al.,* 1988; *Scaife et al.,* 2017].

- **Do the tropics play a role in the link between Arctic sea ice and the extratropical circulation?**

The second results chapter investigates this co-variability between tropical rainfall, the NAO, and sea ice using a skilful hindcast model to attribute where NAO skill originates from, by sub-sampling ensemble members based on skilful polar and tropical predictability to determine if they lead to enhanced NAO prediction. Additionally, identifying potential links between tropical/polar drivers and the NAO is conducted through examination of the model signal-to-noise ratio [*Scaife and Smith,* 2018]. Polar and tropical sources of variability are combined; first within a multiple linear regression framework to identify coincident relationships, and then with sophisticated causal effect network approaches [*Runge et al.,* 2015; 2017].

Coupled model simulations and reanalysis are useful in identifying teleconnections between regions, but do not allow teleconnections to be isolated in determining causal pathways. Atmosphere only models have been employed widely to interpret the response to boundary condition forcings, such as sea ice (e.g. *Mori et al.* [2014]; *Lim et al.* [2012]; *Seierstand and Bader* [2008]; *Xue et al.* [2017]), as well as sea surface temperatures [*Rodwell et al.,* 1999] and their impact on the extratropical circulation. They allow causal responses to the forcing imposed to be evaluated in a controlled environment. Coupled simulations can mask this direction of causality as the atmosphere may drive ice and ice may drive the atmosphere.

- **What is the response to sea ice variability in atmospheric only models?**

The third results chapter investigates the causality of the link between autumn Arctic sea ice and winter extratropical circulation further through a variety of multi-model experiments. Multi-model approaches have been used to investigate Arctic sea ice variability on northern hemisphere temperature variability [*Sun et al.,* 2016; *Ogawa et al.,* 2018; *Koenigk et al.,* 2019], but not on mean sea level pressure variability and its links with tropical sources. Large ensemble atmosphere-only simulations, with either time-varying

or climatological sea ice can be used to infer a causal extratropical response to sea ice variability in the models. Additionally, they can be used to determine the origins of any co-incidental variability between the Arctic, extratropics and tropics.

A teleconnection that links the tropics to the Arctic is the basis for the covariance between Arctic sea ice and the extratropical circulation. MJO and ENSO dynamics have been related to the Arctic climate, through Rossby wave dynamics and perturbations in the mid-latitude circulation; which affect poleward heat and moisture fluxes into the Arctic [*Gong et al.,* 2017; *Park et al.,* 2015; *Henderson et al.,* 2014; *Woods et al.,* 2013; *Woods and Caballero,* 2016].

- **Can polar variability be reconstructed through knowledge of autumn tropical variability alone?**

Within the final results chapter, in order to investigate whether interannual sea ice variability can be reconstructed through knowledge of tropical atmospheric variability alone, tropical nudging experiments are conducted. These have been used effectively in studies both looking at case study winter responses to tropical variability [*Knight et al.,* 2017; *Maidens et al.,* 2019], as well as over decadal timescales [*Jung et al.,* 2014; *Greatbatch et al.,* 2015]. Using a model with known ability to simulate global teleconnections, tropical nudging is performed using tropical atmospheric conditions from different years during autumn to infer a response in sea ice in late autumn.

The overall outcome of this research is to better understand the causality of the link between autumn Arctic sea ice and the winter extratropical atmosphere, and the role that tropical variability may play in mediating this relationship. Better understanding of causal relationships in the climate system enable more rigorous empirical predictions of the NAO to be made, more confident real time forecasts of the NAO and also direct model development in representing real teleconnections to better aid skilful NAO predictions. It also helps reconcile a widely disputed body of research on links between Arctic sea ice and the extratropical circulation.

This thesis is structured at follows: firstly, a literature review collates NAO predictability and its links to polar and tropical sources of variability. This is followed by methodology, summarising key techniques used for analysis, as well as the datasets/models used. The results chapters then follow, sequentially based on the key research questions

above. A concluding remarks section follows this, summarising findings and the wider application, with suggestions for future work on this important topic.

Chapter 2

Literature Review

To motivate and provide context to the key questions laid out in the introduction, this chapter collates published research related to variability, and predictability, of the NAO. The chapter is organised as follows; firstly providing an overview of the NAO, how it is measured, and methods employed to obtain skilful seasonal predictions of the NAO. The chapter then looks at how commonly proposed remote drivers, such as Arctic sea ice and tropical rainfall can impact mid-latitude circulation patterns and subsequently the NAO, and how these drivers contribute to NAO predictability. Discussion of other proposed causal drivers of the NAO and AO are also included. Finally, this chapter concludes with an evaluation of NAO drivers, and how existing research informs the thesis key questions and aims providing opportunity for novel research. Some of the work in this chapter has been published in *Warner et al.,* [2018] (see list of publications at start of thesis).

2.1 The North Atlantic Oscillation

Overview

The North Atlantic Oscillation (NAO) is a measure of the meridional gradient of atmospheric mass over the North Atlantic basin, commonly diagnosed using mean sea level pressure or lower tropospheric geopotential height [*Hurrell,* 1995a; *Ambaum et al.,* 2001]. This pattern of variability is a regional manifestation of the Arctic Oscillation (AO); a dominant mode of variability in boreal winter. Like the NAO, the AO describes the meridional distribution of atmospheric mass but instead across the polar region and the mid-latitudes, and approximately zonally symmetric [*Thomson and Wallace,* 1998]. Therefore,

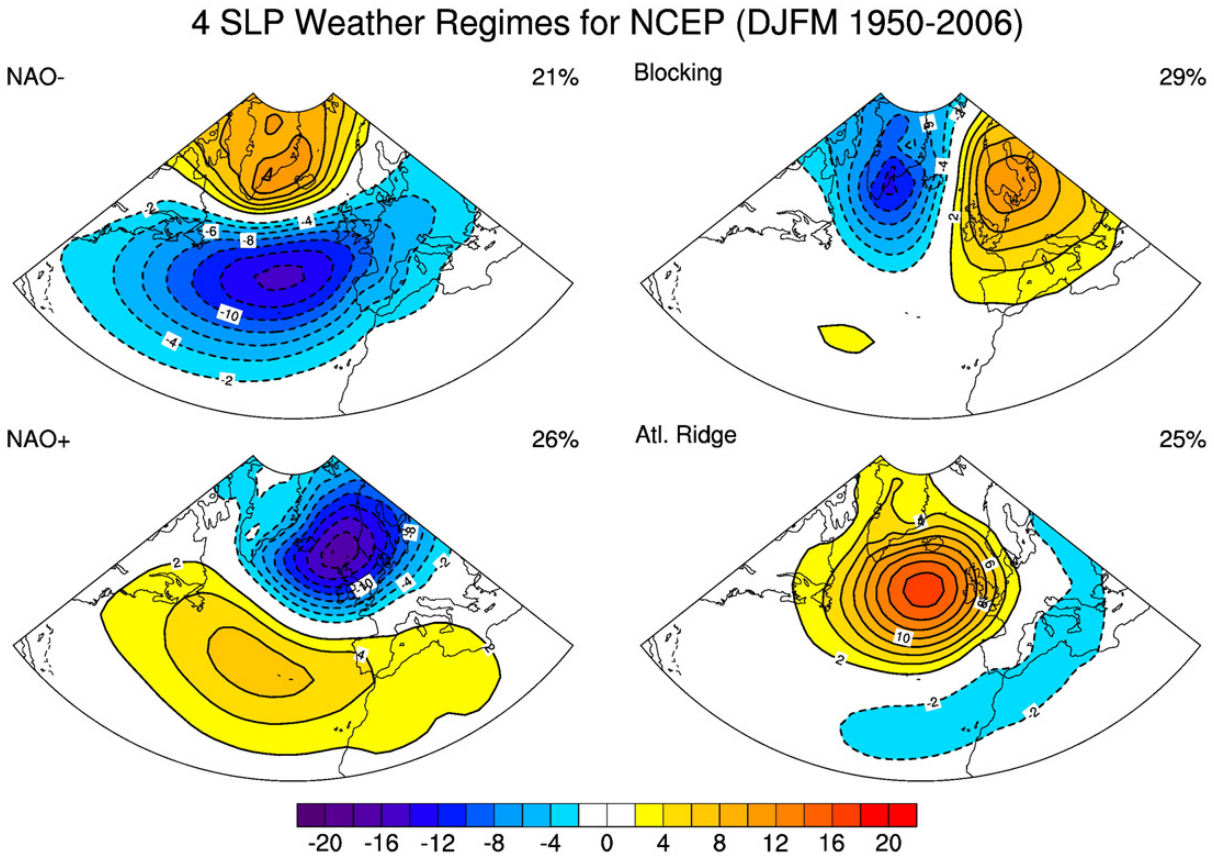

Figure 2.1: Modes of winter climate variability. December-March climate regimes identified using sea level pressure (hPa) over the North Atlantic domain (20-70°N, 90W-40°E) using daily data between 1950-2006, from NCAR reanalysis. The percentage at the top right expresses the frequency of occurrence out of all winter days since 1950. The contour interval is 2 hPa. From *Hurrell and Deser* [2009].

the NAO and AO are intrinsically related modes of atmospheric variability [*Ambaum et al.,* 2001]. Studies which investigate AO variability are generally applicable to the NAO [*Vallis and Gerber,* 2008].

Variability in the NAO explains to a large degree weather variability over the north Atlantic and surrounding land mass in winter [*Hurrell,* 1995a]. The NAO is therefore a useful index for summarising weather characteristics over large regions [*Anthanasiadis et al.,* 2017]. A positive NAO index is defined as a stronger than average pressure gradient between the climatological low pressure around Iceland (the Icelandic low), and high pressure that resides around the Azores (the Azores high). A stronger than average pressure gradient between the two nodes is related to enhanced extratropical storm activity in the Atlantic and a stronger westerly jet, leading to milder and wetter conditions over north-west Europe. The reverse is true for a negative NAO, with colder, drier conditions

over north-west Europe [*Hurrell,* 1995a].

Figure 2.1 reveals the two phases of the NAO by clustering daily sea level pressure patterns, and shows that the NAO captures almost half of the variance over the North Atlantic domain during boreal winter [*Hurrell and Deser,* 2009]. It is important to note, however, that other weather regimes are revealed when decomposing winter variability, such as blocking over Scandinavia and in the Atlantic, as shown in the right hand panel of figure 2.1. In such states, depending on the specific location of the blocking, cold air advection can lead to particularly cold conditions over Europe, such as in December 2010 [*Sillmann et al.,* 2011], but this pattern may not project on to the NAO. Even though weather variability at a particular location may be a combination of multiple circulation patterns [*Hall and Hanna,* 2018], the NAO remains the leading mode of atmospheric variability during winter over the north Atlantic sector.

The presence and location of the NAO is related to the eddy storm track that spans the north Atlantic ocean, which drives the eddy driven jet [*Ulbrich and Christoph,* 1999; *Woollings et al.,* 2015]. The strong sea surface temperature (SST) gradient across the ocean that exists as a result of warming from the Gulf Stream, leads to a highly baroclinic region [*Minobe et al.,* 2008] and the development of eddies, which maintain the NAO through eddy-feedback mechanisms [*Peng et al.,* 2003]. It is the spatial organisation of this baroclinic activity into coherent large-scale patterns such as storm tracks that produces patterns like the NAO, which is the stationary component of the eddy forcing [*Vallis et al.,* 2004]. The location of the storm track and the NAO is also in part a result of orographic features such as the Rocky mountain range, which force climatological stationary waves downstream [*Hoskins and Valdes,* 1990; *Brayshaw et al.,* 2009].

Case Studies of Extreme NAO Phases

Recent examples of winters where the NAO was strongly negative include the exceptionally cold winter of 2009/10, the coldest since 1978/79, with the lowest NAO and AO index observed in the last 150 years [*L'Heureux et al.,* 2010; *Jung et al.,* 2011; *Fereday et al.,* 2012; *Wang and Chen*, 2010; *Cohen et al.,* 2010]. Resultant impacts from snow and ice in the UK alone grounded transport networks [*Palin et al.,* 2015], and resulted in up to 18 times as many hospital admissions as in previous winters [*Benyon et al.,* 2011]. By analysing hindcasts from the European Center for Medium range Weather Forecasting

(ECMWF), *Jung et al.* [2011] found that remote drivers in the Arctic or tropics could not explain why the NAO was so negative, and that its strength and persistence were in part a result of internal dynamical processes and feedbacks. Despite this, *Fereday et al.* [2012] and *Maidens et al.* [2013] showed this extreme winter was predictable, suggesting sensitivity in the models used to interpret sources of NAO predictability. Work by *Song et al.* [2019] suggest persistent NAO phases depend highly on the overall evolution of the AO; though this is expected given the strong relationship between the NAO and AO [*Ambaum et al.,* 2001].

Charlton-Perez et al. [2018] found that negative NAO phases are more predictable than positive phases owing to sensitivity of the initial stratospheric state, which itself is more predictable than tropospheric variability [*Baldwin et al.,* 2003; *Stockdale et al.,* 2015]. Some studies such as *Weisheimer et al.,* [2017] suggest there may be periods where the NAO was less predictable in the 1960's, but this may be due to sparser observational records. The severe winter of 2009/10 was followed by severe cold the following winter in December. Persistence in the Atlantic sea surface temperatures were linked to this repeat severe winter through dynamical coupling with the NAO [*Buchan et al.,* 2013; *Maidens et al.,* 2013], suggesting interannual persistence in the NAO in certain extreme cases. Actual temperature extremes during negative NAO phases may be mitigated because of climate change warming the base temperature state, suggesting future negative NAO phases may not have the same impacts as present [*Cattiaux et al.,* 2010; *Screen,* 2017b]. Transient periods of extreme negative NAO index, such as February/March 2018, occurring in response to sudden stratospheric warming, led to severe cold over western Europe [*Karpechko et al.,* 2018], but may not be captured in traditional winter averages defined from December to February.

Positive NAO phases can also be associated with extreme weather, such as the winter of 2013/14, where large regions of the UK were inundated with severe flooding from heavy and persistent rainfall [*Huntingford et al.,* 2014; *Knight et al.,* 2017]. This was associated with a anomalously powerful jet stream, driving a succession of extratropical cyclones towards the UK [*Kendon and McCarthy,* 2015]. A positive NAO index is also indicative of an environment conductive for the development of intense extratropical cyclones [*Pinto et al.,* 2008], where wind damage can be considerable; windstorm Daria in 1990 alone led to insured losses of $8.2 billion [*Clark and Gray,* 2018]. Mitigation against such extremes

is aided substantially through accurate seasonal predictions of the NAO, which governs frequency and likelihood of these extreme events.

Socio-Economic Importance

Skilful NAO predictions aid a multitude of businesses and industries, such as the transport sector which directly ingest NAO forecasts and make decisions based on predictions in road, rail and aviation sectors, allowing for mitigation solutions [*Palin et al.,* 2015]. Applications of NAO forecasts also extend to hydrology such as river management, run off and flood risk, providing the potential to implement flood adaptation measures [*Svensson et al.,* 2015]. Commodities such as energy can be traded with an advantage by using skilful predictions of the NAO well in advance of the winter season, leading to huge financial gain [*Clark et al.,* 2017]. Re-insurance from windstorm damage is a multi-billion pound sector, and risk is intimately tied to the phase of the NAO, which controls the probability of extreme windstorms [*Pinto et al.,* 2012]. Additionally, variability in the NAO controls the distribution and survival of flora and fauna of all sizes, bio-geochemistry, and more broadly the marine ecosystem in the Atlantic ocean [*Drinkwater et al.,* 2003]. Weather predictions at some locations are more skilful when using the NAO index rather than parameters such as near surface air temperature or rainfall, given that models demonstrate better skill at getting large scale dynamics correct rather than mesoscale details, which are dependent on model resolution [*Anthanasiadis et al.,* 2017]. Given the strong application of NAO forecasts, it is important that causal drivers that control NAO variability are identified for better prediction.

2.1.1 Measuring the NAO Index

There is no general consensus on the best metric to use to construct the NAO index [*Hurrell and Deser,* 2009]. The 2 methods commonly used are EOF analysis, which is a statistical decomposition of a data field, and station/box based methods, where a time-series is created by subtracting the difference between two regions or locations.

EOF analysis is a statistical technique used to decompose a dataset into orthogonal functions, and can be used to obtain information about spatial and temporal patterns of variance. A principal component time series can be obtained from a dataset varying in space and time, such as mean sea level pressure, which reduces the dataset into a one

dimensional time series that captures maximum amount of information in as few degrees of freedom as possible [*Hannachi et al.,* 2007]. The equations behind this method are not repeated here, but can be found in the review paper by *Hannachi et al.* [2007]. To use this technique, a suitable domain bound has to be chosen; to contain the spatial pattern of the NAO a domain bounded 20°N to 80°N and 90°W to 40°E is suggested in *Hurrell* [1995a]. This statistical technique can be used effectively to isolate modes of variability, such as the NAO or AO, but must be used with caution given they maximise variance over the entire domain, and are therefore sensitive to the domain chosen [*Monahan et al.,* 2009]. Atmospheric modes picked up from EOF analysis are also not statistically independent from other modes of variability [*Monahan et al.,* 2009].

The station based method is commonly used given its simplicity, which involves taking the pressure difference at a gridbox between the location of the two nodes of the NAO over Iceland and the Azores [*Hurrell,* 2018]. By subtracting the mean difference and standardising this time series, an NAO index can be constructed. Other variations of this method include taking an spatial average of multiple grid boxes over each node, in order to eliminate any local variations of the variable being used to calculate the NAO index at the grid-point scale, which can be sensitive to interpolation.

There are relative advantages and disadvantages of these methods. The NAO node locations can shift over decadal timescales [*Wang et al.,* 2003], where the EOF methods will be capture this, if the domain sufficiently captures the node and the EOF is recalculated for the new period. The station based approach will no longer capture as much variance of the NAO given its fixed location in space. This can be partially overcome by taking a box average before taking the difference between Iceland and the Azores. By projecting the EOF of the NAO onto the surface fields, other regimes as shown in figure 2.1 will not be picked up unlike in the station based case, and therefore the EOF is a better method in isolating NAO variability. A disadvantage of the EOF approach is that it relies on well structured gridded data, which limits its use to recent climate periods, compared to station based indices, where in-situ weather stations in the Azores and Iceland go back a lot further [*Hurrell,* 2018].

2.1.2 Dynamical vs Statistical NAO Predictions

The two main methods used to predict the NAO on seasonal timescales involve dynamical approaches, such as running coupled GCMs forward in time, or through constructing empirical models that consist of a few predictors that are combined within a multiple linear regression framework.

Dynamical models

NAO/AO predictability in dynamical models depend on 3 factors; the initial states provided to the model components, the model mean climate state, and the representation by the model of the physical processes associated with teleconnections and seasonal predictability [*Athanasiadis et al.,* 2017]. The use of an ensemble is essential in order to account for uncertainty in model initial conditions and the non-linear and chaotic nature of eddy dynamics [*Murphy,* 1998], which is commonly achieved by using a stochastic physics perturbation scheme [*Anthanasiadis et al.,* 2017], along with perturbations to the initial conditions such as in the GloSea5 system. The NAO is an inherently noisy process as a result of non-linear feedbacks on a range of spatial and temporal scales, and therefore an ensemble is required to obtain a predictable signal. This can be achieved through calculating the ensemble mean, which eliminates noise given a sufficiently large ensemble [*Eade et al.,* 2014]. Even if the dynamical model used was a perfect representation of the real world, one realisation would not be sufficient to determine the predictable signal because of internal variability in the NAO [*Eade et al.,* 2014; *Anthanasiadis et al.,* 2017].

The NAO signal in the model can be considered as two separate components - one that contains unpredictable noise resulting from internal variability, and a component that is potentially predictable as it is constrained by predictable factors such as teleconnections or boundary forcings [*Eade et al.,* 2014; *Douville et al.,* 2018]. *Keeley et al.,* [2009] estimate that 70% of interannual variability in the NAO is externally forced, suggesting the NAO may be largely predictable. Potential predictability is supported by statistical space-state modelling approaches, which suggest 60% of interannual variance is attributable to external forcing, and 8% due to trends [*Sansom et al.,* 2018]. *Domeisen et al.,* [2018] find there is no significant difference in predictability of the NAO and AO, despite their difference in spatial scale.

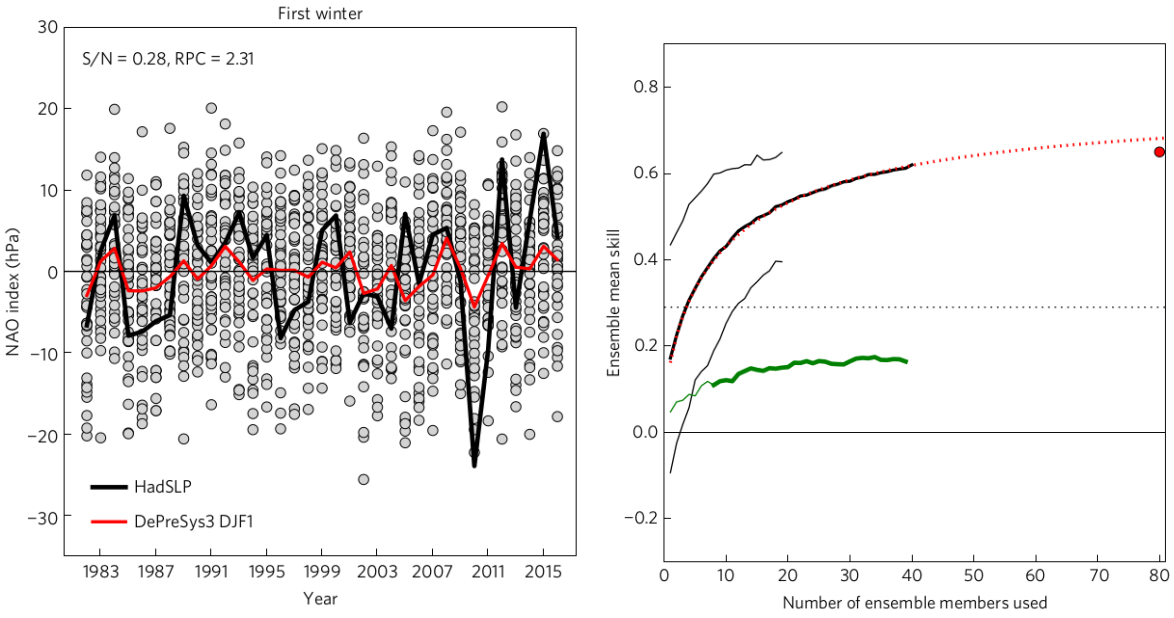

(a) (b)

Figure 2.2: The Met Office DePreSys3 hindcast ensemble skill in predicting the winter NAO. a) shows the ensemble mean in red, reanalysis in black, and individual ensemble members in grey. The signal to noise ratio (S/N) and ratio of predictable components (RPC) are displayed. **b)** shows the skill as a function of ensemble size (thick black line showing ensemble mean skill, black curves represent 5-95% confidence intervals. Red dotted line is theoretical relationship. Green curves show the average skill in predicting a single model member (changing to a thick line when this is significantly less than predicting the reanalysis). Adapted from *Dunstone et al.,* [2016].

Signal to Noise 'Paradox'

To characterise how well models capture the predictable component of the NAO in models relative to the noise in the ensemble, *Eade et al.,* [2014] proposed the following equation 2.1, where SN is the signal to noise ratio, σ_{obs} is the real world variance, and σ_{mod} is the model ensemble mean variance. This ratio can be expanded by incorporating the correlation coefficient (r), and normalising this with the ratio of variance explained by the model, producing the ratio of predictable components (RPC) value.

$$SN = \frac{\sigma_{mod}}{\sigma_{obs}} \qquad RPC = \frac{r}{\sqrt{\frac{\sigma_{mod}}{\sigma_{ens}}}} \tag{2.1}$$

This implies a system with an RPC equal to 1 perfectly reflects predictability of the real world, with values above 1 suggesting under-confidence in the model. Model

under-confidence can be interpreted as the ensemble mean skilfully predicting observations (high correlation) but ensemble members agree less well with each other indicating a low model SN ratio as seen in the green curve in 2.2(b) [*Eade et al.,* 2014, *Dunstone et al.,* 2016; *Scaife and Smith,* 2018]. A similar interpretation is that each ensemble member contains too much noise and not enough predictable signal, suggesting the model is under-confident [*Scaife et al.,* 2014; *Eade et al.,* 2014]. The ensemble spread is unrealistically large given the skill of the ensemble mean, such that the skill in the model predicting itself is significantly lower than the observations, suggesting that the simulated model NAO is less predictable than the real NAO [*Dunstone et al.,* 2016]. Such signal to noise paradox has been identified in multiple dynamical modelling systems [*Scaife and Smith,* 2018], with the models signal to noise ratio becoming increasingly large as ensemble size increases [*Baker et al.,* 2018].

The presence of such a low signal to noise ratio makes it difficult to use ensemble NAO predictions operationally, given the magnitude of the NAO response is incorrect as seen in figure 2.2(a), although the NAO index can be recallibrated to correct for the variance. Identifying the source of this signal to noise problem, which is found in a wide range of different models, is an active research problem [*Baker et al.,* 2018; *Scaife and Smith,* 2018]. Various reasons behind the existence of this have been put forward, such as the model atmosphere not being constrained strongly enough to relevant drivers and teleconnections proposed to control NAO predictability, such as North Atlantic SST's [*Eade et al.,* 2014], the QBO [*O'Reilly et al.,* 2019], or fundamentally underestimating regime persistence [*Strommen and Palmer,* 2019]. More recently, it has emerged models at very high resolution simulate eddy feedbacks across the Atlantic better, which in turn strengthens the model signal [*Scaife et al.,* 2019]. The signal/noise paradox is important to consider in analysis, given the models may be deficient in representing teleconnections (anomalously weak signals), and may in part explain weak model signals related to the NAO, particularly if the ensemble size is small.

Empirical Models

Empirical approaches to predicting the NAO have also been employed, using only a statistical framework focusing on key proposed drivers of the winter NAO. This includes multiple linear regression analysis, where the relative contribution of each driver can be

assessed given its weighting. To derive a predictor, EOF analysis can be used to determine which boundary forcings, such as sea ice or sea surface temperatures, contain the most variability month to month, and each of these can be tested in their correlation with the winter NAO using a lag, which implies a direction of the connection [*Hall et al.,* 2017; *Wang et al.,* 2017]. Development of simple stochastic models to fit the NAO time-series have been employed, testing different timescales of variability using power spectra [*Stephenson et al.,* 2000].

Statistical predictions can be tested using training periods, but given the limited observational record there is a risk of over-tuning parameters in the statistical model and over-fitting data [*Hall et al.,* 2017]. Choices of what predictors to choose can also be subjective, with uncertainty with regard to what lag to use [*Kretschmer et al.,* 2016]. Methods such as causality discovery mechanisms, which take into account auto-correlation, co-variance between drivers and different lag times have been utilised to identify causal drivers of the NAO and AO [*Kretschmer et al.,* 2016]. These techniques are better than a simple correlation between a predictor and the NAO, but have caveats; results are conditional on all related predictors being included in the analysis, but these may not be known. Therefore, this statistical tool is dependent on prior physical knowledge of the climate system. These simple models also may fail to replicate covariance between drivers on a variety of timescales that a dynamical model would, particularly non-linear interactions. These caveats and their implications are discussed in more depth later when causal effect network analysis is performed.

Both dynamical and statistical methods are useful in determining what physically drives NAO variability. Dynamical models require the use of large ensembles to obtain an NAO signal, which are expensive to run, but can be better at understanding the core physical processes. Statistical approaches are much faster, but are subjective to the data used, the training periods chosen, and are difficult in determining causality. Ideally, a combination of both should be employed to better aid understanding what controls NAO variability, especially given dynamical models can represent non-linear interactions between the predictable components of the climate system [*Folland et al.,* 2012], which may then be utilised in statistical models. For future predictions, dynamical predictability is particularly useful given possible non-stationarity of predictors such as sea ice [*Kolstad and Screen,* 2019].

2.1.3 Skilful NAO Predictions

Predictability of the NAO depends on the timescale in question. Earlier studies such as *Collins* [2002] suggested limited NAO predictability beyond a few weeks. While *Feldstein* [2000] find the e-folding time of the NAO to be approximately 10 days, *Rennert and Wallace* [2009] find extended persistence on intermediate 10-30 day timescales, explained through a positive feedback with eddies and larger scale vorticity anomalies associated with the NAO [*Barnes and Hartmann,* 2009].

Predictability on sub-seasonal timescales that originates from persistence also depends on the phase of the NAO event; *Barnes and Hartmann,* [2009] found that negative NAO events last significantly longer than positive NAO events, given that negative NAO events are synonymous with an equatorward-shifted jet, with stronger eddy feedbacks that help to maintain the NAO polarity. Despite this enhanced persistence, *Weisheimer et al.* [2017] found that negative NAO periods such as in the 1960's were less predictable than more recent positive NAO periods. Dynamical factors attributable to better predictability of negative NAO events include sudden stratospheric warmings, partly responsible for negative NAO phases [*Kidston et al.,* 2015]; this is covered in more depth later in this chapter.

Earlier studies such as *Johansson,* [2007] argued it is necessary to employ coupled atmosphere-land-ocean models to obtain NAO skill beyond a few weeks. While this is supported by recent studies such as *Dunstone et al.* [2016], who find NAO skill a year ahead and must therefore originate from boundary conditions, other recent studies have challenged this conventional view and argued the importance of initial stratospheric conditions. *Stockdale et al.* [2015] obtained winter AO correlations of 0.6 in an operational forecast model, through initial stratospheric conditions alone. However, this result only uses a sampling period of 8 years (2004-2011), and despite a large ensemble, may not be a representative result over a longer period. More robust studies include *Nie et al.* [2019] who show a downward propagation of initial stratospheric conditions during winter, contributing to NAO skill, and *O'Reilly et al.,* [2019], who found NAO skill substantially improve with QBO initial conditions. Stratosphere-troposphere coupling is particularly important in late winter [*Baldwin and Dunkerton,* 2001], to realise NAO predictability through eddy feedback mechanisms [*Kidston et al.,* 2015; *Saito et al.,* 2017].

Predictability of the winter NAO is non-stationary in time, and has varied over the

twentieth century [*Weisheimer et al.,* 2017]. This is in part due to data uncertainty and quality of observational data used to verify model performance [*Fletcher and Saunders,* 2006], and low frequency variability in the tropics, such as a dominance of central Pacific events post 2000 which coincided with higher skill [*Kumar and Chen,* 2018], or more generally ENSO variability [*L'Heureux et al.,* 2017]. Short datasets of just 20 years can be over-dispersive, with skill varying considerably over a longer 40 year period [*Shi et al.,* 2015], therefore, if sufficiently long periods are not used to test predictions particularly using empirical methods, sampling errors can lead to large departures from their actual value [*Kumar,* 2009].

Hall et al. [2017] achieved similar levels of NAO skill as dynamical models using a statistical model containing information about SST's, sea ice, and tropical rainfall, though this analysis is limited given the testing period is short with the risk of over-fitting the regression [*Hawkins,* 2004]. Even higher levels of skill using a simple multiple linear regression model are found in *Wang et al.* [2017], with correlations as high as 0.7 using just a few predictors such as SSTs, sea ice and stratospheric conditions in autumn. This study is highly selective in its use of predictors, by exhaustively testing 18 different principal components (2 months, 3 predictors, and the 3 leading PC's) and using the top 3 to construct the MLR. Additionally, the sea ice index, derived through projecting sea ice onto the September-February EOF loading pattern, may build in information from the DJF NAO and therefore be biased.

Modelling systems other than the Global Seasonal forecasting system 5 (GloSea5) have also been able to obtain high levels of statistically significant NAO and AO skill [*Siegert et al.,* 2015], suggesting that sources of predictability are unanimously being captured by various models [*Anthanasiadis et al.,* 2017; *Kang et al.,* 2014; *Riddle et al.,* 2013; *Butler et al.,* 2016]. Additionally, *Sun and Ahn* [2014] found NAO predictability using a more simple coupled GCM; NAO predictability may not require full complexity.

Lagged ensembles are used to improve NAO prediction; where subsets of the ensemble are initialised at different times taking into account sensitivity to initial conditions [*Chen et al.* 2013], and is actively employed in the DePreSys3 hindcast [*Dunstone et al.,* 2016]. Another technique is creating a multi-model ensemble; better NAO skill can be obtained by taking a large ensemble using a multi-model average [*Anthanasiadis et al.,* 2017]. By creating a large multi-model ensemble of 126 members, *Baker et al.* [2018] found winter

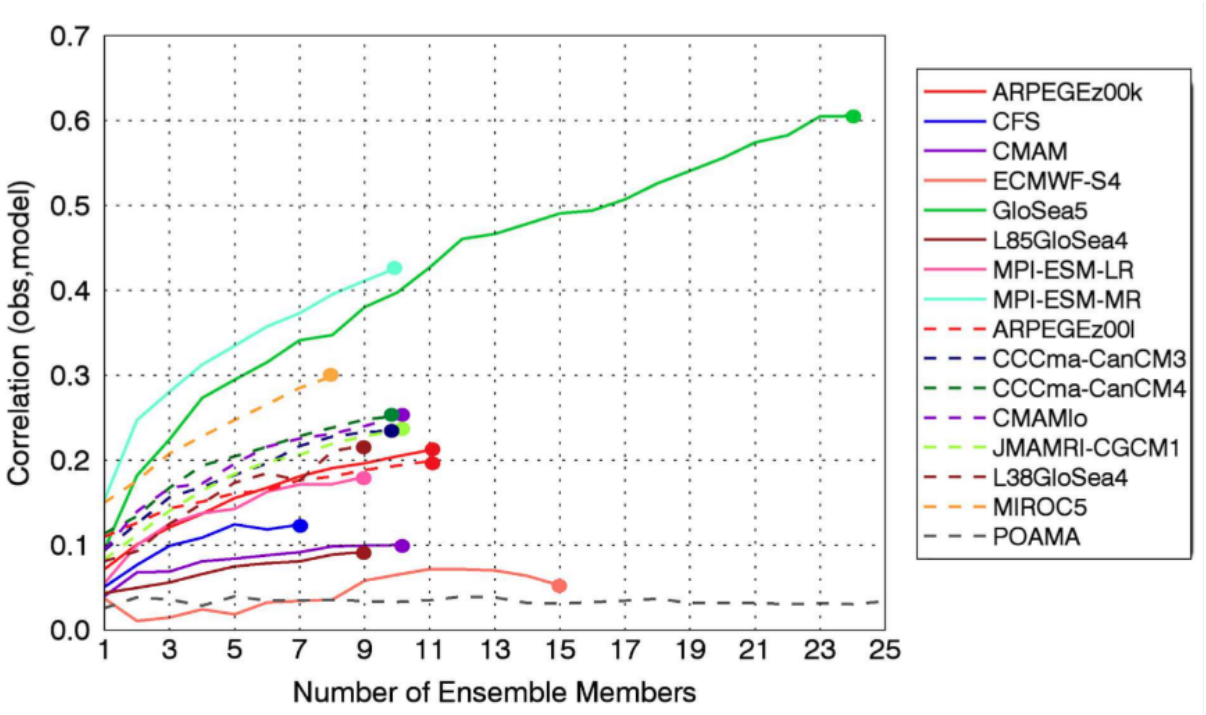

Figure 2.3: Skill of different model forecasts of the winter NAO as a function of their ensemble size. The correlations are calculated by randomly selecting ensemble members 100 times, averaging them together, and then correlating the ensemble mean with the observed DJF NAO index using ERA-Interim reanalysis [*Butler et al.,* 2016].

NAO correlations of r=0.7; higher than any individual system. Other methods exist involving sub-sampling and filtering the model ensemble prior to winter such as *Dobrynin et al.* [2018], but these are usually biased, as they require hindsight knowledge of rejecting members based on their representation of processes linked with the NAO.

Butler et al. [2016] examined NAO skill across different models initialised from November, and determined the benefit of implementing a resolved stratosphere (high-top model). There is a large disparity across models in their ability to predict the NAO; skilful models such as GloSea5 and ARPEGE, whilst many others show no significant skill at all. From a multi-model mean perspective, high top models have increased skill in predicting the NAO; though when isolating models where only the model lid height and vertical resolution are changed, there is no significant impact on NAO skill [*Butler et al.,* 2016]. There is a clear dependence on ensemble size, as discussed earlier in *Scaife et al.* [2014]; *Dunstone et al.* [2016]; *Eade et al.* [2014], in order to obtain a predictable NAO signal, and this is well reproduced across all skilful models as shown in figure 2.3. These skill with ensemble size curves follow what would be expected theoretically with increasing the

ensemble size, eventually reaching an asymptotic value of maximum skill [*Murphy,* 1990; *Dunstone et al.,* 2016]. GloSea5's high skill may be resultant of enhanced ocean resolution and initialisation of Arctic sea ice, not only due to its large ensemble size [*Butler et al.,* 2016]. These results show the current operational limit of NAO predictability is around r = 0.8 in dynamical systems (e.g. [*Anthanasiadis et al.,* 2017; *Scaife et al.,* 2014; *Dunstone et al.,* 2016; *Butler et al.,* 2016; *Baker et al.,* 2018]), and demonstrates recent progress in predictability of the NAO along with future potential [*Smith et al.,* 2016].

2.2 Polar Drivers of NAO Variability

2.2.1 Arctic Sea Ice and NAO Links

Rapid decline in Arctic sea ice over the past few decades has been the subject of intense research, with model projections suggesting that September Arctic sea ice could disappear within the next few decades [*Collins et al.,* 2012]. Arctic amplification; the positive heating feedback over the Arctic, is heating this region 2-4 times faster than the global average [*Screen et al.,* 2013]. The last couple of decades have experienced unexpectedly low sea ice concentrations such as in 2007 [*Stroeve et al.,* 2007; *Comiso et al.,* 2008], due to positive feedback processes such as the albedo feedback [*Screen and Simmonds,* 2010]. Declines are not only confined to sea ice extent, but also ice thickness and reductions in multi-year ice [*Kwok and Rothrock,* 2009]. Many modelling studies only incorporate sea ice concentration and do not take thickness into account; and typically prescribe a uniform sea ice thickness of 2 meters [*Peings and Magnusdottir,* 2014], despite studies such as *Rinke et al.* [2006] emphasising the important influence of thinning sea ice on both regional and wider circulation patterns. Sea ice thickness is however poorly constrained, with limited observations [*Lindsay and Schweiger,* 2015], and makes it difficult to provide accurate boundary conditions for models, especially in recent decades where sea ice is thin [*Krinner et al.* 2010].

Melting sea ice is highly non-uniform across the Arctic; sea ice loss is particularly strong (loss of 2-8% per decade) in the Barents and Kara (BK) seas as revealed from satellite data [*Liu et al.,* 2004]. This Arctic sea ice loss has led to many studies investigating how this will affect atmospheric circulation patterns, both locally and remotely in the extratropics [*Vihma et al.,* 2014]. Decrease in autumn Arctic sea ice is linked with

changes in northern hemisphere atmospheric circulation, particularly the negative phase of the AO/NAO, broader meridional meanders in the midlatitude jet [*Francis and Vavrus,* 2015; *Barnes and Screen,* 2015], and more frequent cold air outbreaks [*Liu et al.,* 2012; *Collow et al.,* 2019], though these links are disputed [*Overland et al.,* 2016].

The earliest studies such as *Newson,* [1973] identified a weakening of mid-latitude westerlies due to Arctic sea ice loss using an idealised model, well before the trend in sea ice became strong. Since, model complexity ranges from idealised dry-core to fully coupled comprehensive GCMs. These experiments, however, have produced a spectrum of NAO responses with no consensus even regarding the sign of the NAO [*Smith et al.,* 2017], as well as in case study experiments of extreme low sea ice years such as 2007 [*Bluthgen et al.,* 2012]. Discrepancies in these responses could be related to model configuration, sampling uncertainty due to large internal variability in the model [*Screen et al.,* 2012], the limited period of time since major amplification of the Arctic warming [*Overland,* 2016], as well as the climatological state of the model [*Overland et al.,* 2016; *Smith et al.,* 2017]. Studies also vary in the way they prescribe sea ice anomalies, and the time of year that the forcing is applied, among others [*Cohen et al.,* 2014]. These discrepancies have led to a coordinated effort (PAMIP) contributing to the CMIP6 project [*Smith et al.,* 2019].

Negative NAO response to low sea ice

Many studies suggests a negative NAO/AO response to decreased Arctic sea ice [*Wu and Zhang,* 2010; *Sun et al.,* 2015], particularly in the Barents-Kara seas [*Yang and Christensen,* 2012]. This teleconnection is suggested to occur through both tropospheric and stratospheric adjustment mechanisms [*Kim et al.,* 2014; *Zhang et al.,* 2018]. Sea ice in autumn also emerges as one of the strongest positively correlated predictors of the winter NAO index [*Wang et al.,* 2017], when using observational data, implying a strong statistical link between the two, though note the previous identified issues with this study, along the dependence of detrending the data to obtain this link. Importance of sea ice as a boundary forcing for Eurasian weather has also been shown using AMIP experiments, forced with either climatological sea ice or observed ice; the latter leading to better temperature variability over Eurasia [*Lim et al.,* 2012]. However, studies such as *Lim et al.* [2012] are restricted by a small sample size (3 ensemble members), and other

studies such as *Sun et al.,* [2016], *Ogawa et al.,* [2018] and *Koenigk et al.,* [2019] suggest limited role for sea ice affecting temperature variability over these regions.

Using observational data, *Honda et al.* [2009] found that sea ice minima in autumn coincided with significant cold anomalies across Siberia, extending westwards towards Europe and becoming zonally elongated in late winter, projecting onto the negative NAO phase. This response was reproduced using an AGCM, which revealed a thermally generated stationary Rossby wave through turbulent heat flux anomalies in the Barents-Kara seas during late autumn, which amplifies the climatological Siberian high. Reproducibility in the model suggests the dynamics are sufficiently captured using an atmosphere only model, and are supported by studies such as *Blackport and Kushner* [2016] and *Zhang et al.* [2018]. *Seierstand and Bader* [2008] find that by forcing the ECHAM5 AGCM with present and projected future Arctic sea ice concentrations separately, that storminess in early to mid winter decreases significantly, due to increased likelihood of the negative NAO phase. *Seierstand and Bader* [2008] also find greater atmospheric sensitivity to sea ice anomalies in late winter, suggesting temporal dependence on how the atmosphere responds to sea ice variability and may explain in part discrepancies in model response. The result of *Seierstand and Bader* [2008] contradicts that found in *Garcia-Serrano et al.* [2015], who find that only November BK ice anomalies have a significant cross-validated correlation with the winter circulation anomalies over the Atlantic and Euro sector using reanalysis data. Studies such as *Jaiser et al.* [2012] find that sea ice loss and resultant heat fluxes modify vertical static stability; such that baroclinic instability is altered in both storm tracks which feedback onto the NAO, although the study is limited in its small composite size (using two 10 year samples in reanalysis representative of low/high ice).

Nakamura et al. [2015] support the mechanism proposed in *Honda et al.* [2009]; that BK anomalies force a stationary Rossby wave, but also conclude that this is a positive feedback which cools the midlatitudes and warms the Arctic further, accentuating the process. *Nakamura et al.* [2015] also found an important role of the stratosphere; high top models simulate a deeper tropospheric annular mode response, and stronger modulation of the NAO in mid to late winter to sea ice variability. A stratospheric mechanism involving the polar vortex is proposed by *Kim et al.* [2014]. Decreased sea ice cover during the early winter months in the Barents-Kara sea enhances upward wave propagation of wave 1 and 2 into the stratosphere, which subsequently break, disrupting and weakening the

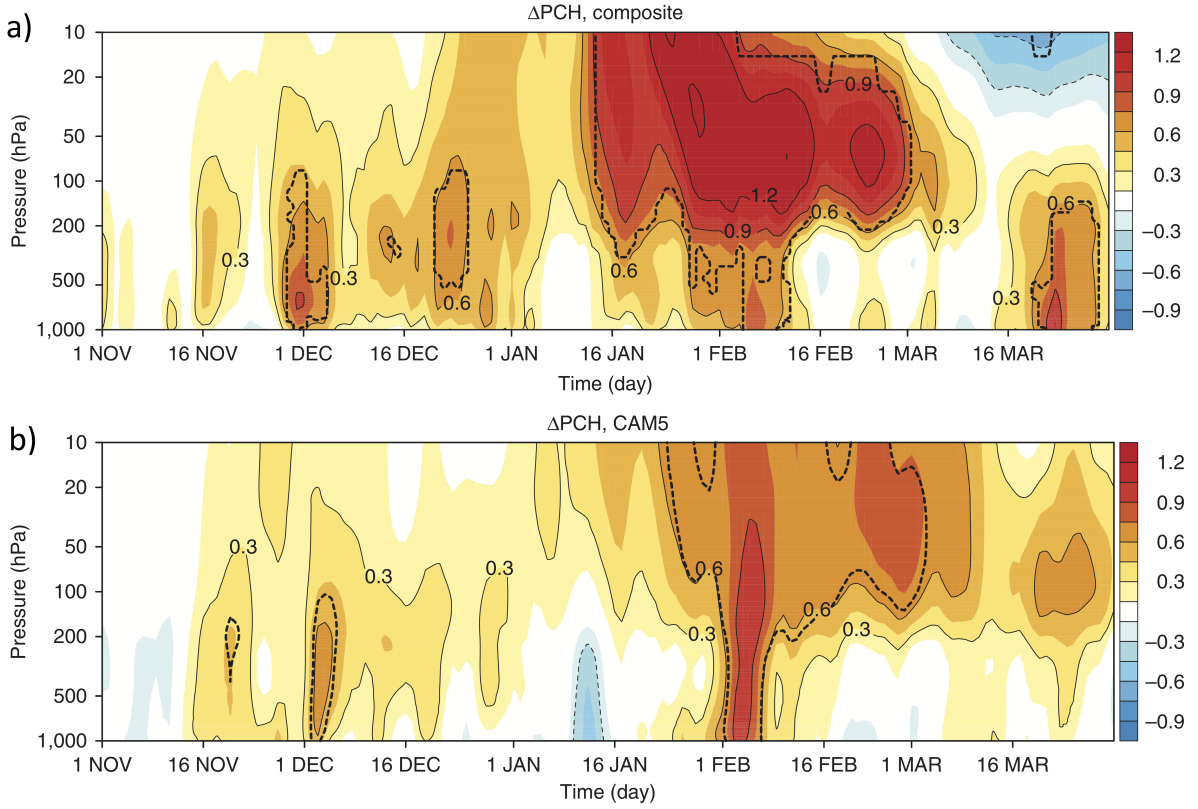

Figure 2.4: Polar Cap Height and its relation to BK ice variability. a) Composite of early winter (November-December) BK sea ice on the subseasonal evolution of the polar cap height using HadISST and ERA-Interim data. Units are the standard deviation anomaly. **b)** Same as in **a)**, but using the CAM5 ensemble mean. Values enclosed by a dotted line are significant at the 95% confidence level. Adapted from *Kim et al.* [2014].

polar vortex in mid winter. A weaker polar vortex has an increased tendency to undergo a sudden stratospheric warming, which can affect tropospheric weather after a lag of 1-2 weeks projecting onto the negative phase of the NAO depending on the nature of the breakdown [*Hitchcock and Simpson,* 2014]. Given that removal of sudden stratospheric warmings from model hindcasts removes almost all skilful predictability of the NAO [*Scaife et al.,* 2016], and that the stratosphere controls a lot of predictability in the troposphere and at the surface [*Baldwin et al.,* 2003; *Jia et al.,* 2017; *Stockdale et al.,* 2015], these results suggest that the stratosphere may be critical in mediating a response from Arctic ice to the NAO, given some lag [*Ruggieri et al.,* 2016], if such Arctic sea ice link to the NAO is causal. Additional multi-model simulations by *De and Wu* [2019] confirm the importance of stratospheric representation in simulating this link between the Arctic and mid-latitudes.

Figure 2.4 from *Kim et al.* [2014] captures this lagged disruption of the polar vortex

related to anomalously low Barents-Kara sea ice using sub-seasonal data, both in observational data and in their model ensemble mean (CAM5). Intermittent increases in tropospheric polar cap height are seen in early winter, mainly confined below 100 hPa, before major increases in geopotential height are seen in the stratosphere in late winter (increase in geopotential height indicates a weaker polar vortex). This can be seen to propagate down to the troposphere, with impacts on the lower tropospheric circulation and subsequently the NAO. This polar vortex weakening as well as the troposphere-stratosphere coupling in early February is consistent across observations and the model ensemble mean, with a similar pathway found by *Jaiser et al.* [2013].

Given the large amount of internal variability present in the NAO [*Eade et al.,* 2014], large ensembles have been employed to obtain a statistically significant signal in the context of Arctic sea ice-NAO links. By using a 100 member ensemble AGCM, as well as 22 independent climate simulations, *Mori et al.* [2014] found that sea ice concentration reduction in the Barents-Kara seas has doubled the probability of severe winters in central Eurasia, with an increased tendency for a negative NAO due to more frequent Eurasian blocking. Analysis of these climate models, however, suggest that in the future as the climate warms, sea ice driven cold winters are will be less severe given the source regions of cold air are also warming [*Screen,* 2017b]. Synthesis of 6 ocean-atmosphere coupled models show an intensification of the Siberian high and weakening of the Icelandic low, which project onto the negative NAO phase, with sensitivity to the magnitude and geographic pattern of sea ice loss (explored later) [*Screen et al.,* 2018].

Positive NAO response to low sea ice

Singarayer et al. [2006] found that forcing HadGEM3 with sea ice from 1980-2000 and then with reduced sea ice in 2100 (following a moderate climate change scenario), led to enhanced precipitation and cyclone activity in extratropical storm tracks, indicating a positive NAO response. Additionally, *Orsolini et al.* [2012] tested this atmosphere response by forcing the ECMWF seasonal forecast model with either prescribed or reduced sea ice, finding that the initial local heating response from reduced ice expanded outwards in winter, deepening the Icelandic and Aleutian low, favouring a positive NAO. This study focused on one year of anomalously low ice (2007), so may not be representative of other years where the background climate state is different. Other studies that have looked at

case study years include *Balmaseda et al.* [2010], who find that low sea ice in 2007 led to an increase in pressure of Arctic and Greenland and the negative NAO phase; an opposite response of *Orsolini et al.* [2012]. Additionally, *Strey et al.* [2010] find Atlantic sector blocking by re-simulating the case study of 2007.

Physical mechanisms that explain a positive NAO response to Arctic sea ice loss involve the notion that a warmer Arctic leads to a thermal low pressure, which can extend out of the polar region and accentuate the Icelandic node of the NAO [*Cassano et al.,* 2014; *Orsolini et al.,* 2012]. This idea is not only supported by climate simulations, but also higher resolution modelling studies using the Weather and Research Forecast (WRF) model; *Strey et al.* [2010] configured a high resolution WRF to look at case study years of extremely low sea ice, and found that low sea ice led to reduced sea level pressure over the Arctic, and drove a barotropic ridge/trough structure over North America, leading to increased storm activity over the Atlantic basin and a positive NAO index. These case study style experiments should be treated with caution however, given large internal variability year to year; studies looking at simulations spanning longer periods of time, such as *Rinke et al.* [2013] who looked at forcing HIRLAM with sea ice anomalies in autumn and winter from 1949-2008 using a 6 member ensemble found internal variability leads to significant uncertainty in the impacts of ice loss. This is due to the simulated atmospheric feedback pattern dependent on the position and strength of the regional sea ice anomalies, as well as the time period chosen [*Rinke et al.,* 2013].

Inconclusive NAO response to low sea ice

Not all studies conclude a particular NAO phase response to reduced ice, with signals originating from ice perturbations small and indistinguishable from internal variability [*Chen et al.,* 2016], given that high latitude variability is so large [*Gerber et al.,* 2014]. By performing single year model runs starting in April, and perturbing the sea ice thickness, *Petrie et al.* [2015] found NAO responses in summer but not in winter. Similarly, *Blackport and Kushner* [2016] find that modifying the ice albedo leads to a weak and insignificant response in the midlatitude circulation. Given how large internal variability is, it is challenging to obtain a forced signal, with the additional caveat of models potentially underestimating teleconnections due to the signal/noise issues [*Scaife and Smith,* 2018]. While local responses to ice variability are distinguishable from internal variability,

more remote responses in the mid-latitudes may be partially or wholly masked by internal variability [*Screen et al.,* 2013]. This is supported by comprehensive evaluation of CMIP5 models, which provide no support for a relationship between declining Arctic sea ice and negative AO polarity [*Boland et al.,* 2017].

Studies have attempted to address the uncertainty in the atmospheric response to sea ice loss by looking at how model configuration plays a role in determining the influence of sea ice; *Deser et al.* [2015] highlight the importance of ocean-atmosphere coupling with Arctic sea ice loss, given ice loss induces changes elsewhere in the ocean. They find that the response to sea ice loss is much more confined to the polar regions when fully coupled models are not used, and that full dynamical models support teleconnections much further out from the Arctic. The sensitivity of this is investigated using a full depth, slab and non-interactive ocean. A full ocean model leads to ice variability impacts across the globe, including the tropics [*Deser et al.,* 2015]. Other studies have found that although ocean-atmosphere coupling enhances the response to sea ice loss, it doesn't change the overall structure or pattern of the forcing [*Deser et al.,* 2016]. Not only is model configuration important, but also the background state of the model; differences in the climatological state in the mid-latitudes can mediate the response of Arctic sea ice loss by controlling the refraction of planetary waves, and therefore the sign of the NAO [*Smith et al.,* 2017], and could therefore help explain the discrepancies in these results in conjunction with atmosphere-ocean coupling. By analysing sea ice loss with and without an ocean coupled model, *Blackport and Kushner* [2018] found that the response to Arctic sea ice loss extended into the mid troposphere only when ocean coupling is used, suggesting that AGCM experiments will underestimate mid tropospheric warming.

Bi-directional relationship between ice and the NAO

Relationships between ice and the NAO may be resultant of the atmosphere driving, and not responding, to sea ice variability [*Sorokina et al.,* 2016; *Peings et al.,* 2019; *Blackport et al.,* 2019]. The NAO can drive changes in sea ice extent, concentration and thickness through changing large scale wind stress [*Guemas et al.,* 2016], thus sea ice variations may be forced by large scale variability in the atmosphere [*McCusker et al.,* 2016].

Kwok [2000] showed that in observations, the intensity of the Icelandic low modulates the quantity and location of ice transport over this region, changing the sea ice export

as well as sea ice import from the BK seas, which significantly alter the sea ice mass balance and geographical distribution of sea ice in the Arctic ocean. Studies focusing on decadal variability such as *Mysak and Venegas* [1998] reveal a feedback cycle between sea ice concentration and winter sea level pressure, with a 10 year cycle according to decadal variability of the NAO. Hemispheric wide oscillations such as the AO have been shown to control sea ice on these timescales, where a deepening of the AO of 3hPa during the 1980's led to stronger cyclonic motion in sea ice motion [*Rigor et al.,* 2012]. Using regression with leads and lags, *Kelleher and Screen* [2018] found that CMIP5 models showed atmospheric precursors and responses to low sea ice, but regressions are stronger when atmosphere leads sea ice, including a weaker polar vortex, with low sea ice a response to enhancement of mid-latitude eddy heat flux.

On shorter seasonal and interannual timescales, the processes are still relevant. Interannual persistence of the AO can partly be attributed to the preceding winters dynamical influence on sea ice concentration, which leaves an imprint in heat fluxes over the Arctic ocean [*Rigor et al.,* 2012]. The complexity of this feedback is extended further when considering ocean interactions with sea ice and the NAO, with exchanges of ice volume, heat and freshwater at the Greenland-Scotland ridge strongly correlated with the NAO [*Zhang et al.,* 2004]. Supporting these findings, *Krahmann and Visbeck* [2003] used a general circulation model with an interactive boundary layer to investigate northern annular mode like forcings on sea ice, finding that ice changes rapidly to changes in forcing, leading to widespread variations in sea ice thickness and concentration. Intra-seasonal relationships have also been identified where NAO phases affecting sea ice variability can then re-enforce each other later in winter [*Yamamoto et al.,* 2016]. Determining cause and effect between sea ice and the atmosphere remains a challenging research topic.

Spatial Dependence of Sea Ice Variability

Early studies such as *Sokolova et al.* [2007] demonstrated that variations of Arctic sea ice exert a strong influence on storm tracks in the Atlantic and Pacific, as well as implying that there may be nonlinear dynamic feedbacks between sea ice and the Arctic Oscillation. Diagnosing the atmospheric response to sea ice variability using Eliassen-Palm fluxes, they found reduced wave activity during high sea ice phases, which correspond to the positive phase of the AO [*Sokolova et al.,* 2007]. The BK region in isolation has been shown to

exert an influence directly onto the NAO producing a negative NAO response to low BK sea ice [*Liptak and Strong,* 2014]. Systematic experiments where sea ice is decreased in different regions of the Arctic can help identify key regions of importance. For example, *Screen* [2017a] forced an AGCM prescribed with sea ice loss in 9 different regions to obtain distinct atmospheric responses, as well as a pan-Arctic ice loss case, to see whether the response for different regions was additive or non-linear. These winter responses for each of the regions are shown in figure 2.5.

Different responses to sea ice loss are found in each region, with some triggering large scale dynamical responses, where as others are confined to local thermodynamic induced changes instead. Although sea ice in most regions leads to a weakening of the Azores high, as seen in figure 2.5, sea ice loss in the Barents-Kara region produces the strongest response in the NAO. Polar cap height analysis reveals that Barents-Kara sea ice loss is able to modulate the polar stratosphere, therefore exerting an indirect influence on the mid-latitude troposphere, whereas there is no general consensus among other regions of ice loss to the effect on the stratosphere [*Screen,* 2017a]. These results are also supported by *Koenigk et al.* [2016], who used detrended ERA-Interim data to analyse the atmospheric response of sea ice variability in 8 regions found that BK ice has the strongest relationship with the NAO, or regions similar to this including the Laptev Sea [*Li and Wang,* 2012]. Of interest also is the non-linearity of the response in different regions; the net addition of ice loss responses is not equal to the response in the pan-Arctic case, suggesting that sea ice loss in one region affects sea ice in another region, potentially via induced circulation anomalies locally [*Screen,* 2017a]. Sea ice loss in the Okhotsk, for example, drives a positive NAO response in multiple models [*Mesquita et al.* 2011], in which the NAO may then alter the distribution of sea ice later (as discussed in the previous section).

Zhang et al. [2017] imposed a thermal anomaly in the Barents-Kara sea to simulate sea ice loss in an idealised GCM in winter, which led to a geopotential height increase throughout the polar atmosphere. The use of calculating Eliassen-Palm (EP) fluxes to better interpret divergence and wave activity in the atmosphere (e.g. [*Edmond et al.,* 1980; *Andrews.* 1987]) and how this changes in time can help to diagnose a causal chain of events. An analysis of EP fluxes shows that BK ice anomalies lead to linear constructive wave interference in the troposphere, as to amplify and accentuate the climatological waves meridionally, leading to enhanced upward wave propagation which weakens the

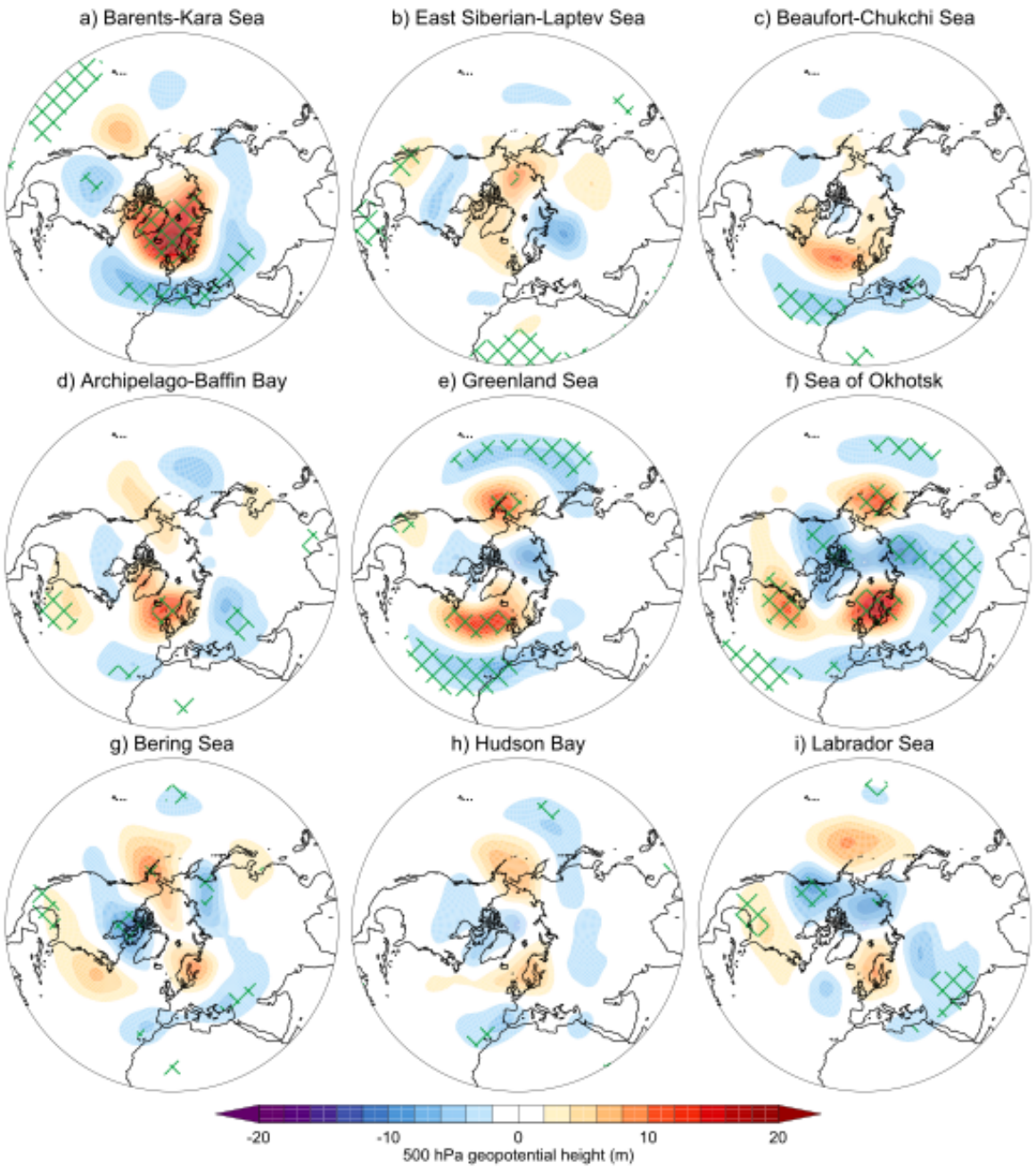

Figure 2.5: Contrasting response of sea ice loss in different regions. Sea ice loss response in 500hPa geopotential height during October-March in the Barents-Kara Seas (65-85°N, 10-100°E), East Siberian-Laptev Seas (68-85°N, 100-180°E), Beaufort-Chukchi Seas (68-85°N, 180-240°E), Canadian Archipelago-Baffin Bay (63-80°N, 240-315°E), Greenland Sea (63-85°N, 315-360°E), Sea of Okhotsk (40-63°N, 135-165°E), Bering Sea (55-68°N, 165-205°E), Hudson Bay (50-63°N, 260-290°E), and Labrador Sea (40-63°N, 290-315°E). From *Screen* [2017a].

polar vortex, similar to that found in *Honda et al.* [2009] and *Kim et al.* [2014]. Given the chain of events and lagged response in the stratosphere, this stratospheric response persists for 1-2 months accompanied by a downward migration to the troposphere and surface. Finally, this amplifies and extends the low level jet, de-accelerating it, with the BK region most effective in eliciting this strength of response [*Zhang et al.,* 2017]. *Yang et al.* [2016] also find anomalies in the BK sea lead to large scale atmospheric changes through a series of dynamical adjustments, with slower zonal mean anomalies propagating from the sub-Arctic to the mid-latitudes after around 1 month. The AO pattern is driven by wave mean flow interaction, and therefore it is modified through warming and weakening of the polar stratospheric vortex [*Yang et al.,* 2016].

McKenna et al. [2018] found contrasting responses in stratospheric polar vortex strength from ice loss in the Barents and Kara seas and the Pacific sector; with a weakening of the polar vortex associated with BK ice loss. These results are also supported by *Kelleher and Screen* [2018], who found that low BK ice drives a weaker polar vortex, and that low sea ice in the Sea of Okhotsk is correlated with a stronger polar vortex. *Mckenna et al.* [2018] also found that tropospheric mechanisms become relatively more important than stratospheric mechanisms as the sea ice loss magnitude increases, given the AO response for moderate and large sea ice loss is similar. Impacts of BK ice variability have been explained through tropospheric mechanisms solely; *Petoukhov and Semenov* [2010] argue that decreases in ice in this region could lead to increased cold extremes in Europe, given anticyclonic conditions develop over the polar ocean leading to anomalous easterly advection of cold air from the continent. Despite this, they find the response highly non-linear as sea ice is decreased from 100% to ice-free conditions. They proposed that this was due to opposing effects from local heating and convection, and baroclinic effects from modifying the temperature gradients surrounding the heating area. The sensitivity of this response also suggests a large role for internal variability, again reiterating the requirement for large ensembles [*Koenigk et al.,* 2018]. However, *Peings et al.* [2019] find that this anticyclonic circulation over Eurasia causes sea ice loss, and is not a response through sensitivity experiments.

Variability and Predictability of Sea Ice

If there is a causal link between Arctic sea ice and the NAO, skilful predictions of sea ice may lead to improved NAO predictions, especially given studies have shown seasonal forecasts are sensitive to Arctic sea ice biases [*Bunzel et al.* 2016]. Despite sea ice persistence on seasonal timescales [*Blanchart-Wrigglesworth et al.,* 2011; *Chevallier et al.,* 2013; *Guemas et al.,* 2016], sea ice is sensitive to high frequency atmospheric variability such as storm-induced breakup [*Kohout et al.,* 2014; *Guemas et al.,* 2016].

Empirical models find that upper ocean conditions are particularly important for sea ice predictions [*Lindsay et al.,* 2008; *Luo et al.,* 2018], as well as the sea ice downward trend [*Sigmond et al.,* 2013; *Chevallier and Salas-Melia,* 2012; *Msadek et al.,* 2014]. *Bushuk et al.* [2017] found initialising the ocean subsurface effectively can lead to significant gain in sea ice predictability. Additionally, *Dirkson et al.* [2017] found importance and benefit of initialising ice thickness, despite this potential limited by sparse observations. Current multi-model predictions report robust skill up to 5 months lead time [*Wayand et al.,* 2019], although prediction skill varies depending on the period chosen; year to year variability in sea ice has increased post 2000 making it more challenging to forecast [*Bushuk et al.,* 2019].

2.2.2 Eurasian Snow Cover & October Siberian Precursors

Autumn snow cover over Eurasia has been linked to interannual and interdecadal variability in the winter NAO, through thermodynamic forcing of the larger scale circulation, linked to cooling of the lower atmosphere over snow covered surfaces [*Watanabe and Nitta,* 1999]. Snow cover can drive strong radiative cooling at the surface, as well as the the air above through radiative long-wave emission. This cooling enhances subsistence and strength of anticyclonic circulation anomalies [*Cohen and Entekhabi,* 1999]. This anomalously strong anticyclone can then interact with the stationary wave pattern in the troposphere, in such a way to constructively or destructively interfere and amplify planetary waves, particularly over north-east Asia [*Inoue et al.,* 2012]. Wave interference affects vertical wave propagation into the stratosphere [*Saito et al.,* 2001], which modulate the strength of the polar vortex [*Kryjov,* 2015]. Changes in the strength of the polar vortex can affect tropospheric weather through troposphere-stratosphere coupling [*Christiansen,* 2001; *Scaife et al.,* 2005; *Hitchcock and Simpson,* 2014].

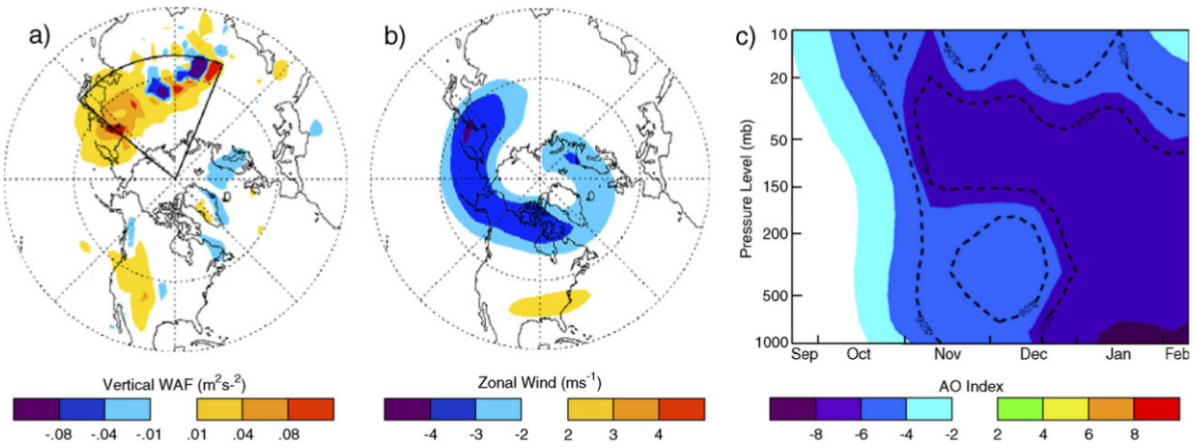

Figure 2.6: Climate response to a realistic, observation based positive snow forcing over Siberia, during autumn. (a) Vertical wave activity flux on the 850 hPa pressure level during autumn (SON). **(b)** Zonal wind on the 50 hPa pressure level during winter (DJF). **(c)** Weekly evolution over the atmospheric column of normalized 42-day running mean hemispheric Arctic Oscillation index. From *Gong et al.* [2007].

This chain of events is shown in figure 2.6 from *Gong et al.* [2007]. Snow anomalies induce tropospheric anomalies, which lead to vertical wave propagation downstream, as diagnosed by vertical wave activity flux during autumn **(a)**. This weakens the polar vortex **(b)**, producing a negative Arctic Oscillation signature at all pressure levels by winter **(c)**, descending from the stratosphere to the surface during late winter given increased tropospheric coupling to the stratosphere in late winter [*Christiansen,* 2001; *Hitchcock and Simpson,* 2014].

Model simulations

Despite strong observational evidence for a link between snow cover and the AO, model experiments show varied relationships, some implying that snow cover forcing is insufficient to initiate the telelconnection pathway to produce an Arctic Oscillation response in winter [*Gong et al.,* 2007]. *Hardiman et al.* [2008] investigated different coupled GCM's ability to reproduce observed correlations of Eurasian snow cover extent in autumn to wave activity in winter. Based on work by *Cohen and Entekhabi* [1999] and *Saito et al.* [2001], *Hardiman et al.* [2008] tested Rossby wave propagation from the troposphere into the stratosphere, using prescribed snow cover, and reproduced the coupled troposphere-stratosphere response later in winter, though this chain of events is disputed [*Henderson et al.,* 2018].

Models also fail to capture the observed snow-Eurasia MSLP teleconnections [*Peings et al.,* 2017], potentially due to weak forcing from the snow [*Hardiman et al.,* 2008], or more generally sea ice-atmosphere coupling [*Cohen et al.,* 2013]. The results from *Hardiman et al.* [2008] showed that the response to snow forcing was too longitudinally constrained, hence minimising wave propagation into the stratosphere. More encouraging studies demonstrate weak, but reproducible wave train structures linked to Siberian snow forcing [*Handort et al.,* 2015]. It cannot be ruled out that these weak signals in the model could be due to signal to noise issues. By using the CMIP5 model suite to investigate this further, *Gastineau et al.* [2017] found that only 4 out of the 12 models simulated the same relationship between Eurasian snow cover and winter sea level pressure as that identified in observational reanalysis. Using 500hPa geopotential height in October over northern Siberia as a predictor for the winter Arctic Oscillation, *Kryjov and Min* [2016] found a statistically significant correlation of 0.6, although this correlation is temporally dependent on the time period chosen [*Kryjov and Min,* 2015].

There are strong relationships between snow cover and Barents-Kara sea ice [*Gastineau et al.,* 2017], which share the large scale circulation pattern above. Reduction of sea ice increases moisture sources and therefore atmospheric water vapour content over the Arctic, increasing snowfall at high latitudes [*Liu et al.,* 2012]. *Luo et al.* [2018] explored different circulation patterns on BK sea ice variability, and found Ural blocking leads to pronounced BK sea ice decline. This is supported by *Peings et al.* [2019], who forced an atmospheric model with either BK sea ice or snow cover anomalies, while separately nudging a simulation with blocking over the Ural region. They found the model reproduced the tropospheric, and subsequently stratospheric response, to Ural blocking when evaluated with reanalysis. More significantly, no atmospheric response was found in reducing BK sea ice or varying snow cover anomalies. A further coupled experiment confirmed a response in both snow cover and BK sea ice to imposed Ural blocking anomalies [*Peings et al.,* 2019]. These findings rebut the role of sea ice influencing Eurasian snow cover as found by *Mori et al.* [2019], and caution against using model deficiencies to argue the weak snow cover atmospheric response, e.g. *Gastineau et al.* [2017]. Additionally, recent trends in Eurasian cooling that coincide with sea ice loss may be simply due to internal variability [*McCusker et al.,* 2016].

2.2.3 Stratospheric Polar Vortex

The stratospheric polar vortex can absorb forcings from the troposphere and later affect the troposphere after some lag [*Baldwin and Dunkerton,* 2001], in the most extreme case during a sudden stratosphere warming [*Hitchcock and Simpson,* 2014]. Vertically propagating planetary waves can enter the stratosphere, where they break and release energy which warms the stratosphere, weakening the vortex [*Charney and Drazin,* 1961]. During a vortex breakdown where the stratospheric flow becomes easterly, the vortex can either be split into daughter vortices, or displaced off the pole, which have differing surface impacts [*Mitchell et al.,* 2013].

Accurate model coupling between the stratosphere and troposphere is imperative to propagate disturbances in the stratospheric polar vortex correctly [*Gerber and Polvani,* 2009]. For example, *Scaife et al.* [2005] found that models can only reproduce decadal trends in the NAO if trends are imposed in the lower stratosphere. More applicable to interannual variability, initial stratospheric conditions are important for winter NAO predictability [*Nie et al.,* 2019; *O'Reilly et al.,* 2019]. Additionally, the recent trend in strengthening of the polar vortex over the past 20 years can be attributed to a trend in warming of SSTs in the central North Pacific [*Hu et al.,* 2018]. Physically, is it argued this SST trend weakens the Aleutian low, which weakens wavenumber 1 flux into the stratosphere, preventing energy transfer into the stratosphere and wave breaking, warming the vortex [*Hu et al.,* 2018]. Trends in the stratospheric polar vortex are important, given the strong stratosphere-troposphere coupling in winter.

The response, if any, in the troposphere to a sudden stratosphere warming depends on non-linear wave-mean flow interactions [*Matsuno,* 1971]. Forecast skill of the NAO vanishes completely if model ensemble members that contain a sudden stratospheric warming are excluded [*Scaife et al.,* 2016], emphasising the importance of stratospheric variability in the model. The stratosphere does not only provide a pathway for high latitude drivers to have a lagged affect on the winter circulation, but tropical modes of variability also. How well models reproduce any link between sea ice and the NAO may be heavily tied to its ability to simulate this troposphere-stratosphere coupling correctly [*Sun et al.,* 2015; *De and Wu,* 2019; *Romanowsky et al.,* 2019].

2.3 Tropical Drivers of NAO Variability

Tropical Pacific SST's are closely linked to the wider atmospheric circulation above; the strongest mode of this coupled ocean-atmosphere system is the El-Niño Southern Oscillation (ENSO) [*Bjerknes,* 1969]. The lower atmosphere either heats or cools as a result of the anomalous SST's beneath it, i,e, warm SSTs induce heating, which changes the lower atmosphere lapse rates leading to positive buoyancy and convection. This rising air reaches the top of the troposphere, and diverges horizontally, triggering planetary waves and perturbing the midlatitude jet [*Sardeshmukh and Hoskins,* 1988; *Trenberth et al.,* 1998; *Wang,* 2002]. Tropical rainfall is commonly used as a proxy for sources of upper divergence and planetary wave sources given it is intrinsically related to tropical convection [*Scaife et al.,* 2017], through the condensation of water as air rises and cools. Of interest is how these planetary waves propagate poleward out of the tropics, interact with circulation patterns at higher latitudes, and affect the extratropics and polar regions. Once an El Niño has been established, one of 4 mechanisms are required to trigger its decay; Kelvin waves reflected at the ocean western boundary, a discharge process due to Sverdrup transport, western Pacific wind-forced Kelvin waves, and anomalous zonal advection, some of these occurring in conjunction with each other [*Wang and Fiedler,* 2006].

2.3.1 Mechanisms Connecting Tropics to Mid-Latitude Weather

Divergence in the upper tropical troposphere, associated with convection, can be linked to poleward and eastward propagating Rossby waves, particularly in the north Pacific but also Atlantic [*Trenberth et al.,* 1998]. Figure 2.7 by *Trenberth et al.* [1998] shows this propagation out of the tropics, leading to downstream changes in storm track characteristics as well as large scale modes of variability such as the NAO. Different methods have been employed to determine Rossby wave source regions and permitted propagation routes of Rossby waves through ray tracing experiments, initially through studies using an idealised barotropic atmosphere [*Karoly,* 1983]; identifying Rossby wave propagation characteristics [*Held et al.,* 1985; *Yang and Hoskins,* 1996], and more recently *Scaife et al.* [2017]. This section discusses some of the key mechanisms and model experiments used to test tropical to mid-latitude teleconnections.

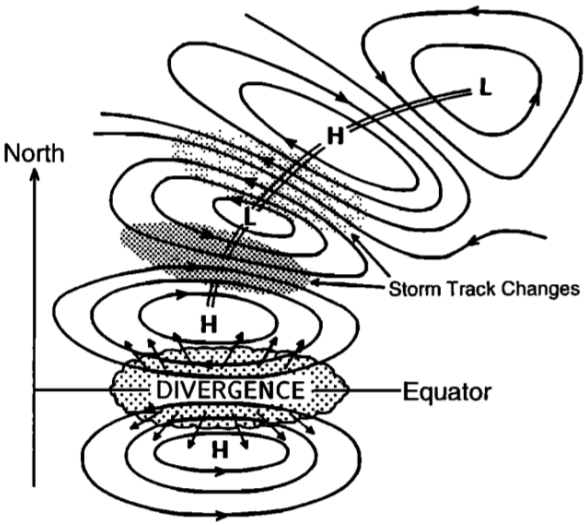

Figure 2.7: Schematic of Rossby wave propagation out of the tropics. Divergence over the equator leads to convergence in the subtropics, which leads to a pattern which tilts eastwards due to the prevailing mid-latitude westerlies. This leads to enhanced storm activity to the south (dark stipple) and reduced activity to the north (light stipple) of the cyclone center, from *Trenberth et al.* [1998].

Extratropical response to El Niño

Bell et al. [2009] used an intermediate complexity GCM with a well resolved stratosphere to reproduce the late winter negative NAO response to El Niño, by weakening the polar vortex and therefore increasing the probability of sudden stratospheric warmings during all winter months [*Hitchcock and Simpson,* 2014]. Sensitivity experiments where the mean state and variability of the stratosphere were deliberately degraded resulted in the model no longer being able to resemble the spatial and temporal response seen in observations, as shown in figure 2.8. Despite this, however, the strongest El Niño events appear insensitive to stratospheric representation and had a correct response over Europe, as shown in the bottom panels of figure 2.8.

These results suggest dependence on the stratosphere as a medium for transporting such teleconnections from the tropics to the mid-latitudes, although when the El Niño forcing becomes strong enough, this can be bypassed, potentially via a tropospheric route [*Bell et al.,* 2009]. A physical route linking El Niño to the NAO was proposed by *Toniazzo and Scaife* [2006], where El Niño strengthens the Aleution low, as part of a stationary wave train emanating from the tropical Pacific. Further downstream into the Atlantic sector, particularly over western Europe, the response to El Niño becomes non-linear

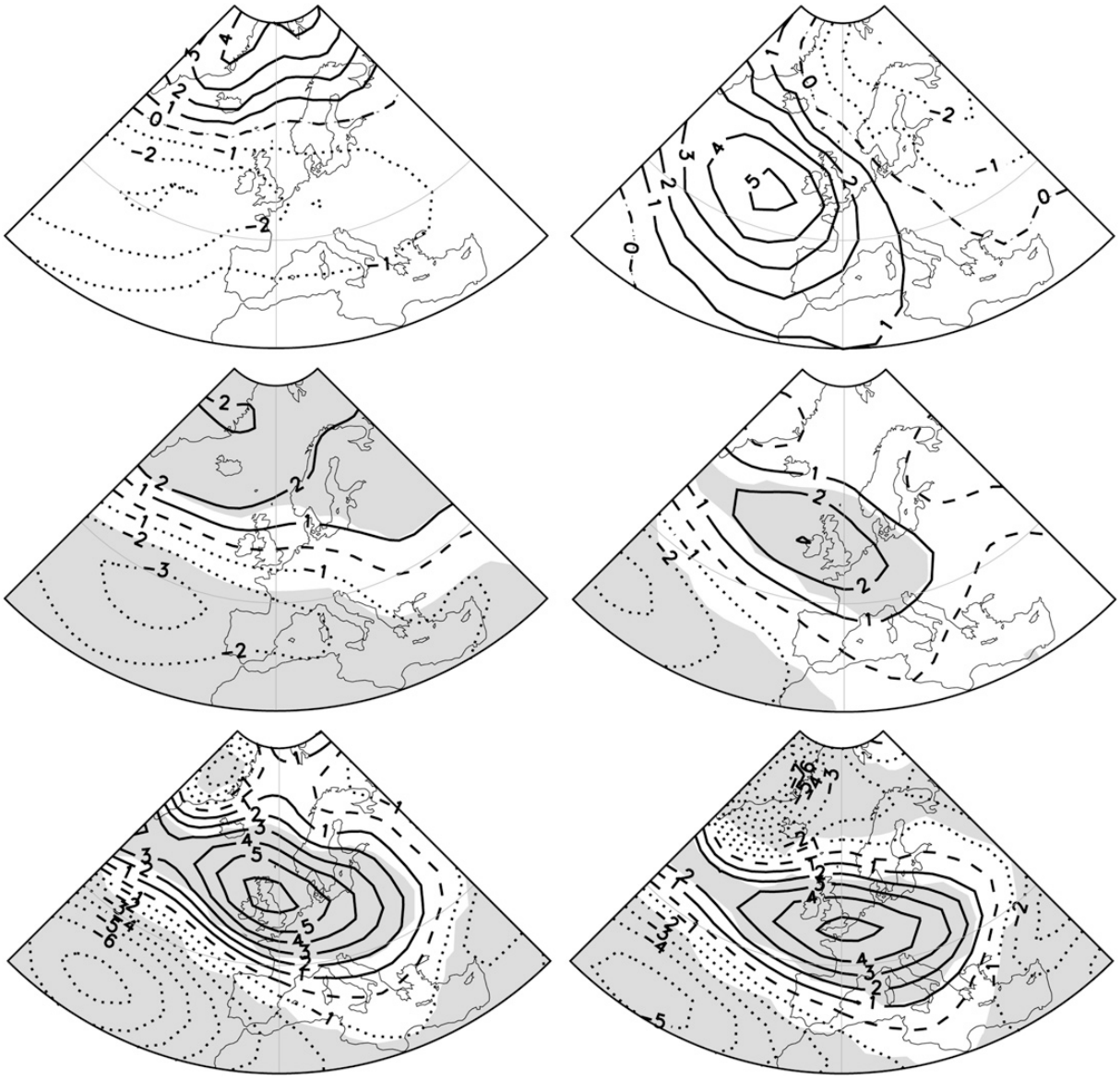

Figure 2.8: European MSLP sensitivity to El Niño forcing. Top Left: Composite of observed January - March averaged MSLP response (El Niño years - neutral years) taken from HadSLP2 data for moderate El Niño events. **Top Right:** Similar diagnostic, but for observed strongest events. **Middle Left:** January - March averaged MSLP response taken from the IGCM experiments with a fully evolving stratosphere. **Middle Right:** Similar diagnostic, but for the IGCM experiments with a degraded stratosphere. **Bottom Left:** Same as middle left, but for a doubled El Niño SST anomaly. **Bottom Right:** Same as middle right, but for a doubled El Niño SST anomaly. Contour intervals are in hPa, with shading representing significance at the 95% level. From *Bell et al.* [2009]

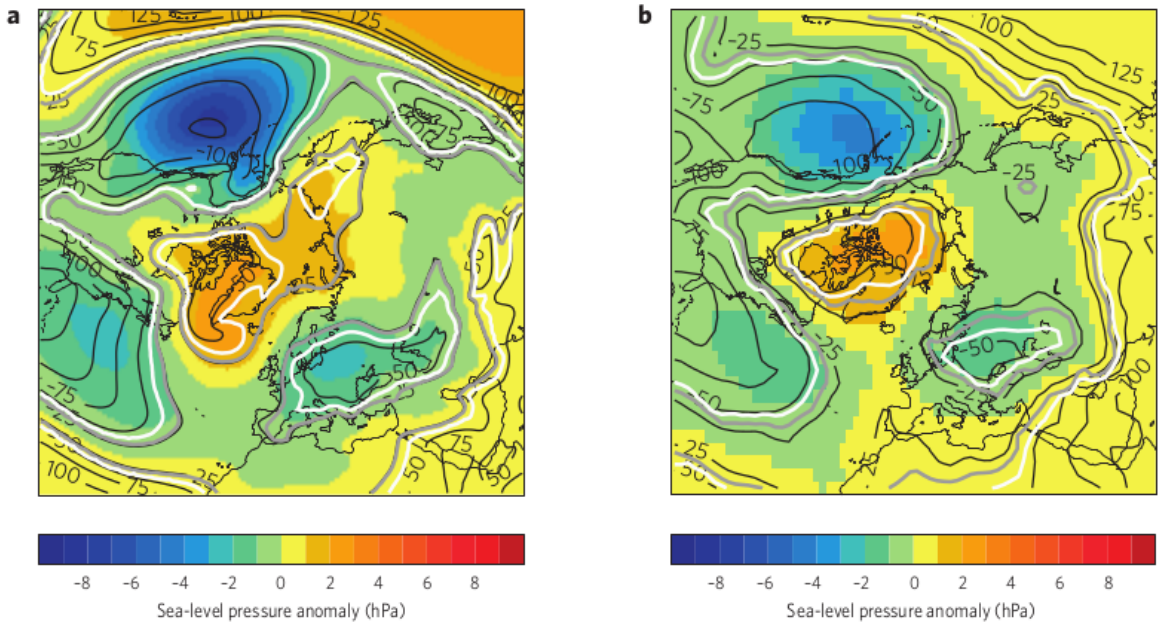

Figure 2.9: Response to El Niño in models and observations. Composite surface climate response to El Niño in sea level pressure anomaly (hPa) for the **a)** model and **b)** observations, from *Ineson and Scaife* [2009]

with anomalies of opposite signs in moderate and strong events. By testing this with the HadAM3 model, *Toniazzo and Scaife* [2006] found upper tropospheric anomalies are modelled well compared to reanalysis, extending into the mid-latitudes, but the pattern is not sensitive to the magnitude of ENSO events unlike other studies, such as *Zhou et al.* [2018], who found the strength of the stratospheric polar vortex dependent on the intensity of the ENSO event. Coarse vertical resolution in *Toniazzo and Scaife* [2016] may in part explain the discrepancy in results between *Toniazzo and Scaife* [2016] and *Zhou et al.* [2018].

Importance of a well resolved stratosphere in accurately capturing El Niño signals in the midlatitudes is found in most studies, bar particularly strong El Niño 's. Figure 2.9 from *Ineson and Scaife* [2009] show the response to El Niño forcing is captured well spatially and in terms of magnitude compared to reanalysis. This response is only generated when sudden stratospheric warmings occur, which subsequently affect mid-latitude weather and complete the teleconnection pathway [*Ineson and Scaife,* 2009]. These results project onto the NAO nodes; with El Niño increasing the change of a negative NAO to occur as a result of high latitude blocking, seen both in model and observations (figure 2.9).

Extratropical response to La Niña

La Niña occurs when SST's over the east tropical Pacific become cooler than average. Studies such as *Iza et al.* [2016] find a robust stratospheric response during strong La Niña events, characterised by a significantly stronger and cooler polar vortex, leading to changes in tropospheric weather [*Baldwin and Dunkerton,* 2001; *Hitchcock and Simpson,* 2014]. *Iza et al.* [2016] found this is due to a weaker propagation of upward wave activity into the stratosphere, as a result of destructive interference between climatological and anomalous La Niña forced tropospheric stationary eddies over the North Pacific region. This is a similar pathway to El Niño, which uses the Pacific-North American (PNA) teleconnection pattern route via the Aleutian low to modulate the polar vortex [*Garfinkel and Hartmann,* 2008]. *Bromimann et al.* [2007] examined reconstructed indices over the past 500 years to find consistent and symmetrically opposing El Niño and La Niña responses over Europe in winter, which is stationary in time. *Bromimann et al.* [2007] also found strong dependence on the north Pacific climate in modulating a downstream affect into the Atlantic sector, as in *Garfinkel and Hartmann* [2008].

Studies have compared atmospheric responses between El Niño and La Niña more directly, as well as addressing the sensitivity to the size of the forcing. *Pozo-Vazquez et al.* [2001b] looked at ENSO indices from 1873 to 1995, and by restricting their analysis to ENSO events that were well developed during winter they found La Niña events composited onto the positive phase of the NAO, with no significant patterns associated with El Niño. This supports the idea that La Niña has a more stable and robust influence on the NAO compared to El Niño. This analysis again supports earlier findings that the main route that connects the tropics to the mid-latitudes is the PNA teleconnection, which mediates the downstream response through stationary wave trains. A potential caveat to studies investigating the extratropical response of El Niño is the sensitivity of the thresholds used to detect events, as well as some El Niño's occuring in tandem with other sources of variability [*Iza et al.,* 2016], diffusing the strength of an El Niño signal.

Temporal dependence of response to forcing

Responses of the midlatitude circulation in the North Atlantic to ENSO forcing depends strongly on the time of forcing; most studies focus on winter averages or late winter responses. *King et al.* [2018] found substantial differences when regressing the Niño 3.4

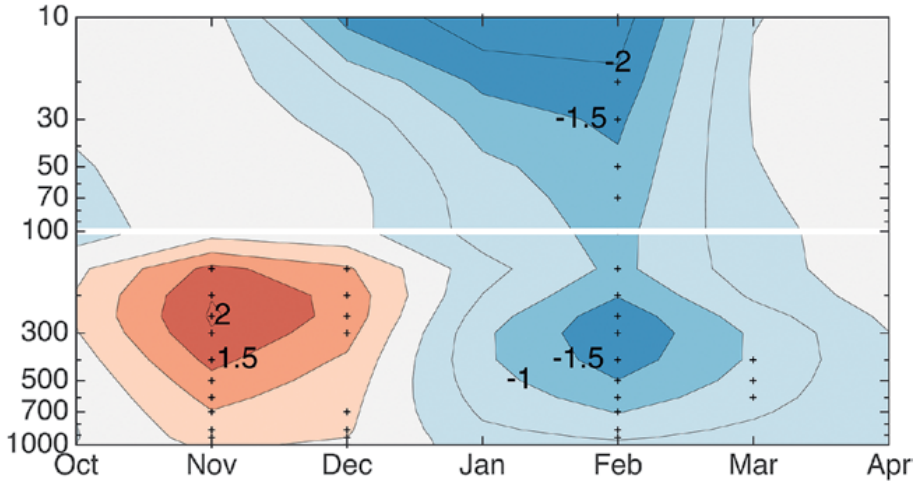

Figure 2.10: Regressing Niño 3.4 onto Atlantic zonal wind. Regression of the zonal wind (m s-1) on the Niño 3.4 index on a pressure level-month plane. The zonal wind is defined as the area average of the zonal wind in the area 40-50N, 90W-0 for levels below 100 hPa, and the zonal mean is in the latitude band 50-60N for levels at and above 100 hPa. Crosses mark values with statistical significance at the 95% level according to a two-tailed t test. Data is from NCEP-NCAR Reanalysis and HadISST. From *King et al.* [2018].

index onto zonal wind averaged over the Atlantic sector from autumn to winter, as shown in figure 2.10. Figure 2.10 shows marked differences between the late autumn and mid to late winter ENSO teleconnections, with a decrease in zonal wind during late winter which projects onto a negative NAO index. Before winter, teleconnections from the tropics to the midlatitude occur only in the troposphere, and differences from autumn and winter are due to a combination of differences in the background atmospheric flow and associated Rossby wave-guide at this time of year [*King et al.,* 2018]. These factors dictate the preferred mode of natural variability and stratosphere preconditioning, with late winter tropospheric weather much more controlled by stratospheric variability [*Baldwin and Dunkerton,* 2001]. The stratosphere is important to resolve tropical to mid-latitude teleconnections, with the exception of particularly strong ENSO events where poleward Rossby wave propagation is possible via a purely tropospheric route. This is supported by *Ineson and Scaife* [2009], where model simulations with an inactive stratosphere still show impacts on the NAO from the strongest El Niño forcings, which through analysis of the wave patterns strongly support a tropospheric origin from the tropical Atlantic.

Other Ocean Basins

El Niño responses vary depending on the intensity and timing of the event, although this variability could be explained through other basin teleconnections. Variability associated with ENSO can also affect SSTs in the equatorial Atlantic, with a lag of around 6 months, which can then source anomalous Rossby waves that propagate poleward and affect the NAO [*Rajagapalan et al.,* 1998; *Watanabe and Kimoto,* 1999; *Robertson et al.,* 2000]. *Toniazzo and Scaife* [2006] proposed that a secondary wave train could emanate from the tropical Atlantic associated with re-arrangement of the large-scale tropical circulation resultant from ENSO anomalies, even in the absence of SST anomalies in the tropical Atlantic itself. This is complicated further with tropical Atlantic variability exerting an influence on the tropical Pacific and Indian Ocean basins, with circulation patterns over the Atlantic modulating both the Indian summer monsoon as well as ENSO events through SST patterns and Walker circulation anomalies [*Wang et al.,* 2009]. Relaxation experiments exploring the influence of the tropics on the extreme winter of 2015/16, suggest that the Atlantic basin modulates wavelike activity stemming from the tropical Pacific [*Maidens et al.,* 2019], similar to that found in *Toniazzo and Scaife* [2006].

Decadal variability in the NAO may in part be associated with a warming trend in the Indian Ocean [*Bader and Latif,* 2003]. Model experiments simulating this warming trend suggest a weakening of the both Icelandic and Azores nodes of the NAO, and is consistent with the NAO trend observed over recent decades [*Bader and Latif,* 2003]. This is also found in other studies [*Hoerling et al.,* 2001], though these are limited by not isolating individual tropical basins.

Rossby waves propagate polewards out of the tropics [*Trenberth et al.,* 1998], but despite this mechanism, it has been proposed that some of ENSO variability is resultant from mid-latitude weather variability. Mid-latitude winter weather drives SST changes in the north Pacific that persist into summer, where SST anomalies forces a subtropical circulation anomaly that extends north and south of the equatorial Pacific. This circulation anomaly leads to wind stress that affects the oceanic Kelvin signal, which in part controls the modulation of ENSO [*Vimont et al.,* 2001]. These results suggest bi-directional influence on ENSO and the mid-latitude circulation, albeit on timescales longer than seasonal forecasting.

2.3.2 Remote Links to the Arctic

Recent research suggests that tropical forced atmospheric variability can extend beyond the mid-latitudes into the Arctic. On decadal timescales, positive phases of the AO linked to ENSO produce a dipole-like response in sea ice across the Arctic; although the positive AO and negative ENSO trend is much smaller than regional ice trends themselves [*Liu et al.,* 2004]. *Lee et al.* [2011] used ECMWF reanalysis data and found that ice covered regions of the Arctic warm primarily due to dynamic stationary eddy heat fluxes and adiabatic warming, and ice free ocean is dominated by infra-red (IR) long wave radiation fluxes. Using a lag, enhanced convective precipitation in tropical regions was followed 3-6 days by mid-latitude circulation anomalies, and 1-2 days later by variations in downward IR fluxes [*Lee et al.,* 2011]. These tropical sourced waves are poleward propagating Rossby waves, common to that shown to affect the NAO in the troposphere, and lead to changes in adiabatic warming, poleward stationary eddy heat transport, and downward IR radiation when the energy budget of the Arctic is considered [*Lee,* 2012].

Evidence substantiating a link between the tropics and polar regions include attribution studies investigating trends as well as interannual variability in sea ice. *Gong et al.* [2017]; *Park et al.* [2015]; *Henderson et al.* [2014]; *Woods et al.* [2013]; *Woods and Caballero,* [2016] all suggest an important role of poleward moisture fluxes in controlling regional sea ice variability. *Gong et al.* [2017] largely attributes the trend in sea ice to an increasing trend in downward infrared, and that greenhouse gas forcing is changing frequency and intensity of moisture intrusions into the Arctic. Advection of moisture into the Arctic is dominant over locally increased evaporation rates due to exposed ocean [*Park et al.,* 2015]. By examining poleward (70°N) intense moisture intrusions in reanalysis, *Woods et al.* [2013] attributed blocking on the eastward flanks of regional ice loss, associated with a poleward deflection of extratropical cyclones and their respective heat and moisture. Strong intrusion events lead to sea ice retreat that persists, with an increased frequency of these events in the past few decades [*Woods and Caballero,* 2016].

Sea ice predominantly responds to mid-latitude atmospheric circulation anomalies and their associated poleward heat and moisture fluxes in a top down manner (i.e. atmosphere drives sea ice variability) [*Henderson et al.,* 2014]. Studies have increasingly linked ENSO variability, particularly La Niña, to regional sea ice variability, either through theoretical arguments [*Lee,* 2014], or through model experiments introducing thermal heating per-

turbations, resembling atmospheric variability associated with ENSO [*Trenberth et al.,* 2014]. Compositing El Niño and La Niña in observations produces the following pattern in winter 2m temperature, shown in figure 2.11 from *Lee,* [2012]. To construct this composite, they identified 13 El Niño and 14 La Niña events, and composited these onto detrended DJF 2M temperature.

Figure 2.11 relates variations in ENSO to remote temperature responses at high latitudes around the Arctic. This has significant impacts on ice melt/growth during the winter season, predominantly as a result of modifying IR fluxes through cloud/water vapour. Arctic air temperature is anomalously warm during La Niña and cold during El Niño, as a result of changes in poleward moist static energy inferred through surface energy fluxes [*Lee,* 2011]. The magnitude of these responses may be different, however, because poleward propagating Rossby waves are stronger during La Niña than El Niño [*Lee,* 1999]. Fluxes in IR over the Arctic associated with tropically excited waves has also been discovered using station data, and supports such theory [*Flournoy et al.,* 2016]. Tropical rainfall in the western Pacific and the Indian ocean has also been shown to preceed strong downward IR events in the Arctic within a week or two, and can be associated with up to 10% decline in sea ice concentration over the BK seas, with this IR influence more dominant that wind-induced sea ice loss [*Park et al.,* 2015].

Ding et al. [2014] found that the region of most prominent warming in the Arctic is over north-east Canada and Greenland, where sea ice variability is mostly controlled by large scale circulation patterns such as the NAO. By using observations, and a model forced with tropical SST's, they found that warming in this region was strongly associated with the recent negative trend in the NAO, which itself is a response of an anomalous Rossby wave train emanating out of the tropical Pacific [*Ding et al.,* 2014]. This suggests that some of the recent warming trend in the Arctic is driven by natural tropical variability and not greenhouse gas forcing. *Ding et al.* [2019] further supports this, by attributing 52% of the recent trend in Arctic sea ice due to internal modes of variability. They also find sea ice loss related to barotropic ridging across the Arctic, which leads to adiabatic warming and enhanced ice melt. Using wave diagnostics, they related this to enhanced and suppressed convection tied to ENSO variability via a wave train over the North Pacific and Greenland [*Ding et al.,* 2019]. Additionally, extreme years such as the Arctic warmth in 2016 was 30-40% attributable to forcings outside the Arctic [*Sun et al.* 2018]. Other

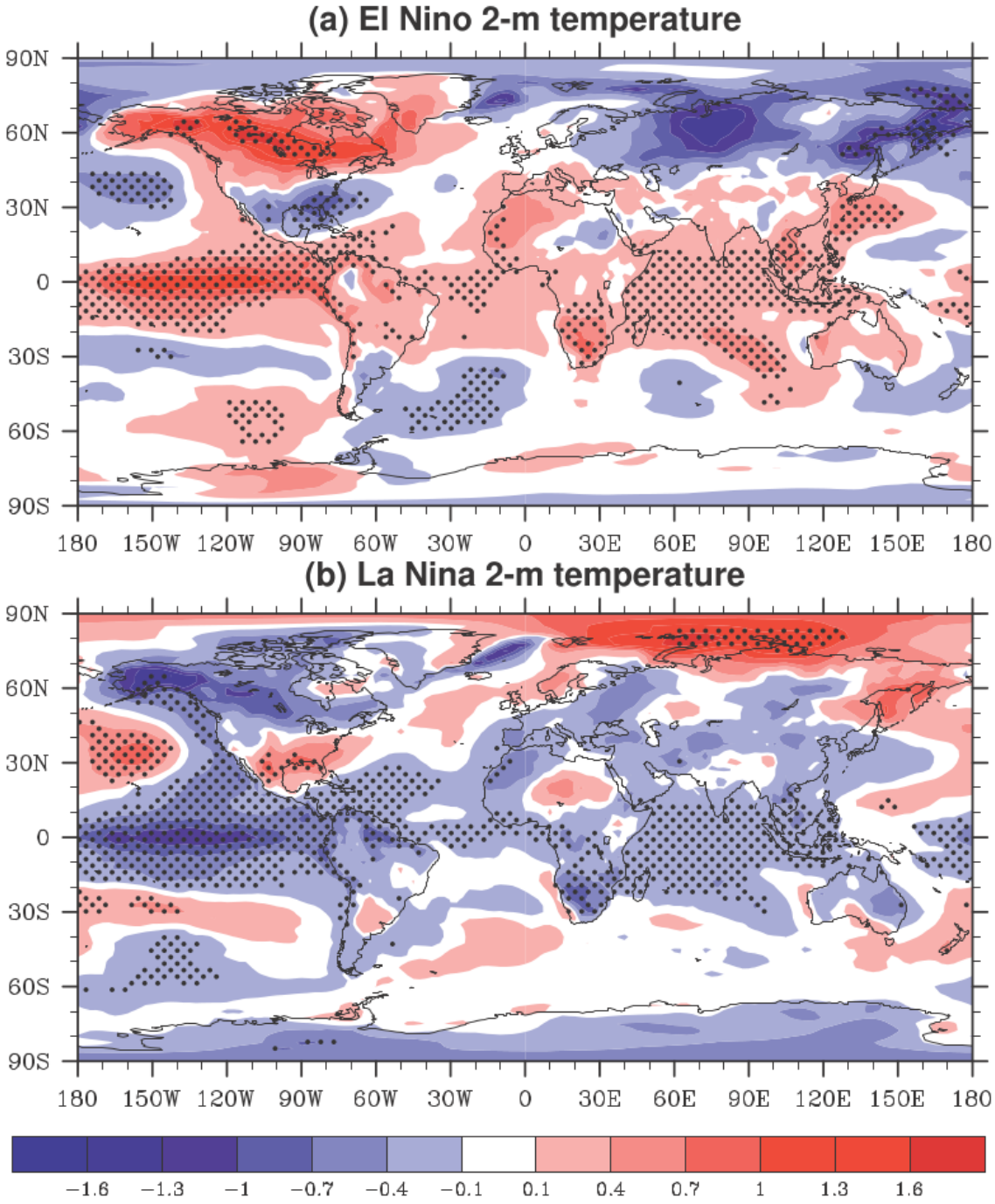

Figure 2.11: Compositing El Niño and La Niña events on 2M temperature. Compositing **(a)** El Niño and **(b)** La Niña events onto surface air temperature, using ERA-40 1958-2001 data. Dots indicate regions where the composite values exceed the 95% confidence level for a two-sided test, from *Lee,* [2012].

recent studies find strong sensitivity to the spatio-temporal sea ice variability related to internal variability, particularly in the Barents-Kara sea [*England et al.,* 2019].

2.3.3 Madden-Julian Oscillation

The Madden-Julian Oscillation (MJO) is an intra-seasonal mode of variability with enhanced convection that propagates eastwards over the Indian and Maritime continent [*Madden and Julian,* 1972], which governs local climatology over the region and more remotely [*Zhang,* 2005]. The MJO is related to ENSO; given ENSO alters the large scale tropical circulation and can therefore modulate the strength of the MJO [*Moon et al.,* 2011]. Impacts of the MJO extend well outside the tropics and into the midlatitudes [*Cassou,* 2008], with remote association with variability in the Arctic [*Yoo et al.,* 2011; *Henderson et al.,* 2014].

MJO activity is characterised by convection strength and region; the latter commonly segmented into 8 phases [*Wheeler and Hendon,* 2004]. Phases 5-7 correspond to enhanced convection in the tropical west Pacific, where upper tropospheric vortex stretching can generate Rossby waves that propagate into the mid-latitudes [*Trenberth et al.,* 1998]. This wave propagation can induce anomalies in the north Pacific such as the Aleution low [*Zhou and Miller,* 2005], with perturbations in the Pacific sector advected downstream into the Atlantic sector and the NAO [*Lin et al.,* 2009]. More widely, the sign and tendency of Arctic Oscillation can be shifted through active MJO phases in the west Pacific [*L'Heureux and Higgins,* 2008]. These teleconnections are reproducible in idealised model experiments forced with imposed thermal anomalies representing the MJO [*Matthews et al.,* 2006], suggesting the tropical-midlatitude link is robust. However, additional non-linearities arise given this teleconnection is modulated in the eastern Pacific by ENSO variability [*Moon et al.,* 2011].

Typical mid-latitude response time to the MJO entering its active western Pacific phase is 1-2 weeks; both in idealised model experiments [*Matthews et al.,* 2006], observations [*Lin et al.,* 2009] and climate model experiments [*Ferranti et al.,* 1990]. Links with mid-latitude weather variability have encouraged investigation to how MJO knowledge can be utilised for NAO sub-seasonal predictability; more widely *Ferranti et al.* [1990] found significant increases in mid-latitude predictability when the nudging the tropics to observations. Additionally, *Cassou* [2008] found daily NAO forecasts have a 70% success

rate when using the previous 12 days MJO phase as a statistical predictor in winter. The time-lagged NAO relationship when MJO convection is over the Indian Ocean (west Pacific), the probability of a positive (negative) NAO around 10 days later is increased significantly [*Barrett,* 2019]. Additionally, all regimes of weather over the North Atlantic and European sector can be affected, not just the NAO [*Cassou,* 2008]. The response is complicated because of longer-lagged relationships; *Schwartz and Garfinkel* [2017] found phase 6/7 of the MJO preceded more than half of sudden stratospheric warming (SSW) events, and that these MJO phases could only lead to a long-lived impact on the tropospheric AO if it modulates the stratospheric polar vortex. Studies have widely documented how mid-latitude circulation anomalies can modulate upward wave flux into the stratosphere [*Baldwin and Dunkerton,* 2001], with a lagged feedback later on tropospheric weather [*Hitchcock and Simpson,* 2014]. Disentangling tropospheric and stratospheric pathways and their associated non-linearities remains a research challenge.

As discussed earlier, recent emergence links between ENSO and Arctic variability have become apparent; with a large degree of the trend in Arctic sea ice attributable to tropical variability [*Ding et al.,* 2019]. Additionally, MJO phases have been linked to temperature changes in the Arctic; through modulating the mid-latitude circulation, poleward heat fluxes into the Arctic and sea ice melt are partly controlled [*Lee,* 2011; *Park et al.,* 2015]. For example, *Henderson et al.* [2014] found that phases of the MJO have a detectable lagged influence on daily sea ice both in summer and winter. Additionally, *Yoo et al.* [2011] determined that the MJO in phase 5 leads to warming in the Arctic 1-2 weeks later during winter, by modifying heat fluxes into the Arctic from the mid-latitudes.

2.3.4 Quasi-Biennal Oscillation

The Quasi-Biennal Oscillation (QBO) is a highly predictable oscillation of equatorial stratospheric zonal winds, where the winds oscillate between westerly and easterly phases with a period of around 28 months [*Baldwin et al.,* 2001]. Through modulating extratropical wave propagation, it exerts considerable control on the stratospheric polar vortex, and subsequently sudden stratospheric warmings which can affect the NAO [*Scaife and Marshall,* 2009] and more widely the high latitudes [*Anstey and Shephard,* 2014]. By taking a composite difference between easterly and westerly QBO phases, *Watson and Gray* [2013] found that the anomalous structure had a close resemblance to the north-

ern annular mode, including its wave components, and by isolating the QBO in a model experiment its relationship to the polar vortex was causal.

When the QBO is in its easterly phase, an increased frequency of the occurrence of sudden stratospheric warmings is observed [*Holton and Tan,* 1980]. This is because the easterly phase leads to greater drag on the polar vortex, as a result of the wave-guide for planetary waves becoming narrower, which increases the strength of extratropical wave activity [*Marshall and Scaife,* 2009]. Given that there are strong links between ENSO and the QBO, is it difficult to disentangle signals from each, though *Garfinkel and Hartmann* [2007] found that the effect of each phase on the stratospheric polar vortex are of comparable magnitude with each other, using a composite based approach. Although the influence of the QBO is only briefly discussed here, given its highly predictable nature and being a well documented driver of the winter NAO, it should be considered in any future analysis. The QBO has been suggested to modulate the extratropical response to future Arctic ice loss; during westerly phases, the QBO strengthens the polar vortex in response to sea ice forcing [*Labe et al.* 2019].

2.3.5 ENSO Predictability

Skill in ENSO predictability on seasonal and decadal timescales has increased with time, predominantly due to better resolution and more advanced understanding of atmosphere-ocean coupling [*Barnston et al.,* 2011]. Early studies using idealised atmosphere-ocean models to predict ENSO found that potential forecast lead time could be of the order of years [*Goswami and Shukla,* 1991]. Its predictability is in part due to the slow timescale of ocean processes, where persistence can explain a large degree of skill in the first few months [*Chen and Cane,* 2008]. All models, whether statistical and physical, perform considerably better than a persistence forecast in predicting typical indices of ENSO on lead times of 6 to 12 months [*Latif et al.,* 1998]. Correlations as high as 0.7 have been found between rainfall in tropical rainfall basins and the NAO, when combined using multiple linear regression [*Scaife et al.,* 2017]. Additionally, *Black et al.* [2017] found that tropical convection was particularly important in predicting the NAO on sub-seasonal to seasonal scales on lead times up to 5 weeks using empirical methods.

Federov et al. [2003] found that predictability of each El Niño event varied considerably, as a result of sensitivities in the model capturing random disturbances such as

westerly wind bursts which interact with the ocean and longevity of the El Niño. Additionally, a 'spring barrier' in ENSO prediction across all model systems in boreal spring is found [*Chen et al.,* 2004] for reasons that are not yet well understood [*Zheng and Zhu,* 2010]. If ENSO is predictable on seasonal timescales, and links to both the extratropics and Arctic, these links could be exploited for improved seasonal NAO prediction.

2.4 Other NAO Drivers

Polar and tropical sources of variability are not the only documented sources of NAO variability. This section will briefly overview other drivers including Atlantic SST's and radiative forcings to provide a complete context.

2.4.1 Atlantic Sea Surface Temperatures

SST's in the Atlantic ocean can modulate the strength of the NAO through localised forcing of baroclinic instability, and conversely the atmosphere exterts wind stress and thermodynamic fluxes on the ocean surface [*Bjerknes,* 1964]. Much of the NAO variability over past decades can be reconstructed using only knowledge of SST patterns in the North Atlantic [*Rodwell et al.,* 1999]. This 'information exchange' at the interface between the atmosphere and ocean is communicated through moisture and heat fluxes, as well as kinetic energy [*Rodwell et al.,* 1999]. Atmosphere-ocean coupling is important in NAO representation given it has a significant impact on how the model simulates NAO variance, even though it doesn't necessarily change the climatology of the NAO [*Bhatt et al.,* 1998]. Resolution of the ocean in coupled models also matters; the skilful GloSea5 model utilises a 0.25 degree ocean, which reduces biases in blocking over the Atlantic sector [*Scaife et al.,* 2011; *Scaife et al.,* 2014]. Owing to the slower timescales on which SSTs evolve over the Atlantic [*Boer,* 2004], information about the preceding winters NAO can be carried through to the following winter [*Scaife and Knight,* 2008; *Taws et al.,* 2011; *Maidens et al.,* 2013] as discussed earlier.

2.4.2 Radiative Forcings

Radiative forcing includes the 11 year solar cycle [*Ineson et al.,* 2011], and aerosol forcing from volcanic eruptions [*Stenchikov et al.,* 2006].

Solar variability, for example the 11 year sunspot cycle, has long been linked to weaker westerly winds in the stratosphere when in the minimum phase [*Labitzke,* 1987; *Kodera,* 1995; *Kodera,* 2002; *Ineson et al.,* 2011], as a result of weaker heating in the tropical stratosphere. This weakens the stratospheric meridional temperature gradient, and therefore winds, through thermal wind balance with this wind anomaly migrating polewards and downwards through wave-mean flow interaction [*Andrews et al.,* 2015], as well as modulating the Brewer-Dobson circulation [*Metthes et al.,* 2006]. Climate models, however, have consistently struggled to reproduce this signal and its influence on surface conditions such as the Arctic Oscillation [*Tsutsui et al.,* 2009; *Schmidt et al.,* 2010]. More recent model simulations have yielded much better results using coupled ocean-atmosphere-climate models with a well resolved stratosphere [*Ineson et al.* 2011]. This may in part be due to the importance of the ocean to communicate lagged responses [*Andrews et al.* 2015; *Yukimoto et al.* 2017]. More recently, *Chiodo et al.* [2019] argue this lagged relationship could be chance occurrence due to internal variability, using evidence from both extended observational periods and a chemistry-climate model. Sensitivities to the metric used for solar strength could in part explain some of these differences; *Woolings et al.* [2010] found that the relationship between solar flux and the NAO was stronger than other solar measures, and is also more linearly related.

Stratospheric aerosol particles from volcanic eruptions produce transient cooling of the troposphere [*Mitchell,* 1961] and warming of the lower stratosphere [*Labitzke et al.,* 1983; *Stenchikov et al.,* 1998]. This generally corresponds to a positive phase of the AO in winter [*Groisman,* 1992; *Kirchner et al.,* 1999], with a typical persistence of 2 years if observed eruption magnitudes in the past century are considered [*Robock and Mao,* 1992; *Stenchikov et al.,* 2006]. *Marshall et al.* [2009] forced the HadGEM model with volcanic emissions which produced a strengthening of the winter polar vortex and a positive AO, as found using observational data, although analysis of CMIP5 models by *Gillett and Fyfe* [2013] found no significant relationship between volcanic forcings on the NAO. Sampling uncertainty given the infrequent volcanic event in reanalysis could account for these discrepancies.

2.5 Discussion and Summary

Multiple modelling systems are now reporting significant NAO skill on extended lead times of a season or more [*Dunstone et al.,* 2016; *Butler et al.,* 2010], but there is scope for further skill based on estimates of externally forced variability, as well as space-state modelling approaches [*Keeley et al.,* 2009; *Sansom et al.,* 2018]. However, large uncertainty remains with regards to what physically controls variability of the NAO, with minimal consensus on whether Arctic sea ice is a causal driver. There is also no physical reason to expect each of the various polar and tropical drivers proposed to affect the NAO to act independently without interacting with each other, which poses a complex non-linear problem, varying across temporal and spatial scales.

The link between the NAO and Arctic sea ice varies considerably across model experiments. The sensitivity and lack of robust inter-model response to Arctic sea ice probes the question of whether such a causal connection really exists. Caveats to model analysis investigating causal drivers to the NAO include the unexpectedly low signal to noise ratios [*Eade et al.,* 2014; *Scaife and Smith,* 2018], which weaken forced signals and require very large ensembles. Select choice of months for statistical predictions of the winter NAO, such as October ice in *Wang et al.* [2017], along with the dependence of detrending the sea ice time series to obtain a stronger correlation further make the ice-NAO link sceptical, or at least non-robust. This ambiguity motivates further investigation using both observations as well as model experiments, to better quantify the link between Arctic sea ice and the NAO.

Literature which explores how the tropics can force midlatitude weather reveal a substantial link and cross-study consensus that variability, particularly in the tropical Pacific, generate planetary waves either via the troposphere or stratosphere, which have the ability affect the winter NAO. Although studies show variable response depending on the magnitude of the ENSO event, there is broad consensus that ENSO processes affect midlatitude weather in the Atlantic sector and subsequently the NAO. There is also emerging evidence of the tropics driving variability in the Arctic, including the trend in key regions such as the Barents-Kara seas, as a result of perturbing the midlatitude circulation, which controls heat and moisture fluxes into the Arctic. If these connections are robust, which need to be tested in tropical nudging experiments performed here, it suggests that tropical variability could be the largest component of forced NAO variability, and potentially

could explain why there is an apparent correlation between Arctic sea ice and the NAO given that tropical rainfall has been shown to force both. Further work needs to be undertaken to determine whether the relationship between sea ice in the Barents-Kara seas and the NAO has tropical origins.

The uncertainty of autumn precursors such as Eurasian snow cover, and their connection with the NAO/AO, may also be incidental to the tropics. Model response to Eurasian snow cover varies considerably in terms of the strength of the resultant atmospheric circulation anomalies. While in observations there appears to be a link, it is not clear whether snow cover is driving anticyclonic circulation patterns, or whether the anticyclone is providing conditions that are more favourable for snow extent to increase, or a combination of both (bi-directional relationship). If tropical rainfall can demonstratively force mid-latitude variability, then it may drive variations in snow cover and anticyclone strength which have been linked to the AO. There is a need to further extend analysis of the influence of Arctic sea ice in multi-model experiments to isolate a role of ice from other drivers; performed here in the third and fourth results chapter.

This chapter has explored remote polar and tropical drivers and how studies have linked these to midlatitude, and therefore NAO/AO variability. Open questions remain about the causality of the link between sea ice and the NAO, motivating the remainder of this thesis.

Chapter 3

Methodology

The analysis in this thesis draws on many observational and reanalysis datasets, as well as model simulations. The chapter is laid out as follows; first describing the different datasets and models used, then a discussion of the statistical tools used in the project. Finally, the methods used to derive each index are then discussed.

3.1 Datasets

3.1.1 Observational & Reanalysis Data

Briefly, observational reanalysis products are produced by running a free model simulation, typically coupled, whilst being heavily constrained to observations of temperature, humidity, pressure from a variety of sources such as surface stations, aviation measurements, weather balloons and satellite retrievals. It is not without imperfections, particularly in areas with sparse observations to constrain the model, such as the mid and upper troposphere as well as the stratosphere [*Saha et al.,* 2010], and over polar regions [*Jung et al.,* 2014]. Despite these limitations, it is the best estimate of the current climate available. Newer reanalysis such as ERA5 contain ensembles in order to gauge uncertainty in the model simulation with respect to uncertainty in observations constraining it [*Hersbach and Dee,* 2016], though given its recent release and lack of testing/benchmarking, it is considered unreliable at this stage to use.

The reanalysis product used is the ERA-Interim reanalysis [*Dee et al.,* 2011]. The atmospheric component of the model itself has a horizontal resolution of 79km, with 60 model layers and a lid at 0.1 hPa. Details of model components, performances and

benchmarking can be found in *Dee et al.* [2011], but it is widely considered one of the leading reanalysis products available. Variables for different pressure levels are taken, as well as surface variables at both daily and monthly resolution. The data is retrieved at 1 degree horizontal resolution, which means some interpolation from the models native resolution to the requested resolution is involved. Data from the 1st of January 1980 through to December 2017 is used; longer reanalysis exists, but pre-satellite era (< 1980) ingests substantially less observations and is therefore less reliable. An exception to this is sea level pressure observations, where records extend much further back and is relatively well sampled. To ensure that the NAO index method chosen is robust over longer periods of time where the NAO has been shown to exhibit non-stationary behaviour [*Pozo-Vázquez et al.,* 2001a], a longer record will be used, such as the HadSLP2 dataset [*Allan and Ansell,* 2006]. This dataset, although coarse at 5 degree horizontal resolution, provides an extended reanalysis period to ensure that the methodology to construct the NAO is robust.

For boundary variables (sea ice cover and sea surface temperatures), HadISST2 and HadISST datasets are used respectively [*Titchner and Rayner,* 2014; *Rayner et al.,* 2003]. Data is provided on a 1 degree Gaussian grid, and extends from 1850 through to 2007 (with subsequent updates to extend the period to 2017). Large bias adjustments were applied pre-release, particularly during the summer months for HadISST2, where this product contains more ice than the previous release of HadISST [*Titchner and Rayner,* 2014]. Data prior to 1980 will not be used in this analysis because of the lack of satellite records before this date to verify the data. Data from the National Snow and Ice Data Center (NSIDC) provide satellite obtained Arctic sea ice extent for all months post 1979 [*Fetterer et al.,* 2017]; this will be used to verify the accuracy of sea ice in the reanalysis later in this chapter.

In order to obtain rainfall data for tropical regions, the Global Precipitation Climatology Project (GPCP) data is used [*Adler et al.,* 2003]. GPCP data ingests a variety of data sources such as rain gauge observations as well as satellite derived rainfall estimates. This dataset is used rather than ERA-Interim for rainfall, given biases in precipitation derived from reanalysis simulations [*Decker et al.,* 2012]. Its coarse 2.5 degree horizontal resolution is sufficient given the domain sizes used in the tropics for the analysis, and the global spatial scales in this project.

3.1.2 The Met Office Decadal Prediction System 3

The Met Office Decadal Prediction System 3 (DePreSys3) is a coupled model system developed at the Hadley Center, using a HadGEM3-GC2 configuration, with a horizontal resolution of 0.83 degrees longitude and 0.55 degrees latitude [*Williams et al.,* 2015; *Dunstone et al.,* 2016]. It contains a well resolved stratosphere, with 85 vertical levels and a model lid near the mesopause. The ocean has a resolution of 0.25 degrees and is fully coupled to the atmosphere, whilst also containing interactive sea ice, which supports ice-atmosphere interactions [*Dunstone et al.,* 2016]. The system uses the Los Alamos sea ice model CICE [*Maclachlan et al.*, 2015], where sea ice is initialised using NEMO 3D data assimilation system [*Hunke et al.,* 2010].

The model contains 40 ensemble members, perturbed using stochastic physics, and is re-initialised every year on the 1st November. Therefore, a set of ensemble members for one particular year is independent from the next year. The hindcast is run for 16 months, providing an opportunity to explore predictions of the second winter in the model. Recently, it has been demonstrated that DePreSys3 can skilfully predict not only the first but the second winter NAO [*Dunstone et al.,* 2016], which implies the model retains predictability on extended timescales. Given the low persistence in the NAO on timescales beyond a few weeks, predictability of the NAO must stem from slower varying boundary drivers such as SST's or sea ice [*Johansson,* 2007], or initial conditions such as the stratosphere [*Nie et al.,* 2019], that are linked to the NAO. DePreSys3; containing interactive sea ice and a well resolved ocean, allows these boundary forcings to interact with the atmosphere, and have a much longer memory than the atmosphere alone, therefore could be a source of the extended NAO skill found in *Dunstone et al.* [2016].

The hindcast period extends 1980-2017, which provides a suitably long test period to examine Arctic sea ice to NAO teleconnections in this model, with an effective sample size of 2960 (37 years x 40 ensemble members x 2 winters) winters to analyse. Data is sampled as monthly averages, at the models native resolution, but is interpolated to 1 degree resolution.

3.1.3 Atmosphere Model Intercomparison Project

An atmosphere only dynamical model allows the atmosphere to interact, but not modify the boundary forcings supplied (usually at the surface, such as land, sea and ice charac-

Model	Horizontal Resolution	Vertical Resolution	Ensemble Size
GFSv2	1° x 1°	64 Levels	30 Members
CAM4	1° x 1°	25 Levels	20 Members
ECHAM5	0.75° x 0.75°	31 Levels	30 Members
CAM5.1	1° x 1°	25 Levels	20 Members

Table 3.1: Summary of the atmosphere only models used for the AMIP simulations.

teristics). These boundary forcings are prescribed, and therefore the atmosphere responds to these forcings. This unidirectional relationship enables causal links to be established; by perturbing the boundary forcings relative to a control simulation to ascertain a response which is attributable to the perturbation. The model simulations span 1979 to 2015 inclusive.

In order to isolate the response of the NAO to variations in Arctic sea ice, models from the Atmosphere Model Intercomparison Project (AMIP) are used, within the Facility of Climate Assessments (FACTS) repository. It includes 4 models; GFSv2 [*Saha et al.,* 2014], CAM4 [*Neale et al.,* 2010], CAM5.1 [*Neale et al.,* 2012] and ECHAM5 [*Roeckner et al.,* 2003], where each of these models are forced with a repeating climatological cycle of sea ice and polar SST's as the control [*Hurrell et al.,* 2008]. The models are then forced in the same configuration with observed sea ice and polar SST's, to determine the effect of including realistic sea ice and polar SST's in the model. An additional experiment, forced with observed sea ice and the leading EOF pattern of SST's is also used, though this comprises of only GFSv2, CAM4 and ECHAM5. The leading EOF SST pattern globally primarily picks up ENSO related variability in the tropical Pacific.

Both the control and test simulations are forced with observed radiative forcing, and all other boundary forcings outside the polar regions are observed variability. A summary of the models resolutions and ensemble size are shown in 3.1. Combining these into a multi-model ensemble means there are 100 ensemble members in both the control and perturbation runs, where such a large ensemble supports sub-sampling based on different criteria. Only 20 members are used from each experiment to ensure that there is equal weighting to each model, unless otherwise specified. The experiment forced with observed sea ice and the leading EOF of SSTs, which only contains 3 models, therefore has a reduced ensemble size of 60.

3.1.4 CESM Large Ensemble

The Community Earth System Model (CESM) is a fully coupled climate model allowing two way interaction between the atmosphere and ice/ocean components [*Kay et al.,* 2015]. The ensemble spans the period 1920 through to 2005, forced with historical radiative forcing throughout [*Lamarque et al.,* 2010], and contains 41 ensemble members perturbed using error round-off on the 2m air temperature field. The model horizontal resolution is 1 degree, with 30 atmospheric levels and 60 ocean levels [*Kay et al.,* 2015]. The large ensemble allows internal variability to be investigated more thoroughly. An additional deterministic model run is used, spanning 1800 years with pre-industrial radiative forcing. This longer simulation provides an opportunity to evaluate stationarity of the link between sea ice and the NAO, especially if they are linked to slower ocean variability.

3.1.5 Tropical Nudging Experiments

Experiments where a free running model is nudged towards a known state (using reanalysis) have been employed in a variety of studies to determine sources of predictability in the climate system [e.g. *Jung et al.,* 2014; *Knight et al.,* 2017; *Maidens et al.,* 2019]. Analysis of relevant literature will be contained within chapter 7. Here, the model setup will be described.

The model (GloSea5 HadGEM3) is consistent with the model used within the skilful DePreSys3 dataset, with identical horizontal resolution of 0.83 degrees longitude and 0.55 degrees latitude with 85 vertical levels. It contains interactive sea ice (CICE) and ocean (NEMO). The experiment design initialises the model with a case study year, and then nudges the tropics to a variety of years (specific choices and justifications related to the project will be outlined in chapter 7). The tropical nudging profile extends across all longitudes and from the second vertical atmospheric level from the surface through to the top model level (85), and is applied equally across all levels. The latitude boundary of maximum nudging (+/- 19.5 degrees) is tapered to zero over 8 degrees, in order to minimise shock to the zonal trade winds at the edges of the domain, as in *Maidens et al.* [2019] and *Knight et al.* [2017]. The nudging profile is demonstrated in figure 3.1.

The model is nudged to ERA-Interim atmospheric reanalysis in the domain shown in figure 3.1, at each timestep. The atmospheric variables temperature (T), and horizontal components of wind (u and v) are relaxed towards reanalysis with an e folding timescale

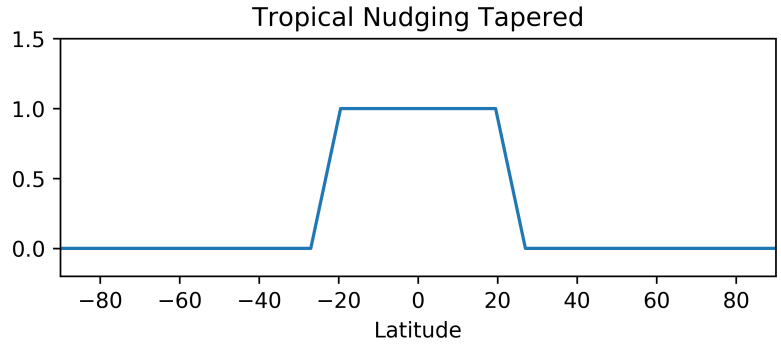

Figure 3.1: Tropical Nudging Profile Schematic - Spatially. Schematic of the tropical nudging profile in the experiment, values are relative to the maximum nudging at the equator.

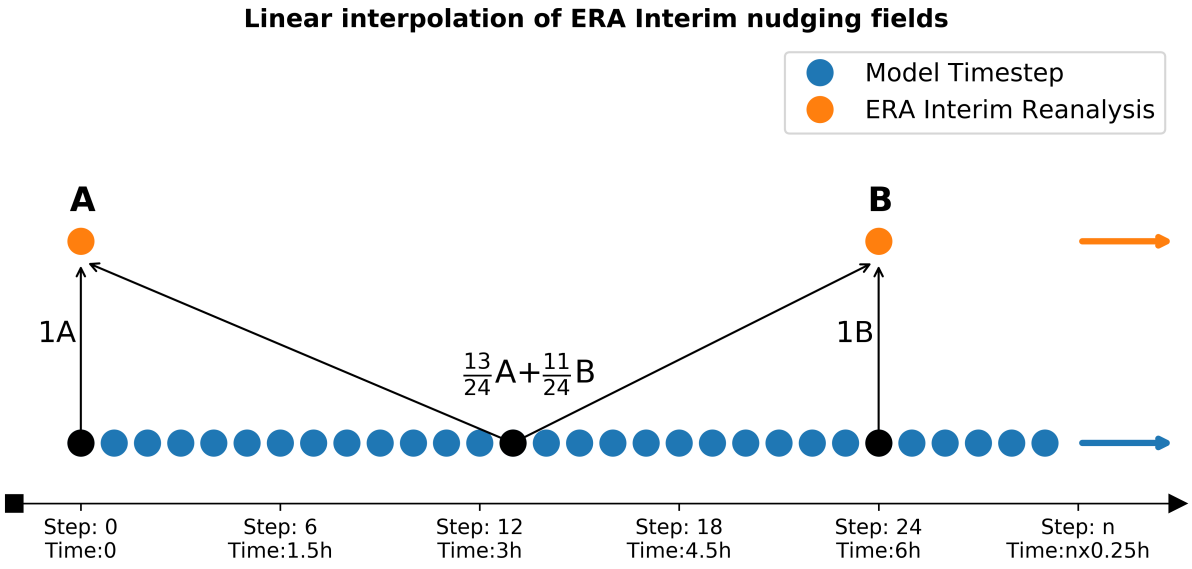

Figure 3.2: Tropical Nudging Profile Schematic - Temporally. Schematic of the tropical nudging temporal frequency and linear interpolation of reanalysis. This is demonstrated by displaying the weighting at a given timestep, in this case timestep 13.

of 6 hours between +/-19.5 degrees latitude. A fraction of the difference between the model field and reanalysis field was added at each timestep; as ERA-Interim reanalysis is available 6 hourly; a linear interpolation was made at each timestep as shown in figure 3.2.

3.2 Statistical Tools

This sections outlines different statistical methods employed within the project.

Data Distributions: Determining the underlying properties and distribution of data means better informed choices can be made regarding the statistical tools to use. For example, making the assumption that data is normally distributed can lead to poor choice of statistical tests when evaluating results, leading to false conclusions. Data can be characterised by attributes such as skewness, symmetry or uniformity, among others [*Groeneveld and Meeden,* 1984].

To test whether the data can be treated as normally distributed, a D'Agostino and Pearson's test can be employed [*D'Agostino and Pearson,* 1973]. This test combines skewness and kurtosis to produce a test of normality, providing a p value to test whether the data comes from a normal distribution or not, given some significance threshold. Many alternate tests can also be employed, such as the Kolmogorov-Smirnov test which identifies how well the sample data fits a normal distribution by determining differences between the sample distribution and a normal distribution [*Massey,* 1951]. The relative merits of each method are not discussed further, but an appreciation of the underlying data distribution is made within analysis. This is particularly relevant for sea ice, which is bound between 0 and 100%; unlike continuous fields like mean sea level pressure. Non-normal data can also be transformed to make it normally distributed; this is discussed later for comparing/adding correlations using the Fisher-Z transform.

Correlation: In order to identify how well two variables are related, the linear Pearson's correlation is used. There is no known physical justification to using a higher order correlation, so the linear correlation is used, like in many climate studies investigating the relationship between two normally distributed variables. The Pearson's correlation coefficient is intrinsically related to the variance of the data, and produces a value between -1

and 1, which represent data that is perfectly anti-correlated and correlated respectively, with 0 implying no correlation. The equation that defines the Pearson's correlation coefficient, r, is:

$$r = \frac{cov(x,y)}{\sigma_x \sigma_y} \qquad cov(x,y) = \frac{\sum_{i=1}^{n}(x_i - \bar{x})(y_i - \bar{y})}{n-1} \tag{3.1}$$

Where x is the independent variable, y is the dependent variable, *cov* denotes covariance, σ is the standard deviation, the overbars denote an average, and n is the number of data points. Essentially, it is a measure of the linear relationship of the two variables (the covariance between x and y), scaled by the product of the standard deviation in order to obtain a value between -1 and 1. A useful interpretation of the Pearsons correlation coefficient, r, is that the % linear variance explained in y by x can be calculated by squaring the coefficient ($100 \cdot r^2$).

A two-tailed p value is also calculated, which explains the probability of a random correlation being at least as extreme as the one being tested. The null hypothesis is that there is no correlation between the two variables, but if p is outside a significance threshold the null hypothesis can be rejected (either at the 2σ ($p < 0.05$) or 3σ ($p < 0.01$) level). Two ways to achieve a smaller p value is if the correlation between the variables increases, or the sample size increases (assuming the correlation remains constant).

The Pearson's correlation method is not only dependent on normally distributed data, but is also sensitive to extreme outliers in a dataset. An alternative correlation is the Spearman's rank correlation, where the data is ranked and so outliers have less of an affect on the correlation. Should data violate the core assumptions that are integral to the Pearson's method then this alternate correlation shall be used, but the Pearsons method will be the a priori method to determine the strength of the linear relationship between two variables. It can be adapted to find two patterns that look similar spatially (of 2 dimensions), through dimension reduction and calculating the correlation. This pattern correlation approach on gridded latitude-longitude data can adapted by weighting the average in 3.1 by the cosine of latitude, to account for the smaller grid-boxes at the pole (avoiding dis-proportionate area weighting at higher latitudes).

Fisher-Z Transform: Correlation values are bounded between -1 and 1, and are also non-Gaussian. To transform the data so it is Gaussian, and therefore so it can be added,

averaged as well as comparing to other correlation values, a Fisher-Z transform is applied [*Fisher,* 1915; *Silver and Dunlap,* 1987]. The procedure to transform correlation values is to first take the inverse hyperbolic tangent function of the correlation values as in equation 3.2.

$$Z = \frac{1}{2}\left[\ln\left(1+r\right) - \ln\left(1-r\right)\right] \qquad Z = \operatorname{arctanh}\left(Z\right) \tag{3.2}$$

The transformed r values (z) can then be averaged, or confidence intervals be constructed, before the z values are transformed back to correlation values using the hyperbolic tangent function $r = \tanh\left(z\right)$. This method is particularly important with stronger correlations ($r > 0.5$) where the distribution of r values is more skewed nearer -1, 1; if this transform isn't applied, the average correlation coefficient will be an underestimate [*Silver and Dunlap,* 1987].

Linear Regression: Linear regression is closely related method to correlation in investigating the linear relationship between variables. It is based on fitting a straight line that best describes the the relationship between the two variables, typically using a least-squares fitting approach by minimising the sum of the squares of the vertical deviations from each data point to the best fit line. The line $y = mx + c$, where y is the dependent variable, x is the independent variable, m is the line gradient and c is the line intercept ($y = 0$), is calculated using the following formula:

$$m = \frac{\sum_{i=1}^{n}(x_i - \bar{x})(y_i - \bar{y})}{\sum_{i=1}^{n}(x_i - \bar{x})^2} \qquad c = \bar{y} - m\bar{x} \tag{3.3}$$

The gradient of the line m provides a useful metric to predicting a change in y based on a change in x, i.e. how strongly do these variables linearly scale. It is important to determine whether the slope of the best fit line is statistically non-zero (i.e. whether the relationship is significant or could occur by chance) using a p value, as well as determining how well the slope fits the data, by testing the least squares approach through calculating the standard error about the regression line using the following formula:

$$\sigma_{stderr} = \sqrt{\frac{\sum_{i=1}^{n}(y_i - y_i')}{n}} \tag{3.4}$$

where σ_{stderr} is the standard error, y denotes the actual y value and y' denotes the

prediction of y based on the regression line. A t-statistic, which is proportional to $\frac{1}{\sigma_{stderr}}$, is then generated, and a p value is obtained from a normal distribution to determine whether the slope is statistically non-zero.

Linear regression can be expanded to incorporate multiple variables $(x_1, x_2, x_3...x_n)$ predicting a variable y, using multiple linear regression using the following equation:

$$y = \beta_1 x_1 + \beta_2 x_2 + \beta_3 x_3 + ...\beta_n x_n + \epsilon + c \tag{3.5}$$

where x_n are the predictors, β_n are the coefficients, ϵ is an error/residual term and c is the y intercept. This method calculates the optimal coefficients (β_n) to explain maximum variance in the predictand (y). It is particularly useful for evaluating how much variance different climate components explain in the NAO; for example, different proposed drivers such as Arctic sea ice and tropical rainfall can be combined using multiple linear regression to determine whether the variance they explain in the NAO is shared.

A caveat to this method is that there is a limited number of predictors that can be used given a sample of fixed length. In a extreme case, if a data sample of length n was being predicted by n predictors, this would be heavily over-fit, therefore if this model was then applied to some new data, it would fail. Though there is no defined maximum to the amount of predictors that can be used on a dataset, given it depends on the data itself, there are methods to detect over-fitting, such as cross validation. Multiple linear regression produces positive, inflated correlations by construction. Figure 3.3 demonstrates this by sequentially increasing the number of predictors in a multiple linear regression by creating timeseries of random numbers predicting another timeseries of random numbers. Using one predictor (single linear regression), correlations are normally distributed around zero. By using two or more predictors (multiple linear regression), then the correlation between the model prediction and the predictand is always positive. This becomes increasingly strong with increased predictors, where many predictions become statistically significant as the correlation is artificially skewed.

Cross Validation: Cross validation is used to test the fit, or prediction, of a linear model to some data, by calculating the coefficients (either a single or multiple linear regression model) using a subsection of the data, and then using this to predict the remaining withheld data. This is also known as k-fold validation, where k=2 implies half

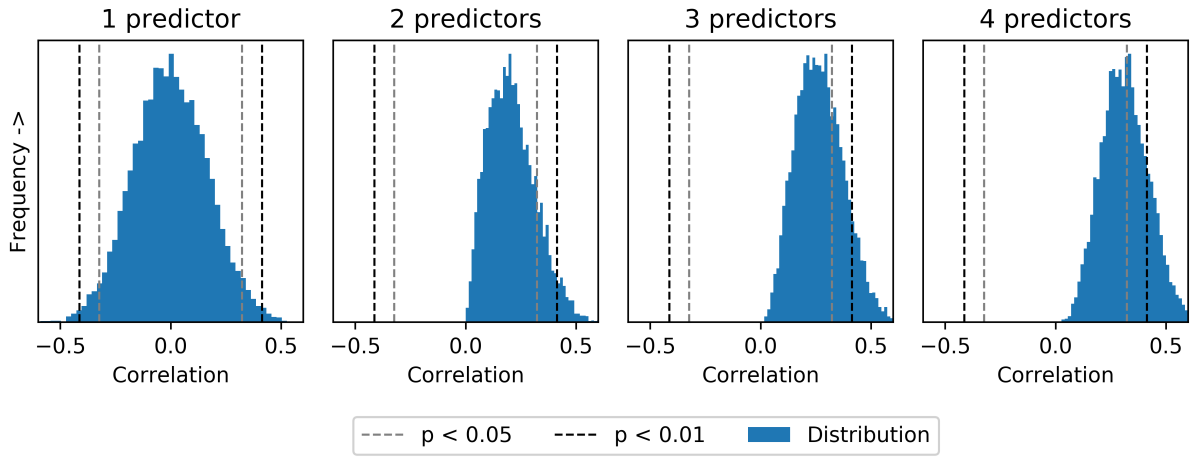

Figure 3.3: Multiple linear regression inflates correlations. Correlation coefficient of fitting a linear regression model with random timeseries, in predicting a random timeseries (of length 37). This is repeated 10000 times to obtain a smooth PDF.

the data is used for creating the model, and the other half is then used to test the data. Both folds of data are used as the training data and the test data subsequently.

The most rigorous cross validation is leave one out (LOO) cross validation, where in a dataset of length n, 1 data point is withheld, with $n - 1$ data points being used to generate the model. This is the most resource intensive validation, as it involves repeating the process n times, but is appropriate for smaller datasets such as being used in this project, where larger k fold validation would not be appropriate (for example, most data is sampled between 1980-2017, so $n = 37$). LOO validation is also the most strenuous cross validation on the data, and is widely employed. Cross validation can be used to validate whether a model is over-fit when large numbers of predictors are used; the LOO validated model explains no variance. This means the model is over-tuned to the data, and when some data is excluded for testing, it cannot predict this. Typically, for every predictor there should be 10-15 samples [*Babyak,* 2004], though this is subject to underlying characteristics of the data [*Austin and Steyerberg,* 2015; *Babyak,* 2004]. For the main period of observations used in this thesis, 1980-2016, this means no more than 3-4 predictors. An alternate approach to varying the number of predictors, is to use a larger sample size where over-fitting becomes less problematic.

An additional method for interpreting the variance a multiple linear regression model explains of some data is using the adjusted r-squared, which takes into account inflation from adding additional variables in the regression. The equation is shown below in 3.6,

where n is the sample size, k is the number of independent predictors, and r^2 is the variance the model explains.

$$R^2 = 1 - (1 - r^2)\left[\frac{n-1}{n-(k+1)}\right] \qquad n \gg k \tag{3.6}$$

Resampling/Bootstrapping: Another method used to determine error in statistics such as the standard error of the regression line, is re-sampling (also known as bootstrapping). This involves sampling from a population repeatedly with replacement, such that the new sample is not likely to be identical to the population. Some values may be drawn repeatedly whilst others do not get drawn; repeating this process many times enables a more robust statistic to be derived. This is particularly useful when comparing model ensembles to reanalysis, the latter of which is one realisation by construction. Randomly sub-sampling a member from each year can produce an equivalent and comparable model time-series to reanalysis, and can be repeated many times.

T and F tests: T-tests can be employed to investigate whether the means of two different sets of data are significantly different. The null hypothesis is that the mean difference between the two datasets is indistinguishable from variability in the datasets, which can be rejected based on which confidence interval is chosen (either at $p = 0.05$ or $p = 0.01$ level), assuming a normal distribution and typically similar variance (if the later is not true, a Welch test can be employed [*Welch,* 1947]). An F-test involves the same principals, except the null hypothesis is that the difference in variance between the two distributions is indistinguishable.

Re-gridding data: Re-gridding data to a different resolution enables like-for-like comparisons between fields in different models, as well as ensuring homogeneity among analyses. Interpolation is nearly always done to decrease the resolution. Data is interpolated using a nearest neighbour or bi-linear approach onto a 1 degree grid. There are higher order interpolations, such as cubic interpolation, but these can introduce spurious and un-physical artefacts into the data. The simplest, and default employed here, is nearest neighbour. This does not smooth the field and is particularly useful for re-gridding sea ice given discontinuities in the field (i.e. near coastline where sea ice cover can go from 1 (full) to 0 (none) where there is land), unlike continuous fields such as sea level pressure.

Detrending data: The correct order trend to use depends on the nature of the data; in most cases, a linear trend suffices. In any case, an assessment whether this is suitable is made. To linearly detrend the data, a linear regression is performed between the variable to detrend, and time, using a least-squares fit approach (as discussed earlier). This produces a line of best fit using the slope coefficient and the y intercept. This is subtracted from the original time series, leaving detrended data as a remainder.

3.3 Climate Indices

It can be beneficial to summarise information about modes of atmospheric/oceanic variability into a single value, to create a timeseries. This can include taking an average over an area, or using EOF analysis to decompose multi-dimensional data into a single dimension. This section describes how the NAO index is calculated, with a measure of how robust this is. It also explains how sea ice data is processed and quality controlled, along with the tropical rainfall indices and other indices used in the analysis.

3.3.1 NAO Calculation & Sensitivity

There is little consensus on which method should be used to construct the NAO index. These methods vary from station (one grid box) differences between Iceland and the Azores, box approaches (taking the average of a region), and EOF analysis over the North Atlantic domain. Sensitivity tests are conducted to determine the best method. ERA-Interim data is used for the period 1980-2016 inclusive, as well as HadSLP2 (1850-2005 with a native resolution of 5° horizontally) to test each method over a longer period of time where there may be decadal variability and non-stationarity in the nodes of the NAO. Both datasets are interpolated to 1 degree resolution using a nearest neighbour approach.

Using mean sea level pressure data, a station pressure difference is taken between Reykjavik, Iceland (64.1°N, 21.8°W) and Lisbon, Portugal (38.7°N, 9.1°W) [*Hurrell,* 2018]. The box method, which is the difference between the spatial average of two boxes located around Iceland (25°-16°W, 63°-70°N) and the Azores (28°-20°W, 36°-40°N) [*Dunstone et al.,* 2016], will be used as the primary NAO method, as it was recently used in demonstrating prediction skill in the DePreSys3 system [*Dunstone et al.,* 2016]. These pressure

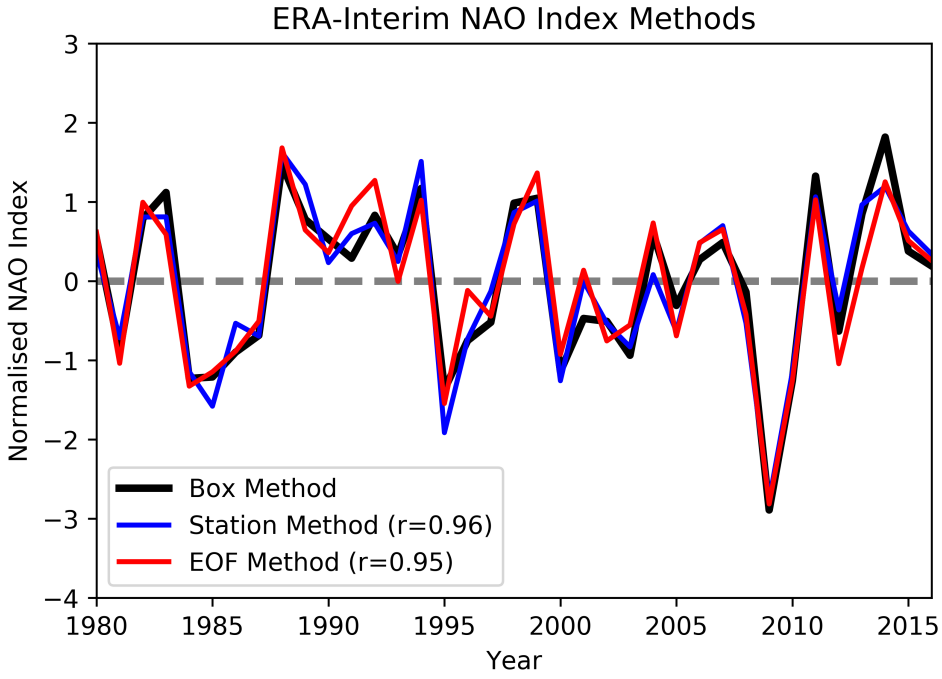

Figure 3.4: Comparing NAO Index Methods. Intercomparison of winter NAO methods between the station, box and EOF approach, using ERA-Interim data 1980-2016. The Pearsons correlation coefficient (r) with the box method is also shown in the legend.

difference time series are then standardised by their mean and variance. Finally, the EOF approach involves calculating the anomalies of mean sea level pressure in the domain (20°-80°N, 90°W-40°E) from the climate mean, as defined in *Hurrell* [2018]. The data is then cosine-weighted to take into account latitude and grid box size reduction towards the pole, and the leading principal component (PC) is extracted. Given the signs of the eigenvectors are arbitrary [*Jolliffe and Cadima,* 2016], the principal component sign is corrected to be positively correlated with the other two methods.

The timeseries for each method is shown in figure 3.4. This analysis demonstrates a very high correlation between both the station and EOF method with the box method that share at least 90% variance. The box method also captures NAO extremes well, such as in the winter of 2009/10 and 2014/15. Given the high variance shared between the methods, the choice of method is somewhat arbitrary and should not change the later results significantly, despite *Baker et al.* [2018] finding a variation in model skill depending on the choice of method, mostly because some models have large biases in the nodes of the NAO.

The EOF approach works by characterising orthogonal modes of variability, where each

mode explains a percentage of variance [*Monahan et al.,* 2009]. The maximum number of modes is equal to the length of the data, in this case 37 years (37 modes). Though the NAO captures the most variance in mean sea level pressure during winter, it cannot be assumed this is the case for all months. For example, figure 3.5 explores how the leading mode of mean sea level pressure varies for each month of the year, and how well each of the 5 leading principal component series correlate with the NAO index derived through the box method. Firstly, though the leading PC (PC1) is the best correlated with the NAO index for most of the year, in the summer months, particularly September, the leading PC captures a lot less variance than the winter months suggesting it is not such a dominant mode of variability during the summer months, or that the box method no longer addresses the nodes of the NAO (figure 3.5A).

The breakdown of how much variance each mode explains is shown in figure 3.5C. The analysis also suggests that the NAO in months close to boreal winter, such as November, are not dominated by the NAO, and instead by a tripolar pattern over north west Europe (figure 3.5B) described by the east Atlantic pattern [*Wallace and Gutzler,* 1981; *Barnston and Livezey,* 1987]. These results highlight the importance of carefully selecting the appropriate NAO method, either because the NAO is no longer the leading mode of variability, or the box method no longer captures the nodes of the NAO.

The box method is tested over a longer period of time, using the HadSLP2 dataset, to test for non-stationarity where the NAO has been shown to have decadal variability [*Woollings et al.,* 2015]. This provides a larger sample to test each NAO index. Figure 3.6A displays each of the 3 methods over this extended period, along with the correlation of the station and EOF method with the box method. Correlations of 0.93-0.97 agree well with the recent 1980-2017 period using ERA-Interim data in figure 3.4, suggesting the methods covariance is not unique to the recent period. By calculating a moving 30 year correlation between both the station and EOF method with the box method over the extended period, how sensitive the methods are to longer multi-decadal variability over the Atlantic can be examined. 30 years is sufficient to smooth out interannual and decadal variability.

These results are displayed in figure 3.6B, which reveals that although the correlation remains high between the box and station method, the correlation drops between the box and EOF approach. Given the EOF approach allows the nodes of the NAO to vary

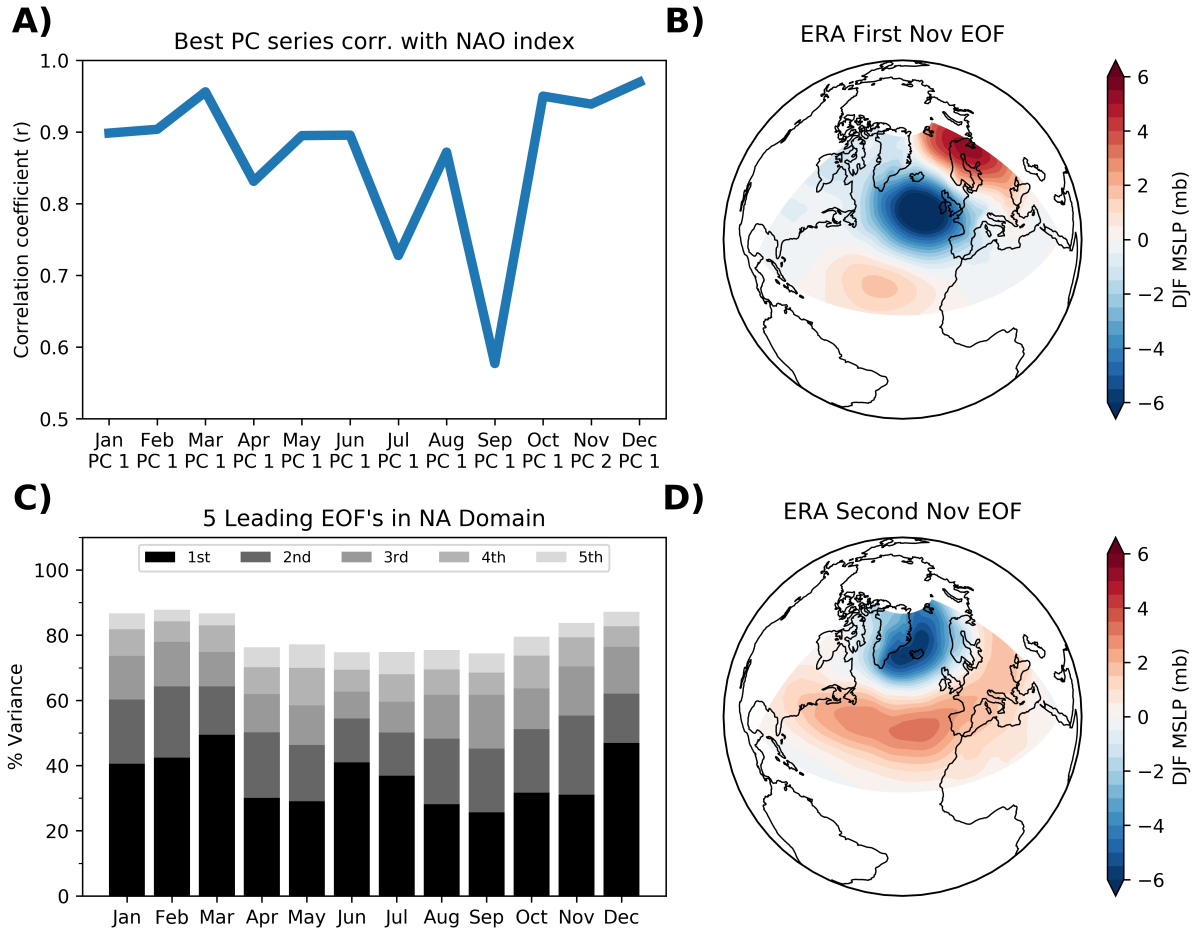

Figure 3.5: Modes of variability in the North Atlantic Domain. A) Pearsons correlation coefficient of the leading EOF principal component for each month with the box method NAO index. The principal component that correlates most strongly is listed for each month under the month heading. **B)** The spatial pattern of the leading EOF for November, using mean sea level pressure (MSLP). **C)** The variance explained by each of the leading 5 EOF's for each month separately. **D)** Same as in B), but displaying the second leading EOF for November.

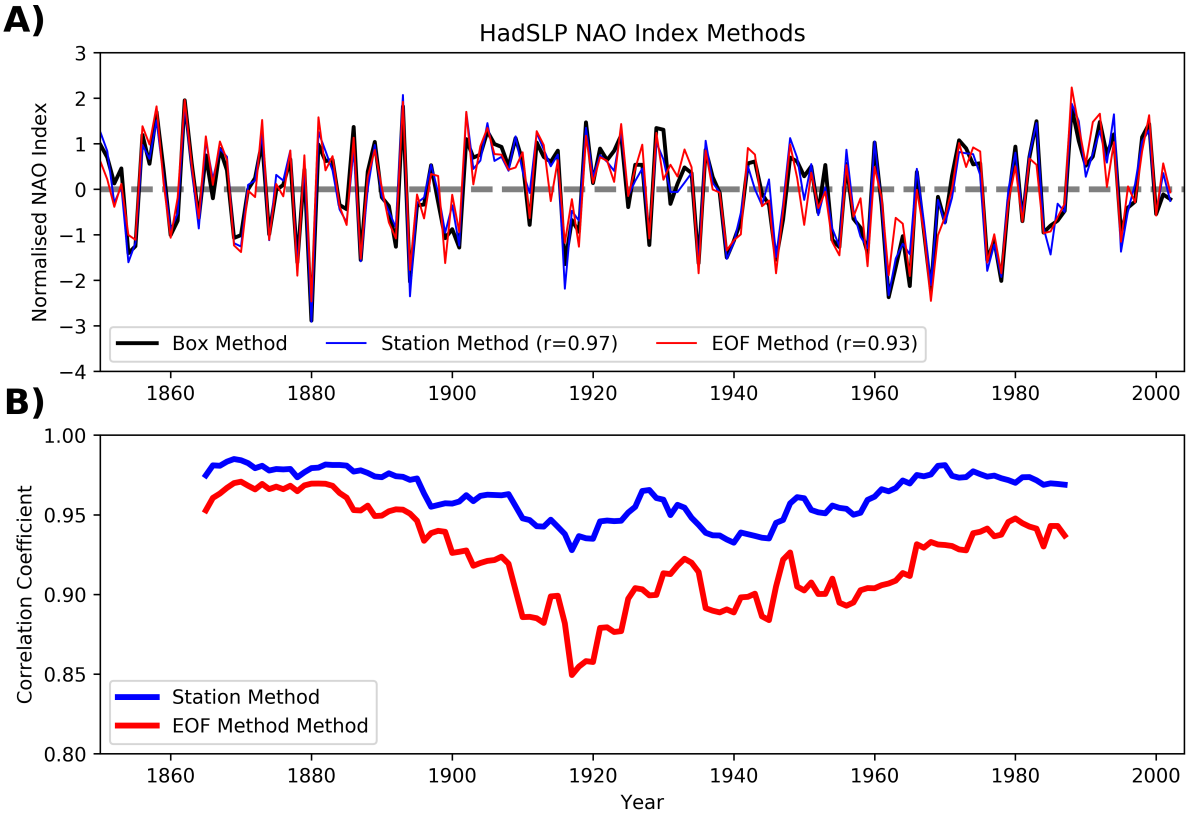

Figure 3.6: Testing NAO methods over centenial timescales. A): Timeseries of the NAO index using the 3 different methods in HadSLP over the period 1850-2004 inclusive. Pearsons correlation coefficient (r) shown in the legend with the box method. **B)** Pearsons correlation coefficient of a 30 year moving window between the box method and the station/EOF methods.

spatially with time, this result could suggest that the displacement of the NAO modes between 1900 and the mid 1900's leads to the box method becoming a more limited measure of capturing NAO variability. This does, however, have to be interpreted with caution, given data availability and accuracy in creating the gridded dataset with more sparse measurements in the early 1900's. Additionally, the coarse original resolution of the data (5 degrees) may affect the EOF analysis to accurately pick up an NAO like pattern. In general, these results provide confidence that the box method in determining the NAO index is sufficient in capturing NAO variability during winter in the recent period of 1980-2017. The box method is also easier and quicker to implement when it comes to sub-sampling ensembles later in the project.

In figure 2.1 the NAO was one of 4 predominant modes of variability over the North Atlantic. Here, the relationship between NAO variability and European winter climate variability is explored in figure 3.7, by calculating the regression of the NAO index onto typical meteorological variables using ERA-Interim data from 1980-2016. The regression of the NAO index onto mean sea level pressure reveals a dipole pattern of sea level pressure extending from Azores to Iceland. It can be seen that surface temperatures over western, central and northern Europe are significantly warmer (3.7B), as a result of relatively mild air being advected off the North Atlantic ocean which is warmer than the surrounding continents during winter. Lower atmospheric winds are also significantly stronger (3.7C), as a result of a stronger pressure gradient across western Europe (3.7A). Finally, precipitation across northern and western Europe increases, though this field is more noisy. These three fields imply a positive NAO, associated with a stronger storm track, leads to stronger winds, more heat advection into Europe as well as precipitation; vice-versa with a negative NAO.

3.3.2 Sea Ice

Sea ice is sensitive to a variety of atmospheric and ocean processes in models, and because of this there are discrepancies and biases among reanalysis products [*Lindsay et al.,* 2014]. Systematic differences are due to model resolution which affects how well the land-sea border is represented, which is especially important in regions of the Arctic that are compromised of many islands near the continent edge, such as northern Canada. In order to calculate sea ice extent in different regions of the Arctic, and as a whole, it is important

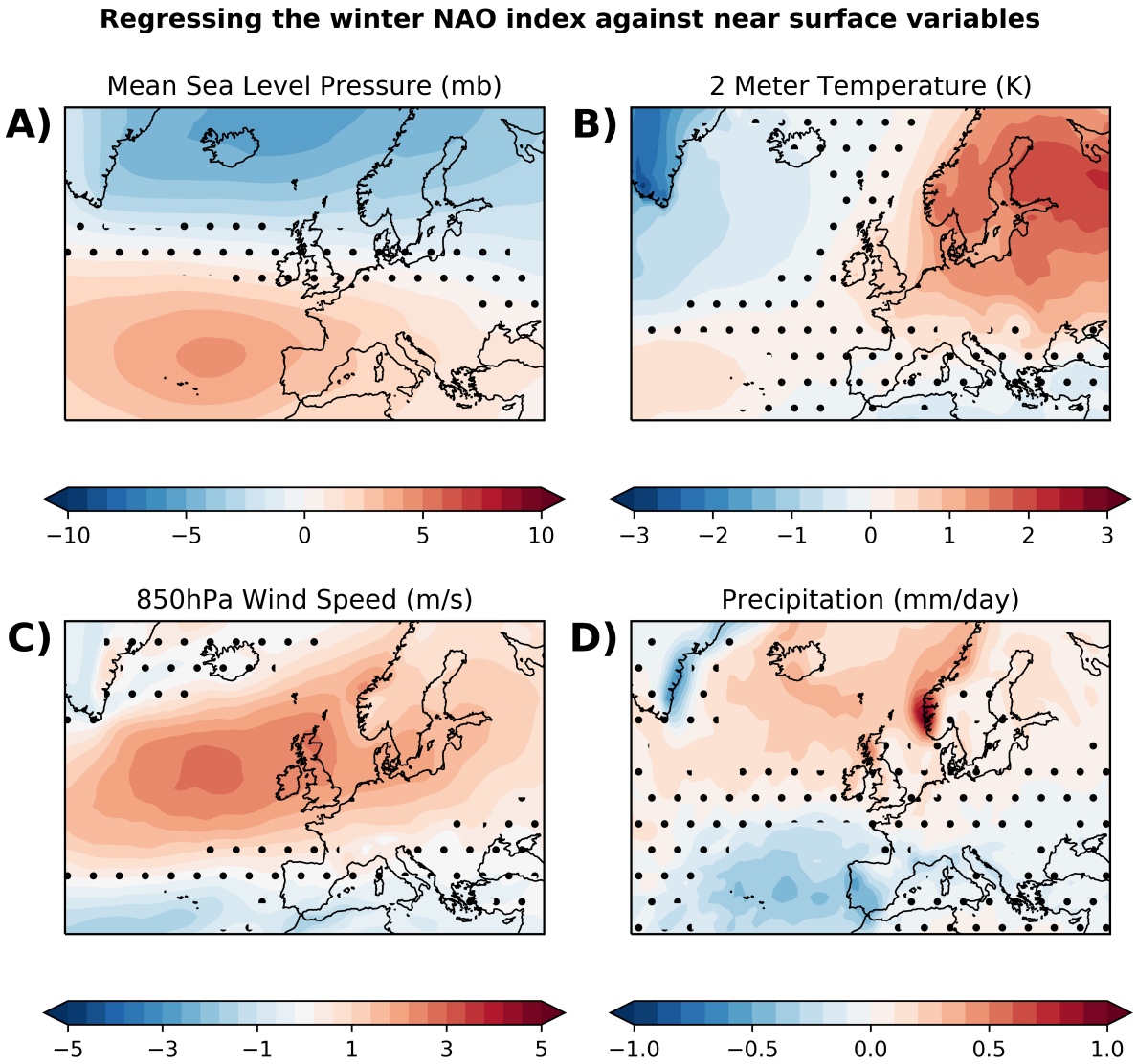

Figure 3.7: Regression of the NAO index onto typical variables. Regression of the normalised NAO index onto **A)** mean sea level pressure, **B** 2 meter temperature, **C)** 850hPa wind speed and **D)** precipitation at each gridpoint. In all cases, the response is an increase in the NAO index by 1σ (i.e. a positive NAO index). Hatching indicates areas where the regression coefficient is not significant at the 5% level.

to assess which reanalysis products are most suitable, and benchmark gridded products against a known, published time-series of sea ice, such as the satellite-derived NSIDC pan-Arctic time series. Given discrepancies in resolutions and land-sea masks in different datasets, the following processing is employed;

- The gridded data is interpolated down to be equal with the lowest resolution dataset, in this case 180x360 (1 degree grid box) using a nearest neighbour interpolation.
- A gridbox contains sea ice if the ice concentration is greater than 15%. Making the approximation that a 1 degree grid box at the equator is 111km by 111km, a simple formula for the size of a grid box at a given latitude (in km^2) is

$$Area = 12321 \cdot \cos\left(\frac{\pi \cdot Latitude}{180}\right) \tag{3.7}$$

- The total sea ice extent is then integrated over the domain required.

To compare how the two gridded datasets that contain sea ice data perform using this methodology with the NSIDC values, a pan-Arctic sea ice timeseries is produced for September between 1980 and 2016 as a first test, shown in figure 3.8. September is chosen for this comparison as this month contains the most interannual sea ice variability.

This demonstrates that although both HadISST and ERA-Interim capture interannual variance and the trend well, there is a large bias between them and satellite derived ice extent even after applying the procedure above. While additional data processing such as concatenating both datasets land-sea mask together, to ensure they all contain the same number of land/sea points, biases are only reduced slightly between products (not shown). A simple but effective bias correction is to remove each timeseries mean, producing figure 3.8(B)). The correlation between HadISST2, ERA-Interim with NSIDC measurements over the year are shown in 3.9. This demonstrates a discrepancy in performance of ERA-Interim and HadISST2, particularly in late spring. It is expected that correlation may drop during this time as there is less interannual variability, given sea ice is at its maximum and is constrained by coastline, and less interannual variability makes it more sensitive to noise in the reanalysis products. Months where the trend is stronger, such as late summer/early autumn, will also have a higher correlation.

HadISST2 performs consistently during the period with little variation in month to month performance, whereas ERA-Interim performs erratically at times, and is thus

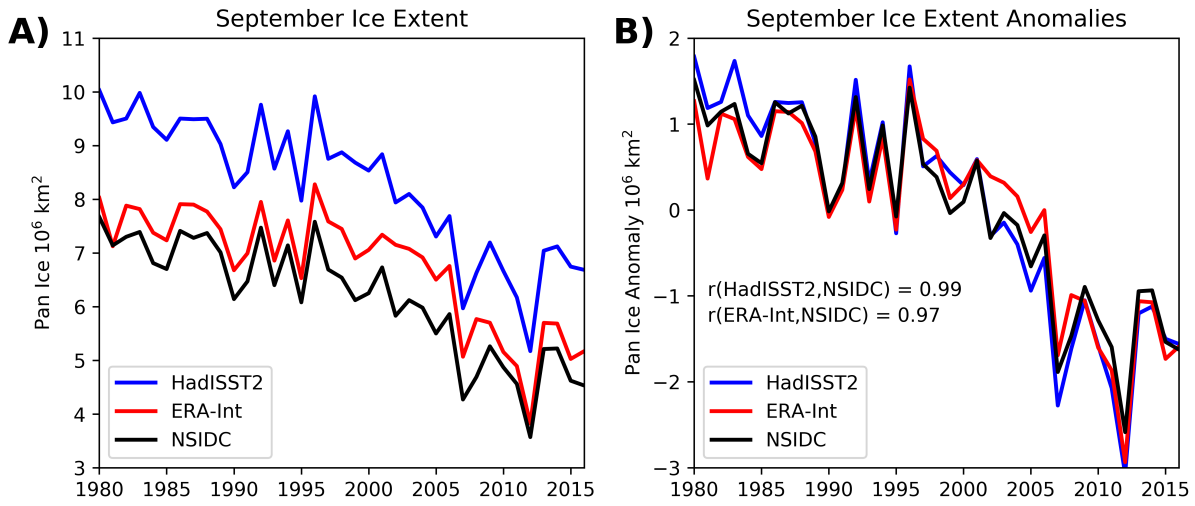

Figure 3.8: September sea ice biases in different reanalysis products. **A)** Time series of September Pan Arctic ice using HadISST and ERA-Interim, along with NSIDC values for the period 1980-2016. **B)** Same as in A), except the mean has been subtracted from each time series. The Pearson correlation coefficient between HadISST,ERA-Interim and NSIDC is shown.

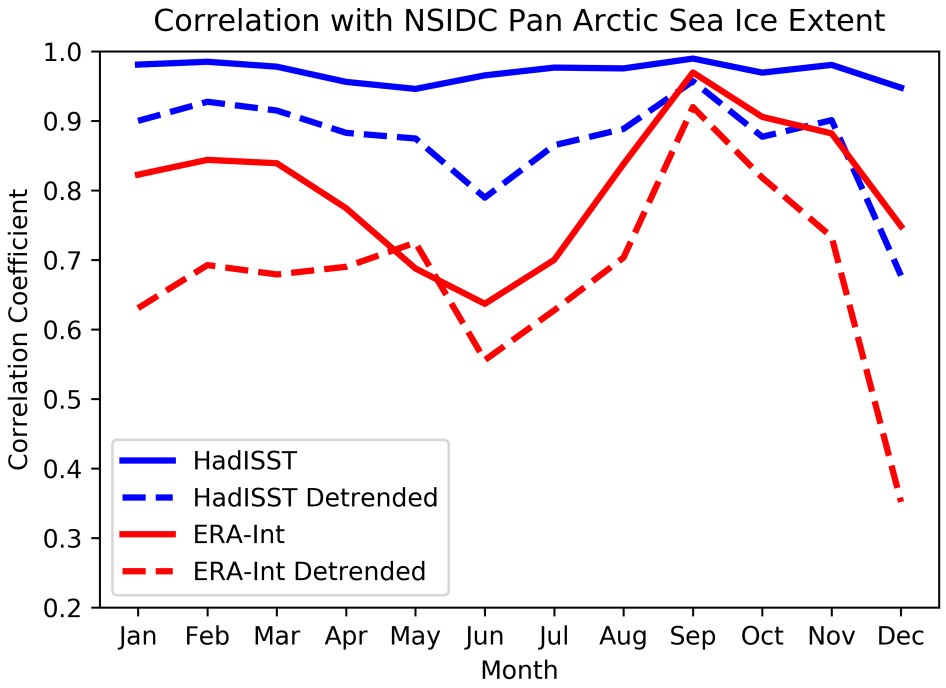

Figure 3.9: Monthly performance of sea ice extent reanalysis products. Monthly Pearson's correlation coefficients between the two gridded products, ERA-Interim and HadISST, with NSIDC values for the period 1980-2016 inclusive. The linear trend is removed from the dashed lines before computing the Pearson's correlation coefficient.

deemed unsuitable for use for ice extent. Nearly all correlations are lower when the timeseries is detrended prior to analysis; isolating interannual variability indicates that HadISST remains well correlated with satellite derived measurements. ERA-Interim ice fields, which are prescribed in the reanalysis, are formed of a variety of products [*Dee et al.,* 2011], so it is possible that processing and re-gridding of data has led to this discrepancy.

Finally, a subregion is defined in the Arctic guided by the domains defined in *Screen* [2017a]. Of particular interest is the Barents-Kara region, defined as (10-100°E, 65-85°N), which has been regularly cited as a pivotal area of sea ice for affecting the NAO (e.g. *Petoukhov and Semenov* [2009]). The motivation to sub-divide the Arctic stems from studies showing that different regions of the Arctic exhibit different responses on the midlatitude circulation, e.g. *McKenna et al.* [2018]; *Screen* [2017], discussed earlier in the literature review.

Autumn variability in Arctic sea ice has been regularly linked to NAO variability [*Honda et al.,* 2009; *Nakumura et al.,* 2015; *Wang et al.,* 2017; *Hall et al.,* 2017]. Variability in Arctic sea ice is explored through EOF decomposition in autumn and winter, and analysing the 3 leading EOF's as shown in figure 3.10, where the Barents-Kara sea ice domain is overlayed. The leading EOF in both seasons captures the dominant climate change downward trend, which manifests itself primarily in the Barents-Kara and Chuckchi seas. The second EOF predominantly demonstrates interannual variability, where this variability is predominantly confined to the Barents-Kara seas in both seasons. Given interannual variability is so large in the Barents-Kara seas, intuitively it may have the biggest effect on the atmosphere if the two are causally linked.

3.3.3 Tropical Rainfall

To capture variability in tropical rainfall in different basins, 4 boxes are used across the tropics, as defined in *Scaife et al.* [2017] as these are linked to the NAO in both observations and models, and are regions of enhanced predictability. These are comprised of the Tropical Atlantic (5°S-5°N, 60°W-0°W), East Pacific (5°S-10°N, 160-270°E), West Pacific (5°S-25°N, 110-140°E), and the Indian Ocean (5°S-10°N. 45-100°E). These regions have been selected based on tropical regions where the rainfall is highly predictable on seasonal timescales and correlated with the NAO [*Scaife et al.,* 2017]. Additionally, they

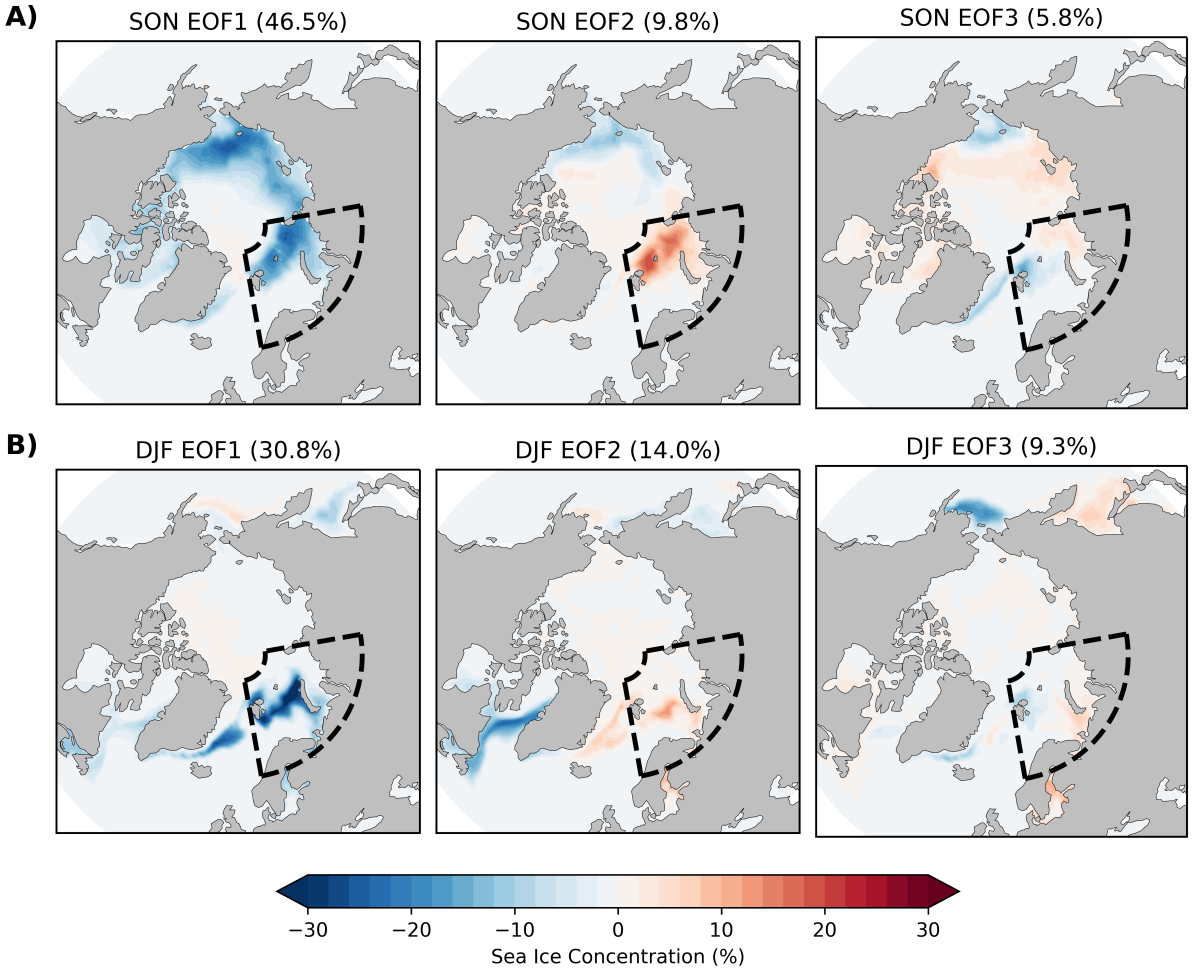

Figure 3.10: Modes of variability in Arctic sea ice. The 3 leading empirical orthogonal functions for autumn (SON) and winter (DJF) averages using HadISST2 data. The Barents-Kara seas region is denoted by the dotted line. The variance each EOF explains is shown in brackets.

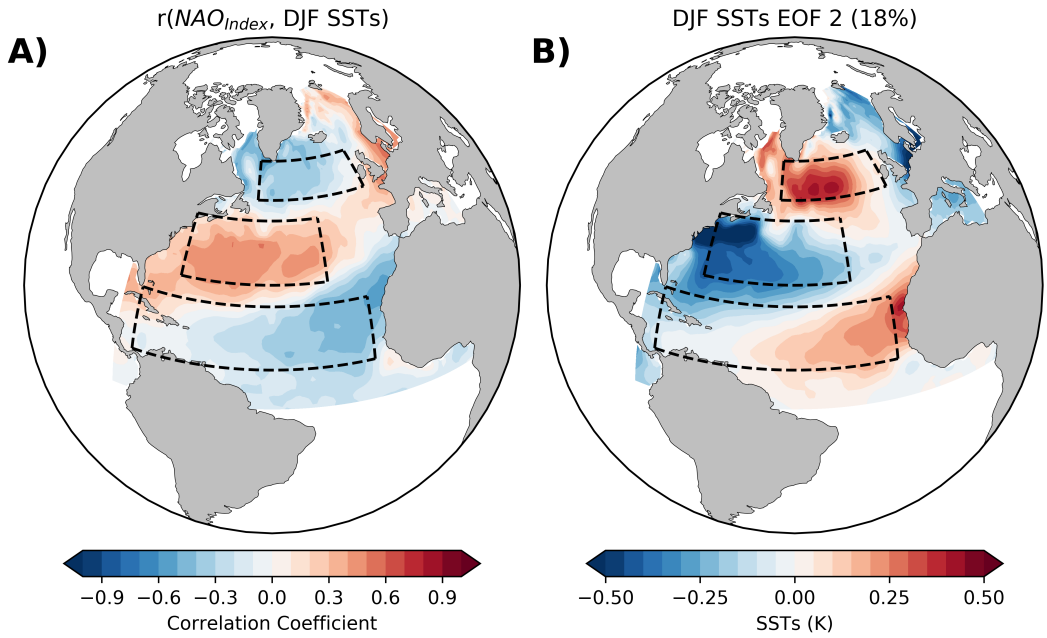

Figure 3.11: Sea surface temperature variability during winter in the North Atlantic. A) Grid point correlation between the winter NAO index and winter averaged SST's in the Atlantic. **B)** The second leading EOF of winter SST's over the Atlantic, with the variance this mode explains in brackets. For both plots, the 3 boxes used to calculate the Atlantic tripole index are shown, with HadISST data used for the SSTs and ERA-Interim to derive the NAO index.

contain variability from the MJO and ENSO regions; two key teleconnections linked to the NAO and sea ice. Rainfall is a good proxy for divergence/convergence in the upper troposphere through vertical motion, and thus Rossby wave sources.

3.3.4 Other Indices

A wide range of other drivers have been suggested to control NAO variability, such as the tripole pattern of SST's in the north Atlantic [*Rodwell et al.,* 1999], the stratospheric polar vortex [*Hitchcock and Simpson,* 2014], ENSO [*Toniazzo and Scaife,* 2006], and the QBO [*Marshall and Scaife,* 2009].

Knowledge of Atlantic SST's, in particular the Atlantic tripole, allows some NAO variability (20%) to be reconstructed [*Rodwell et al.,* 1999]. Figure 3.11A shows a gridbox correlation between the winter NAO index and winter SST's in observational reanalysis, and demonstrates a tripolar pattern extending from high latitude seas into the tropics. The pattern is orientated such that a positive NAO is correlated with colder than average SST's south of Greenland, with warmer SST's across much of the subtropical Atlantic;

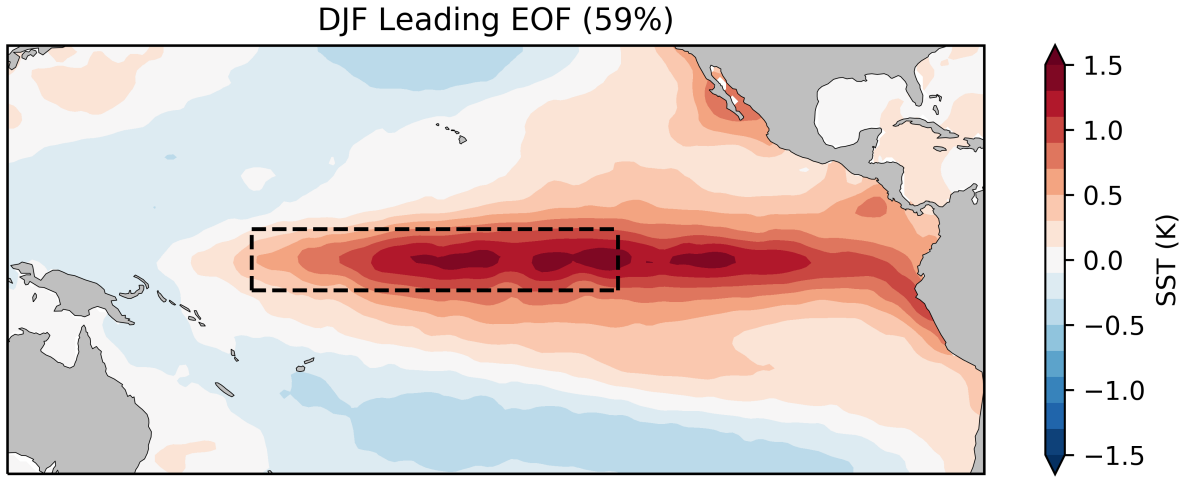

Figure 3.12: Domain used for NINO3.4 Index. The leading EOF of SST's over the tropical Pacific for inter-annual winter (DJF), with the region used to calculate the NINO 3.4 index encapsulated in dashed lines. The variance this leading EOF captures is shown in brackets.

as found in *Visbeck et al.* [2001]. To capture this tripole in a simple index, 3 boxes are constructed with SST's averaged in each, as in *Dunstone et al.* [2016], and shown in figure 3.11.

More specifically, the 3 boxes are defined as the northern box (50-10°W, 50-60°N), central box (30-70°W, 30-45°N) and southern box (20-80°W, 10-25°N) of the North Atlantic, and the tripole index is the average rainfall in each of these boxes calculated as middle-(north+south). The pattern emerges as the second EOF of winter SSTs, containing 18% of variability in the North Atlantic SST's during winter (figure 3.11B); with the leading EOF capturing a general warming trend over the period 1980-2016, or perhaps low frequency variability in the Atlantic meridional overturning circulation.

While tropical rainfall is highly correlated with tropical SST's as discussed in the literature review, it is advantageous to have an index which captures SST variability of ENSO in the central Pacific, more commonly known as the NINO 3.4 index. The same domain is used as in *Dunstone et al.* [2016], bounded by 170-120°W, 5°S-5°N, shown in figure 3.12. The leading EOF of winter SSTs is also overlayed, to demonstrate that the node of SST variability is largely contained within this box, and that this EOF contains a large proportion of variance in this basin during winter. Note that this doesn't consider different types of El Niño given the fixed box location; eastern Pacific El Niño's may not be as well captured by this index but still influence the mid/high latitude circulation.

Other indices are constructed based on their links with NAO variability in the literature; these include the polar stratospheric vortex, and the Quasi-Biennal Oscillation. To calculate the strength of the stratospheric vortex, the zonal mean of the zonal wind on the latitude band at 60°N is taken, on the 10hPa pressure level. To calculate the Quasi-Biennal Oscillation, zonal winds at 30hPa are averaged between 5°N and 5°S.

Chapter 4

Arctic Sea Ice & Extratropical links

This chapter identifies key links between Arctic sea ice variability and the mid-latitude circulation, particularly between autumn Barents-Kara sea ice and the winter NAO. This is approached using observational reanalysis, DePreSys3 (a prediction system that can skilfully predict the NAO at extended lead time), and the CESM large ensemble (a free-running coupled simulation). The overall purpose of this chapter is to provide grounding to the well documented link between sea ice variability and the mid-latitude circulation in autumn and winter. Understanding the relationship between sea ice and the extratropics, and its reproducibility within a model environment provides the basis for further experimentation on the issue of causality.

4.1 Introduction

Sea ice is bounded by the ocean and atmosphere, both of which contain variability on a range of spatial and temporal scales. Intuitively, therefore, the sea ice must also respond to these variations in the atmosphere and ocean given its physical proximity to both of these. Atmosphere-ocean-ice relationships are more complicated than thermodynamics alone, given that the atmosphere can drive motion in the upper ocean through wind stress, and vice versa, through bi-directional heat and momentum fluxes. What complicates this further is that large areas of the Arctic contain first year sea ice, which is thin relative to multi-year ice and can be broken up easily through wind stresses and ocean wave motion, and is therefore sensitive to the state of the atmosphere and ocean. Thermodynamically, sea ice prevents heat flux from the ocean to the atmosphere, therefore a large ice breakup

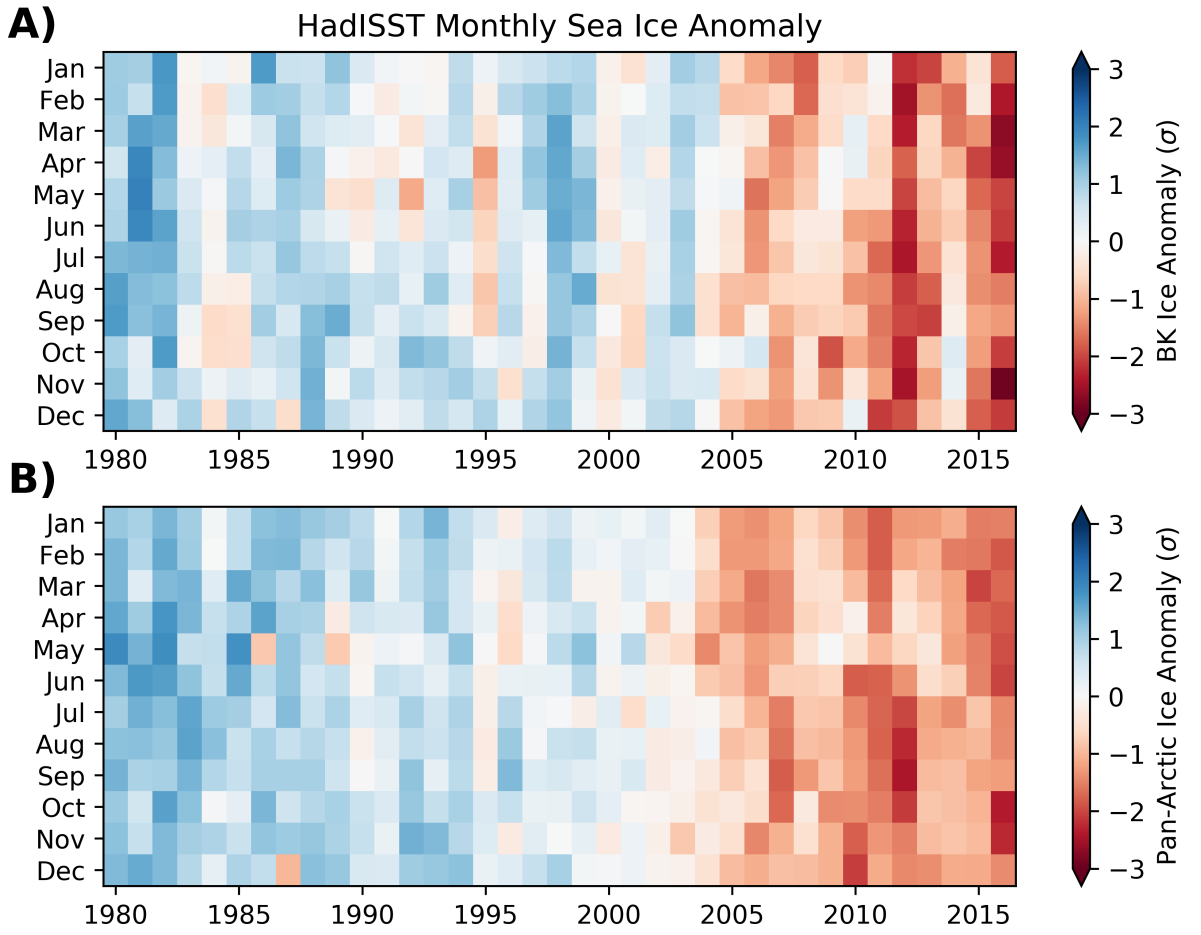

Figure 4.1: Interannual variability in sea ice. **A)** Monthly sea ice standardised anomalies in the Barents-Kara seas, relative to 1979-2016. **B)** Same as A), except for Pan-Arctic sea ice.

event from a synoptic-scale storm can significantly alter the energy balance in the lower atmosphere. Modifications of the lower atmosphere temperature gradients are intrinsically linked to atmospheric stability and dynamic motion.

Figure 4.1 demonstrates the interannual variability of sea ice both across the (a) whole Arctic (Pan-Arctic) and (b) the Barents-Kara (BK) seas. Sea ice has decreased consistently across all months, particularly during the autumn months. Extreme years such as autumn 2007 have received much attention, because of the magnitude of sea ice loss compared to other years [*Comiso et al.,* 2008]. Interannual variability is particularly prominent in autumn in both the BK seas and across the Arctic. If there is a link between regional sea ice variability and the wider circulation as summarised in *Smith et al.* [2017], year to year variations of millions of km^2 of ice may produce significant changes in circulation patterns not only locally but also remotely. Secondly, if regional

sea ice is not persistent on multi-year timescales and has a causal influence on the wider circulation, there may be un-tapped extratropical predictability if simulations of sea ice can improved. The relationship between sea ice and the atmosphere is bi-directional, so low sea ice might be the response of a particular atmospheric harbinger, or may cause a response in the atmosphere, making it particularly difficult to disentangle causality.

- **Is the relationship between autumn Arctic sea ice and the winter NAO reproduced in a skilful prediction system?**

Here, relationships are identified between sea ice and the wider circulation by determining whether the observed strong correlations found by *Wang et al.* [2017] and others prior is reproduced within a skilful model hindcast.

- **How does autumn Arctic sea ice relate to the wider winter circulation in observations and the skilful prediction system?**

The analysis is then extended to the relationship between autumn sea ice and the boreal hemispheric circulation; both in the troposphere and also the stratosphere. While a direct link between sea ice and the NAO may not be reproduced, deducing the link between sea ice and other parts of the climate system may provide clues as to why the model cannot reproduce the direct link, taking into account internal variability and model issues such as the signal to noise paradox [*Scaife and Smith,* 2018].

- **Does the relationship between Arctic sea ice and the NAO vary in time, using a long running coupled simulation?**

Separately, the CESM Large Ensemble is used to assess how stationary the link between sea ice and NAO is over the past century, complementing the recent work of *Kolstad and Screen* [2019]. Furthermore, a multi-century coupled simulation is also analysed to determine whether there is any periodicity in the relationship between sea ice and the NAO, perhaps due to slow-varying ocean variability.

These results provide the grounding for more specific experiments and analysis deducing the causality of these relationships. Therefore, this chapter focuses on the link, and not the causality, of sea ice with the wider circulation.

4.2 Ice-Atmosphere Co-Variability in Reanalysis

The observed statistical relationship between sea ice and the mid-latitude circulation is first explored. Key months preceding winter include October, identified by *Wang et al.* [2017] as containing the strongest correlation between Arctic sea ice and the winter NAO through PC analysis. Physical reasoning also suggests October is important for driving the winter AO through circulation anomalies over Siberia [*Kryjov,* 2015; *Kryjov and Min,* 2016]. To identify the statistical relationship between both pan-Arctic sea ice and regional ice variability in the Barents-Kara seas, a grid point correlation is performed with sea ice in October and Boreal winter, displayed in figure 4.2.

The instantaneous relationship between October sea ice and October mean sea level pressure is shown in the first column of figure 4.2. It has been shown that sea ice, snow cover and pressure patterns over Siberia are all related during autumn [*Gastineau et al.,* 2017], but recent studies show that pressure patterns over the Ural mountains drive changes in sea ice and snow [*Peings et al.,* 2019]. An anti-correlation extending from north-west Europe into Siberia is observed, implying that low sea ice is linked to high pressure over this region, both using regional BK ice as well as pan-Arctic sea ice. Particularly in the pan-Arctic case, an -AO like pattern can be seen in relation to low sea ice, also projecting onto the -NAO. Although instantaneous correlations can't help in deducing which drives which, it confirms a relationship between sea ice and the wider circulation during this important month.

Next, the lagged correlation between October ice and the winter mean sea level pressure pattern is analysed. This month has been employed as a predictor of the winter NAO using sea ice across the Arctic in other studies such as *Wang et al.* [2017], although they used EOF analysis to extract principal variability (much of which is contained in the Barents-Kara seas, see figure 3.10 in Chapter 3), rather than a weighted grid box area total to construct a sea ice index. Coherently when both October Pan-Arctic and BK sea ice is used, Eurasian/Siberian winter blocking occurs in relation to low sea ice. This pattern persists when winter sea ice is used. However, in the Atlantic sector, a strong relationship is only found when a lagged correlation between October BK sea ice and the winter circulation is used.

In order to better quantify the lagged relationship between Arctic sea ice and the winter NAO, figure 4.3 investigates the temporal variability of this correlation, along with

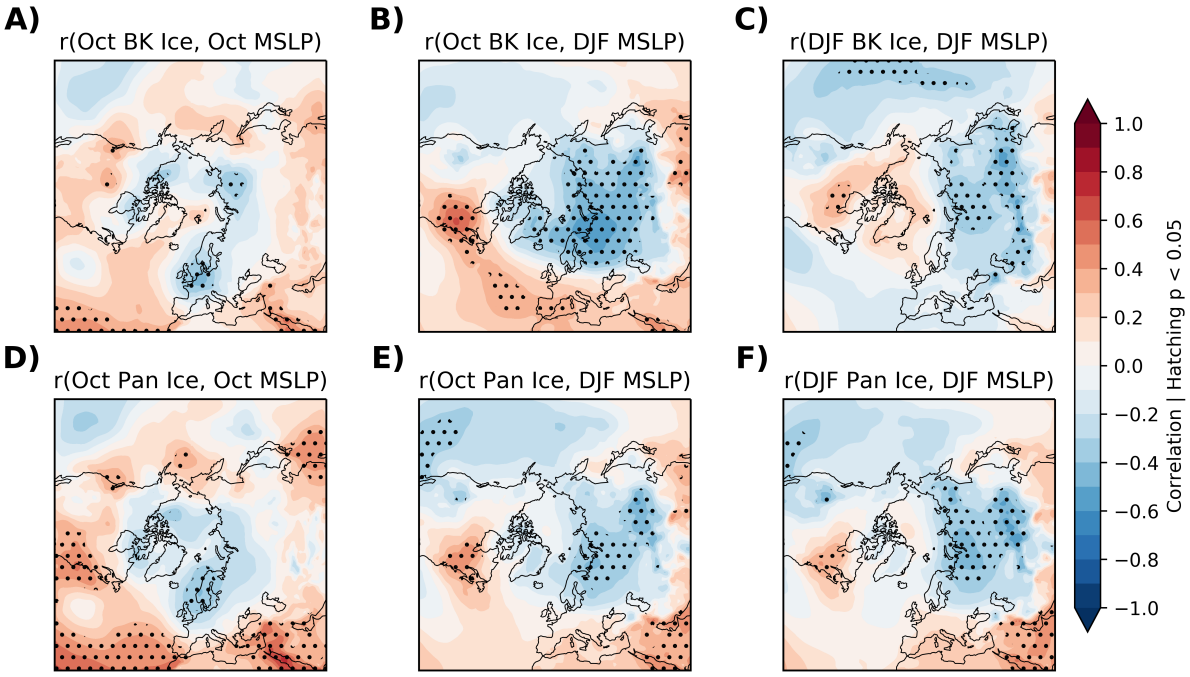

Figure 4.2: Correlation between both pan-Arctic and regional sea ice and October/Winter circulation patterns. Grid point correlation between the timeseries of sea ice, and mean sea level pressure. Hatching denotes regions in which the correlation is significant at the 5% level ($p < 0.05$). Ice region/time and mean sea level pressure months correlated are defined in the title of each panel.

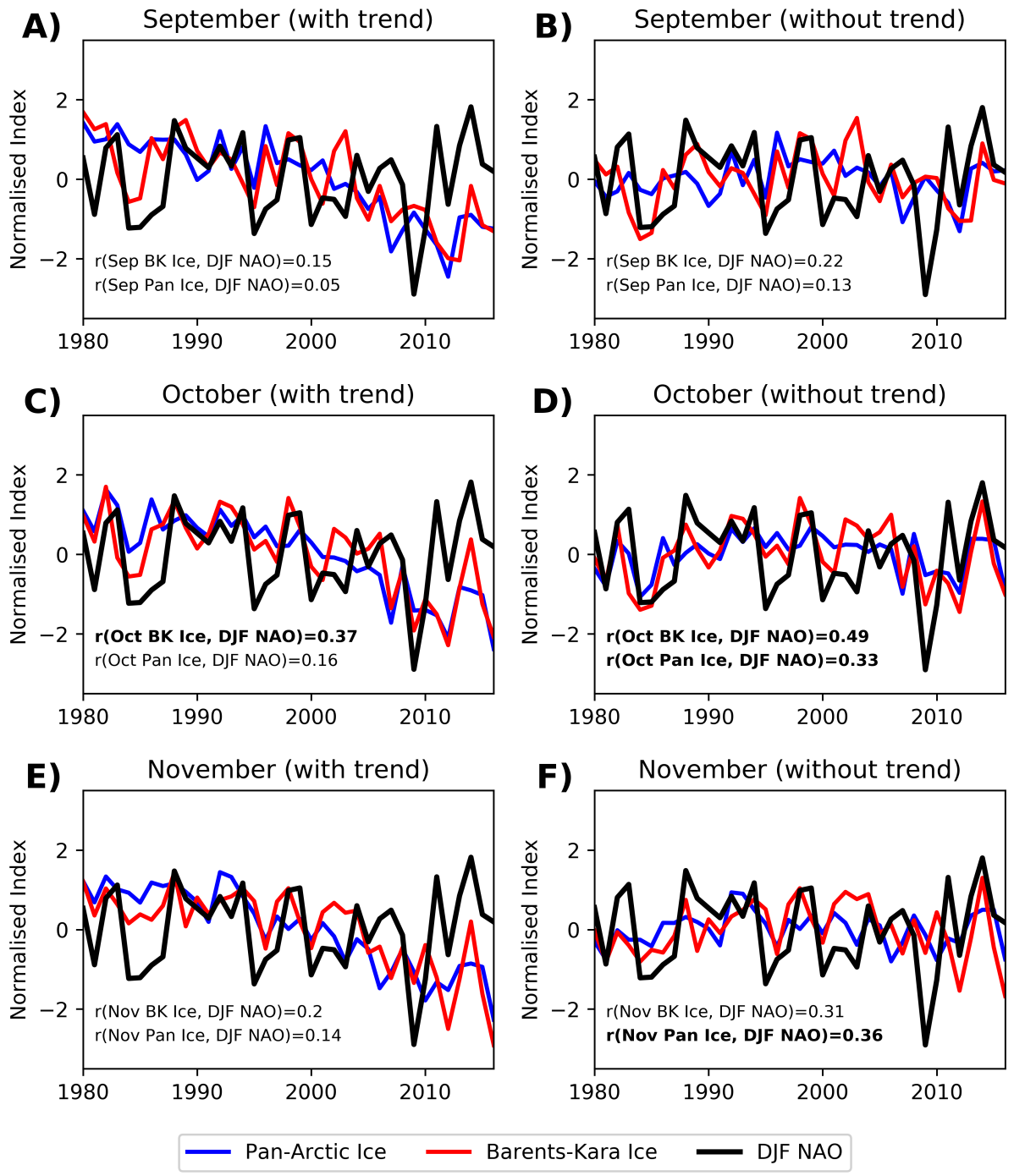

Figure 4.3: Correlation between both BK and pan-Arctic sea ice and the following winter NAO index. Normalised timeseries of autumn months sea ice (September - November) for both BK and pan-Arctic sea ice, along with the detrended timeseries. The linear Pearsons correlation coefficient is shown in each panel, statistically significant correlations at the 5% level are shown in bold.

its sensitivity to the trend pertinently present in sea ice. Correlation between sea ice and the winter NAO varies considerably from month to month, both regionally in the Barents-Kara seas as well as across the Arctic. A more surprising result is that the correlation between sea ice and the winter NAO weakens from October to November, despite being temporally closer to the NAO, and with sea ice carrying persistence on monthly timescales [*Blanchard-Wrigglesworth et al.,* 2011]. A physical relationship that could be proposed to explain this is that sea ice variability induces circulation anomalies locally which affect snow cover over Eurasia as proposed in *Gastineau et al.* [2017], which can reinforce the prior anomalous pattern in mid-Autumn, modulating wave propagation into the stratosphere in late autumn/early winter [*Kryjov,* 2015], where the stratosphere can later affect the NAO through troposphere-stratosphere coupling and sudden stratospheric warmings [*Hitchcock and Simpson,* 2014]. Given this chain of events, therefore, it could be posited that October sea ice is more important than November given increased sensitivity of the atmosphere to forcing in mid-autumn. This chain of events can be explored using an ensemble from a skilful coupled climate model, as discussed later in this chapter.

There is an increase in correlation is all autumn months and sea ice regions when the sea ice is detrended prior to computing the correlation. This suggests that the trend in sea ice is not linked to a trend in the NAO, or potentially offset by a tertiary component, or that the interannual variability is physically linked between sea ice and the NAO, but not the trend. Relationships of other components associated with the NAO variability (set out in Chapter 3) are explored more in the following chapter. BK sea ice in October correlates more strongly with the winter NAO without the trend; increasing from r=0.37 to 0.49, which is almost a doubling of variance explained in the NAO. When testing different months as predictors for the winter NAO, *Wang et al.* [2017] found correlations between the leading principal component of sea ice in October and the winter NAO of 0.51. However, in addition to detrending the data, to compute the principal component of sea ice they projected the EOF of October sea ice onto the SONDJF loading pattern of sea ice variability. This loading pattern builds in information about the NAO as it extends into winter, which can artificially inflate the correlation.

The reanalysis product used here, ERA-Interim, is driven by HadISST sea ice [*Dee et al.,* 2011]. A separate test is conducted outside of model simulations using sea ice concentrations from the Nimbus-7 passive microwave dataset [*Cavalieri et al.,* 1996] in

the BK seas region, along with station observations for mean sea level pressure in Iceland and Portugal [*Hurrell,* 2003], for the same temporal period/domain as used prior. This test is therefore independent of reanalysis and uses observations only. The correlation between the reanalysis NAO index (box method used in this thesis) and the station series is r=0.76 (for the same period 1980-2016), with the HadISST BK sea ice index and the microwave derived dataset correlated r=0.99. Using the observational products only, October BK sea ice and the winter NAO are correlated r=0.36 (0.45 when detrended). These values are both significant at the 5% and 1% level respectively, and are statistically indistinguishable from the correlations found in figure 4.3. This relationship between October sea ice and the winter NAO is therefore not an artificial construction from choice of model reanalysis or boundary forcing applied to the model used to generate the reanalysis.

These results suggest a strong but sensitive relationship between Barents-Kara sea ice in autumn and the winter NAO, dependent on the choice of month and detrending. As discussed in the literature review and in *Smith et al.* [2017], there are discrepancies in how models simulate a relationship, if any, between sea ice and the winter NAO. The next section of this chapter explores this further using a skilful decadal hindcast.

4.3 Ice-Atmosphere Coupling in a Hindcast System

Investigating the relationship between Arctic sea ice and mid-latitude winter weather is limited in observations, due to sampling uncertainty. With the observational record used here spanning 37 years (1980-2016 inclusive), internal variability can mask or inflate statistical relationships. For example, *Shi et al.* [2015] found NAO skill sensitive to the temporal period chosen for calculation, with lower skill also found over longer periods of time in similar indices such as the AO [*Shi et al.,* 2015; *Kumar and Chen,* 2017]. Therefore, these results suggest that it cannot be ruled out that the strong correlations between Arctic sea ice and the NAO found in figure 4.3 may be due to internal variability alone. To approach this issue, the skilful hindcast dataset DePreSys3 is used, spanning the equivalent period but with the inclusion of a 40 member ensemble. An advantage of this dataset is a sufficiently large sample to account for internal variability, and given the model has demonstrated skill in predicting the NAO well in advance [*Dunstone et al.,* 2016], is able to simulate at least some of the physical processes & teleconnections that

lead to NAO predictability.

Initially, Barents-Kara sea ice evolution in the model 16 month run (initialised at the start of November) is evaluated in figure 4.4. Modelled sea ice follows the very predictable seasonal cycle with a minima during September, though displays an ice loss bias during the summer months. This could be due to a variety of physical processes; sensitivity to the initialisation of sea ice thickness which is poorly constrained [*Dirkson et al.,* 2017], biases in wind which drives sea ice motion [*Blanchard-Wrigglesworth et al.,* 2011], or imbalances in the sea ice radiative energy budget (such as cloud biases). Sea ice biases have been reported in models throughout the year, not just in summer [e.g. *DeWeaver and Bitz,* 2006]. Here, this model bias recovers during winter; partly due to coastal constraints on ice growth area, reducing variability. Model skill (B) decreases steadily slowly with time, but skill is largely attributable to the trend as found in *Lindsay et al.* [2008], *Chevallier and Salas-Melia* [2012] and *Sigmond et al.* [2013], with little suggestion that skill is lost in a particular season. Despite this, skill after detrending is attainable at the 5% significance level 12 months after initialisation, longer than what other studies such as *Msadek et al.* [2014] have found. Model performance beyond 2 months is better than a simple persistence forecast at nearly all lead times, so the model has added value in simulating the atmosphere-ocean-ice system.

Interannual variance with month is represented well in the model, closely following reanalysis (C). A minimum in variability is found in February/March, attributable to maximum ice extent and the sea ice extent being constrained by the coastline. Maximum variance is found in summer surrounding the ice minima, but dips in September as there is little ice left in the Barents-Kara seas towards the end of the period. Finally, the model simulates an expected RPC of 1 throughout the seasons (D); unlike the signal-to-noise issues found within the NAO [*Scaife and Smith,* 2018], which means that variability in the ensemble mean is equatable to real world variability.

4.3.1 BK Sea Ice and the Winter Extratropical Circulation

The relationship between autumn sea ice in the Barents-Kara seas and the winter extratropical circulation is examined in the model, and compared to observational reanalysis. October-November averaged BK sea ice is used, given both October and November have been separately linked to the NAO from observations (e.g. *Wang et al.* [2017] and *Garcia-*

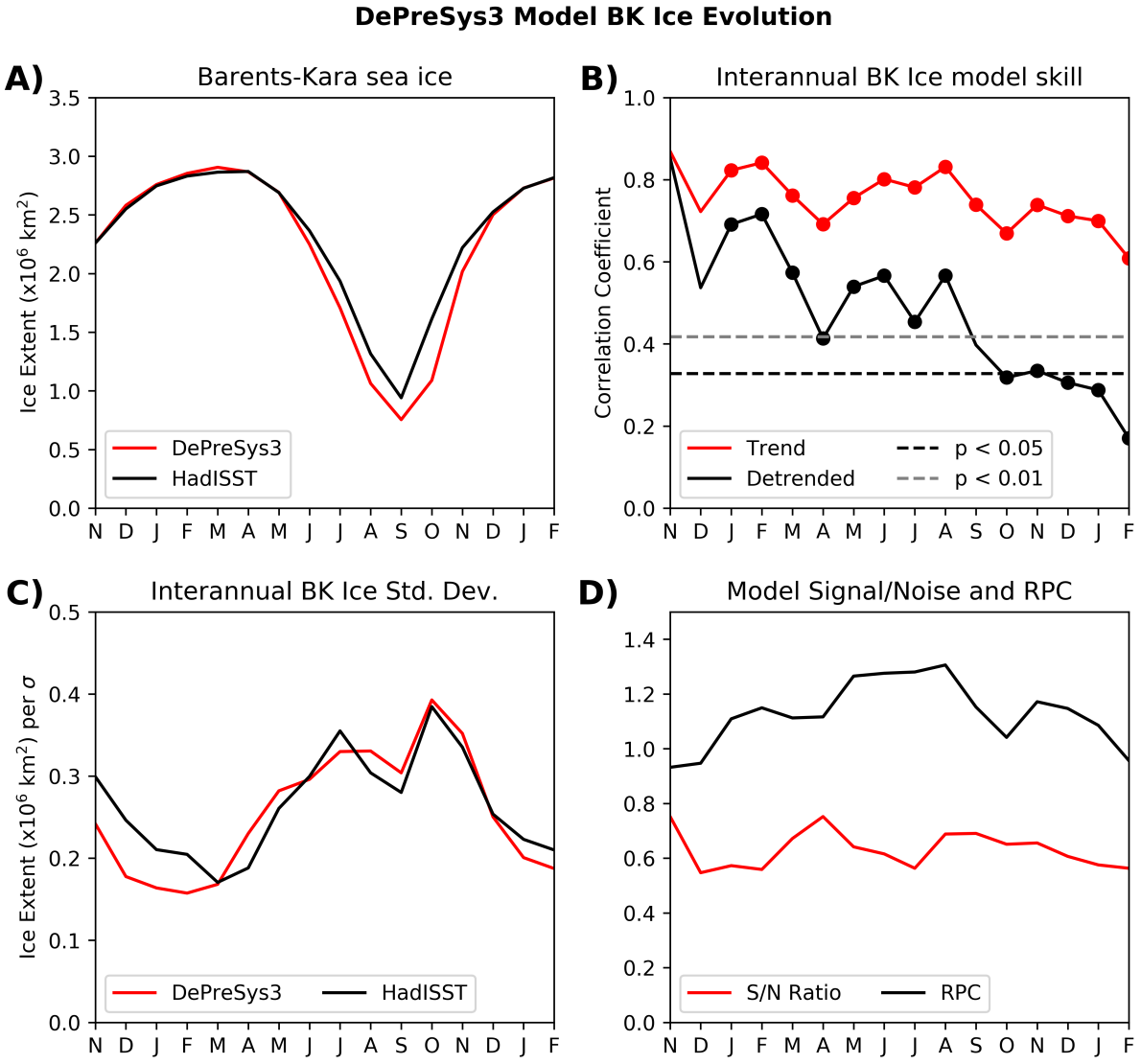

Figure 4.4: Evolution of Barents-Kara sea ice in DePreSys3. **A)** Seasonal cycle of sea ice extent in the Barents-Kara seas in HadISST and DePreSys3 for all years. **B)** Interannual correlation between the model ensemble mean and HadISST. A linear trend is removed for the detrended correlation. Thresholds for a statistically significant correlation are shown for a sample size of 36 years. Dots are plotted where the correlation is greater than the interannual correlation of November ice (initialisation) and the month in question (i.e. persistence). **C)** Standard deviation across all years (HadISST) as well as across all members (Model) for each month. **D)** Signal to noise ratio and the ratio of predictable components for each month (as defined in equation 2.1).

Serrano et al. [2015] respectively). While *Wang et al.* [2017] argues that October sea ice has the strongest link with the NAO, supported by analysis here in figure 4.3, *Garcia-Serrano et al.* [2015] argue that only November ice is statistically significantly linked to NAO variability when applying cross validation. Given that sea ice is known to carry a high degree of persistence [*Blanchart-Wrigglesworth et al.,* 2011; *Chevallier et al.,* 2013; *Guemas et al.,* 2016], a simple test of interannual persistence in BK sea ice from October to November is shown in table 4.1.

Dataset	**Correlation (%)**	**Detrended Correlation (%)**
Observations	0.85 (72%)	0.73 (53%)
Model Ensemble	0.82 (67%)	0.73 (53%)
Model Ens. Mean	0.98 (96%)	0.91 (83%)

Table 4.1: Linear Pearson's correlation coefficient (variance) between BK sea ice in October and November, as well as the linearly detrended version. For the model ensemble, as each year is statistically independent, the model is randomly sampled repeatedly to select an ensemble member for each year to generate a timeseries, equivalent to reanalysis, and the average correlation is computed. For the ensemble mean, all ensemble members are averaged before computing the correlation. Variance is calculated as the r^2 value. The second model winter is used.

These results demonstrate consistency in sea ice persistence across observations and the model ensemble. It also highlights that a large component (approximately 20%) of the variance between October and November sea ice is attributable to the trend. By removing this trend, less variance is shared, suggesting that October and November sea ice may have somewhat differing relationships with the winter circulation, which could explain the differences in *Wang et al.* [2017] and *Garcia-Serrano et al.* [2015], also discussed earlier. A very strong relationship is found in the model ensemble mean compared to treating ensemble members separately, suggesting a large degree of internal variability (which is removed by taking the ensemble mean, assuming the ensemble is large enough that residual internal variability is zero). Given the strong correlations throughout ($r > 0.7$), the choice of combining October and November BK sea ice is justifiable, whilst the two-month average will smooth out any synoptic-scale variability in the ice. The lag between October-November and the winter helps infer direction of a link between BK ice and the winter circulation, but cannot be used to argue causality.

The model, which is run for 16 months, contains two winters, both of which are skilfully predicted [*Dunstone et al.,* 2016]. The second model autumn and winter were used, given sufficient time for the model to evolve from initial conditions. Additionally, October ice cannot be evaluated in the model during the first autumn, as the model is initialised in November. Therefore, October-November averaged BK ice corresponds to 12-13 months lead time within the model, and the winter circulation patterns evaluated hereafter correspond in 14-16 months lead time in the analysis that follows.

The NAO

The relationship between October-November averaged BK sea ice and the NAO is explored within the model ensemble in figure 4.5. Firstly, a scatter plot of BK sea ice against the winter NAO, both in the model ensemble and observations. The advantage of using a model ensemble is the many realisations (sample size of 1440 used here, 40 members x 36 years), which can better account for internal variability during the period 1981-2017 inclusive analysed here. The model ensemble represents a Gaussian profile of BK sea ice and NAO variability, with few extreme outliers. It also suggests a low ice bias in the model compared to reanalysis (the latter of which are clustered at higher BK ice values), first suggested in figure 4.4.

The correlation of October-November averaged BK sea ice and the NAO is explored through randomly sub-sampling an ensemble member for each year, to construct a time-series which is directly comparable to observations. This is done 10000 times to produce a more robust statistic, and is shown by the kernel density estimate (KDE) in figure 4.5B. The average member correlation, along with the model ensemble mean correlation (taking the ensemble average first before calculating the correlation) is shown in the plot. Additionally, the correlation found in observations (along with the linearly detrended correlation) are displayed in the figure for reference. The model suggests the average relationship between October-November averaged BK ice and the winter NAO is weakly positive through sub-sampling ($r = 0.05$); much weaker than found in observations ($r = 0.3$). However, sub-sampling the ensemble reveals that the model can simulate the strong correlations found in observations (in the tail of the PDF), within its own internal variability. These results signify the average relationship between BK sea ice and the NAO is weak, but possible. Interestingly, the ensemble mean correlation, which

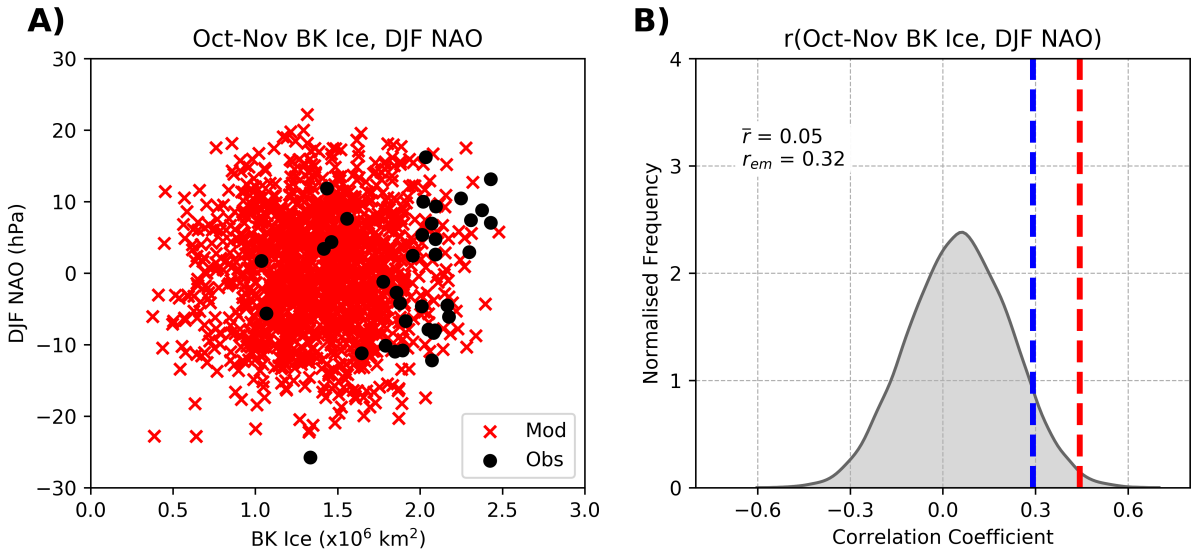

Figure 4.5: Relationship between late autumn sea ice and the winter NAO in the DePreSys3 model. **A)** Scatter plot of October-November averaged BK sea ice area, and the corresponding winter NAO index relative to population mean. This is shown for both all model ensemble members (second winter), and observations, for the period 1981-2017. **B)** PDF of the interannual correlation between BK sea and the winter NAO during 1981-2017, by repeatedly randomly sampling an ensemble member for each year and calculating the correlation of this with observations 10000 times, shown as a KDE distribution. Observed correlation (blue line), along with the detrended observations correlation (red line) are shown for comparison, along with the ensemble average correlation and ensemble mean correlation (averaging ensemble members before calculating correlation).

retains the predictable part of the relationship (cancelling out internal variability given a sufficiently large ensemble) indicates a positive correlation of similar strength/sign to observations. Although these two cannot be directly compared as one is a single realisation and the other is a combination of many, it suggests the model simulates some forced relationship between sea ice and the NAO (but may not be causal at this stage). The results found here are similarly reproduced when sea ice in the first model winter is used (e.g. November BK sea ice, DJF NAO at lead time 1, 2-4 months respectively).

The weak ensemble average relationship could be explained by the models signal-to-noise issue; where its simulation of extratropical teleconnections is erroneously weak [*Scaife and Smith,* 2018], and therefore may be underestimating the relationship between BK sea ice and the NAO. Additionally, the stronger link found in reanalysis may be due to selection-bias; studies such as *Wang et al.* [2017] exhaustively test different months

to find a strong correlation between sea ice and the NAO for use as a predictor. As demonstrated here, combinations of ensemble members in different years can produce equally strong correlations. Later in this chapter, a longer running coupled simulation is used to determine how likely this strong, observed correlation is over the past centuries.

Wider Hemispheric Relationship to BK Sea Ice

Analysis so far suggests the model underestimates the magnitude of the relationship between sea ice and the NAO compared to reanalysis. This may be due to signal-to-noise issues in the model, selection-bias or that the model relationship between ice and the midlatitude circulation manifests itself differently to reanalysis and doesn't project onto the NAO as strongly. The latter is explored here through evaluating the link between October-November averaged BK sea ice and the winter circulation patterns in figure 4.6.

3 different winter metrics are chosen to infer the link between sea ice and the winter circulation; MSLP (to understand circulation dynamics near the surface), 10 hPa geopotential height (to understand stratospheric polar vortex strength), and 2 metre temperature (to understand near-surface temperature variability).

The first row of panels shows the regression of October-November averaged BK sea ice on winter MSLP, for observations and the model. The model ensemble is re-sampled, through choosing a random ensemble member each year to create a timeseries which is directly comparable to observations. This is repeated 1000 times, and a pattern correlation is performed between each combination and the observed pattern in (A). This demonstrates whether the model can simulate the same regression pattern found in observations through its own internal variability, shown in (B). Finally, the model ensemble mean relationship is calculated and shown in panel (C), indicating the forced relationship separately from internal variability. The strong +NAO pattern related to high BK sea ice is shown in 4.6A; as previously learned in figure 4.2. Only regions over eastern USA and over the BK seas themselves are statistically significant; implying large interannual variability in this relationship (particularly over a limited 36 year period). Like the analysis presented earlier in 4.5, the model can simulate the same NAO relationship, as well as over the BK seas itself (4.6B). The forced relationship appears much weaker however (4.6C), although agrees largely on the sign of the relationship over the Atlantic sector. It doesn't show a strong relationship over the BK seas, however. Note that standardised

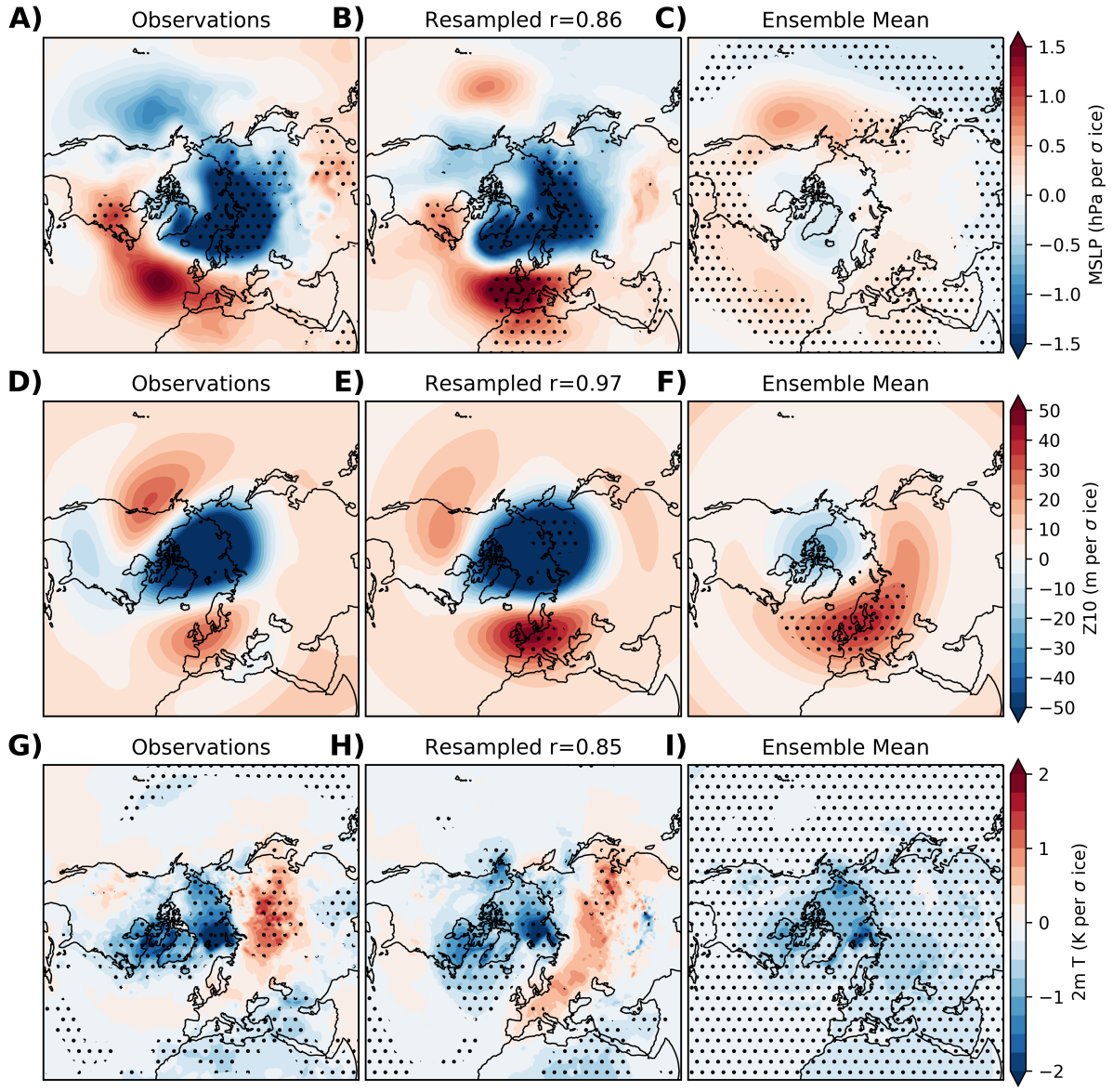

Figure 4.6: Relationship between late autumn sea ice and the winter circulation in the model and observations. A) Regressing standardised October-November averaged BK sea ice onto winter MSLP at each grid-point, in observations **B)** Randomly sampling an ensemble member for each year and applying the same procedure as in A. This is repeated 1000 times, and a pattern correlation is calculated to find the closest correlation with observations and plotted. The second model winter is used. **C)** Calculating the ensemble mean and repeating the procedure in A. **D-F)** Same as A-C except for 10hPa geopotential height. **G-I)** Same as A-C, except for 2 meter temperature. In all plots, regression coefficients that are statistically non-zero at the 5% level are stippled.

BK sea ice is used to regress onto the circulation; variance in BK sea ice is lower in the ensemble mean to that in observations ($\sigma_{OBS} = 0.35, \sigma_{MOD} = 0.23 \quad [\times 10^6 km^2]$).

The central panels D-F explore the relationship between sea ice and the winter stratosphere. Observations show a strong polar stratospheric vortex (decreased geopotential height) related to high BK ice. This is similar to studies such as *McKenna et al.* [2018] which show a weakening of the polar vortex associated with low BK sea ice, although this study was looking at end of century sea ice loss and not interannual variability explored here. Again, the model can reproduce this relationship within its own internal variability (4.6E), although the forced relationship is weaker. It does however capture the weak response over Eurasia found in observations, and is statistically significant too. This ridging related to high BK sea ice appears to be barotropic when comparing MSLP to stratospheric geopotential height in observations (A vs D) and within the models internal variability (B vs E), but not in the forced component (C vs F).

Ice variability has a strong thermodynamic relationship immediately surrounding the region through anomalous heat fluxes, identifiable throughout the model and observations in panels G-I. Secondary thermodynamic links are found over Siberia and east Asia, with cooling due to anticyclonic blocking found in both observations and within the models internal variability. This 'warm Arctic - cold continent' pattern has been identified in studies such as *Mori et al.* [2014], though it is proposed some modelling studies fail to capture this pattern due to incorrect sea ice-atmosphere coupling [*Cohen et al.,* 2013]. Other studies forcing a model separately with anthropogenic background warming or sea ice loss do not find a cooling trend over Eurasia, and conclude this is a strong articulation of internal variability [*Sun et al.,* 2016], though this is disputed by *Cohen et al.* [2012] who argue the recent cooling trend over Eurasia are physically justifiable. The forced link here shows that the model does not simulate any Eurasian warming in association with low sea ice, but again may be underestimating this due to signal-to-noise issues.

Polar Cap Height

The relationship between October-November averaged BK sea ice and the strength of the polar vortex is investigated, using the polar cap height. This is defined as the geopotential height averaged north of 60N, on each avaliable pressure level, and is therefore an effective integrative method of determining the strength of the polar vortex, which is inversely

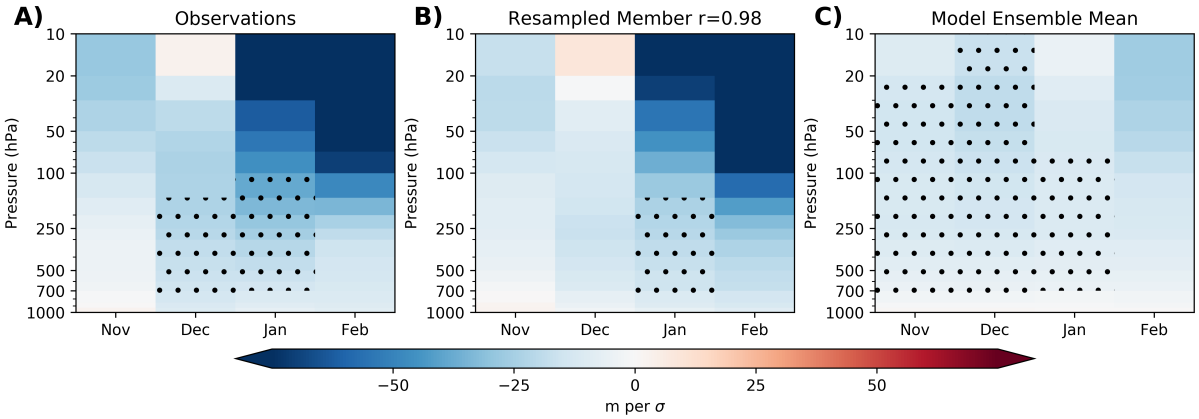

Figure 4.7: Regression of late autumn sea ice against the winter polar cap height in the model and observations. **A)** Regressing standardised October-November averaged BK sea ice onto winter polar cap height, defined as geopotential height averaged north of 60N across all longitudes, in observations. **B)** Randomly sampling an ensemble member for each year and applying the same procedure as in A. This is repeated 1000 times, and a pattern correlation is calculated to find the closest correlation with observations and plotted. The second model winter is used. **C)** Calculating the ensemble mean and repeating the procedure in A. In all plots, regression coefficients that are statistically non-zero at the 5% level are stippled.

proportional to the geopotential height surface [*Baldwin and Dunkerton,* 2001].

Studies have physically linked sea ice decline to a weakening of the polar vortex [*Kim et al.,* 2014]. Later in winter, troposphere-stratosphere coupling identified in reanalysis and reproducible in models suggest a NAO response in late winter [*Nakamura et al.,* 2015; *Ruggieri et al.,* 2016; *Jaiser et al.,* 2013]. Model evidence also suggests regional sea ice loss has differing impacts on the polar vortex [*McKenna et al.,* 2018]; Barents-Kara sea ice being one of the most influential in weakening the vortex. Mechanisms involve increased wave propagation into the stratosphere, weakening the polar vortex, as explained in Chapter 2. The analysis shown here in figure 4.7 suggests that the model can reproduce the strong polar vortex associated with high BK sea ice, particularly in late winter, extending down towards the surface by February. Given large interannual variability in the strength of the polar vortex, this stratospheric link in late winter is not statistically significant in the 36 year period. The forced relationship in the model agrees with the sign of the link (strong vortex with high ice), but is weaker than that found in observations. It also shows broader overall strengthening of both the tropospheric and stratospheric vortex associated with high BK ice, significant through the majority of the

early winter.

Jet Stream and Eddy Driven Jet

The extratropical jet stream (both the sub-tropical and eddy driven components) are well related to the NAO [*Woollings and Blackburn,* 2012; *Woollings et al.,* 2010]. The spatial structure of the winter jet and how it is related to variability in sea ice, both in observational reanalysis and the model, is investigated. Two approaches are taken; computing a zonal hemispheric average to examine the large-scale subtropical jet structure across the northern hemisphere, and a zonal average across the Atlantic sector, which isolates the localised eddy driven storm track across the North Atlantic directly related to the NAO [*Blackmon et al.,* 1977]. The Atlantic sector is averaged between 90°W and 30°E.

The regression pattern using observed BK sea ice on the winter jet shows a marked acceleration of the polar jet, extending down into the troposphere from the stratosphere (figure 4.8A). Strengthening of the polar vortex related to high BK ice is expected given the earlier result in figure 4.7; a decrease in geopotential height and cooling of the polar stratosphere will lead to stronger zonal winds through thermal wind balance. There is also evidence of a poleward shift of the eddy driven jet focused near 250hPa, 40°N in relation to high BK sea ice, which is linked to the +NAO favoured earlier. Additionally, despite many regression plots earlier being marginally significant at the 5% level, due to the limited sample length and large internal variability, this signal stands out. The signal in the troposphere becomes particularly amplified when the Atlantic sector is isolated (figure 4.8D); this might be in part due to the strong eddy-driven jet over this region than the hemispheric zonal average in general.

As found in prior analysis, the model can again simulate this BK sea ice link with the zonal wind profile through its own internal variability, matching the strength of the relationship as well as the key features in the stratospheric vortex and tropospheric eddy driven jet. Climatologically, contours show the model has no obvious bias in simulating the zonal mean jets either across the hemisphere or in the Atlantic sector during the period analysed (1981-2017). Finally, the forced link shown in figures 4.8C and D for the zonal hemispheric and Atlantic averages respectively show a similar link to that found in observations, albeit to a weaker degree. It captures the stronger polar vortex, and shifting

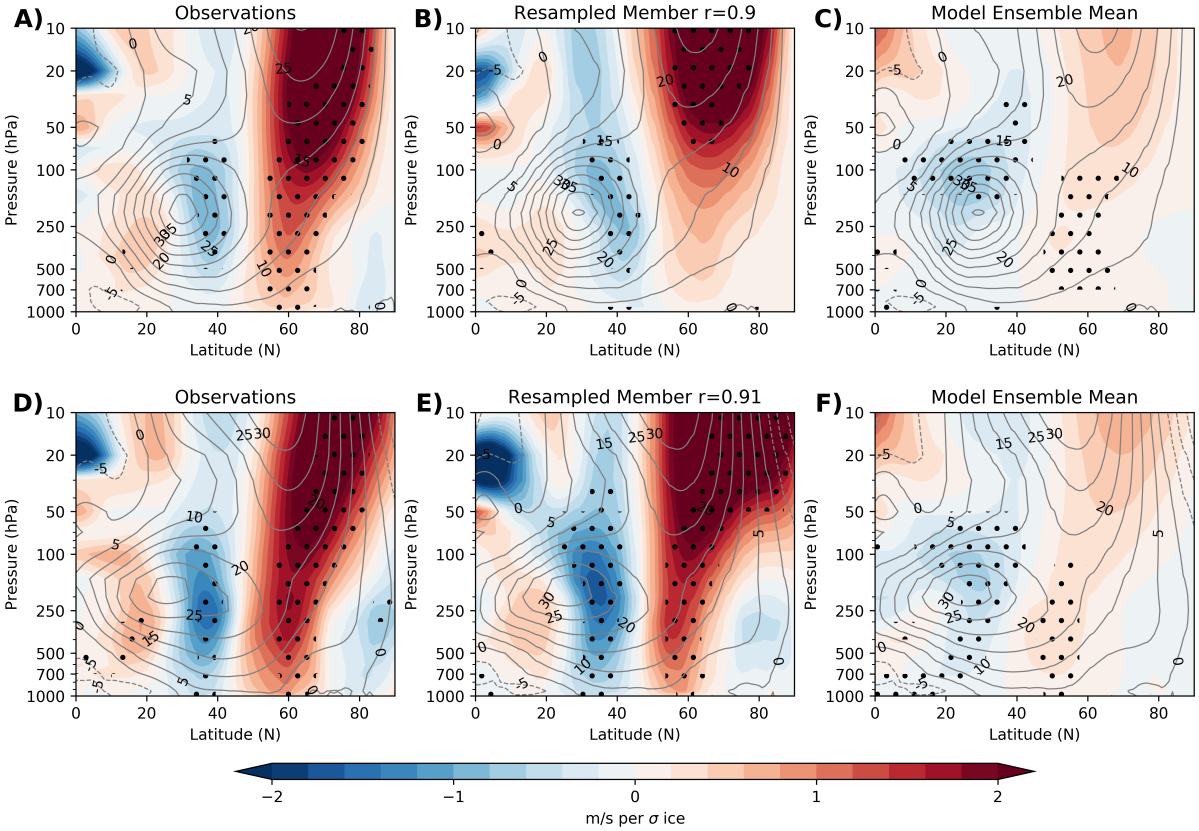

Figure 4.8: Regressing late autumn BK sea ice against cross sections of zonal wind in winter. **A)** Regressing standardised October-November averaged BK sea ice onto zonal-mean wind in winter, in observations. Climatological winds are shown in contours. **B)** Randomly sampling an ensemble member for each year and applying the same procedure as in A. This is repeated 1000 times, and a pattern correlation is calculated to find the closest correlation with observations and plotted. The second model winter is used. **C)** Calculating the ensemble mean and repeating the procedure in A. **D-F** Same as A-C, except calculating the zonal average wind over the Atlantic sector only (90°W-30°E). In all plots, regression coefficients that are statistically non-zero at the 5% level are stippled.

of the subtropical jet. These results, akin to that found in the polar cap height analysis as well as the analysis in figure 4.6, all suggest a large role for internal variability in explaining the observed strong links between late autumn BK sea ice and the winter circulation, whilst also suggesting there is a small forced component (that may be erroneously weak due to the signal-to-noise issue in dynamical models).

Dependence on QBO phase

It has been suggested that the QBO can modulate responses to Arctic ice loss in the extratropics and polar regions, and that during westerly phases, the QBO strengthens the polar vortex in response to sea ice forcing (vice-versa with easterly QBO forcing [*Labe et al.* 2019]. While this study focuses on sea ice decline in the future, it may be applicable to interannual variability in the recent climatological period assessed here; is a stronger link found when compositing based on QBO phase? The QBO here is defined as the zonal wind averaged averaged +/- 5° at the equator at 30hPa. The QBO is predictable, with strong interannual correlation between the model ensemble and observations even on the extended multi-year model lead time analysed here (winter QBO model ensemble mean correlation with observations $r = 0.7$, shown in figure 4.9A).

A key limitation of any analysis compositing the 36 year period into two groups based on the strength of the zonal wind associated with the QBO is the small sample size. Whilst the model contains a large ensemble, there is little ensemble spread even by the second model winter (figure 4.9A). This means that a composite will contain the same years (i.e. in any given year, all members will be in the same composite group, rather than being split, bar 2002-2004). Nevertheless, compositing using the ensemble mean will remove some internal variability and may demonstrate a statistically significant regression. The ensemble mean is taken, and years are split in half based on the upper and lower zonal wind speed in the region defined earlier. In the two groups (containing 18 years), October-November averaged BK sea ice is regressed onto the zonal mean zonal wind, shown in figure 4.9B,C for each group respectively. This analysis reveals that during the westerly phase, the link between high BK sea ice and a stronger polar vortex is substantially larger than when the QBO phase is easterly, to the degree where the link is significant even though the sample only contains 18 years. These results, although limited, support the conclusions of *Labe et al.* [2019] and hint that tropical variability in the QBO may

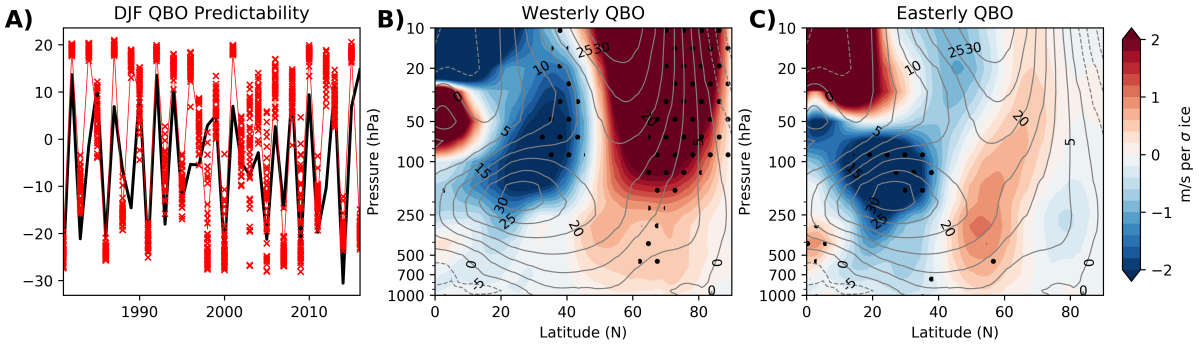

Figure 4.9: Regressing late autumn BK sea ice against zonal mean winter winds during QBO phases. **A)** Observed winter QBO index (here defined as 30hPa wind averaged between 5°N/S), along with the second model winter QBO index (red line showing ensemble mean, red crosses ensemble members). **B)** Regressing October-November averaged BK ice onto winter zonal winds, for the 18 lowest QBO years (Westerly phase), using the model ensemble mean. Stippling indicates the regression coefficient is statistically non-zero at the 5% level. Climatological winds are shown in the contours. **C)** Same as B, except for easterly phases.

mediate the relationship between sea ice and the extratropical circulation.

4.4 Stationarity of the Link Between BK Ice and the NAO

Sampling uncertainty with a relatively short observational period (37 years) restricts interpretation of the recently observed relationship between Barents-Kara sea ice and the NAO. Internal variability can be interrogated using model ensembles, although the periods used thus far matches that to observations, so do not take into account different background states which may be important in mediating a relationship between the Arctic and the midlatitudes [*Smith et al.,* 2017]. The CESM large ensemble provides a longer, free running coupled simulation that may pick up decadal and multi-decadal variability in slower varying processes in the ocean, which may mediate the interannual relationship between BK sea ice and the NAO evaluated in this thesis. Here, the strong link between October BK sea ice and the winter NAO is focused on [*Wang et al.,* 2017].

Firstly, the evolution of both October sea ice in the Barents-Kara seas and the winter NAO is explored in figure 4.10. Panels A and B display the timeseries of all members over the model run period (1920-2005), with C and D displaying the 30 year moving

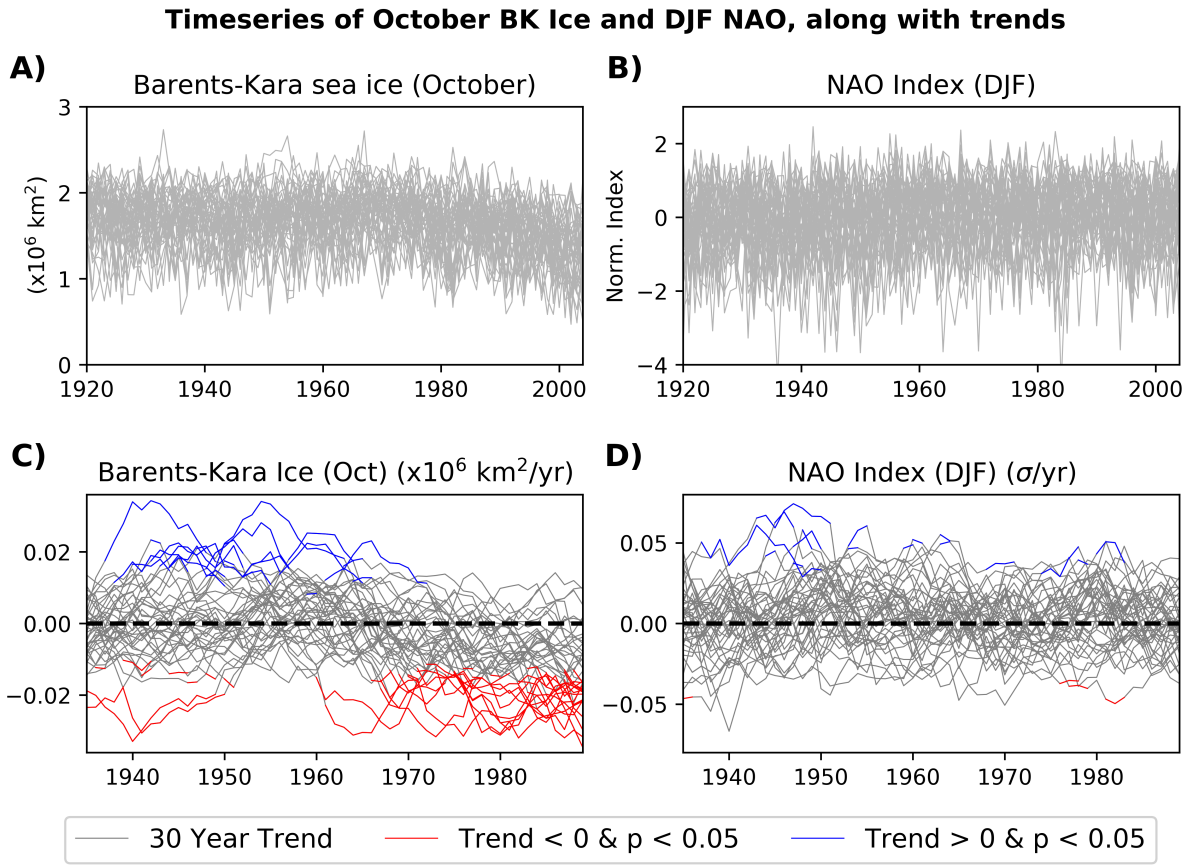

Figure 4.10: Evolution of October Barents-Kara sea ice and the winter NAO in the CESM Large Ensemble. **A,B)** Timeseries of Barents-Kara sea ice in October and the DJF NAO over the model run, with each ensemble member in grey. **C,D)** 30 year linear trends in the above timeseries; trends that are significantly non-zero at the 5% level are coloured depending on whether they are negative or positive

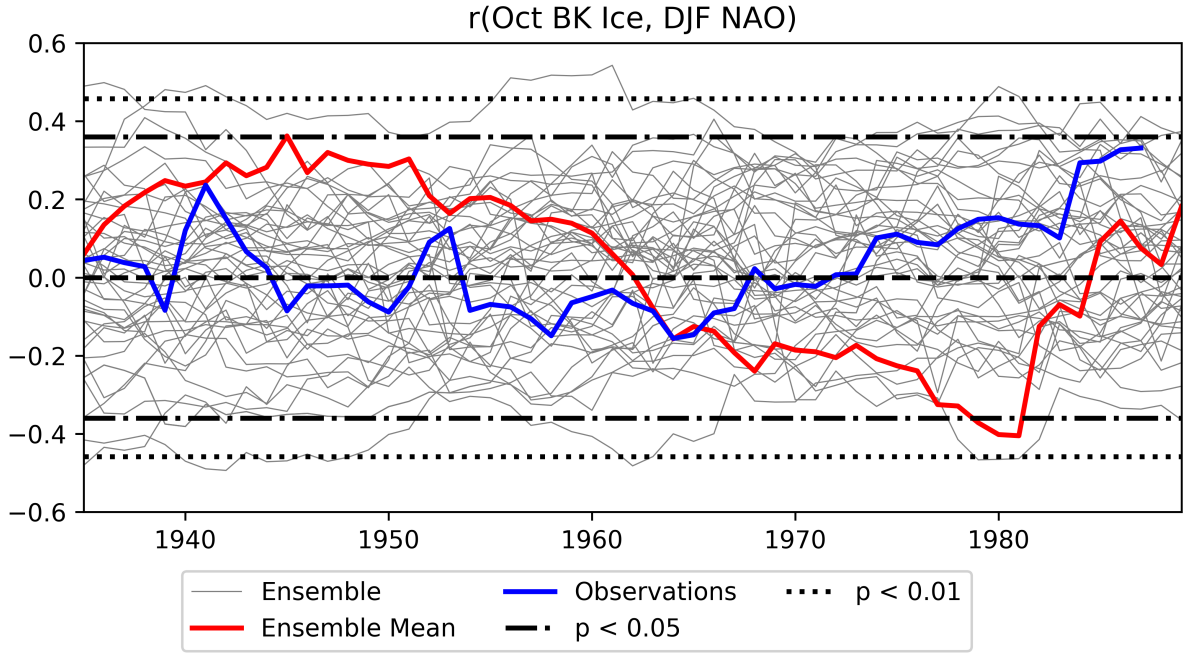

Figure 4.11: Correlation between sea ice and the NAO over multi-decadal timescales. 30 year moving correlation between October Barents-Kara sea ice and the winter NAO for the CESM ensemble (grey lines), ensemble mean (red line), and observations using HadISST/HadSLP data (blue line). Significance thresholds for a 30 year period are also shown at the 5% and 1% level.

trend. A negative trend is observed in sea ice towards the end of the century, with no obvious trend in the NAO index. There is little suggestion of significant decadal - multi-decadal variability in either of these fields, implying stationarity (bar the downward trend in sea ice), or at least not detectable from internal variability. Note that there is some uncertaintly in the HadISST derived sea ice pre satellite era (1979), given much less observational data to generate the product.

Trend analysis reveals that despite approximately half of ensemble members showing a significant decline in sea ice post 1980, many show a weak or even positive trend in sea ice. Between 1940-1960 there is support from a sub-sample of members for an significant increasing trend. Despite the model being forced with historic radiative forcing [*Kay et al.,* 2015], Barents-Kara sea ice post the summer minima can vary substantially due to internal variability. The 30 year moving correlation between October Barents-Kara sea ice and the winter NAO is next considered, both for the ensemble, the ensemble mean, and observations. This analysis, presented in figure 4.11, demonstrates a highly variable relationship over the past century that regularly switches sign. Recent correlations of 0.3-

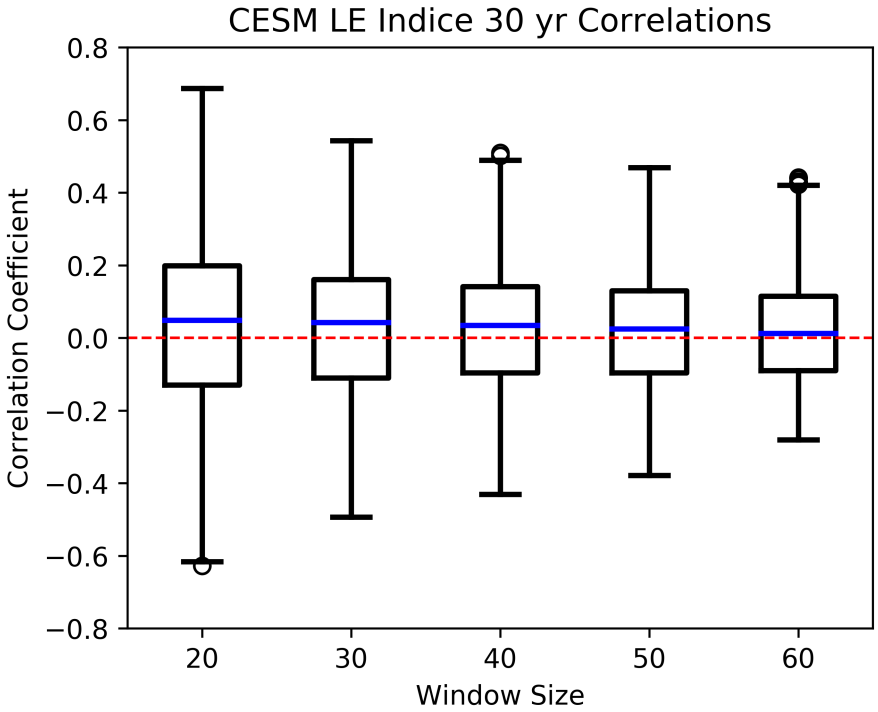

Figure 4.12: CESM sensitivity to the size of the window used for moving correlations. Box and whisker plot of all CESM ensemble members correlation between October Barents-Kara sea ice and the winter NAO, using different window sizes.

0.4 as found in the 1980-2017 reanalysis period appear unique, with a few isolated members replicating such a high correlation over the past century. The ensemble mean, which retains the predictable part of the signal, suggests a slow variation in the relationship between BK ice and the NAO relationship; varying from a positive correlation 1940-1960 towards a negative correlation by 1980. Possible factors that may modulated this relationship may be multi-decadal oceanic variability such as the Atlantic Meridional Overturning circulation.

Sensitivity to the window size used for the moving correlation is investigated in figure 4.12. Window sizes from 20 years (short, high frequency variability) to 60 years (long, low frequency variability) was tested. This analysis shows the correlation, with the median around zero, is influenced little by the choice of window; although high correlations can be found within the ensemble. Statistically significant correlations can be found over long, 60 year periods, but these are rare, and can be expected given the p threshold of 5 % (i.e. 1 in 20 chance that the correlation could be randomly observed). These results suggest strong internal variability within the sea ice and the NAO, and that the recently observed strong correlations may be by chance and have occurred previously, even though

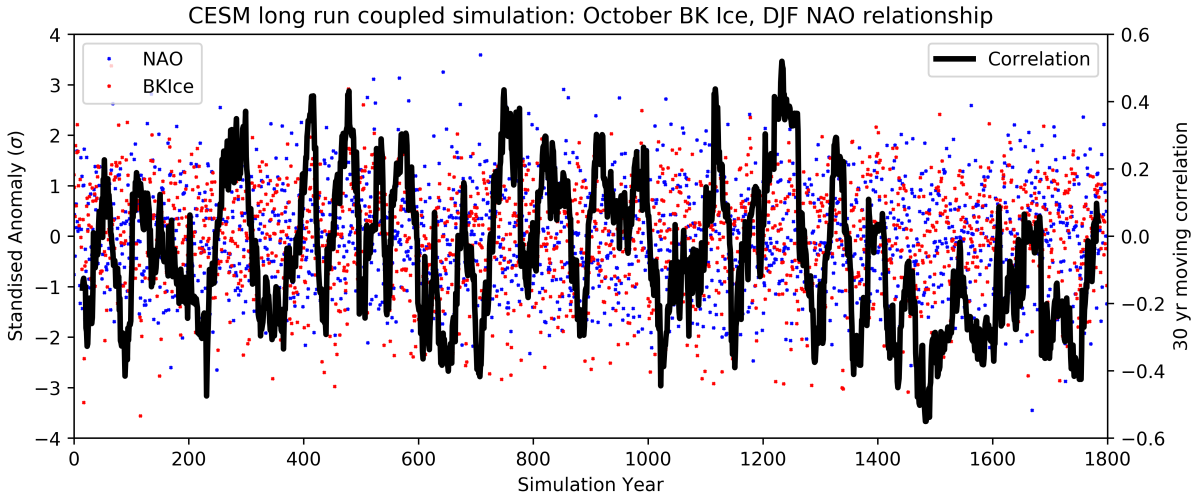

Figure 4.13: Correlation between October BK ice and the winter NAO in a long run CESM simulation. October BK sea ice and the winter NAO over the 1800 year CESM coupled simulation (standardised about their mean and variance), shown by crosses to indicate general spread through the model run. The thick black line is a 30 year (representative of a climate period) moving correlation between October BK sea ice and the DJF NAO.

the average correlation is near zero. This non-stationarity of the relationship casts doubts on the viability of sea ice to be used as a linear statistical predictor for the NAO, such as in *Wang et al.* [2017], as the relationship changes over time.

Finally, the potential of multi-decadal variability mediating the relationship between BK sea ice and the NAO is explored using the coupled free-running CESM model. While this model is deterministic, is provides an opportunity for slower oceanic components to vary on multi-century timescales. BK sea ice and the NAO are highly variable during this 1800 year simulation (figure 4.13). Additionally, the 30 year moving correlation between BK sea ice and the NAO is calculated as in figure 4.11. The results, presented in figure 4.13, imply a highly variable relationship, fluctuating between positive and negative correlations with no obvious periodicity behind this. Again, the magnitude of recently observed correlations (0.4) in reanalysis are found during periods in the model.

These results using the CESM support the the idea that the strong correlations between BK sea ice and the NAO could well be due to internal variability, and that models can reproduce this.

4.5 Conclusions

This chapter explored the relationship between Arctic sea ice and the mid-latitude circulation, using both observational reanalysis, as well as a coupled hindcast forecast model which has skill in predicting the NAO up to a year out [*Dunstone et al.,* 2016]. An advantage to using a model containing a large ensemble is that it can better account for internal variability; additionally the model in question here has a proven record of simulating teleconnections effectively (in order to predict the NAO on timescales where persistence alone cannot account for the predictability). Additionally, a longer free running ensemble simulation was used to assess the stationarity of the relationship between BK sea ice and the NAO.

- **Is the autumn Arctic sea ice, winter NAO relationship reproducible in a skilful prediction system?**

Strong lagged relationships were identified between autumn Arctic sea ice and the winter NAO in observations, especially when BK sea ice was used in October. This was particularly strong if sea ice is detrended prior to analysis, akin to studies such as [*Wang et al.,* 2017]. This strong relationship is not observed in the hindcast model however, which demonstrates a weak and variable relationship between BK sea ice and the NAO. However, the model can reproduce the relationship between sea ice and the NAO within its internal variability. Additionally, the forced component of the relationship (through taking the ensemble mean) suggests there is a statistically significant correlation between BK sea ice and the DJF NAO.

- **How does autumn Arctic sea ice relate to the wider winter circulation in observations and the skilful prediction system?**

The model can reproduce the link between BK sea ice and the winter circulation in every metric investigated, through its internal variability. Like the NAO analysis, it was found that the forced component (isolated through taking the ensemble mean) was much weaker, but generally agreed on the sign found in observations. This weaker forced link may be due to the model under-representing the teleconnection, perhaps due to signal-to-noise issues present [*Scaife and Smith,* 2018], or that the real relationship is weaker and the observed links are unusual (but possible). Compositing by QBO phase, as motivated

by *Labe et al.* [2019], revealed a stronger regression between BK sea ice and the polar vortex when the phase is westerly, supporting the conclusions of *Labe et al.* [2019].

- **Does the Arctic sea ice, NAO relationship vary in time in a long running coupled simulation?**

Supporting the findings from DePreSys3, where the relationship between BK sea ice and the NAO was found to be highly variable within the ensemble, the CESM large ensemble also suggests the more recent relationship between BK ice and the NAO is rare, but reproducible within in a model environment. This relationship does not only vary across an ensemble taking into account internal variability, but also over a longer period where trends in sea ice were stationary. Additionally, there appears to be no obvious forced component of the varying correlation of BK sea ice and the NAO through examining a 1800 year coupled simulation.

It is not possible to infer causality from correlation and regression analysis alone, even with lags, when many competing factors are at play. The lack of consensus in literature found between Arctic sea ice and the mid-latitude may be in part due to the difficulty of disentangling causal drivers. Additionally, the non-stationarity of sea ice, and large component of internal variability of the sea ice - NAO relationship makes it challenging to identify causal links. In this chapter evidence has been presented of a relationship between sea ice and variability in the winter circulation, both in reanalysis and observations, which needs accounting for and motivates the remaining chapters in this thesis. Future chapters explore co-varying drivers such as tropical rainfall, and employ statistical and dynamical techniques to better understand the causality of the BK sea ice relationship with the winter extratropical atmospheric circulation.

Chapter 5

Tropical Origins of the Link between BK Sea Ice and the NAO

This chapter builds on the previously identified link between Arctic sea ice and the winter atmospheric circulation in the extratropics, by investigating whether tropical variability can account for these links. This is approached both using a decadal hindcast dataset and observational reanalysis, employing statistical techniques such as multiple linear regression and causal effect network (CEN) analysis.

5.1 Introduction

Teleconnections between the tropics and the mid-latitude circulation have been well documented and known about for many decades [*Sardeshmukh and Hoskins,* 1988]. Changes in the coupled ocean-atmosphere system in the tropical basins, such as ENSO in the Pacific, modify the larger scale atmospheric circulation above [*Bjerknes,* 1969]: vorticity sources in the upper troposphere can generate Rossby waves that propagate polewards [*Trenberth et al.,* 1998], interacting with the mid-latitude jet [*Scaife et al.,* 2017]. Modulation of the Aleutian Low is the most direct tropospheric pathway linking tropical variability to the mid-latitudes via a stationary wave train. More remote teleconnections linking the tropical Pacific to the Atlantic sector, including the NAO, remain more complex and may involve non-linearities [*Toniazzo and Scaife,* 2006]. Additionally, reproducing the relationship within a model may be model dependent, particularly in how well resolved the stratosphere is [*Ineson and Scaife,* 2009]. Recent empirical and dynamical modelling

evidence shows strong links between tropical basins and the NAO [*Greatbatch et al.,* 2012; *Scaife et al.,* 2017; *Maidens et al.,* 2019].

More recently, research has focused on tropical to Arctic teleconnections, mediated by the mid-latitude circulation. Intra-seasonal variability in the tropics, such as the MJO, has been directly linked to poleward fluxes of moisture and heat on sub-monthly timescales into the Arctic [*Henderson et al.,* 2014; *Yoo et al.,* 2011], in both summer and winter. Convection in the west Pacific is typically identified as a key source region that can generate Rossby waves that penetrate the Arctic [*Lee et al.,* 2011; *Lee,* 2012; *Lee,* 2014]. Furthermore, the recent trend in Arctic sea ice has been part attributed to internal modes of tropical variability [*Gong et al.,* 2017; *Ding et al.,* 2019], implying a causal relationship between the two. Much of this recent analysis relies heavily on observational records, which are limited in length and do not isolate forced signals from internal variability; particularly for lower frequency modes of tropical variability such as the Pacific Decadal Oscillation (PDO) which are under-sampled in reanalysis [*Mantua and Hare,* 2002; *Macdonald and Case,* 2005]. Further work needs to be undertaken to understand how the Arctic climate can be modulated by tropical variability.

The previous chapter explored the relationship between BK sea ice in autumn and the winter mid-latitude circulation, specifically the NAO. Both observations and two sets of model simulation were used; a skilful hindcast and a free running coupled model. While a strong relationship between October BK sea ice and the NAO was identified in observations, this was conditional on de-trending and it is sensitive to the month chosen for analysis. Using large ensembles from the two simulations, the relationship between BK ice and the NAO appears to be highly variable and non-stationary over a longer period, as also found in *Kolstad and Screen* [2019]. Both models could however reproduce this relationship of the same strength as observations (as well as a relationship of opposite sign) due to internal variability. These results suggest that the recently observed relationship is within the upper bound of natural variability, but there is no apparent forced relationship. This interpretation is complicated by a weak NAO signal in models (the so-called signal-to-noise paradox, e.g. *Scaife and Smith* [2018], where the sea ice – NAO teleconnection may be under-represented. Additionally, the ensemble mean of the skilful hindcast model, indicates a weak relationship between the BK sea ice and the NAO.

This chapter brings together the idea that tropical variability, that has been shown to

affect both Arctic sea ice and the NAO, may be behind the apparent relationship between sea ice and the NAO. If the relationship between sea ice and the NAO is non-causal and symptomatic of tropical sources, then the non-stationarity and sensitivity of the ice-NAO relationship may be in part controlled by the tropics. This is explored in a variety of ways.

- **Does tropical rainfall contribute to the variance shared between BK sea ice and the NAO in reanalysis?**

Firstly, co-variability between tropical rainfall, the NAO and BK sea ice is explored within a multiple linear regression framework to identify a possible incidental relationship between BK sea ice and the NAO due to tropical rainfall in reanalysis.

- **What predictable components of the climate system contribute to skilful NAO predictions?**

Predictable components that have been linked to NAO variability are investigated in the first and second model winter of the decadal hindcast; the second winter has minimal influence from the initial atmospheric conditions, and any NAO skill must originate from slower varying components of the climate system that exert predictability at this lead time. Additionally, sub-sampling the model ensemble is undertaken to determine whether improved predictability of the NAO can be obtained through improved prediction of these components.

- **Can causal effect network analysis help distinguish causal from incidental drivers of the NAO?**

Finally, the hypothesis that tropical rainfall can partially account for the relationship between BK sea ice and the NAO is tested using a more robust statistical method than correlations and regressions alone. Causal effect network (CEN) analysis [*Runge et al.,* 2015] is employed, a statistical tool to identify causal relationships by identifying auto-correlation, symptomatic and co-varying relationships between nodes. This analysis motivates the final question of this chapter:

These results will provide improved understanding of the co-variability of the link between sea ice and the NAO with tropical rainfall, supporting the next two chapters which employ more idealised experimental designs to determine causal relationships.

5.2 Co-variability in Sea Ice, Tropical Rainfall and the NAO

Co-variability between early autumn tropical rainfall, late autumn Barents Kara sea ice and the winter NAO was explored in reanalysis. With the NAO linked to both tropical rainfall and sea ice variability [e.g. *Toniazzo and Scaife,* 2006; *Mori et al.,* 2014]; the latter two themselves being linked [*Henderson et al.,* 2014], it can be posited that one of these links may not be causal or at least partly symptomatic of the other real, physical relationship. In this section these ideas are explored briefly with a simple linear regression model.

Firstly, linear co-variability is explored between BK sea ice, tropical rainfall and the NAO in a multiple linear regression framework. October-November averaged BK sea ice, September-October averaged rainfall in the 4 tropical basins, and the winter NAO index are used. The choice of 2 month averages is to smooth high-frequency variability (particularly in rainfall) as the interannual relationship is being investigated here. Note that all fields are detrended prior to analysis in order to isolate interannual variability from any trends present. To begin, rainfall in the east and west tropical Pacific are linearly combined within a multiple linear regression framework and optimally fitted to explain variance in BK sea ice, such that:

$$BK = M + E, \qquad M = \alpha EP + \beta WP + c \tag{5.1}$$

Where M and E represent the linear regression model and residual error term respectively, EP is East Pacific rainfall, WP is West Pacific rainfall, α, β are weighting coefficients and c is the y intercept. The variance that the regression model explains in BK sea ice can be calculated by taking the correlation between the regression model and the predictand (in this case BK ice), i.e. $r(M, BK)^2$. This model can explain $\sim 20\%$ of BK variability ($r = 0.41, p < 0.05$). That is, tropical Pacific rainfall in early autumn can explain $\sim 20\%$ of BK ice variability in late autumn. Similarly, using the same two rainfall boxes to fit to the DJF NAO ($NAO = M + E$, where $M = \alpha EP + \beta WP + c$), $\sim 20\%$ of the variance can be explained ($r = 0.42, p < 0.05$). This confirms that in reanalysis, rainfall in the tropical Pacific is related to both BK sea ice and the NAO (i.e. a common link).

Given that late autumn BK ice and the DJF NAO are also well correlated, sharing $\sim 20\%$ variability ($r = 0.44, p < 0.05$), also previously shown in *Wang et al.* [2017], the degree to which tropical Pacific rainfall can explain this correlation is tested. To account for how much of the strong relationship between BK ice and the NAO is incidental to tropical variability, a new regression model is formed including BK ice, to predict the DJF NAO.

$$NAO = M + E, \qquad M = \alpha EP + \beta WP + \gamma BK + c \tag{5.2}$$

Like before, M and E represent the linear regression model and error term respectively, EP is East Pacific rainfall, WP is West Pacific rainfall, BK is BK ice, and α, β, γ are weighting coefficients with the y intercept c. In this case, $r(M, NAO) = 0.52$ (27% variance, $p < 0.05$). This model explains 9% more variance in the NAO than using tropical rainfall alone, as a result of including BK ice. Therefore, of the 19% variance BK ice alone explains in the NAO, 10% co-varies with tropical rainfall. Direction of potential causality can be inferred through the lag between tropical rainfall, sea ice and the NAO, along with literature suggesting tropical Pacific variability can modify sea ice through Rossby wave propagation (e.g. *Lee,* 2011; *Henderson et al.,* 2014). No studies to the authors knowledge have shown a causal link of Arctic sea ice driving changes in the tropics on interannual timescales.

This linear regression analysis suggests part of the relationship between BK sea ice and the NAO is accountable to tropical variability. However, the link between BK ice and the NAO was is dependent on detrending, and has limited reproducibility in a model ensemble. Permutations of the tropical rainfall, ice, NAO links are summarised in figure 5.1. While tropical dynamics exert a tangible influence on the NAO, confirmed in both observations and modelling studies, various combinations of causal and incidental pathways exist. The analysis here suggests 5.1B is likely, with the link between ON ice and DJF NAO partially symptomatic of tropical variability, although at this stage other combinations cannot be ruled out. This is explored further within the DePreSys3 model hindcast.

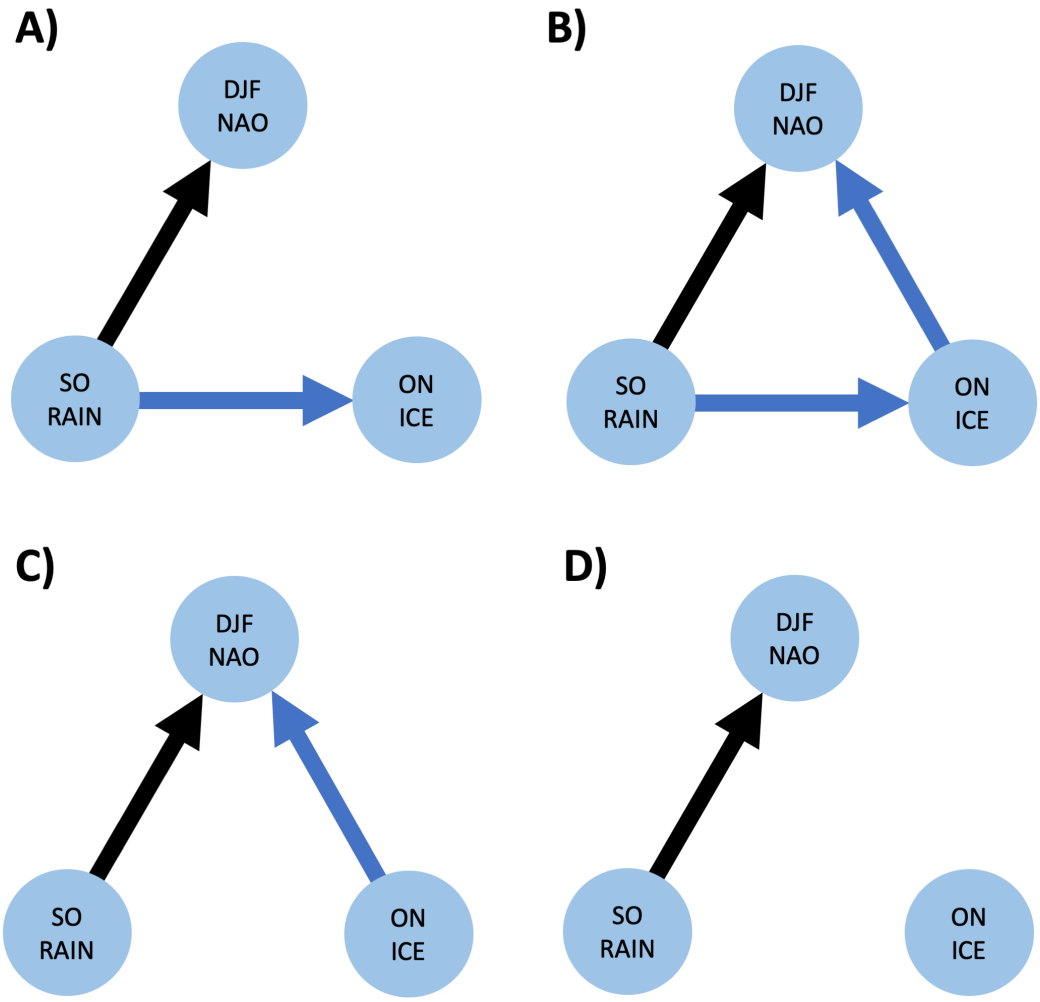

Figure 5.1: Schematic of the permutations of the tropical rainfall, ice and NAO co-variability. In all cases, the link between autumn tropical rainfall variability through to the winter NAO is well understood through ENSO/MJO dynamics. **A)** Case where tropical rainfall can influence sea ice variability, but sea ice variability does not map onto NAO variability. **B)** Case where tropical rainfall maps onto ice variability, which also maps onto NAO variability and may be co-incidental or independent to tropical variability. **C)** Case where tropical variability has no influence on sea ice variability, and that sea ice variability is independently inducing NAO variability. **D)** Case where sea ice is not affected by tropical variability and does not affect the NAO, and is completely independent. In all cases, SO = September/October average, ON = October/November average, DJF = December to February average.

5.3 NAO Predictability

Sources of NAO predictability are explored within the hindcast, for both the first and second winter. *Scaife et al.* [2014] and more recently *Dunstone et al.* [2016] found NAO skill of 0.6 (defined as the correlation of the model ensemble mean and reanalysis NAO index) using HadGEM3 models, with correlations of > 0.8 using large multi-model ensembles [*Athanasiadis et al.,* 2017; *Baker et al.,* 2018]. Despite DePreSys3 being able to reproduce 30% of the variance in the first winter NAO, the model ensemble mean has a weak amplitude compared to observations [*Scaife and Smith,* 2018]. NAO skill in DePreSys3 also extends into the second winter ($r = 0.4$); next the sources of this skill are determined. While many studies posit that NAO predictability originates in the tropics (e.g. *Ferranti et al.* [1990] followed by many others), other studies have suggested Arctic sea ice in the Kara seas (e.g. *Scaife et al.* [2014]) may be a source of NAO predictability. Sea ice is also widely used in statistical models as an empirical NAO predictor, given its correlation with the NAO [*Wang et al.,* 2017; *Hall et al.,* 2017].

Model skill in predicting commonly cited drivers of the winter NAO are explored. Tropical rainfall indices are used as in *Scaife et al.* [2017], along with BK sea ice [*Wang et al.,* 2017], the stratospheric polar vortex [*Nie et al.,* 2019; *O'Reilly et al.,* 2019], ENSO [*Toniazzo and Scaife,* 2006] and the Atlantic SST tripole [*Rodwell et al.,* 1999]. Model skill in the first winter (lead time of 2-4 months) is investigated in each driver and compared to a simple persistence forecast. This persistence forecast is constructed by comparing interannual correlation between November (when the model is initialised) and the following winter for each driver using reanalysis. The analysis is shown in the top half of figure 5.2.

Tropical Pacific rainfall is highly predictable at a few months lead time, particularly in the east Pacific due to the predictable nature of ENSO on these timescales [e.g. *Latif et al.,* 1998]. The model ensemble also contains less spread, with a larger signal-to-noise ratio in the tropical Pacific, compared to other basins. All tropical basins are predicted better than persistence, despite high autocorrelation. A large degree of model skill in sea ice originates from the downward trend (as discussed in figure 3.9), though with a large spread in ensemble members. The stratospheric polar vortex, which is closely related to the NAO, particularly during SSW events [*Hitchcock and Simpson,* 2014], is only reproduced in a limited capacity with a very large ensemble spread, despite persistence in initial

conditions [*Stockdale et al.,* 2015; *Nie et al.,* 2019]. Finally, the Atlantic tripole index is well reproduced; though carries a lot of persistence through late autumn into winter.

Predictability of BK sea ice, the stratospheric polar vortex and Atlantic tripole may also be symptomatic of a predictable winter NAO, given relationships are bi-directional. Predictability of the stratospheric polar vortex may be hindered by large month to month variability, which is damped in the DJF average. Given the high predictability in the tropical Pacific, as well as BK sea ice due to persistence in the initial conditions in the model and real world, the second winter is also evaluated at model lead times of over a year. The system has then had time to evolve from initial conditions (as tested through persistence), and yet retains NAO predictability [*Dunstone et al.,* 2016].

During the second winter of the model simulation (lead time 14-16 months, figure 5.2B), model skill reduces as expected. Persistence in all drivers is non existent from November through to the winter the year after, bar BK ice due to the strong trend in sea ice. The tropical Pacific retains some degree of skill on this extended lead time (ENSO skill $r = 0.46$), along with the tropical Atlantic; which is closely related to the tropical Pacific through rearrangement of the large scale tropical circulation [*Toniazzo and Scaife,* 2006]. Interestingly, the stratospheric polar vortex is skilfully predicted; better than in the first winter, though is not significantly different when applying a Fisher-Z transform to the correlations and determining whether they are statistically different at the 5% level. As *Scaife et al.* [2016] found that NAO skill vanishes when SSW events are excluded, this stratospheric pathway could be the origin of NAO skill, and could play a role on extended interannual timescales [*O'Reilly et al.,* 2019; *Nie et al.,* 2019]. It is not clear whether polar sources or tropical sources are generating this stratospheric polar vortex skill.

The components of the climate system in 5.2 are explored within a multiple linear regression (MLR) framework, both in observations and the model ensemble mean. The 4 tropical rainfall boxes are excluded to prevent over-fitting of the MLR; though the west and east Pacific rainfall signal would be expected to be contained within the NINO 3.4 index. The relative weighting of each the 5 predictors in the regression model is also evaluated - all timeseries are standardised about their mean and variance prior to analysis, allowing these weightings to be directly compared. Note that the ensemble mean is not directly comparable with observations, since it is an average of multiple realisations, but allows interpretation of relationships that occur without the presence of internal variability

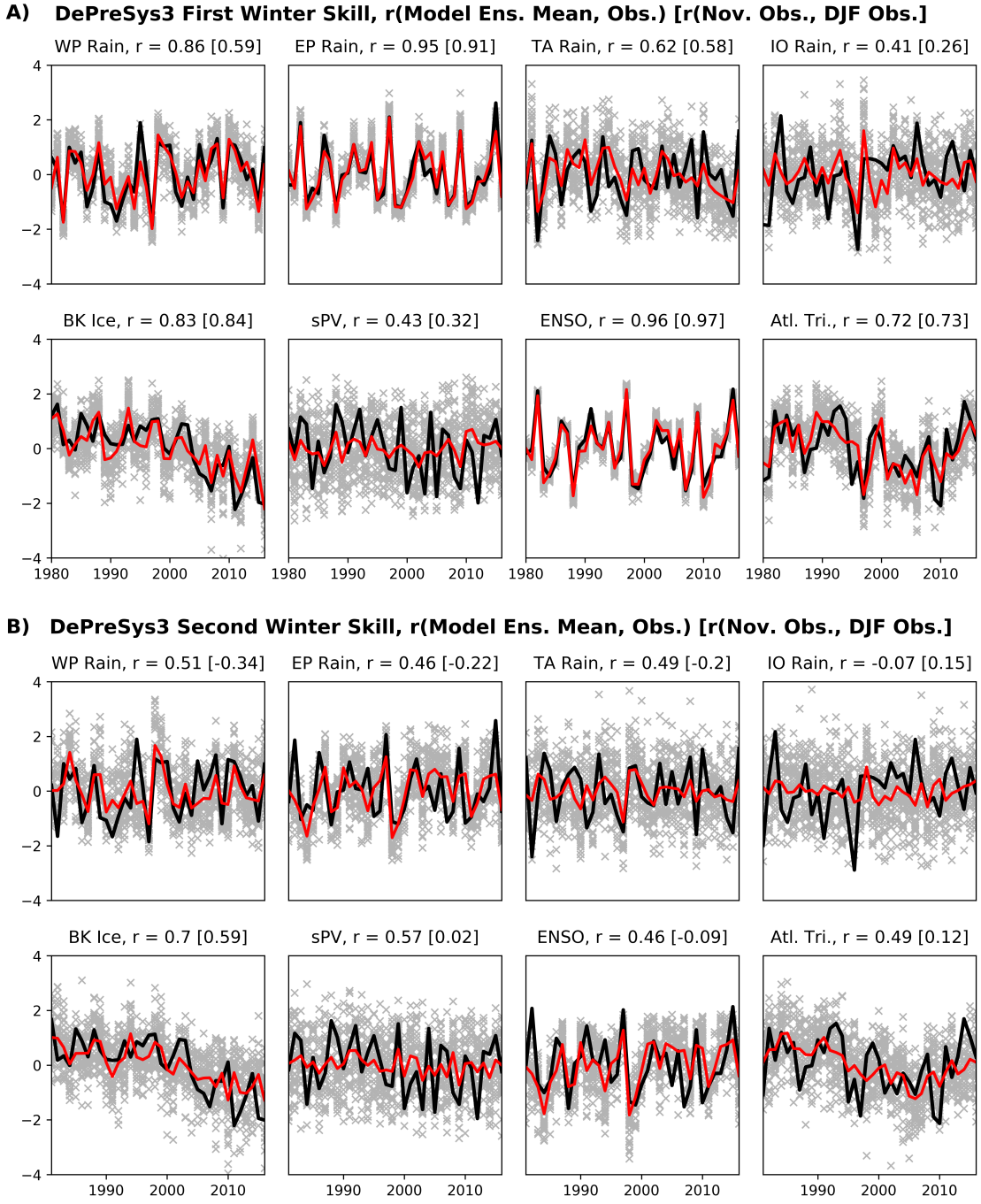

Figure 5.2: DePreSys3 First and Second Winter Driver Skill. Each panel shows either rainfall in the 4 tropical boxes, or commonly proposed NAO drivers including BK sea ice, stratospheric polar vortex at 50hPa (sPV), ENSO and the Atlantic tripole pattern (Atl. Tri.). Crosses indicate individual ensemble members, with the ensemble mean denoted as the red line with observations in black. Correlation between the ensemble mean and observations is shown in the title, followed by the auto-correlation (November correlated with DJF average) for each variable. Each driver is standardised about its mean and variance.

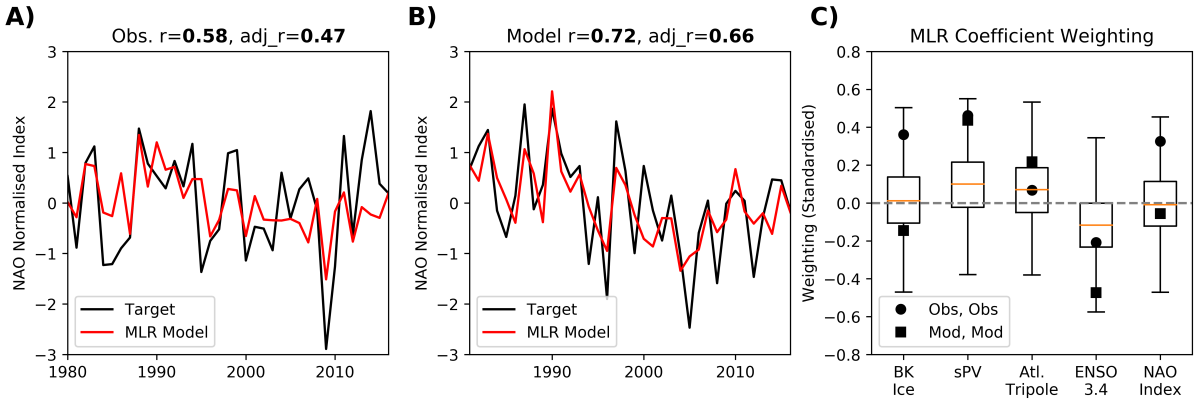

Figure 5.3: Multiple Linear Regression model of predictors in October and November. **A)** Fitting a multiple linear regression model to observed October-November averaged Barents-Kara sea ice (BK Ice), 50hPa stratospheric polar vortex strength (sPV), Atlantic tripole index (Atl. Tripole), ENSO Index 3.4 (ENSO 3.4) and the EOF derived NAO index, predicting the observed winter NAO index. The correlation (along with the adjusted r correlation) between the model fit and the observed NAO index is shown, with significant correlations at the 5% level bold. **B)** As in A), except using the model ensemble mean (averaging ensemble members prior to analysis) for the second winter. **C)** Coefficient weighting in the regression model, for both observations and the model ensemble mean. The model ensemble was randomly re-sampled 10000 times; each time choosing a random member for each year, where a MLR model was constructed. The distribution of coefficient weightings is shown by the box and whisker diagram.

(given sufficient ensemble size), and whether the observed relationship lies close to this or not. Firstly, in figure 5.3A, observed October-November averaged predictors (BK Ice, stratospheric polar vortex, Atlantic tripole, ENSO and NAO) are used to fit a multiple linear regression to the observed winter NAO index. The choice of October-November average means a lagged relationship can be inferred, and a two month average reduces sub-seasonal noise in the indices used. To construct the October, November NAO index, the EOF method is used as the NAO mode may not be centered over the Azores/Iceland boxes commonly used in late autumn vs winter (as found earlier in figure 3.5).

Firstly, using the chosen predictors from reanalysis and fitting to the observed NAO index yields a strong and significant ($p < 0.05$) correlation; even when taking into account the correlation inflation due to 5 predictors using the r-squared metric (figure 5.3A). The analysis is repeated for the model ensemble mean predictors being fit to the ensemble mean NAO index for the second model winter (figure 5.3B). Strong correlations are found using these predictors, suggesting the model NAO is predictable with knowledge of the

predictors in figure 5.3. Interestingly, for some drivers, there is a discrepancy between the coefficient weighting of the model and observations. For example, the model doesn't replicate the strong relationship between BK sea ice and the NAO, as found earlier, but does within its internal variability.

The relative weighting for each predictor in the regression model is investigated in figure 5.3C. In addition to plotting the regression coefficients using reanalysis and the model ensemble mean, a re-sampling procedure was used to randomly select a member from each year and reconstruct a multiple linear regression using only model data. This is directly comparable to observations, and can be performed many times (in this case 10000) to construct confidence intervals, as shown by the box and whisker plots in figure 5.3C. Through isolating the predictable component with the ensemble mean, the stratospheric polar vortex (positively) and ENSO (negatively) are most strongly weighted in the NAO prediction. This is intuitive as a strong polar vortex has been linked to a positive NAO/AO state [*Baldwin and Dunkerton* 2001; *Hitchcock and Simpson,* 2014], and El Niño conditions have been shown to drive negative NAO [*Ineson and Scaife,* 2009]. There is large uncertainty with all 5 drivers and their relative weighting (possibly non-linear interactions between these and the NAO). Within the model ensemble, on average there appears to be no contribution from late autumn BK sea ice. The preceding NAO state before winter also has little effect on the winter NAO; although it may communicate information into winter via the Atlantic SST patterns, which have more persistence [*Rodwell et al.,* 1999].

The large DePreSys3 hindcast ensemble is next used to explore the effect of sub-sampling the ensemble to determine whether members that are more skilful in one aspect, such as providing a better simulation of sea ice in a given year, may produce a better simulations of the winter NAO at extended lead time (12-14 months). This analysis is conducted on the 8 predictable components of the climate system commonly linked to NAO predictability in figure 5.4, where the 20 best/worst members are sub-sampled based on their deviation from observational reanalysis in October/November. Anomalies are first taken respective relative to the 1981-2016 average, to account for model biases. This is particularly important for BK sea ice, where there is a significant negative bias during autumn and such an approach without calculating the anomalies would mean only the members with maximum ice would be sampled in the 'good' member pool. Model

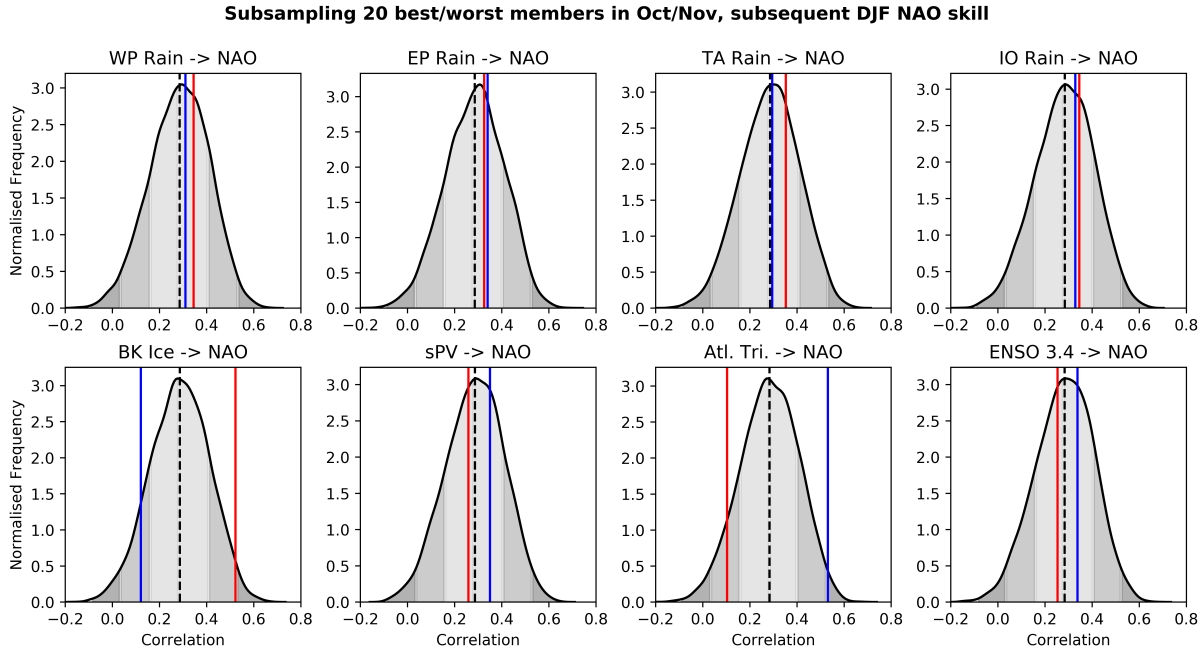

Figure 5.4: Sub-sampling members based on how well they simulate different climate components. For the 8 different predictable components investigated earlier, the 40 members for each year are divided into two groups; members closest and furthest away from the observed value, taking the October/November average. Prior to analysis, the 1981-2016 average is subtracted to account for overall model biases (particularly in BK sea ice as found in figure 4.4). These members in each group are then used to create an ensemble mean NAO of the following winter, where the interannual correlation is displayed in red (bad members) and blue (good members). The PDF shows random sampling of 20 members (10000 times) with replacement and the correlations found.

biases which are non-stationary in time are not considered in this analysis.

These results, presented in figure 5.4, show that there is no measurable improvement in NAO prediction if members are sub-sampled on their prediction of different components prior to winter. In fact, the NAO skill increases when members poorly simulate BK ice in the preceding winter (although this is has marginal significance). Other climate components show no benefit in NAO prediction through sub-sampling, bar sub-sampling the Atlantic tripole. Again, this is marginally non-significant using a Fisher-Z transform, but appreciable gain in skill would be expected given the bi-directional relationship between Atlantic SST's and the NAO [*Rodwell et al.,* 1999], and that Atlantic SST's carry persistence into winter (figure 5.2). This analysis suggests BK sea ice is not an important factor contributing to NAO predictability within the model.

The NAO simulated within the model contains an unexpectedly weak signal-to-noise

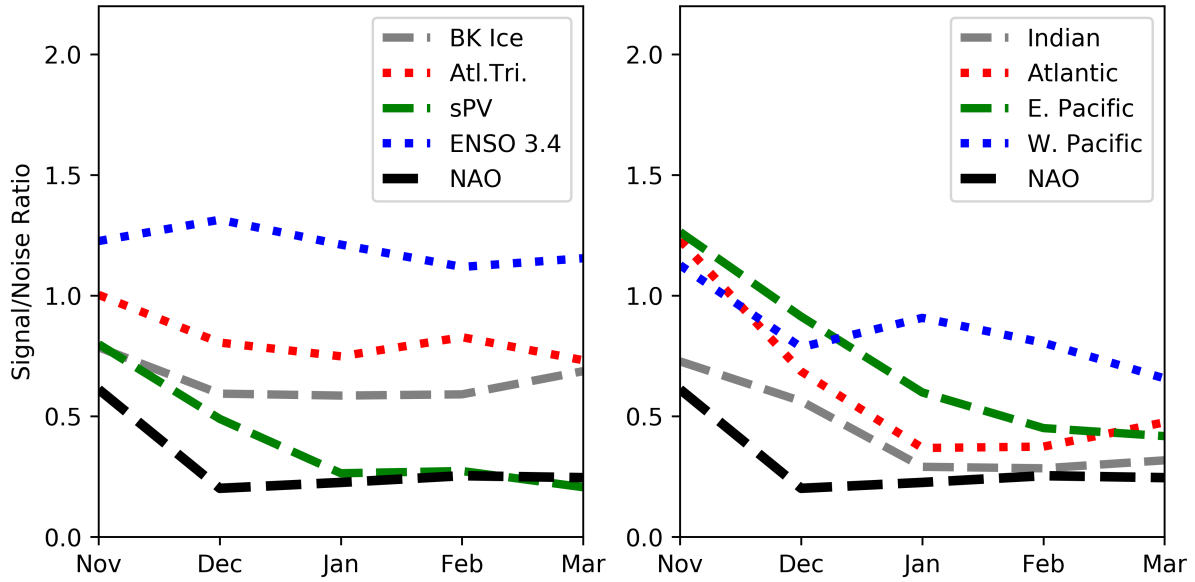

Figure 5.5: Examining the signal/noise ratio with lead time in different climate components.. Left hand panel shows the signal-to-noise ratio in the DePreSys3 model (as calculated in equation 2.1, the ratio of variance in the model ensemble mean to observations) in proposed drivers of the winter NAO, with the 4 tropical basins included in the right hand panel. The first winter is analysed (lead time 1-5 months).

(S/N) ratio [*Dunstone et al.,* 2016]. Here, the S/N ratio is examined in components of the climate system that were analysed earlier (BK sea ice, Atlantic tripole, stratospheric polar vortex and ENSO) during the first 5 months of model integration, to see whether similar low S/N ratios occur (figure 5.5). From initialisation, the S/N ratio of the NAO decreases rapidly down to 0.2, then remains steady. Additionally, after 1 month lag, the stratospheric polar vortex also reaches the same S/N ratio. Dynamical two-way coupling between the two, particularly after December [*Hitchcock and Simpson,* 2014], suggests these may be related. Despite the link between Atlantic sea surface temperatures and the NAO [*Rodwell et al.,* 1999], there appears to be minimal change in the S/N ratio in the Atlantic tripole. The S/N ratio in BK sea ice remains steady throughout the first model winter, implying that it is independent of the low NAO S/N ratio in the model. Furthermore, despite ENSO SSTs showing more variance in the model ensemble mean than observations, the rainfall indices in the tropical boxes (including over the tropical Pacific) all tend to a lower S/N ratio, but higher than the NAO. Boundary conditions in the Atlantic sea surface and Arctic sea ice appear to not be related, or coincidental with the low S/N NAO ratio. Given the strong relationship between the NAO and the stratosphere, the S/N issues may be an entirely atmosphere generated phenomenon (given

S/N ratio found in rainfall but not underlying SSTs), supported by recent work identifying its origin in atmospheric resolution and resolving eddy feedbacks [*Scaife et al.,* 2019].

5.4 Causal Effect Network Analysis

Causal Effect Network (CEN) analysis is a novel statistical technique that can be applied to a variety of complex systems, including climate analysis, neuroscience and transport network systems [*Runge et al.,* 2015], in order to find causal links within a dataset. It involves dimension reduction, in order to extract key regions/processes of interest from a timeseries, applying a causal reconstruction to these, and evaluating causal gateways and mediators [*Runge et al.,* 2015; *Runge,* 2017]. It builds on earlier work using neural network analysis within the climate system [*Pasini et al.,* 2006], and other causal discovery techniques such as Granger causality, which has previously been applied to ENSO - Indian monsoon teleconnections [*Mokhov et al.,* 2011]. This method is more powerful than simple lagged correlations, where autocorrelation can lead to misleading conclusions regarding the relationship between two timeseries [*Runge et al.,* 2013]. However, this data driven method is subject to limitations like most statistical methods, such as assuming that all important variables and processes are included, the temporal resolution of the data (and therefore information about the processes), and assuming stationarity. Physically, a strong trend is present in sea ice, so detrending this prior to analysis is also artificial. Constraint based learning techniques have also been employed to identify causal links between teleconnections in the West and East Pacific, Atlantic and North America [*Uphoff and Deng,* 2012]. However, strong simultaneous coupling between the West and East Pacific make it impossible to infer a direction of causality [*Elbert-Uphoff and Deng,* 2012] and so a physical judgement needs to be made (outside the scope of a purely statistical construction).

CEN analysis was carried out for the relationship between BK sea ice and the NAO, and its link with other drivers, such as tropical variability. Dimension reduction was already performed, given hindsight knowledge of key regions of predictability within the climate system, where time-series can be extracted (NAO, BK sea ice, ENSO etc.). *Kretschmer et al.* [2016] recently applied this method to seasonal teleconnections by identifying causal relationships with sea ice variability, Eurasian snow cover and the Arctic

Oscillation. This study, despite testing relationships over different sampling frequencies (weekly and monthly), is limited in its selection of variables, with tropical variability excluded. If important drivers are excluded then causal links identified through this method may be misinformed. More recently, CEN analysis was actively used in identifying northern hemisphere teleconnections in easterly and westerly QBO composites [*Tyrrell et al.,* 2019; *Schenzinger et al.,* 2016; *Schenzinger et al.,* 2019].

Abbreviation	Description
EP	East Pacific tropical rainfall
WP	West Pacific tropical rainfall
ENSO	ENSO Index 3.4 index
sPV	Stratospheric Polar Vortex (50hPa U at 60N)
QBO	Quasi-Biennal Oscillation (30hPa)
NAO	North Atlantic Oscillation (from *Hurrell* [2003]
BK	Barents-Kara sea ice
Atl	North Atlantic Tripole index

Table 5.1: Acronyms used for different drivers in the CEN analysis, with clarification on levels at which some metrics are computed.

In order to construct suitable timeseries to apply this CEN method to, monthly data is used with the linear trend removed, as specified in *Runge et al.* [2015] who determine stationarity is important prior to constructing this analysis. The assumption that the trend in a component does not physically alter variability in other components of the climate system may not be physically consistent, particularly in sea ice which has a strong downward trend, and may physically drive a trend in other components. In line with the requirements of the method set out in *Runge et al.* [2015], the monthly cycle is removed from the data by standardising each month by the long term monthly mean and variance. A summary of the climate components is shown in table 5.6 for reference. The construction of these climate components is further explained in the methodology chapter. Only pathways that are significant at the 5% level discovered through CEN are retained.

First, CEN is tested on a known teleconnection; the connection between east and

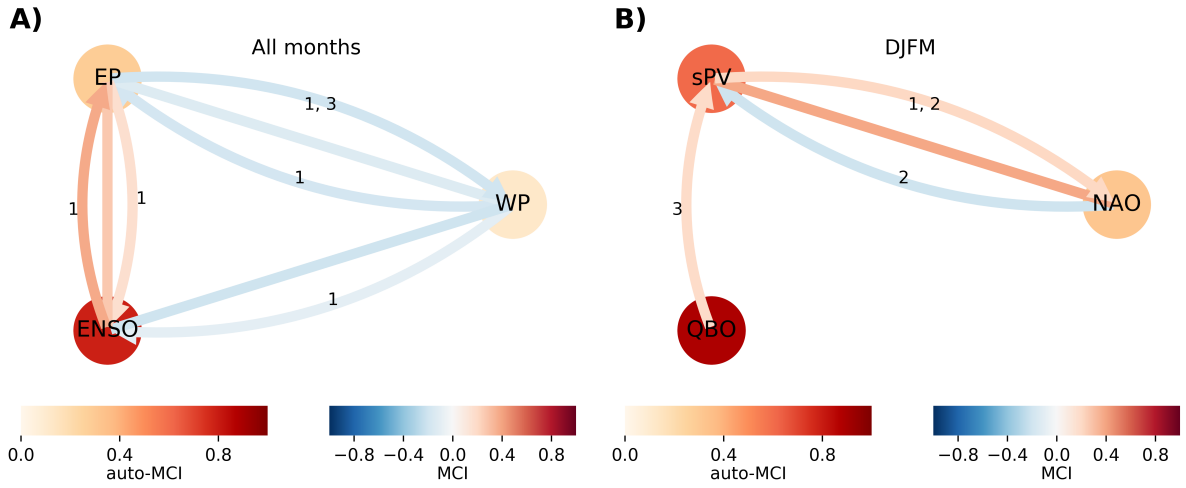

Figure 5.6: CEN analysis for the tropics and tropics to mid-latitude link. A) Using EP, WP and ENSO for all months (no masking). Arrows indicate direction of causality, with the colour representing the strength. The colour of the circle represents autocorrelation. Links are only shown if they are significant at the 5% level. **B)** Using QBO, sPV and NAO as predictors, with the same layout as in A).

west Pacific rainfall and ENSO. Different ENSO phases lead to large scale sea surface changes, which modify the rainfall and hence the larger scale circulation aloft [*Bjerknes,* 1969]. CEN analysis, displayed in figure 5.6(a), shows a strong and positive instantaneous relationship between ENSO and east Pacific rainfall as physically expected. Additionally, it demonstrates an instantaneous anti-correlation with west Pacific rainfall; the latter also being instantaneously anti-correlated with east Pacific rainfall. This is expected given the west and east Pacific act as a dipole, where an El Niño event leads to enhanced rainfall over the eastern tropical Pacific, with suppressed convection over the western Pacific. Instantaneous relationships occur when the sampling frequency (in this case monthly) is too low to distinguish a cause-effect relationship; suggesting such teleconnections could happen on the order of weeks. This analysis also reveals lagged relationships, with bi-directional influences between ENSO and the east Pacific, which is to be expected given that the ENSO process is a coupled atmosphere-ocean phenomenon. Finally, the node colours represent the strength of monthly autocorrelation within each index supplied. ENSO has a strong month to month auto-correlation; as does the tropical Pacific rainfall to a lesser extent.

An additional test is employed on the CEN analysis to analyse teleconnections between the NAO, stratospheric polar vortex and the QBO, all of which are closely related in

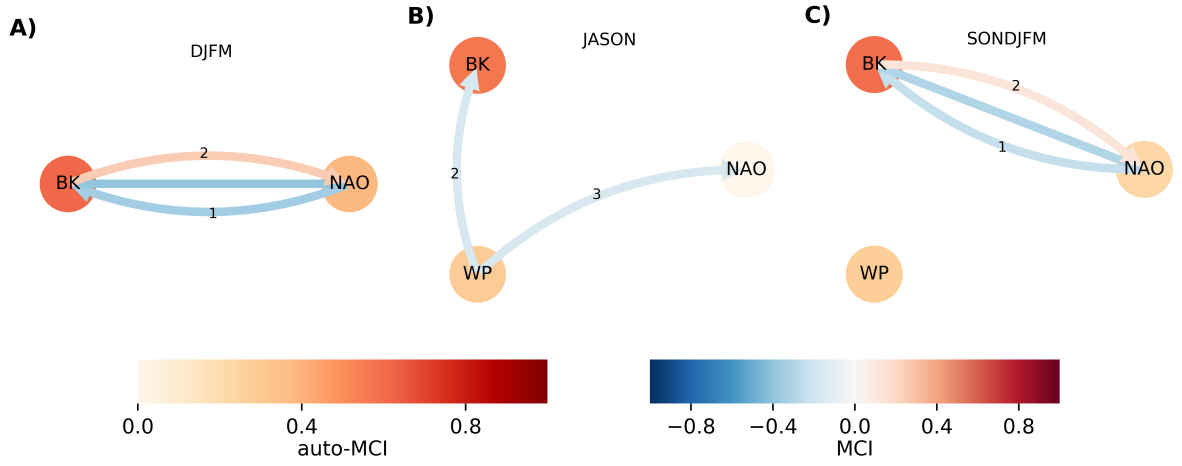

Figure 5.7: CEN analysis on the BK sea ice, NAO link, bringing in west Pacific rainfall A) Using BK and NAO for December to March inclusive. Arrows indicate direction of causality, with the colour representing the strength. The colour of the circle represents autocorrelation. Links are only shown if they are significant at the 5% level. **B)** Same as in A), but including west Pacific rainfall in the analysis and using July to November inclusive. **C)** Same as in B), except using September to March inclusive.

winter [*Anstey and Shepherd,* 2014]. Figure 5.6(b) reveals a long lagged relationship between the QBO and the polar stratosphere vortex of 3 months during winter; though note the QBO may influence the polar vortex in prior months. A strong instantaneous relationship between the NAO and polar vortex is also established; these have a well known feedback between the two through troposphere-stratosphere coupling [*Baldwin and Dunkerton,* 2001]. Very strong auto-correlation exists in the QBO given its low frequency cycle, and the polar stratosphere to a lesser extent. Interestingly, there is a lagged anti-correlation that the NAO exerts on the polar vortex on a 2 month timescale, with the polar vortex also exerting an influence on the NAO at 1 to 2 months lag. This suggests that a strong polar vortex induces a positive NAO, and that a positive NAO can actually weaken the polar vortex at longer lag times. Interpretations should be cautious with CEN analysis, not only due to the limitations discussed above, but also sub-seasonal to seasonal teleconnections require data on a higher temporal frequency than monthly as used here. In these two case studies however, the CEN analysis has successfully identified known teleconnections between key components of the climate system.

Attention is now turned to the question of co-variability between tropical rainfall and BK sea ice; and whether the latter has a causal influence on the NAO. Three tests are performed; investigating the strength between BK sea ice and the NAO in winter, deter-

mining relationships between BK sea ice, tropical rainfall and the NAO during summer and autumn, and finally the relationship between all 3 during autumn and winter.

A strong instantaneous relationship between winter BK sea ice and the NAO is revealed, such that low sea ice coincides with a positive NAO. This also occurs at 1 month lag where the NAO leads BK sea ice. This is physically consistent in that a positive NAO leads to increased poleward heat flux into the Arctic, with increased sea ice melt particularly in the Barents-Kara seas. Additionally, there is a 2 month lag where low sea ice can drive a negative NAO; potentially through dynamical mechanisms such as the stratosphere as suggested by *Kim et al.* [2014].

Analysis in figure 5.7(b) was motivated by studies such as *Henderson et al.* [2014] that suggest MJO can influence the Arctic on weekly timescales, which despite being a higher frequency than the sampling frequency used here (monthly), might be identifiable in monthly anomalies. Additionally, west Pacific rainfall contains variability from ENSO, due to large scale re-arrangement of the tropical circulation. This analysis reveals a lagged anti-correlation between west Pacific rainfall and BK sea ice, such that enhanced west Pacific rainfall leads to low BK sea ice. This was found earlier where an anti-correlation between interannual west Pacific rainfall and BK ice in late autumn exists in reanalysis. Furthermore, a weak anti-correlation between west Pacific rainfall and the summer/autumn NAO is found. Given the relationships found in figure 5.7(a), the ability for tropical variability to modulate NAO variability in autumn means it may have an extended influence on BK ice through winter.

Finally, combining these ideas, autumn and winter links between west Pacific rainfall, BK sea ice and the NAO are analysed in figure 5.7(c). Inclusion of autumn variability, and an additional driver (west Pacific rainfall) does not affect the relationship between BK sea ice and the NAO. This choice of lags/drivers suggests there is no significant causal effect of west Pacific rainfall on either BK sea ice and the NAO, unlike that found in 5.7(b). Further testing the sensitivity of this to the months chosen reveals results can vary substantially, and therefore the method is very sensitive to the seasonal period analysed. The lagged relationship between west Pacific rainfall and BK sea ice in mid summer through to autumn suggests there is some causal influence of west Pacific rainfall on BK sea ice and the NAO, though this is weak and non-significant later through autumn and into winter.

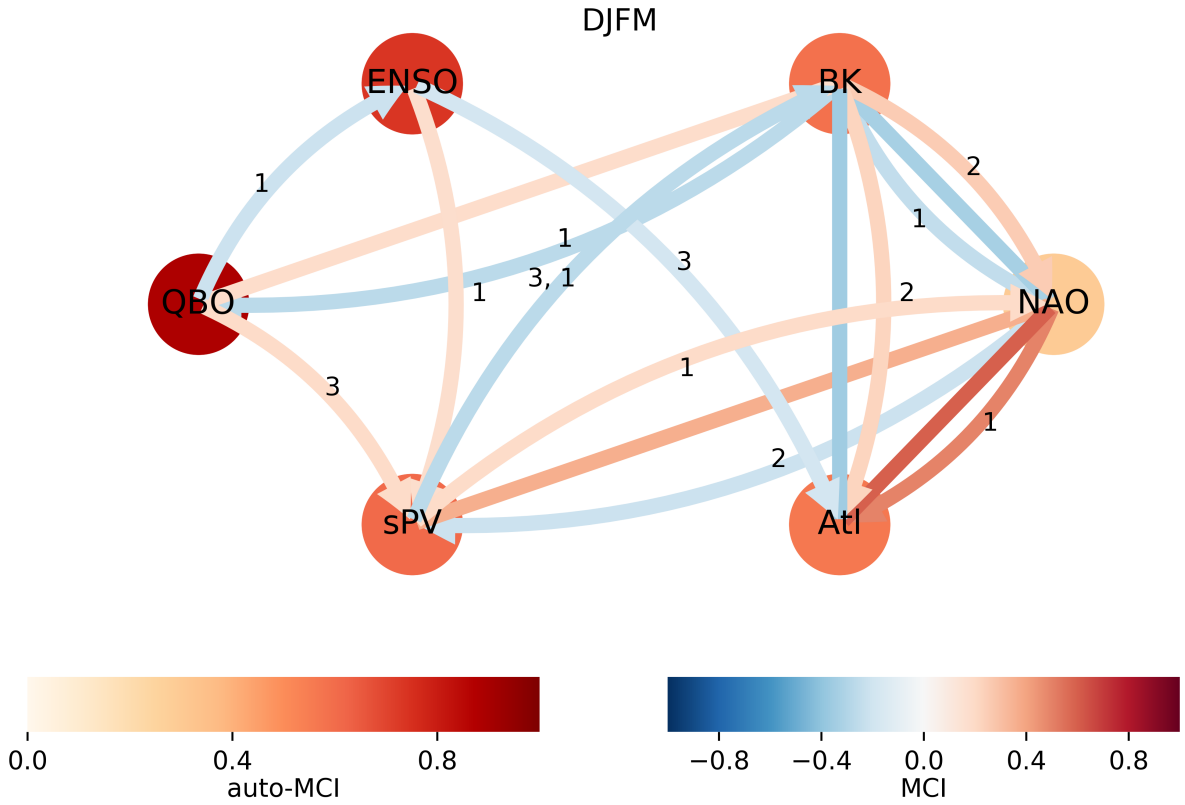

Figure 5.8: CEN analysis on key winter drivers associated with the NAO. Arrows indicate direction of causality, with the colour representing the strength. The colour of the circle represents autocorrelation. Links are only shown if they are significant at the 5% level. Months December to March inclusive are used for the CEN analysis.

Major drivers of the winter NAO are pooled together into the CEN analysis to identify causal drivers. The advantage to CEN analysis is that it can take a large number of drivers and process statistically causal connections between these, forming a sometimes complex network between these nodes. The analysis is shown in figure 5.8. Initially, analysing the auto-correlation in the nodes reveals that the QBO contains the strongest auto-correlation, followed by ENSO, with the NAO containing the least. The strongest relationships are instantaneous links between the NAO and the Atlantic tripole; an expected result given the strong atmosphere-ocean coupling over the Atlantic and reproducibility of the NAO through SST patterns in this area [*Rodwell et al.,* 1999], though the direction of causality is unclear from instantaneous links. Additionally, strong instantaneous links between the BK seas and the Atlantic tripole are identified; heat fluxes in the Atlantic affect the oceans in the Arctic, which in turn affect ice growth and melt particularly in the BK seas region. The additional complication with the causality of the relationship between BK sea ice and the NAO is they may both be incidental to tropical variability from external sources (i.e. ENSO has a lagged effect on Atlantic SST's in this analysis), and that oceanic changes can affect both BK sea ice and the NAO. Additionally, while the direct link between the tropics and BK disappears in this analysis, indirect pathways through the stratospheric polar vortex may still exist.

5.5 Conclusions

This chapter explored potential co-varying relationships between early autumn tropical rainfall, late autumn sea ice, and the winter NAO, based on recent literature suggesting links between all three. This was approached with a combination of observational and model analysis, utilising statistical techniques such as multiple linear regression and CEN analysis to identify co-varying relationships and test whether these are causal or not. Like the previous results chapter, which found the relationship between sea ice and the NAO to be highly variable, the tropical rain to sea ice link is also variable and largely non-reproducible in model simulations except in the east Pacific, which contains a strong ENSO signal. The three key questions are discussed below and in context with the wider research problem.

- **Does tropical rainfall contribute to the variance shared between BK sea**

ice and the NAO in reanalysis?

Creating a multiple linear regression model containing early autumn tropical rainfall, late autumn BK sea ice, and the winter NAO, demonstrated significant correlations between all 3. Through combining both tropical rainfall and BK sea ice in a MLR predicting the NAO, approximately half the variance that BK sea ice can explain in the NAO covaries with tropical rainfall. This suggests some of the relationship between BK ice and the NAO may be symptomatic of tropical variability.

- **What predictable components of the climate system contribute to skilful NAO predictions?**

Motivated by the skilful NAO predictions found in *Scaife et al.* [2014] and more recently at the extended interannual lead time in *Dunstone et al.* [2016], sources of NAO skill are examined. Given sufficient lead time, atmospheric initial conditions will no longer contribute to NAO skill, and slower varying components of the climate system are responsible for NAO skill. Identifying components that are both skilfully predicted at this extended range, and are linked to NAO variability, could give some insight into causal links between the NAO and these drivers. This analysis found that tropical rainfall, particularly in the Pacific, retained skill into the second winter, whilst unexpected skill in the second winter stratospheric polar vortex was also found. Additionally BK sea ice and the tripole are skilfully predicted. However, given the bi-directional influence of these relationships with the NAO, they may be skilfully predicted due to the skilful NAO predictions, not the cause of the NAO skill. There are large discrepancies in the relative contribution of these drivers in the model and observations as found using MLR analysis. Likewise with signal-to-noise analysis, it is hard to disentangle whether the erroneous S/N ratio in the NAO is the result or the cause of erroneous S/N ratios in other components.

- **Can causal effect network analysis help distinguish causal from incidental drivers of the NAO?**

CEN analysis is an auto-regressive statistical technique which encompasses ideas from Granger causality, taking into account shared variance between drivers which may lead to non-causal relationships, as well as auto-correlation contained within drivers. The method verified well when testing the analysis on some well known teleconnections. However,

the analysis identified causal bi-directional relationships between BK ice and the NAO; without influence from west Pacific rainfall. Despite this, inclusion of summer in this analysis reveals a causal link from WP rainfall onto BK sea ice, physically supported by *Henderson et al.* [2014]. Finally, combining all winter drivers and the NAO into this method to produce a high dimensional analysis, strong instantaneous (sub-monthly) links were found between the Atlantic tripole and Barents-Kara sea ice. This could be because both are being driven by the same mediating process; the NAO. This method of identifying causal links is limited by the small number of years contained in the observational period, and there is no reason to assume that different processes should be related linearly. A possible extension would be to apply CEN within the DePreSys ensemble, thus negating a data limitation problem and providing a better context to how robust the connections identified within the analysis hold in the model.

The analysis performed here and in the previous chapter points strongly to a problem where real world relationships may not be representative given the limited sample length (with such large internal variability requiring a larger sample), and potential model deficiencies such as signal-to-noise issues that may be masking relationships [*Scaife and Smith, 2018*]. Furthermore, directions of causality are not addressed fully by the regression and correlation analysis performed in these two chapters. Despite this, there is little evidence to suggest that sea ice is contributing to NAO predictability. To further test the hypothesis laid out in the schematic in figure 5.1, model experiments will be used to test both the sea ice to NAO link, and the degree to which tropical rainfall can affect sea ice (and potentially account for this link).

Chapter 6

AMIP Experiments

This chapter uses atmospheric model experiments to isolate the atmospheric response to sea ice variability. Additionally, the atmospheric response to prescribed tropical SST variability is evaluated, to determine whether the relationship between BK sea ice and winter MSLP identified earlier can be explained by tropical SST variability. Some of the work in this chapter has been published in *Warner et al.,* [2020] (see list of publications at start of thesis).

6.1 Introduction

The Atmospheric Model Intercomparison Project (AMIP) have been employed in a variety of studies and government assessments of anthropogenic climate change [*Gates et al.,* 1999]. This approach has also been extensively used in evaluating the impact of Arctic sea ice loss (e.g. [*Mori et al.,* 2014; *Lim et al.,* 2012; *Koenigk et al.,* 2018; *Ogawa et al.,* 2018]), where sea ice is prescribed as a boundary forcing and the atmosphere is free to respond. These experiments allow a causal response to the forcing imposed to be identified as ocean coupling masks the direction of causality. Many studies using coupled models find similar extratropical responses to sea ice loss as in AMIP simulations (e.g. [*Deser et al.,* 2015; 2016; *Smith et al.,* 2017; *Blackport and Kushner,* 2018]). Experiments have mainly focused on winter sea ice loss and winter impacts. Others investigated the relationship between Arctic sea ice loss and temperature variability [*Sun et al.,* 2016], particularly on the trend of sea ice loss, rather than interannual variability explored here. Additionally, work here builds on single model studies by using large multi-model

ensembles to isolate links between sea ice and winter midlatitude variability. *Xue et al.* [2017] investigated the atmospheric response to BK sea ice variability and SST's in AMIP experiments, finding that the model ensemble mean could not capture the cooling Eurasia trend over Asia commonly linked to Arctic sea ice decline, and that the magnitude found in reanalysis could be explained by internal atmospheric variability. This AMIP set-up has been used effectively to isolate forced (ensemble mean) components from internal variability (ensemble members) [*Sun et al.,* 2016].

The three AMIP model experiments used here are described in more detail in Chapter 3, but a summary is presented here. The first experiment, AMIP$_{OBS}$, contains observed sea ice, observed polar SSTs and observed SST variability elsewhere. Next, AMIP$_{CLIM}$ is forced with climatological sea ice, climatological polar SSTs and observed SST variability elsewhere. AMIP$_{ENSO}$ is forced with observed sea ice variability, observed polar SSTs, and the leading EOF of SST's variability globally (which consists mainly of the ENSO pattern). Therefore, comparisons between AMIP$_{OBS}$ and AMIP$_{CLIM}$ can be used to infer the role of sea ice variability. Additionally, depending on this result, AMIP$_{ENSO}$ can therefore be used to infer the influence of the tropical Pacific once the role of sea ice is known. Although the models are forced with sea ice variability year round, the focus here is on the lagged relationship between late autumn BK sea ice and the winter circulation as identified in observations and reproduced within a model environment in Chapter 4. The inclusion of tropical SST variability provides an opportunity to explore the idea of a symptomatic relationship between BK sea ice and the mid-latitude circulation due to a third common factor; the tropical Pacific.

- **Does sea ice variability affect the wider atmospheric circulation variability and the NAO?**

The first aim of this chapter is to explore how sea ice variability in late autumn affects winter MSLP variability. This is achieved by comparing the experiments AMIP$_{OBS}$ to AMIP$_{CLIM}$, which differ only in sea ice and polar SST's. Additionally, determining whether the inclusion of sea ice variability can increase the models ability to reproduce the observed winter NAO index will support a case for a casual relationship.

- **What is the forced pattern related to sea ice variability in the model, and is this similar in observations?**

Motivated by the previous chapter, where tropical rainfall could partly explain the BK sea ice - NAO relationship, the regression of observed sea ice is performed on AMIP$_{OBS}$ and AMIP$_{CLIM}$ separately, to determine whether the observed regression pattern found in reanalysis is a) reproducible within ensemble members, and b) a forced component within the model ensemble mean.

- **Can tropical variability account for a link between sea ice and the extra-tropical circulation?**

Given a significant correlation between early autumn west Pacific tropical rainfall and late autumn BK sea ice, a regression is performed using tropical rainfall in this region onto the winter circulation to determine whether there is coincident variability of the forced signal found in the prior analysis. AMIP$_{ENSO}$ is also used to identify how much of the relationship between BK ice and winter MSLP can be explained through tropical Pacific SSTs.

This analysis provides a clean test of links between sea ice and the atmosphere, better determining causality between the two; with the caveat of assuming that the model is realistic and can simulate teleconnections effectively (note the signal-to-noise error in models - *Scaife and Smith,* [2018]). These experiments do however make the assumption that ocean-atmosphere coupling is not important in this connection, which is important to consider. This ongoing issue in climate science is also discussed in the context of these results.

6.2 Model MSLP and Temperature Variability

The three model experiments are investigated in their ability to reproduce winter variability in both mean sea level pressure and temperature over the model run period compared to observations. This means the model can be assessed in its ability to simulate dynamic and thermodynamic variability respectively, in the lower atmosphere.

First, winter atmospheric variability in reanalysis (hereafter ERA) is explored in figure 6.1A through taking the standard deviation of DJF averaged MSLP. Three key regions are identified; the Atlantic and Pacific storm tracks, and the Arctic; the latter demonstrating particularly strong internal variability centred over the BK seas. The standard deviation

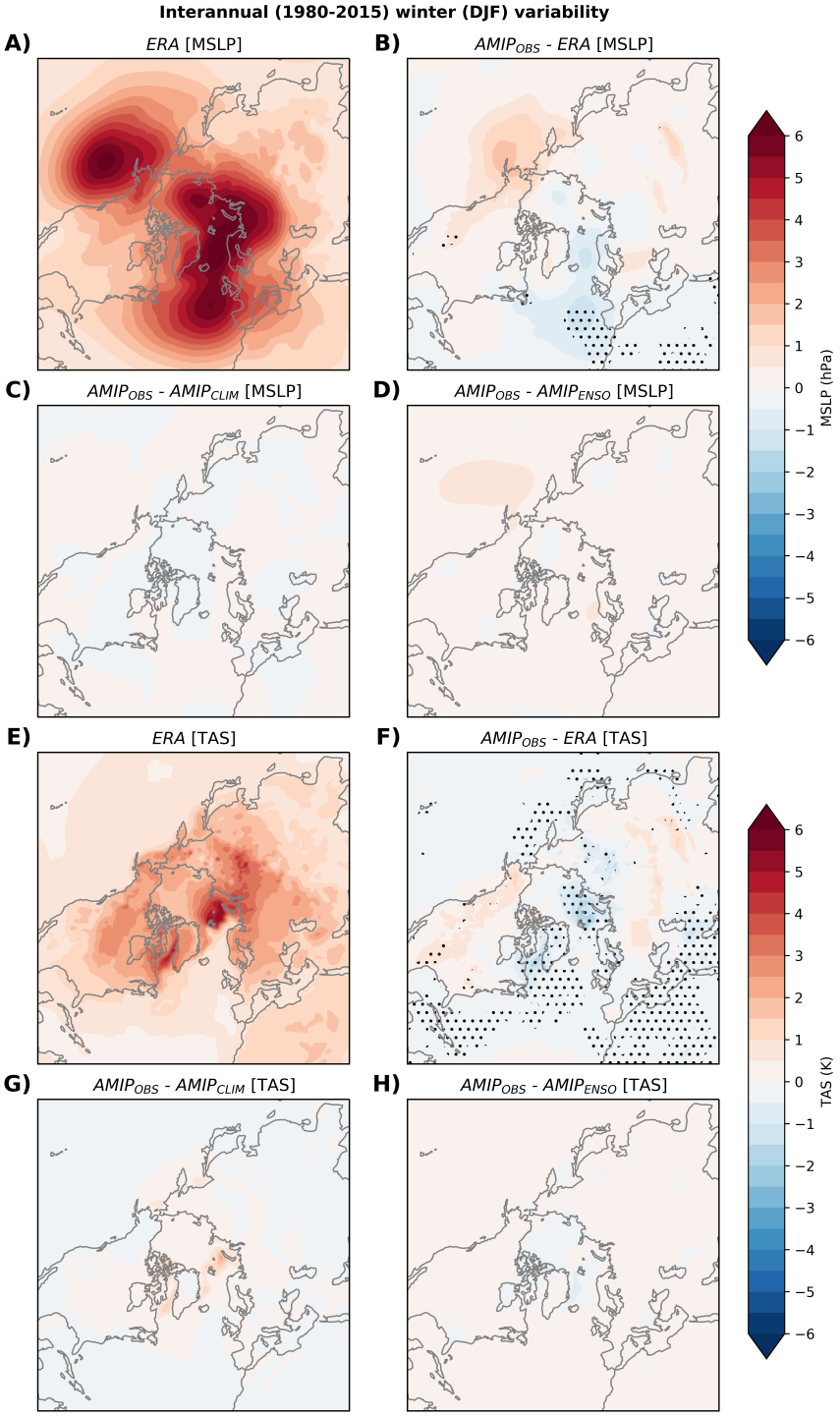

Figure 6.1: Winter interannual variability in observations and AMIP A) Standard deviation of inter-annual winter MSLP in ERA Interim. **B)** Difference between ERA Interim and AMIP$_{OBS}$ standard deviation of winter MSLP (the latter is the average member standard deviation). At each grid-point, the inter-annual variance of MSLP is calculated for each member and for reanalysis; regions where reanalysis fall outside $\pm 2\sigma$ of the ensemble PDF are stippled. **C)** Difference between AMIP$_{OBS}$ and AMIP$_{CLIM}$ inter-annual standard deviation of winter MSLP. **D)** Same as C, except for AMIP$_{OBS}$ - AMIP$_{ENSO}$. **E-H)** Same as A-D respectively, but for 2 meter surface air temperature.

in AMIP$_{OBS}$ is calculated for each member, averaged, and compared to ERA by subtracting the two (figure 6.1B). Slight underestimation in model variability is found over the Azores through to the Barents sea; with slightly too much variability in the Pacific storm track. Examining the variance in individual members and identifying where ERA MSLP variance lies outside the 2σ range reveals that AMIP$_{OBS}$ significantly underestimates variance over the Azores; but other regions are not statistically indistinguishable from ERA. Internal variability present within ERA is likely to be significant even over a 35 year period [*Shi et al.,* 2015]. Further analysis comparing AMIP$_{CLIM}$ and AMIP$_{ENSO}$ to AMIP$_{OBS}$ reveals very little difference in winter MSLP variability (figure 6.1C,D). The striking similarity between AMIP$_{OBS}$ and AMIP$_{CLIM}$ (figure 6.1C) implies that the inclusion of observed sea ice variability and polar SST's has only small effects on total MSLP winter variability.

This analysis is extended to 2 meter air temperature. This is expected to be more sensitive than MSLP, given strong heat fluxes into the boundary layer. In ERA, the strongest temperature variability is found over the continents of America and Eurasia/Siberia, due to the limited heat capacity of the land surface vs the ocean, as well as over marginal sea ice zones such as the BK seas, where sea ice covered surface and open ocean have very different heat fluxes. AMIP$_{OBS}$ underestimates interannual temperature variability over the BK seas (figure 6.1F), as well as over south-west Greenland. Marginal ice zones where AMIP models cannot represent air, sea interactions and feedbacks by definition may result in this underestimate. However, largely over the continents, the model overestimates variability, though this is not significant when comparing individual ensemble members to ERA. Unlike MSLP, some significant discrepancies are found between AMIP$_{OBS}$ and AMIP$_{CLIM}$; the latter underestimating interannual temperature variability as it does not contain sea ice/polar SST variability over the BK seas. The last panel shows negligible difference between AMIP$_{OBS}$ and AMIP$_{ENSO}$ as both are forced with sea ice/polar SST variability.

This analysis demonstrates that all 3 AMIP experiments satisfactorily capture both MSLP and 2 meter temperature variability compared to ERA; and discrepancies between them are accountable due to experimental setup.

r	ERA	$\mathbf{AMIP}_{OBS}$	$\mathbf{AMIP}_{CLIM}$	$\mathbf{AMIP}_{ENSO}$
ERA	1	0.33	0.29	0.25
$\mathbf{AMIP}_{OBS}$		1	0.9	0.33
$\mathbf{AMIP}_{CLIM}$			1	0.36
$\mathbf{AMIP}_{ENSO}$				1

Table 6.1: Correlations between the ensemble mean NAO index in different AMIP simulations and observations (ERA).

6.3 Reconstructing Mid-Latitude Variability

Time series analysis is performed on the ensemble mean of the 3 AMIP experiments to identify how much interannual NAO variability can be reproduced through boundary conditions such as sea ice or SSTs alone. *Cassano et al.* [2014] and *Orsolini et al.* [2012] imply a tropospheric route connecting sea ice variability to the Icelandic node of the NAO; whereas *Kim et al.* [2014] and *McKenna et al.* [2018] explore a stratospheric pathway with a lagged response of the NAO in late winter. Note *McKenna et al.* [2018] focus on the response to extreme sea ice loss at the end of the century, which is not directly comparable to interannual variations of sea ice in the past few decades here. NAO variability has been partly reconstructed with Atlantic SST patterns alone [*Rodwell et al.,* 1999], which AMIP simulations also contain apart from AMIP_{ENSO}.

The AMIP simulations here are predominantly low top models with limited stratospheric representation, apart from GFSv2 which contains 64 vertical levels (see technical model set-up in Chapter 3). Therefore, additional analysis separately analysing the NAO skill in each model is performed. A lack of stratospheric initial conditions means the NAO skill here is lower than hindcast systems with atmospheric initial conditions [*O'Reilly et al.,* 2019; *Nie et al.,* 2019].

The reproducibility of the NAO in AMIP_{OBS} and AMIP_{CLIM} is investigated in figure 6.2A. The 'skill' here is defined as the multi-model ensemble mean NAO index correlation with reanalysis (ERA). Both experiments only reproduce a small amount of NAO variability, with a slight but statistically insignificant increase in skill when observed sea ice/polar SST variability is included. This implies that the inclusion of sea ice variability does not affect the NAO in the models, supported by strong covariance between the ensemble mean NAO index simulated in both AMIP experiments ($r = 0.9$). The correlations between the

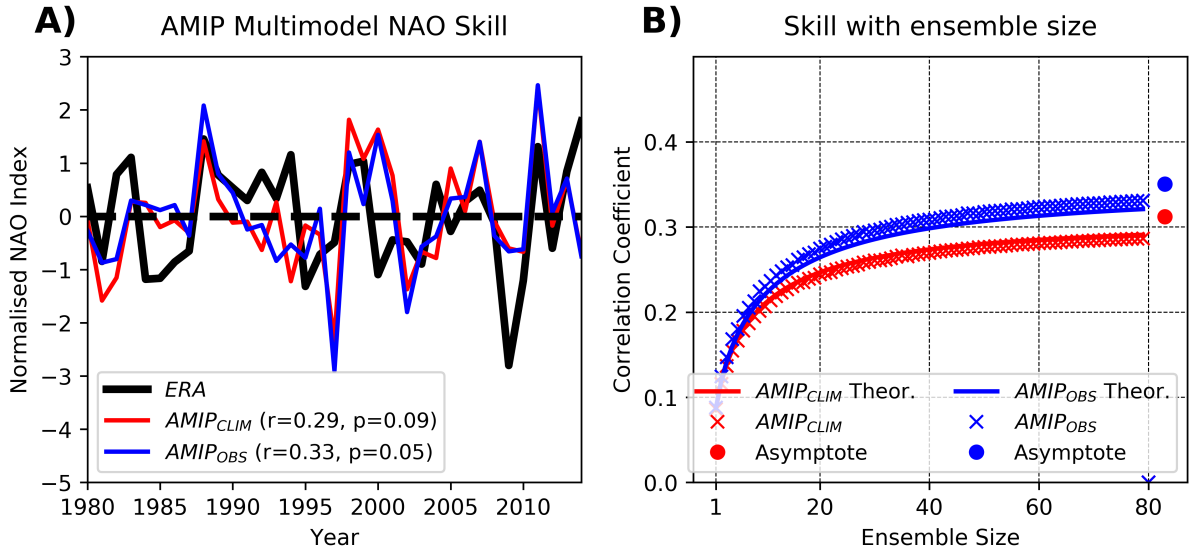

Figure 6.2: NAO variability reproducible in the AMIP model experiments. **A)** Normalised ensemble mean AMIP$_{OBS}$ and AMIP$_{CLIM}$ NAO index, along with the normalised ERA NAO index. Pearsons correlation values and p values are shown between AMIP and ERA. **B)** AMIP$_{OBS}$ and AMIP$_{CLIM}$ NAO index correlation with ERA NAO index as a function of ensemble size, through random sampling without replacement 10000 times and calculating the average correlation. Solid lines show the relationship between correlation and ensemble size according to *Murphy* [1990] (see equation 6.1). The circles show the theoretical correlation an infinite ensemble size according to *Murphy* [1990] (see equation 6.1).

ensemble mean NAO index in the AMIP simulations and reanalysis are shown in table 6.1. AMIP$_{ENSO}$ reproduces little observed NAO variability; r(AMIP$_{ENSO}$, ERA) = 0.25, p=0.14. All three model experiments contain tropical ENSO SST variability, which is the common factor that would explain the low but similar skill (given AMIP$_{ENSO}$ does not contain midlatitude SST variability). Examining the individual model ensemble means and correlating their NAO index with ERA produces coefficients between 0.2-0.3. From this, it appears inclusion of the stratosphere, or better horizontal resolution contained in some individual models such as GFS has limited effect on NAO reproducibility in this experiment configuration, despite studies finding an improvement in NAO simulation with a high top model [*Butler et al.*, 2016].

To determine whether the multi-model ensemble size is sufficient to isolate a stronger NAO signal, a theoretical relationship devised by *Murphy* [1990] is used to explore NAO skill as a function of ensemble size (equation 6.1):

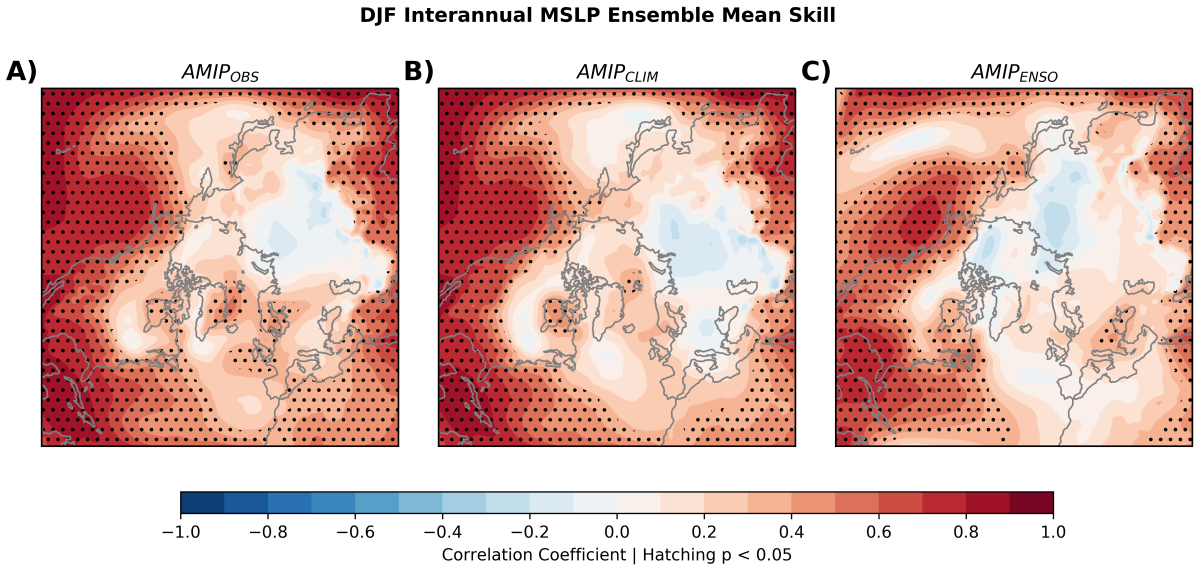

Figure 6.3: AMIP model skill in reproducing interannual winter MSLP. Correlation between the multi-model ensemble mean in **A)** AMIP$_{OBS}$, **B)** AMIP$_{CLIM}$, and **C)** AMIP$_{ENSO}$ with ERA MSLP during winter, with hatching denoting correlations that are significant at the 5% level.

$$r(M) = \frac{\sqrt{M}C_{om}}{\sqrt{1+(M-1)C_{mm}}} \qquad M \to \infty \qquad r \to \frac{C_{om}}{\sqrt{C_{mm}}} \tag{6.1}$$

where:

r = Correlation Coefficient

M = Number of ensemble members

C_{om} = Average member,real world correlation

C_{mm} = Average member,member correlation

Here, a theoretical correlation can be computed for infinite ensemble size to help determine whether the ensemble is sufficiently large (i.e. nearing the asymptote). The curve generated by equation 6.1 can be verified by repeatedly sampling M number of members randomly without replacement, and computing the averaging correlation value. These results are displayed in figure 6.2B. Even with a much larger ensemble, this analysis suggests more limited ability to reproduce the NAO compared to initialised predictions [*Scaife et al.,* 2014; *Dunstone et al.,* 2016]. Therefore, the multi-model ensemble of 80 members for AMIP$_{OBS}$, AMIP$_{CLIM}$ and 60 members in AMIP$_{ENSO}$ is deemed sufficiently large to interpret teleconnections to the NAO.

Finally, reproducibility of MSLP across the northern hemisphere is investigated. In-

clusion of sea ice variability may lead to increased MSLP skill outside the Atlantic sector, and independent of the NAO index. These maps are shown in figure 6.3 for all 3 AMIP experiments. In all three maps, skill is mainly confined to the tropical regions, with the mid and high latitudes less reproducible. The addition of sea ice/polar SST variability leads to some gain in skill around the BK seas and Greenland when comparing AMIP_{OBS} to AMIP_{CLIM}. Additionally, AMIP_{ENSO} which doesn't contain information about mid-latitude SST's leads to much less skill in the east Atlantic sector; although this may be a by-product of containing 20 fewer ensemble members. In particular, predictability over Siberia is low. In the context of seasonal NAO predictions, the evolution of Ural blocking is particularly influential in modulating the strength of the polar vortex, which itself affects the NAO [*Peings et al.,* 2019; *Kryjov,* 2015], which may be why the AMIP experiments are not capturing interannual NAO variability linked to the boundary conditions.

6.4 Relationship between Ice and Winter MSLP

In this section, the relationship between November Arctic sea ice in the Barents-Kara seas and the winter circulation is investigated, to determine whether the strong regression patterns, particularly on the NAO, found in reanalysis are reproducible in the models, and whether it reflects a forced relationship (and not just internal variability). November BK ice is used given its links in observations with the winter circulation found earlier. A linear regression is performed between standardised November BK sea ice and the winter MSLP fields at each gridpoint in reanalysis, and is shown in figure 6.4A.

This analysis reveals a pattern that projects strongly onto the NAO, Arctic, and to a lesser extent, the North Pacific in reanalysis. This observed relationship between low autumn sea ice and the negative NAO relationship has been well documented [*Yang and Christensen,* 2012; *Kim et al.,* 2014; *Petoukhov and Semenov,* 2009], along with blocking over the BK seas and Eurasia [*Mori et al.,* 2014; *Gastineau et al.,* 2017]. Despite such strong projection onto the NAO, there is a large standard error about the regression coefficient in reanalysis due to considerable internal variability (figure 6.1) and limited sample length [*Screen et al.,* 2017], therefore the Azores node of the NAO is not significant. Other regions where the regression coefficient is strong and statistically significant are parts of the North Pacific and over BK seas/northern Siberia.

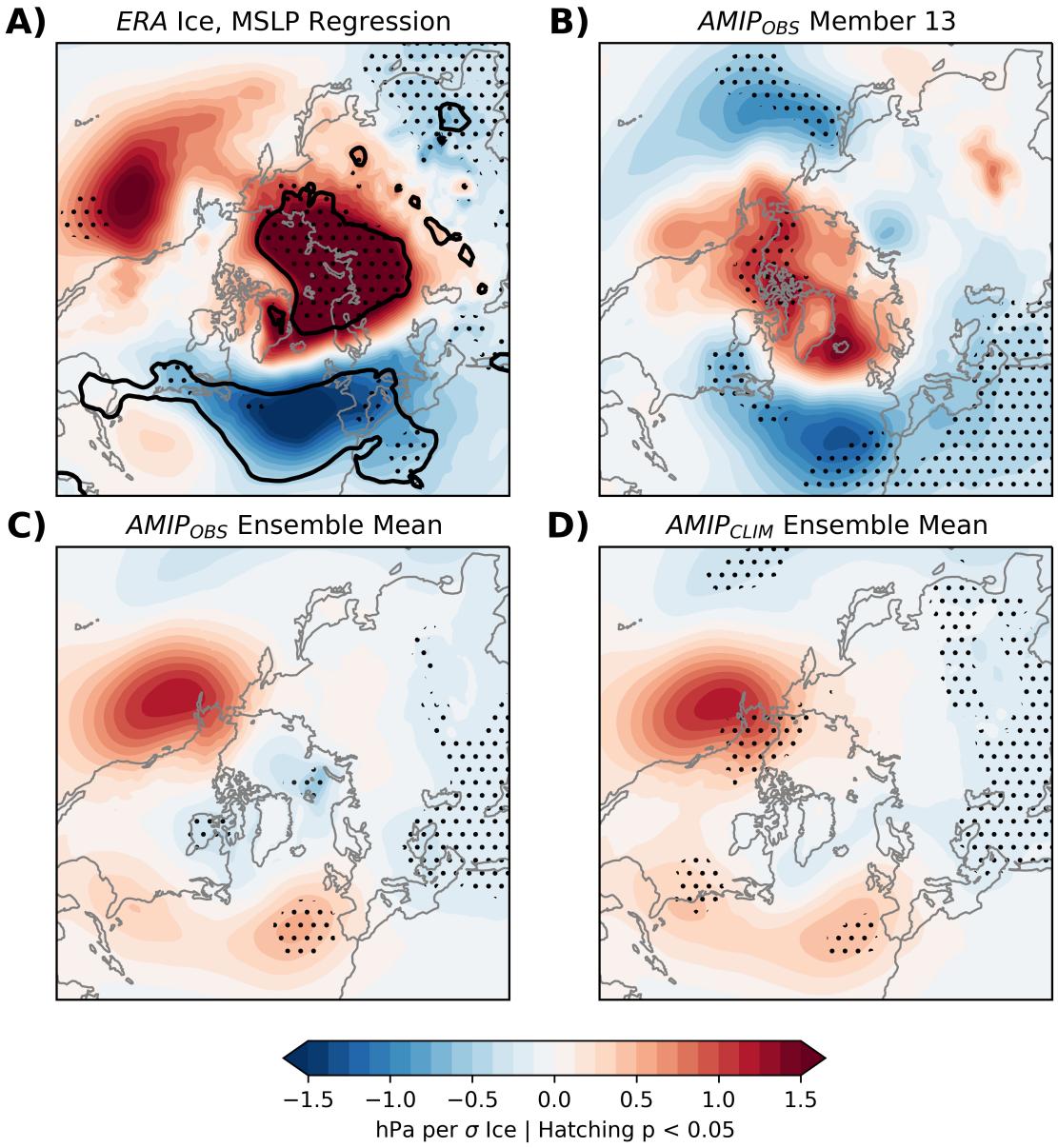

Figure 6.4: Winter circulation patterns related to preceding BK sea ice in reanalysis and model experiments. A) Linear regression of standardised November BK sea ice onto DJF MSLP at each grid-point, showing the regression coefficient. Stippling is where this regression coefficient is statistically non zero at the 5% level. All regression coefficients have been multiplied by -1 to infer the relationship with low sea ice. **B)** Same as A, except on each individual member in both AMIP experiments, and selecting the member with the strongest regression pattern of November BK ice onto the -NAO. Regions where the regression coefficient lies outside $\pm 2\sigma$ of the PDF of ensemble regression coefficients are contained by a thick black line. **C)** Same as in A, except performing the regression of ice onto the ensemble mean in AMIP$_{OBS}$. **D)** Same as in C, except for the ensemble mean in AMIP$_{CLIM}$.

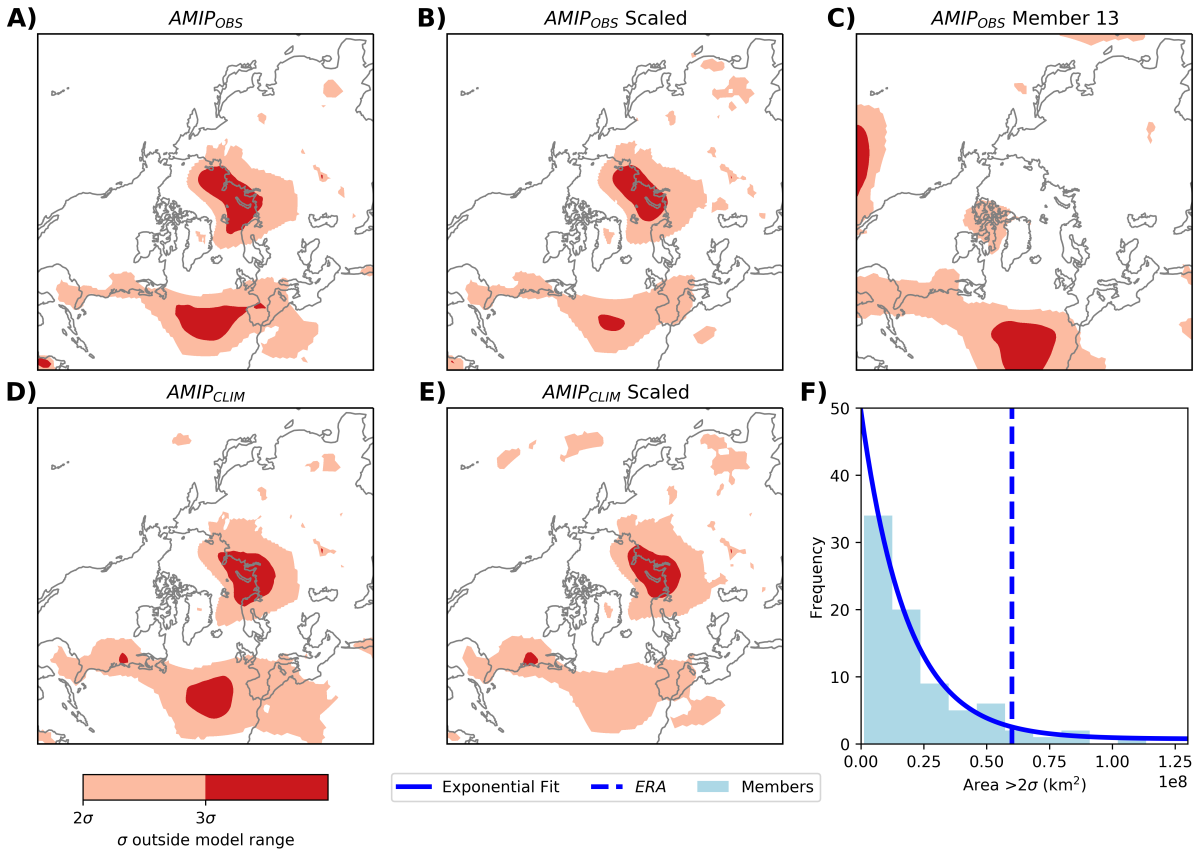

Figure 6.5: Observed regression pattern outside model ensemble range. **A)** At each gridpoint, observed November BK sea ice is regressed onto each AMIP$_{OBS}$ members DJF MSLP (producing 80 regression coefficients). Regions where the reanalysis regression coefficient lies more than 2σ or 3σ away from the average of the 80 regression coefficients is shaded. **B)** Same as in A, except scaling the observed regression coefficient by the ratio of variability in observations/model (as explored in figure 6.1) and repeating the analysis. **C)** Repeating the analysis in A, but replacing observations with a member. Some members produce spurious regions like that found in A. **D)** Same as in A, except in AMIP$_{CLIM}$. **E)** Same as in B, except in AMIP$_{CLIM}$. **F)** Performing a field significance test, where observations are replaced with members in the analysis in A, and the total global area where the member lies 2σ or more away from the average is totalled. A histogram is constructed, with an exponential curve fitted. The area found in A is shown by a dotted line.

Each member in the model ensemble contains internal variability as well as any forced response. Given a sufficiently large ensemble, the ensemble mean only retains the forced response as internal variability cancels out through averaging the ensemble. To determine whether the model can replicate the strong relationship between sea ice and the NAO in reanalysis, the regression of observed BK sea ice onto the winter MSLP fields is repeated for each ensemble member in AMIP$_{OBS}$. The member with the strongest NAO regression pattern (subtracting the regression coefficient over the Azores box from Iceland as in the methods) is plotted in figure 6.4B. Note that although the models can reproduce the relationship between BK sea ice and the NAO, this is still not as strong as in observations (figure 6.4A). Additionally, at each grid point, calculating the regression coefficient for each member in the model (80 coefficients), and determining how far the observed regression coefficient lies within this PDF, regions over the Azores and the BK seas are identified by the thick black line where the observed regression coefficient lies outside 2σ (figure 6.4A). The presence of regions where the observed regression coefficient is outside the model ensemble range might suggest that the model is deficient or under-represents the BK sea ice, MSLP relationship in these regions. This is explored more in depth in figure 6.5.

Firstly, the regions where the observed regression coefficient lies more than 2 or 3σ from the center of the ensemble regression coefficient PDF are identified. The Azores and BK seas regions are identified in AMIP$_{OBS}$, like in figure 6.4A. If the real world regression coefficients cannot be explained by the model, it could be indicative of a model error and the model underestimating the relationship between sea ice and the NAO. In figure 6.1B, it was identified that the model slightly underestimated winter MSLP variance in the Atlantic sector. To determine whether this may account for observations lying outside the spread of member coefficients, the analysis is repeated, except at each grid point the observed regression coefficient is scaled to the models variance (i.e. the observed regression coefficient is multiplied by the model MSLP variance divided by observed MSLP variance at each gridpoint, figure 6.5B). While this partially reduces the issue, it doesn't account completely for the model not being able to represent the observed regression pattern.

To test whether limited regions of statistical significance might occur by chance, the analysis is repeated, but replacing observations with each ensemble member in turn, and comparing that to the ensemble PDF at each grid point. Members can be found that

also contain spurious regions that are outside the PDF and appear, such as member 13 which also demonstrates a deficiency over the Azores (figure 6.5C). Additionally, the model issues do not appear to originate from ice variability; repeating the analysis for AMIP_{CLIM} produces a very similar pattern to AMIP_{OBS} (figure 6.5D), including when the observed regression coefficient is scaled to be the same as model variability (figure 6.5E). Given that entirely within a model environment, spurious regions can be identified as being outside the model typical range when representing the relationship between sea ice and the winter MSLP fields, a field significance test is performed. Like in figure 6.5C, for each member in AMIP_{OBS} the total global area covered by regions more than 2σ is calculated, and compared to using observations. This produces the PDF in figure 6.5F; there are members that show much larger regions of 2σ than the pattern found in 6.5A. While the observed value lies in the top 10% of members, it is not beyond the range of what could occur by chance at the 95% confidence level. Although not very statistically significant this does make it difficult to entirely regard the relationship between sea ice and NAO as entirely internal variability, especially given that models suffer from signal-to-noise issues in the atmosphere over the Atlantic (e.g. *Scaife and Smith* [2018]).

Analysis is performed to explore the relationship between observed November BK ice and the multi-model ensemble mean in both AMIP experiments to identify a forced component, as opposed to internal unforced variability. The analysis of AMIP_{OBS} (figure 6.4C) yields an opposite NAO sign; where reduced sea ice is linked to a weakly positive NAO index. This again implies that the observed relationship between BK sea ice and the NAO could just have occurred due to internal variability, consistent with its high variability over time, as found by *Kolstad and Screen* [2019].

In contrast, a similar relationship is found in the north Pacific in the model and observed regressions in figure 6.4A. When the analysis is repeated for AMIP_{CLIM} which contains no information about sea ice variability, the same pattern is again found in AMIP_{OBS} (figure 6.4D). This suggests that the forced pattern picked up in the sea ice regression originates not from sea ice itself, but from elsewhere in the ocean boundary conditions. The only difference is directly over the BK seas region, where in AMIP_{OBS} strong near surface temperature variability in this region (not shown) leads to local MSLP anomalies. As an additional test of the suitability of using linear regression to explain the relationship between BK sea ice and the winter MSLP, a composite difference of low-high

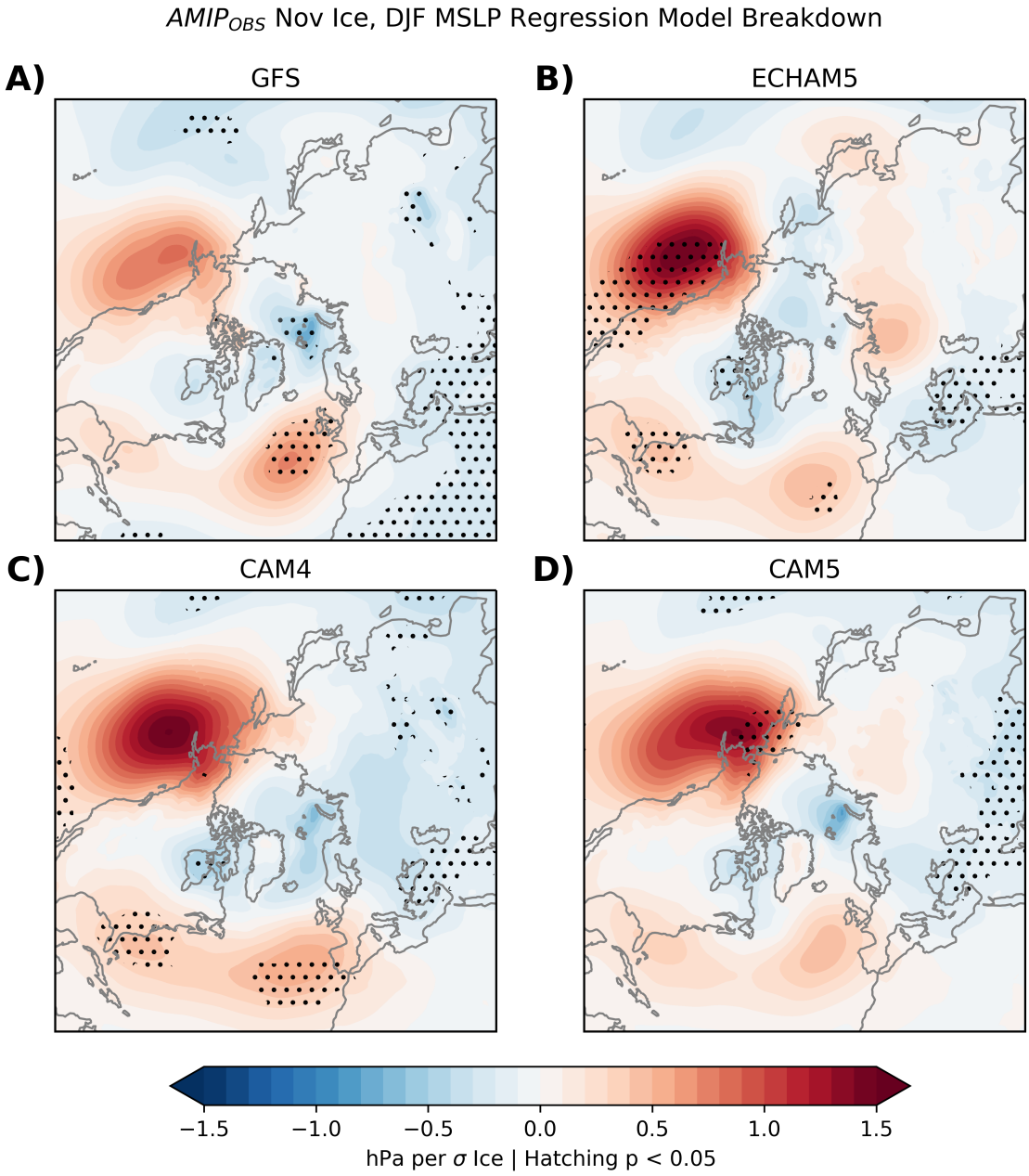

Figure 6.6: $AMIP_{OBS}$ individual model forced ice response. Linear regression of standardised November BK sea ice onto DJF MSLP at each grid-point, showing the regression coefficient. Stippling is where this regression coefficient is statistically non zero at the 5% level. All regression coefficients have been multiplied by -1 to infer the relationship with low sea ice. The ensemble mean for each model is used.

November BK ice is performed, first splitting the 35 years in half, and then compositing the 5 most extreme years. This produces a very similar pattern to that in figures 6.4C,D, which provides additional evidence that the relationship is linear. Note again that despite the similarity between 6.4C,D, there is limited significance over the Aleutian low due to considerable interannual variability given the limited sample length of 35 years.

The relationship between November BK sea ice and the subsequent circulation is explored in each model. Given that the GFS model is high top (64 levels), and therefore may resolve stratospheric teleconnections better, the regression may be stronger in this case. A caveat to this analysis is the small (20 ensemble member) sample in each model which may not be large enough to pick out a signal from internal variability in the BK sea ice, MSLP relationship. The model breakdown is shown in figure 6.6. All 4 models to leading order show a similar pattern (Atlantic, Pacific and local BK seas MSLP regressions are all the same spatially), both spatially and in magnitude. Interestingly, despite the GFS being a high top model, there is minimal difference between this regression pattern and the other 3 low top models. If the link between BK sea ice and Eurasia is physical and not a manifestation of internal variability, then all models may be poorly simulatiing this teleconnection consistently - perhaps due to being unable to simulate atmosphere-ocean interactions by construction.

6.5 Tropical Origins of the Ice-Aluetion Low Link

The analysis is now extended to identify the origin of the forced component found in figure 6.4C, which appears to be independent of sea ice variability given the similarity between figures 6.4C and D. The relationship between early autumn (September-October averaged) tropical rainfall and November BK sea ice is tested for the different tropical regions. A weak but statistically significant anti-correlation is found between West Pacific tropical rainfall (hereafter WP_{SO}) and November BK sea ice ($r = -0.34, p < 0.05$) in reanalysis, implying some lagged relationship picking up ENSO and MJO signals which have been shown to affect the Arctic [e.g. *Lee,* 2012; *Henderson et al.,* 2014].

The procedure used to generate the regressions in figure 6.4 is repeated but using WP_{SO} rather than November BK sea ice. Note that unlike the case in figure 6.4 with sea ice, precipitation is not prescribed and so the regression is performed on the simulated

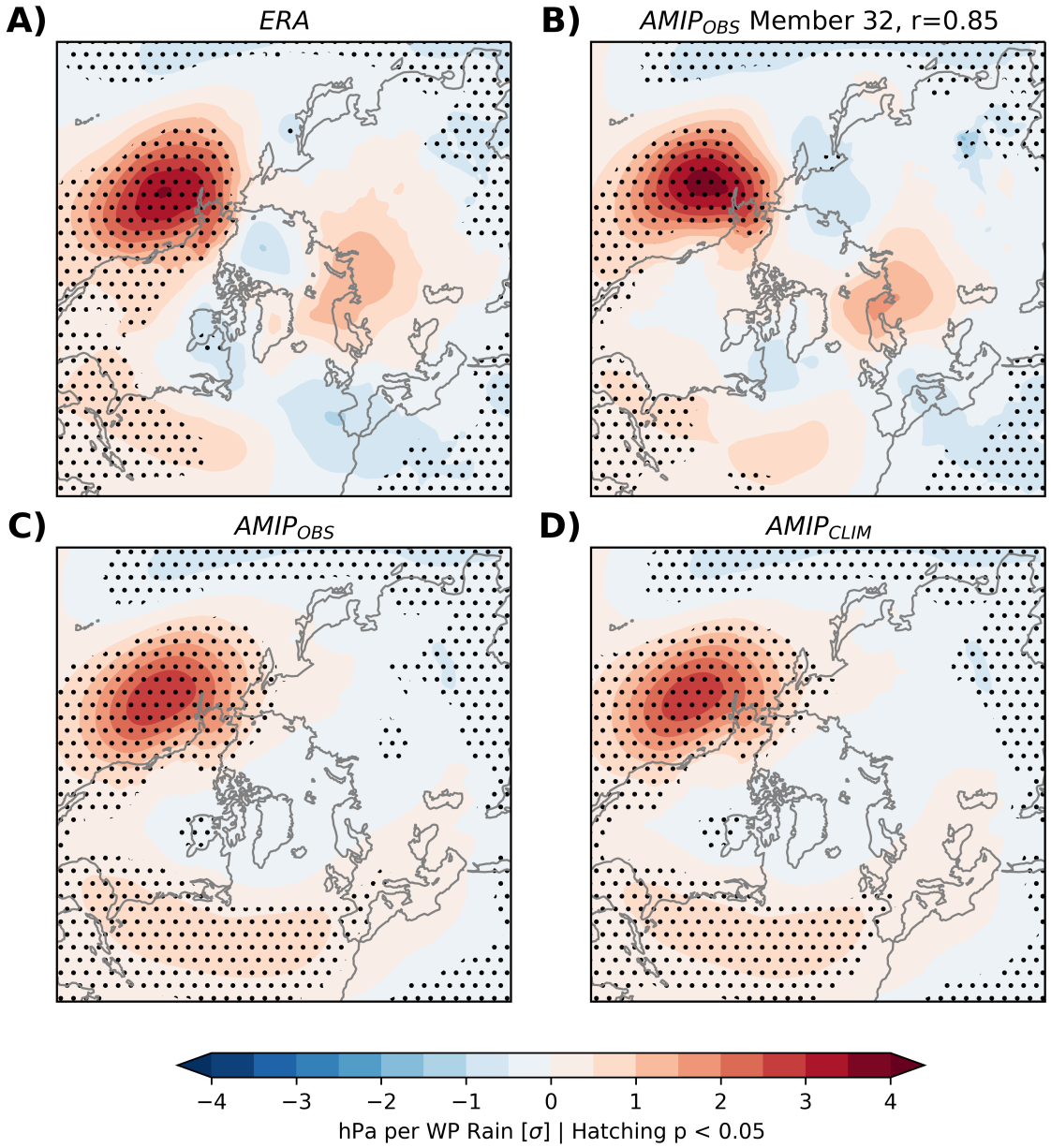

Figure 6.7: Winter circulation patterns related to preceding WP tropical rainfall in reanalysis and model experiments.. **A)** Linear regression of observed WP$_{SO}$ (standardised) onto DJF MSLP at each grid-point in observations, showing the regression coefficient. Stippling is where this regression coefficient is statistically non zero at the 5% level. **B)** Performing the same procedure as A, except on each individual member in AMIP$_{OBS}$ using that members standardised WP$_{SO}$ rainfall. The member with the strongest latitude-weighted pattern correlation north of 20°N is selected, with the correlation coefficient shown. **C)** Same as in A, except performing analysis on the ensemble mean in AMIP$_{OBS}$. **D)** Same as in A, except for the ensemble mean in AMIP$_{CLIM}$.

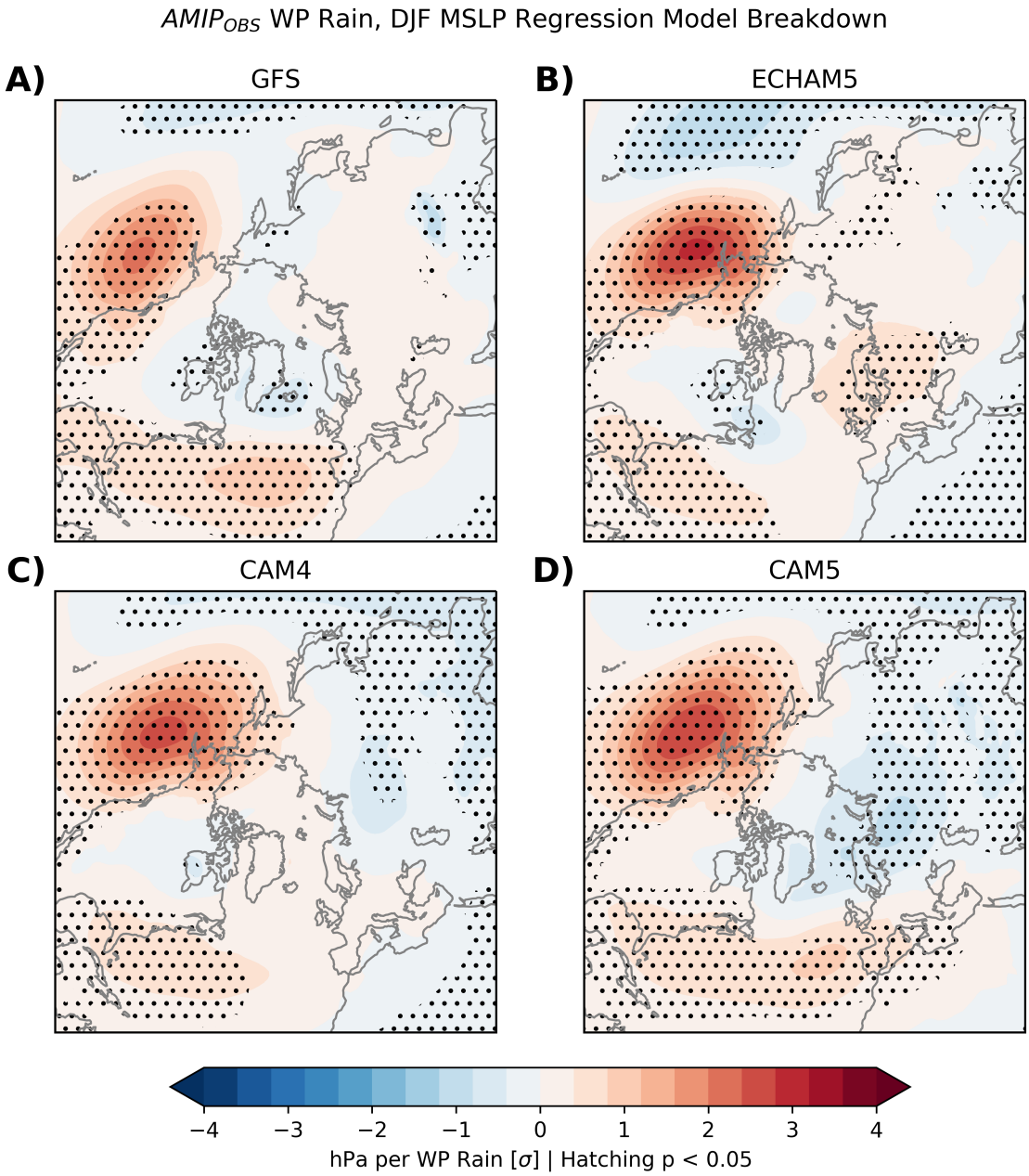

Figure 6.8: AMIP$_{OBS}$ individual model forced ice response. Linear regression of standardised ensemble mean west Pacific rainfall (September, October average) onto ensemble mean DJF MSLP at each grid-point, showing the regression coefficient. Stippling is where this regression coefficient is statistically non zero at the 5% level.

WP_{SO} in each ensemble member. Figure 6.7A shows a strong relationship between the Aleutian Low and WP_{SO} in reanalysis. Given WP_{SO} is increased/decreased during La Niña/El Niño, this confirms the regression pattern related to BK sea ice loss is also related to ENSO. By repeating the regression for each member in $AMIP_{OBS}$ experiments (member WP_{SO} onto member winter MSLP), and performing a weighted linear pattern correlation on the regression patterns north of 20°N, a member is found with the strongest correlation (member 32, r=0.85, Fig. 3B). This member reproduces both the spatial pattern and regression strength closely with reanalysis and indicates that the model can reproduce the observed relationship.

Next the forced model relationship between WP_{SO} and the winter circulation is identified by taking the ensemble mean of WP_{SO} in the AMIP experiments and regressing this onto the respective ensemble-mean winter MSLP. The pattern in $AMIP_{OBS}$ and $AMIP_{CLIM}$ is very similar to the ensemble mean MSLP regression onto BK sea ice (figures 6.4C and 6.4D). Given this pattern, it can be argued that the apparent relationship between North Pacific MSLP and BK sea ice is primarily a consequence of the anti-correlation between WP_{SO} and BK sea ice, and that the variability in the Aleutian Low is forced by tropical variability and not BK sea ice variability. This is supported through studies linking tropical variability to the Aleutian Low [*Yu and Kim,* 2011], with physical mechanisms involving divergence/convergence in the upper tropical troposphere, which excite Rossby waves that propagate into the mid-latitudes modifying the large-scale circulation [*Brönnimann et al.,* 2007; *Garfinkel and Hartmann,* 2008; *Scaife et al.,* 2017]. The regression patterns are not sensitive to the months used (regressing Sep-Nov WP rainfall separately onto the winter circulation produces the same regression patterns).

The model breakdown is investigated to determine any discrepancies in the individual model ensembles (shown in figure 6.8). All 4 models show a similar ability to simulate the relationship between west Pacific rainfall and the winter circulation pattern with minimal differences between them. All models simulate the Aleutian low regression, and even the weak tropical Atlantic relationship with WP_{SO}.

6.6 ENSO Forced AMIP Simulations

The regression patterns in figure 6.4 and the MSLP variance panels in figure 6.1 suggest a minimal role for Arctic ice variability in the recent winter atmospheric circulation. The AMIP_{ENSO} experiments are forced with the leading EOF of SST variability which isolates the ENSO SST pattern, and observed sea ice which has been shown to have minimal influence on the winter circulation. Therefore, AMIP_{ENSO} can be used to account for how much of the regression found in figure 6.4C originates from the tropical Pacific SST boundary condition (rather than other tropical basins, or mid-latitude SSTs). The regression of November BK sea ice onto the ensemble mean DJF MSLP fields in AMIP_{ENSO} is performed in figure 6.9A. The relationship between BK ice variability and the winter circulation can be explained through tropical Pacific SST's alone, which produces a very similar pattern to that found in figure 6.4C. This pattern is however weaker (about 50%) in comparison to the AMIP_{OBS} experiment (figure 6.4C), suggesting that other tropical basins and mid-latitude SSTs are partly responsible for the regression pattern found between BK sea ice and winter MSLP.

The regression of ensemble mean WP_{SO} is also performed on the ensemble mean winter MSLP fields within AMIP_{ENSO}. The regression pattern (figure 6.9B) is as strong as the regression patterns found in figure 6.7C. This confirms that the regression of early autumn west Pacific rainfall onto the winter circulation is causal, and not symptomatic of mid-latitude SST variability.

6.7 Conclusions

The relationship between late autumn BK sea ice and the winter circulation was explored through systematically analysing 3 AMIP experiments. Given that boundary conditions supplied to the model could be controlled, the causality of any relationship between sea ice and the mid-latitude relationship can be identified.

- **Does sea ice variability affect the wider atmospheric circulation variability and the NAO?**

AMIP models forced with time-varying sea ice or climatological sea ice showed no difference in their simulation of interannual MSLP variability, and closely match vari-

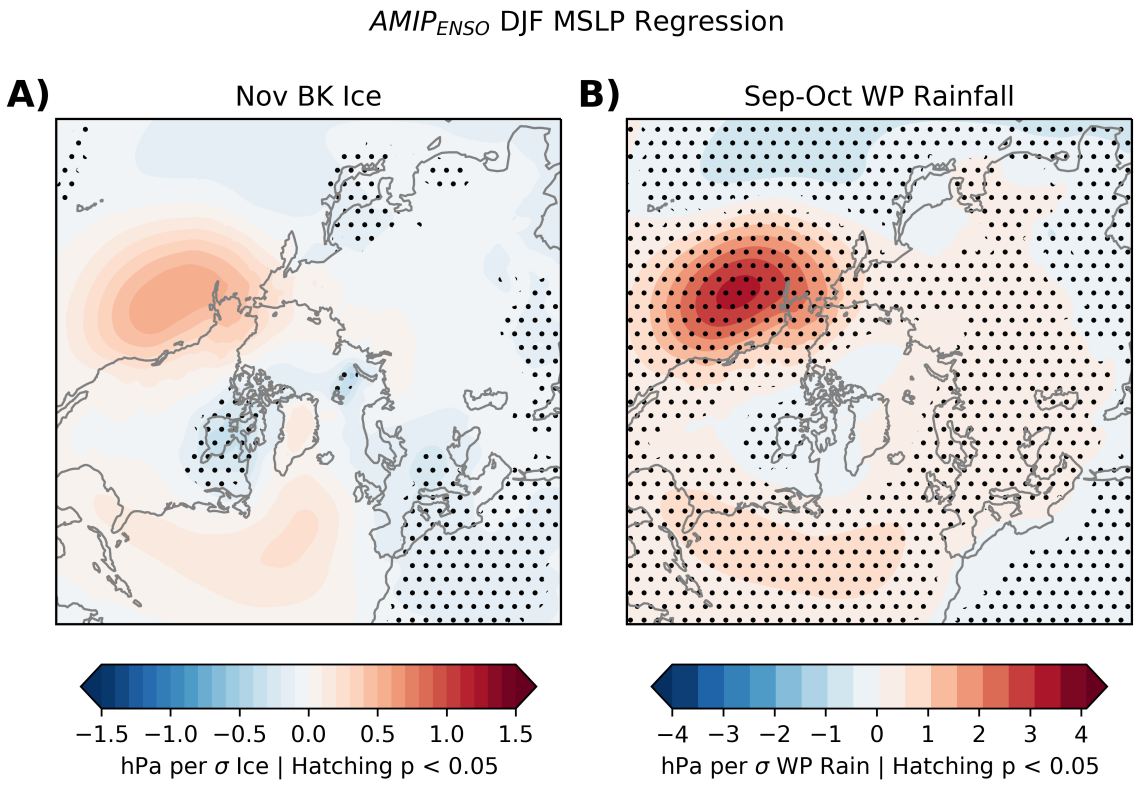

Figure 6.9: Regression of Nov BK sea ice or Sep-Oct West Pacific rainfall onto the winter circulation in the AMIP$_{ENSO}$ experiments. A): Linear regression of November BK sea ice onto the ensemble mean DJF MSLP field in AMIP$_{ENSO}$. **B)**: Linear regression of ensemble mean Sep-Oct WP rainfall onto the ensemble mean DJF MSLP field in AMIP$_{ENSO}$. At each gridpoint, regression coefficients that are statistically non-zero at the 5% level are hatched.

ability in reanalysis. Additionally, AMIP models forced with time-varying sea ice show no difference in their ability to reproduce the observed NAO index, despite sea ice being so commonly linked to NAO variability. Nevertheless, this may still be due to model deficiency, as the models may under-represent a teleconnection between sea ice and the mid-latitudes. This under-representation may be resultant of anomalously weak signals in the model [*Scaife and Smith,* 2018].

- **What is the forced pattern related to sea ice variability in the model, and is this similar in observations?**

The relationship between BK sea ice in November and the subsequent winter circulation was analysed in the AMIP models and reanalysis. While individual ensemble members could reproduce the relationship between -NAO and low BK sea ice, they could not account for the magnitude of this relationship found in reanalysis. Regions over the Azores and BK seas were found where the regression coefficient, which described the BK sea ice, winter MSLP relationship at each gridpoint, was outside the 5-95% range of regression coefficients calculated for all individual members. However, performing a field significance test revealed that spurious similar sized regions could be found when replacing the regression coefficients of reanalysis with individual ensemble members, with an equivalent global area in 10% of cases. This suggested the spurious regions could occur by chance. The regression of observed BK sea ice onto the AMIP$_{OBS}$ and AMIP$_{CLIM}$ ensemble mean winter MSLP revealed a weakly opposite NAO regression to that found in reanalysis; where low BK sea ice related to a weakly positive NAO, unlike that found in reanalysis. A relationship with the Aleutian Low was identified in the models. This relationship to BK sea ice variability is found to be similar in both AMIP$_{OBS}$ and AMIP$_{CLIM}$ and suggests the regression pattern found between BK ice and the winter MSLP is non-causal and originates from elsewhere, in this case the tropical ocean. Using AMIP$_{ENSO}$, this can be partly attributed to tropical Pacific SST variability.

- **Can tropical variability account for a link between sea ice and the extra-tropical circulation?**

The similarity of the forced winter MSLP regression patterns found in AMIP$_{OBS}$ and AMIP$_{CLIM}$ in relation to November BK sea ice variability indicate this regression is

originating from ocean boundary conditions elsewhere. This is investigated further by examining tropical rainfall in the west Pacific, which has been linked to sea ice variability through the MJO [*Henderson et al.,* 2014]. Given the weak but statistically significant correlation between WP_{SO} rainfall and November BK sea ice, it is suggested that the forced pattern found earlier between BK sea ice and the winter MSLP is co-incidental to tropical variability, which drives both. This is investigated through the regression of WP_{SO} onto the winter circulation pattern, which reveals a similar forced pattern.

Remaining questions involve the mechanisms that relate tropical variability and sea ice during autumn. A variety of mechanisms have been suggested in the literature through poleward heat and moisture fluxes. The next results chapter aims to seek better understanding of these through tropical nudging experiments.

Chapter 7

Tropical Nudging Experiments

This chapter explores the relationship between tropical atmospheric variability during autumn, and the extratropical atmosphere. This is achieved through nudging the tropics towards reanalysis in a coupled model simulation using GloSea5, in the same configuration as DePreSys3. This 'clean' model test helps infer causality of the relationship between the tropics and extratropical/polar atmosphere, assuming minimal influence of the extratropics on the tropics. Additionally, it can be used to isolate autumn links between tropical rainfall and sea ice variability.

7.1 Introduction

Dynamical model nudging experiments, also known as relaxation experiments, are an effective tool for identifying regions of climate model error [*Jung et al.,* 2008], or for identifying teleconnections between different regions [*Greatbatch et al.,* 2012; *Knight et al.,* 2017]. It involves nudging a region towards a state, such as observational reanalysis, and allowing the rest of the model to evolve freely as determined by its physics [*Knight et al.,* 2017]. This method has been employed over a range of time-scales; to assess model error on weekly scales [*Semmler et al.,* 2017], intraseasonal and seasonal [*Watson et al.,* 2016], interannual and decadal [*Douville et al.,* 2006; *Greatbatch et al.,* 2012; *Gollan et al.,* 2015], as well as for analysing trends [*Peings et al.,* 2019; *Ding et al.,* 2019]. It is often employed on a case study basis for determining drivers of anomalous winters, such as the historic cold winter of 1962/63 [*Greatbatch et al.,* 2015], or more recently the wet winters of 2013/14 [*Watson et al.,* 2016; *Knight et al.,* 2017] and 2015/16 [*Maidens et*

al., 2019]. The nudging technique involves adding a fraction of the difference between the model field and the nudging field, scaled by some relaxation parameter. This relaxation parameter can be customised to the problem being investigated; it can be a function of latitude, longitude, height and time, with varying strength [*Jung et al.,* 2008]. Technical details of how this method is applied to the experiments conducted here are explained in the methodology chapter.

Early studies investigating how errors in the tropics affect predictability in the midlatitudes found significant improvements in model skill through tropical relaxation on weekly timescales [*Ferranti et al.,* 1990], by affecting the source of Rossby waves that propagate polewards and interact with the midlatitude circulation [*Jung et al.,* 2010]. Nudging regions where these errors occur towards observational reanalysis and examining the resulting change in model skill can help to identify regions that are sensitive to errors and therefore require model development. This can also be used to identify causal relationships between drivers and the midlatitude circulation. *Jung et al.* [2014] nudged the polar atmosphere to reanalysis to determine how removing error in the Arctic atmosphere led to reduction in error elsewhere during winter on sub-seasonal timescales. They found that polar nudging led to error reduction over continental North America and more widely over Asia, but little change over the Atlantic and Pacific. This is similar to many studies which demonstrate a weak causal connection between sea ice and the extratropics, much weaker than that recently observed [*Overland,* 2016].

The winter of 2013/14 was particularly wet over north-west Europe, as a result of anticyclonic clustering around the UK [*Knight et al.,* 2017]. By using nudging analysis in different regions of the atmosphere, tropical conditions were shown to have a significant role in promoting the anomalously cyclonic environment in the Atlantic [*Knight et al.,* 2017], particularly the QBO which strengthened the stratospheric polar vortex. *Watson et al.* [2016] also showed a wave train emanating from the tropics into the midlatitudes during this winter, though nudging the west Pacific alone did not demonstrate a tangible impact on the Atlantic storm track, suggesting other basins such as the tropical Atlantic can be more influential. *Maidens et al.* [2019] found independent contributions from both the tropical Atlantic and Pacific on the anomalous winter of 2015/16, reiterating the importance of accurate representation of tropical processes in models. Furthermore, extreme cold winters such as 1962/63 were also rooted in the deep tropics; *Greatbatch et*

al. [2015] imposed tropical nudging during this winter, revealing a wave train originating from the tropical Pacific sector propagating into the extratropics. These results echo the idea of a causal pathway connecting the tropics to the mid-latitudes, as explored in the literature review.

Inter-annual variability in the mid-latitudes has been explored using nudging experiments. Through relaxing the tropics to reanalysis over 1960 through to 2001, *Greatbatch et al.* [2012] found that the tropics strongly influence the midlatitude Pacific, as well as exerting a weak effect on the Atlantic, as found in other studies such as *Ineson and Scaife* [2009]. Similar studies have attributed tropical sources to midlatitude blocking frequency, with pronounced interannual and decadal variability [*Gollan et al.,* 2015]. These studies demonstrate successful utilisation of nudging set-ups to demonstrate a dominant influence of tropical variability on the extratropical circulation. More recently, *Ding et al.* [2019] nudged the Arctic atmosphere to infer a response in sea ice to better understand the direction of causality between ice variability and the atmosphere above, demonstrating a top down mechanism where the atmosphere can drive ice variability and that feedbacks between the ice and atmosphere are small during summer. Additionally, *Peings* [2019] found that nudging Ural sea level pressure to reanalysis during autumn, stratospheric impacts found later in winter are not linked to sea ice or snow cover as identified in separate experiments. This provides additional evidence that BK sea ice variability and snow cover is symptomatic of the atmospheric circulation above, and does not necessarily induce changes above.

The nudging technique is not without its limitations. For example, *Jung et al.* [2010] noted that tropical nudging, even when the boundary of nudging was tapered (smoothed to avoid a hard transition), the presence of a transition zone could lead to spurious refraction of extratropical Rossby waves, leading to model errors. Additionally, imbalances may occur around and within transition zones particularly if horizontal wind components and temperature are nudged; *Jung et al.* [2010] propose nudging divergence and vorticity fields alone. Idealised models have been used to investigate the sensitivity of different relaxation timescales and the impact on generating Rossby waves from the tropics, through idealised heating anomalies [*Hoskins et al.,* 2012]. An additional caveat, separate to the nudging methodology itself, is the observed reanalysis the model is being relaxed to; it assumes the reanalysis product is accurate, despite biases that may exist in reanalysis products

such as over the Arctic, where weak observational constraints occur due to sparse in-situ records [*Jung et al.,* 2014].

The nudging method is employed here to help determine causality between tropical variability, BK sea ice and the NAO. While the tropics to NAO link is well documented through ENSO/MJO/QBO teleconnections as discussed in the literature review, the tropics to BK ice relationship is less well understood. There is emerging literature on this relationship, particularly during summer [*Henderson et al.,* 2014] and winter [*Lee et al.,* 2011], as well as potential mechanisms involving poleward heat and moisture fluxes into the Arctic [*Gong et al.,* 2017; *Park et al.,* 2015; *Henderson et al.,* 2014; *Woods et al.,* 2013; *Woods and Caballero,* 2016], but the relationship in autumn is less clear, particularly in the context of determining any causality in the relationship between autumn BK sea ice and winter NAO. There are no tropical nudging experiments which have investigated inter-annual variability in sea ice during late autumn; a key period proposed to regulate the polar vortex and the winter NAO [*Petoukhov and Semenov,* 2009].

- **Can tropical interannual variability be used to reproduce variability the wider atmospheric circulation and subsequently sea ice?**

The first objective of these experiments is therefore to determine whether providing a coupled GCM with tropical information alone is sufficient to reconstruct variability in the wider circulation and subsequently sea ice.

- **Does the model reproduce the observed relationship between sea ice and the wider atmospheric circulation?**

Atmospheric conditions that precede variability in autumn Arctic sea ice are investigated, to determine whether they originate from tropical sources as suggested by *Henderson et al.* [2014] in summer and winter. Additionally, studies such as *Peings et al.* [2019] suggest sea ice responds to, and does not cause, Ural blocking in autumn. This is key, given pathways via the stratosphere that allow autumn Ural blocking to affect the polar vortex and subsequent winter weather [*Kryjov,* 2015; *Kryjov and Min,* 2016].

- **Case study: How do sea ice and atmospheric circulation patterns compare between the strong tropical forcing year of 1997 and other years?**

The period analysed here (1993-2015 inclusive) contains strong ENSO years, such as the strong El Niño of 1997 [*Wolter and Timlin,* 1998]. If there is a causal link between the tropics and higher latitudes leading to changes in sea ice, then strong ENSO years should have a larger, detectable impact on sea ice in autumn when computing the ensemble mean.

7.2 Methodology

Firstly, a year was determined where BK sea ice follows a fairly typical concentration through autumn. This year is then re-simulated in autumn with observed tropical variability imposed from different years. An ensemble of 20 members is run, to take into account internal variability disguising any possibly forced signal. Constraints of the model suite mean a year must be chosen between 1993 and 2015; typical ice concentration in this period might not be representative of a longer (1980-2016) climate period, so this was also tested. First, the year between 1993-2015 was identified where BK sea ice in October was closest to the climate mean. Further analysis on the chosen year, 1997, reveals that sea ice evolution into winter doesn't follow a typical evolution (by winter it was anomalously high), and this is also a particularly strong El Niño year. This year was rejected; the second year closest to the mean sea ice is the year 2000.

Sea ice in the autumn of 2000 was examined, as well as August and winter sea ice extents, both in the BK sea and across the whole Arctic to verify evolution remained close to the 1980-2016 mean. In all months analysed, and in both the BK seas and Pan-Arctic case, the year 2000 remains within the 1 to -1 σ spread about the 1980-2016 mean. Additional analysis explored how influential components of the climate system in autumn 2000 compare to the longer term spread (figure 7.1). Rainfall in the 4 tropical basins as defined in *Scaife et al.* [2017] are analysed, along with ENSO, QBO and polar vortex. This analysis reveals a weak La Niña year (slightly negative ENSO index, with enhanced west Pacific rainfall). The QBO, which has been linked to the NAO [e.g. *Marshall and Scaife,* 2009] is in a near neutral phase during autumn 2000. The polar vortex in autumn 2000 was one of the weakest relative to the recent climate period; although tropospheric, stratospheric teleconnections are less significant during autumn compared to winter [*Kushner and Polvani,* 2006].

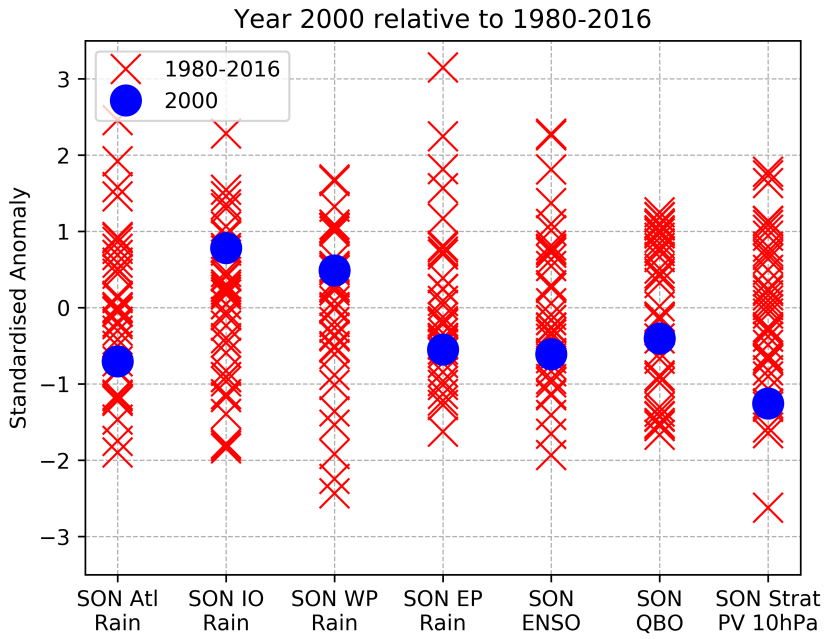

Figure 7.1: Selecting a case study year with typical BK sea ice in late autumn. Standardised tropical Atlantic, Indian, West and East Pacific rainfall as defined in the methodology chapter, along with ENSO 3.4 index, QBO and stratospheric polar vortex during autumn (Sep-Nov average). All indices are standardised about their respective 1980-2016 mean and variance. The chosen case study year 2000 is denoted by a circle.

Despite being fairly typical in terms of global teleconnections examined here, autumn 2000 led to widespread flooding over western Europe causing over £1bn in insured losses [*Howe and White,* 2002; *Pall et al.,* 2011]. This extreme rainfall was generally due to an eastwards displacement of the North Atlantic jet, mapping onto the Scandinavian mode of variability; partly enhanced by anomalous tropical Atlantic upper tropospheric convergence [*Blackburn and Hoskins,* 2001; *Pall et al.,* 2011]. This Scandinavian pattern does not project well onto the NAO mode, so won't be picked up by this index. The Rossby wave pattern generated by this tropical Atlantic convergence propagated north east over Eurasia into the BK seas region (figure 1 in *Pall et al.,* 2011); so may have a secondary impact on Arctic sea ice.

Guided by earlier results in the methodology chapter which revealed that the leading EOF of observed MSLP during November is not the NAO pattern (figure 3.5), EOF decomposition of the MSLP field in the model ensemble and reanalysis is performed [*Monahan et al.,* 2009], with the leading EOF of October-November averaged MSLP shown in figure 7.2A,B. Whilst the leading EOF in the model is centred on the two boxes used to derive the NAO index; the NAO pattern in reanalysis is displaced and so

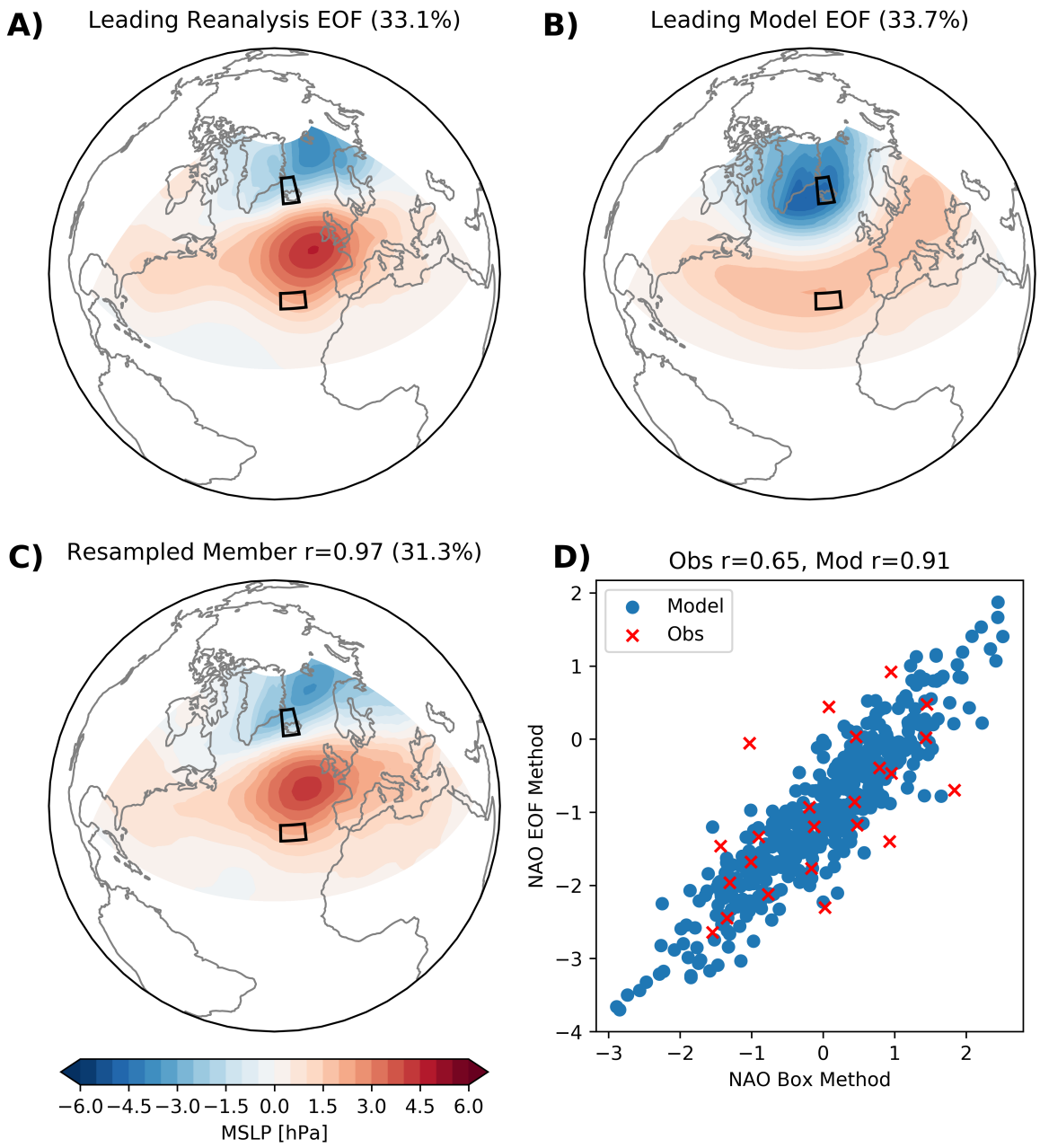

Figure 7.2: EOF analysis of the leading mode of variability in October, November averaged MSLP. A) Leading EOF of reanalysis and **B)** in the model ensemble covering the period 1993-2015 inclusive. The location of the boxes used to contruct the NAO box indice are shown. **C)** Randomly sampling 23 members from the 460 model ensemble members to be representative of the reanalysis sample, constructing the leading EOF of this sample, and calculating the weighted pattern correlation with the leading EOF pattern in reanalysis. This is repeated 10000 times; the sample with the highest pattern correlation is shown. **D)** Scatter plot of the NAO index derived through either principal component analysis or the box method, for all years in reanalysis (23) or all members in the model (460). The respective correlation is also shown between each method in the two datasets. Variance that each pattern explain is shown in the title.

this box method will no longer pick up variability associated with this pattern. Given it could be argued that the leading EOF in reanalysis is picking up the East Atlantic Pattern (or Atlantic ridge, described in figure 2.1), the 3 leading EOFs are checked to determine whether the second or third EOF describes the NAO mode better. All 3 EOFS are ordered in the same way between model and observations, with similar variance (not shown). Next, sampling uncertainty is investigated to see whether the observed NAO pattern can be reproduced within the model via internal variability. Through randomly sampling an equivalent number of ensemble members as reanalysis years, and calculating the leading EOF, a combination is found with the highest weighted pattern correlation with the leading reanalysis EOF, shown in figure 7.2C along with its pattern correlation coefficient. This pattern closely resembles the observed leading EOF; thus suggesting the pattern found in reanalysis could occur via internal variability, rather than a model error.

The lack of suitability of using the box index for the leading EOF in late autumn is summarised in figure 7.2D, through comparing the principal component derived NAO index (based on EOF analysis) and the box index, in reanalysis and the model ensemble. The PC approach well captures NAO variability in the model; both general distribution and extremes, but performs poorly with the limited observational sample and the box index.

Identifying a suitable ensemble size to sufficiently isolate forced signals from internal variability was explored through the model's ability to reproduce the October-November averaged NAO index. The equation of *Murphy,* [1990] was used as defined in equation 6.1. Randomly sampling members without replacement thousands of times using different ensemble sizes, and calculating the correlation between the ensemble mean NAO index with the observed NAO index produces a curve which closely follows the theoretical values predicted by equation 6.1, as shown in figure 7.3. The EOF approach is used to construct the NAO index, given the displaced NAO mode in reanalysis. As a reminder, the coefficients C_{om} and C_{mm} in equation 6.1 represent the average correlation between each member and the real world, and the average correlation between each member and other members respectively. This equation, along with the theoretical correlation value for an infinite ensemble, is useful in determining the trade off between running more ensemble members and gains in skill from isolating a forced signal from noise. To calculate uncertainty about the theoretical curve and infinite ensemble correlation value, coefficients

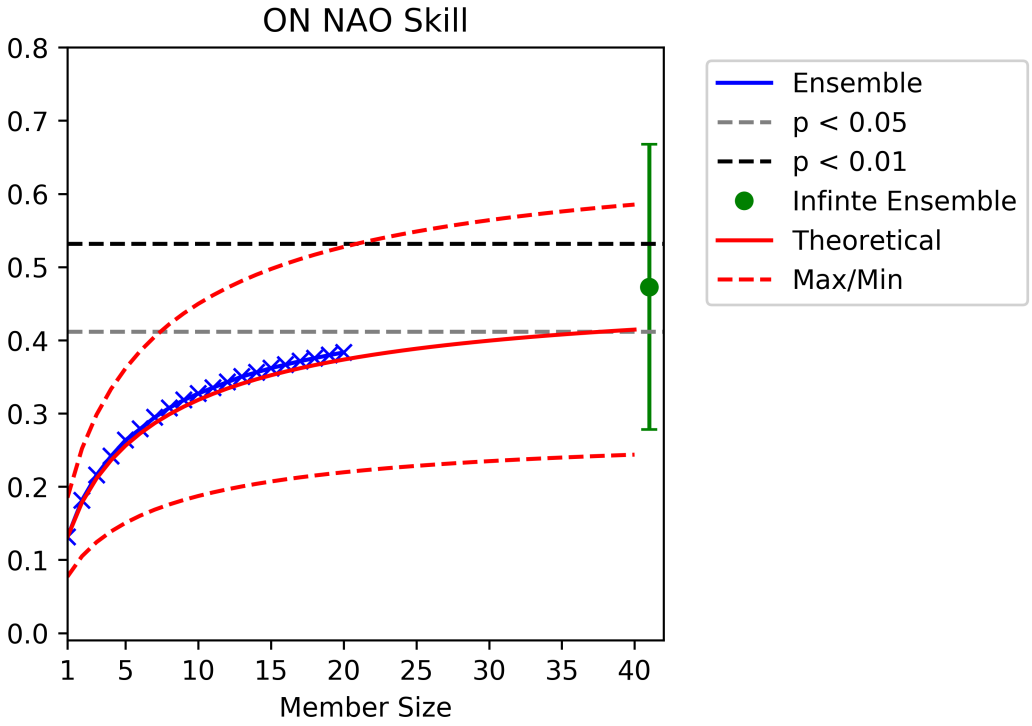

Figure 7.3: Model NAO reproducibility as a function of ensemble size. Using a Monte-Carlo approach to repeatedly sample n members without replacement, and calculate the correlation between the ensemble mean NAO index and observed NAO index (October, November average) as blue crosses (10000 samples). The red line is the theoretical line predicting by *Murphy* 1990 (equation 6.1), along with the asymptote of an infinite ensemble according to this theoretical relationship (green dot). The red dashed lines (green whiskers) indicate the 5-95% confidence interval around the theoretical prediction (asymptote) respectively. Significant correlations at the 5% and 1% level are denoted by dashed black lines.

C_{om} and C_{mm} (which are both averages) have standard error E about the mean.

$$E_{om} = \frac{\sigma_{om}}{\sqrt{N_{om}}} \qquad E_{mm} = \frac{\sigma_{mm}}{\sqrt{N_{mm}}} \tag{7.1}$$

where for an ensemble containing 20 members:

$N_{om} = 20$

$N_{mm} = 190$ (possible unique inter-member correlations).

Error is contained in term $\frac{C_{om}}{\sqrt{C_{mm}}}$. Using error propagation in quadrature allows confidence intervals to be calculated around the theoretical values as shown in figure 7.3. For this experiment, $C_{om} = 0.131 \pm 0.053$ and $C_{mm} = 0.077 \pm 0.015$. However, given

that correlation is a non-linear function, a Fisher-Z tranform can be applied to more accurately construct confidence intervals around this prediction (process can be found in the appendix). This produces 5-95% confidence intervals around the coefficient values $C_{om} = 0.139\,[0.548, -0.324]$ and $C_{mm} = 0.080\,[0.219, -0.063]$.

Note given the small correlation values, the large 5-95% confidence bounds around these coefficient values. It is also not obvious how to propagate non-equidistant uncertainty about the mean in quadrature. Work on understanding potential predictability using ensembles and methods is an active research problem. In the context of this experiment, 20 ensemble members is deemed sufficient given the large uncertainty in skill gain from increasing this and constraints on computing resource.

7.3 Model Validation

The divergence of the model ensemble from initial conditions is investigated. All 460 members (20 members for each of the 23 nudged years) differ only through stochastic physics perturbations initially, and their tropical nudging. Given identical starting conditions (1st September 2000), determining how quickly ensemble members diverge from each other provides an interpretation of the persistence of boundary conditions. Interannual spread for each day during autumn is explored for BK sea ice and the NAO, both in observations and the model ensemble in figure 7.4A,B. The spatial pattern of this variability during November is also displayed in the C and D for sea ice and MSLP respectively in figure 7.4, along with the deviations between reanalysis and the model ensemble (E,F).

Sea ice variability is additionally constrained in extent by coastline. This constraint explains the reduction of variability in sea ice in late October in the Barents-Kara sea (figure 7.4A). There is lower interannual sea ice variability within the model. This is partly because the ocean initial conditions (which are all year 2000) to some degree persist through autumn, limiting sea ice variability compared to observations. Studies such as *Onarheim et al.* [2015] and *Årthun et al.* [2012] indicate the important role oceanic heat content plays in controlling sea ice variability in the BK seas. No suggestion of underestimation of variability over the Arctic in MSLP supports this hypothesis (figure 7.4F). Investigating the spatial structure of sea ice variability in figure 7.4C,D indicates the underestimation of November ice variability is mostly focused over the BK seas. Note

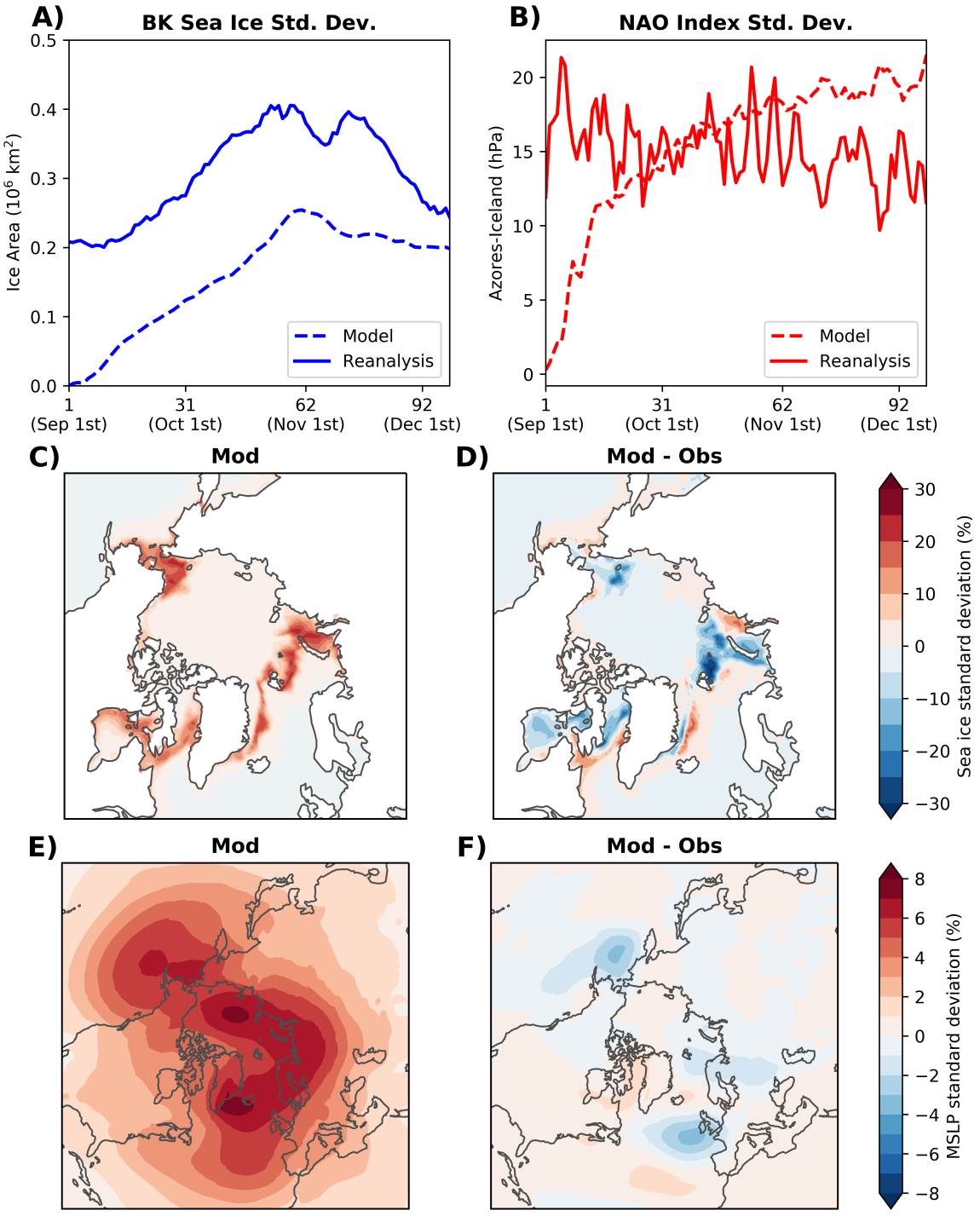

Figure 7.4: Model variability from initialisation compared to observations. **A)** For each day in autumn, the standard deviation of BK sea ice concentration across all years (1993-2015 inclusive) is computed for reanalysis, and for the model (across all members too). **B)** Same as A, but for the NAO index (Azores-Iceland box). **C)** Standard deviation of November averaged sea ice concentration across all members and years in the model. **D)** Same as C but the difference between model and observations. **E)** Same as C, but for mean sea level pressure. **F)** Same as D, but for mean sea level pressure.

other regions that have considerable interannual variability such as the Chuckchi and Bering seas on the Pacific have similar interannual variability to observations.

Inter-annual spread in the NAO increases rapidly beyond initialisation using the box method (figure 7.4B). The NAO index used here is constructed using the box method, to allow a like for like comparison between the model and reanalysis. Therefore, overestimation of variability in the model is likely due to the NAO mode centres (figure 7.2), and not due to a model bias. Analysis of the spatial MSLP variance in figure 7.4E,F reveal only small deficiencies in model variance in parts of the Atlantic and Pacific storm tracks. Given the limited observational sample (23 years), this is easily explained by sampling uncertainty within the observations (i.e. another 23 year period would show different apparent biases).

7.4 Skill in Sea Ice and Atmospheric Patterns

The first objective of the nudging experiments is to determine whether a model containing only tropical information can skilfully reconstruct interannual variability at mid to high latitudes in autumn. Similar studies have investigated the effect of nudging the tropics on mid-high latitude skill and found limited influence into the Arctic [*Jung et al.,* 2014], however this study was limited by its use of an atmospheric model with prescribed boundary conditions. The model set-up here differs as it is coupled between the atmosphere and ocean.

Firstly, key indices of the mid-high latitudes are investigated, comprising: BK sea ice, NAO, Atlantic tripole, and the stratospheric polar vortex (figure 7.5). BK interannual sea ice variability is not reproduced in the ensemble mean, nor is the trend, so a priori, tropical variability cannot directly be related to BK sea ice variability in these experiments. Additionally, tropical variability does not produce a trend in sea ice; *Ding et al.,* [2019] attributed part of the recent Arctic sea ice trend to tropical internal variability, contained within these experiments. It is unclear whether the lack of teleconnection representation from the tropics to Arctic is due to a model deficiency such as the signal-to-noise paradox [*Scaife and Smith,* 2018], in which case the signal could be too weak to be picked up with a limited ensemble. However, 1997 is a notable exception, where the ensemble mean (and majority of ensemble members) simulate anomalously high BK ice; this coincides with a

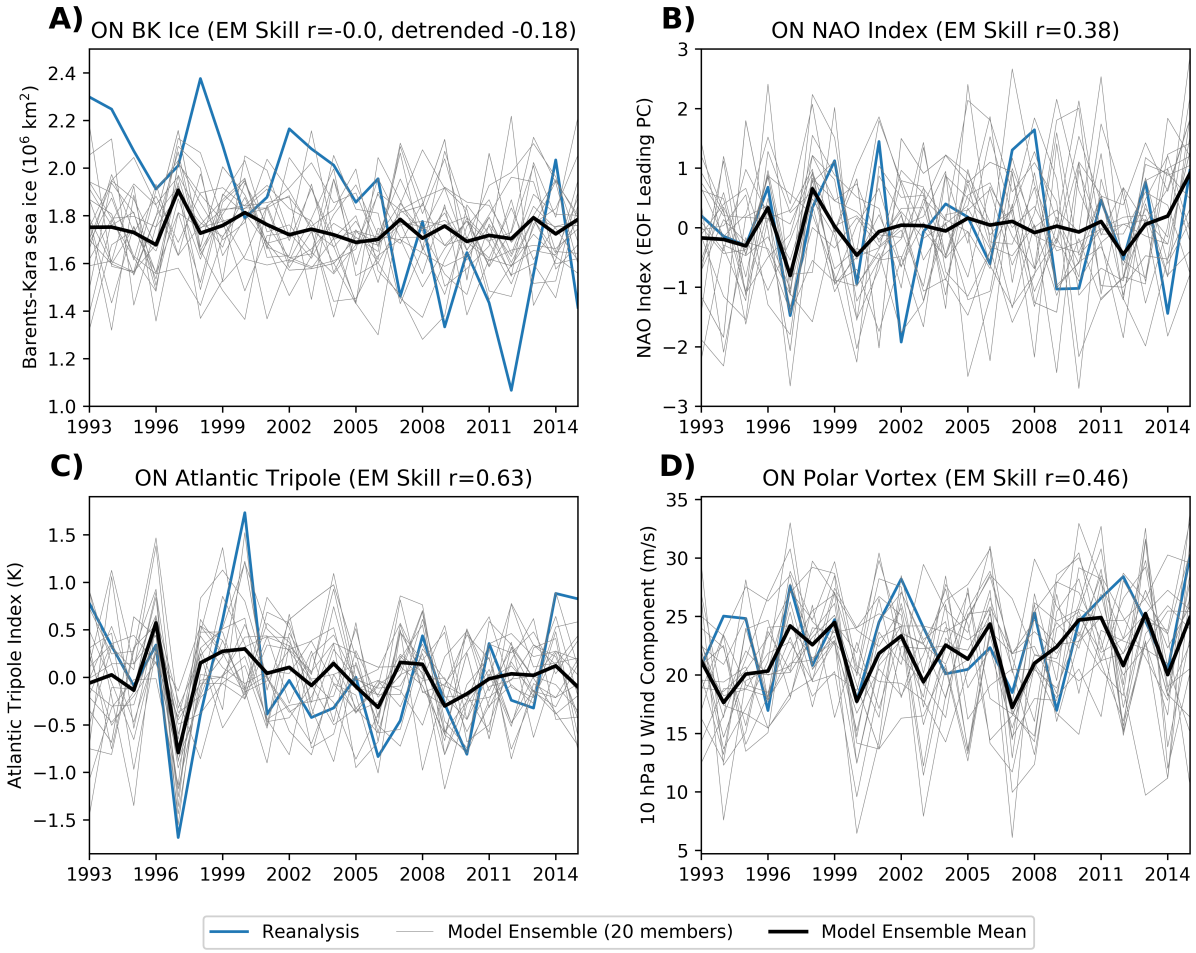

Figure 7.5: Skill in reproducing components of the climate system in late autumn. Interannual timeseries of October, November averaged **A)** BK sea ice, **B)** NAO index (EOF derived), **C)** Atlantic Tripole index and **D)** stratospheric polar vortex at 10hPa for reanalysis, individual ensemble members, and the ensemble mean. Correlation values between the ensemble mean and reanalysis are shown in the respective titles.

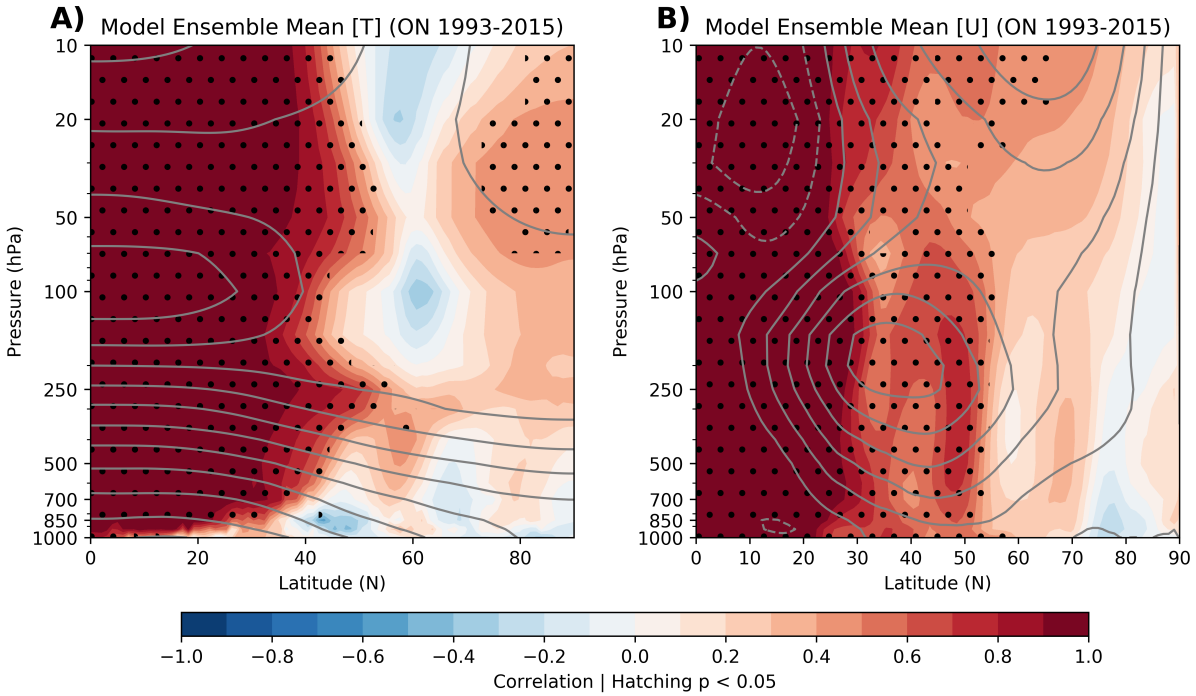

Figure 7.6: Skill in the zonal mean temperature and wind fields. Correlation between interannual **A)** zonal mean temperature and **B)** U component of wind (right panel) with reanalysis, for the October, November average over the period 1993-2015. Contours indicate reanalysis climatology for reference only, each contour interval is 10K or 5m/s for the respective panels. Negative values are contained by dashed contours. Hatching indicates correlation significance at the 5% level.

strong El Niño developing in autumn and tropical influences may be more pronounced. This case study is investigated later in this chapter.

The NAO index (EOF construction) is partly reproduced with a marginally significant correlation of 0.4. Similar to the case with BK sea ice, the NAO is particularly reproducible in the strong ENSO years such as 1997, whereas others show little signal (e.g. 2000-2011); particularly in comparison to ensemble member spread during this period. The Atlantic tripole index is well reproduced in late autumn; though this is in part due to the index being constructed with subtropical SST's (figure 3.11) which underlie the region of nudging, so are well reproduced. The stratospheric polar vortex is skilfully reproduced. Additionally, there is a stronger signal in relation to the ensemble spread, which may carry a signal through into winter [*Nie et al.,* 2019].

Next, spatial correlation maps are generated for both the zonal mean to examine the vertical atmospheric structure, as well as maps of sea ice, SST's and tropospheric variables. Zonal mean plots for temperature and the zonal wind component are shown in

figure 7.6. The nudging boundary is 19.5° (with tapering beyond this - see methodology), throughout the troposphere/stratosphere, therefore any correlation within this tropical region is trivial. Skill in zonal mean temperature extends to 40-50°N, with additional skill in the polar stratosphere. This is reflected in the zonal wind in the stratosphere, as a result of thermal wind balance. Skill is largely absent in the mid to high latitude troposphere. Strong internal variability in these regions may be masking a signal, and may only become apparent using an ensemble sufficiently larger than 20 members due to weak signals.

Skill in predicting the general tropospheric circulation patterns is investigated in figure 7.7. To first order, skill in MSLP and 500hPa geopotential height fields decreases as a function of latitude. Skill also varies strongly with longitude; with a notable difference between the oceans and continents. There is little to no apparent reproducibility of the lower atmospheric circulation patterns over east Asia, the Arctic and large regions of North America; the prior two coinciding with regions of large internal variability; see figure 7.4. Skill in the Atlantic storm track is the cause of the earlier noted NAO skill. The occurrence of skill in the same mid-latitude regions in MSLP fields and 500hPa geopotential suggest the model can largely reproduce the barotropic structure over these regions within the troposphere. Surface fields are also explored, to determine whether sea ice is skilfully reproduced in other regions, and how well mid-latitude SST's can be reconstructed. These results complement those of *Blanchard-Wrigglesworth and Ding* [2019], who find tropical nudging has minimal effect in the Arctic, and that nudging the mid-latitudes is required to have an measurable impact. Additionally, similar to the MSLP pattern here, *Ye et al.* [2018] found more tropically sourced skill over the Pacific than Atlantic sector, consistent with stronger teleconnections here.

The lack of interannual sea ice reproducibility is not confined to the BK seas, and extends more widely across the Arctic, despite mid-latitude storm tracks being skilfully predicted (and widely related to heat/moisture fluxes into the Arctic). SST's are moderately well predicted in the mid-latitude storm tracks; however this is probably a result of the atmosphere being skilfully reproduced over these regions and subsequently driving SST changes. Despite the model being initialised with the conditions of the year 2000, persistence in ocean upper layer conditions does not appear to be present by late autumn (and is modified by atmospheric circulation patterns driven by tropical variability).

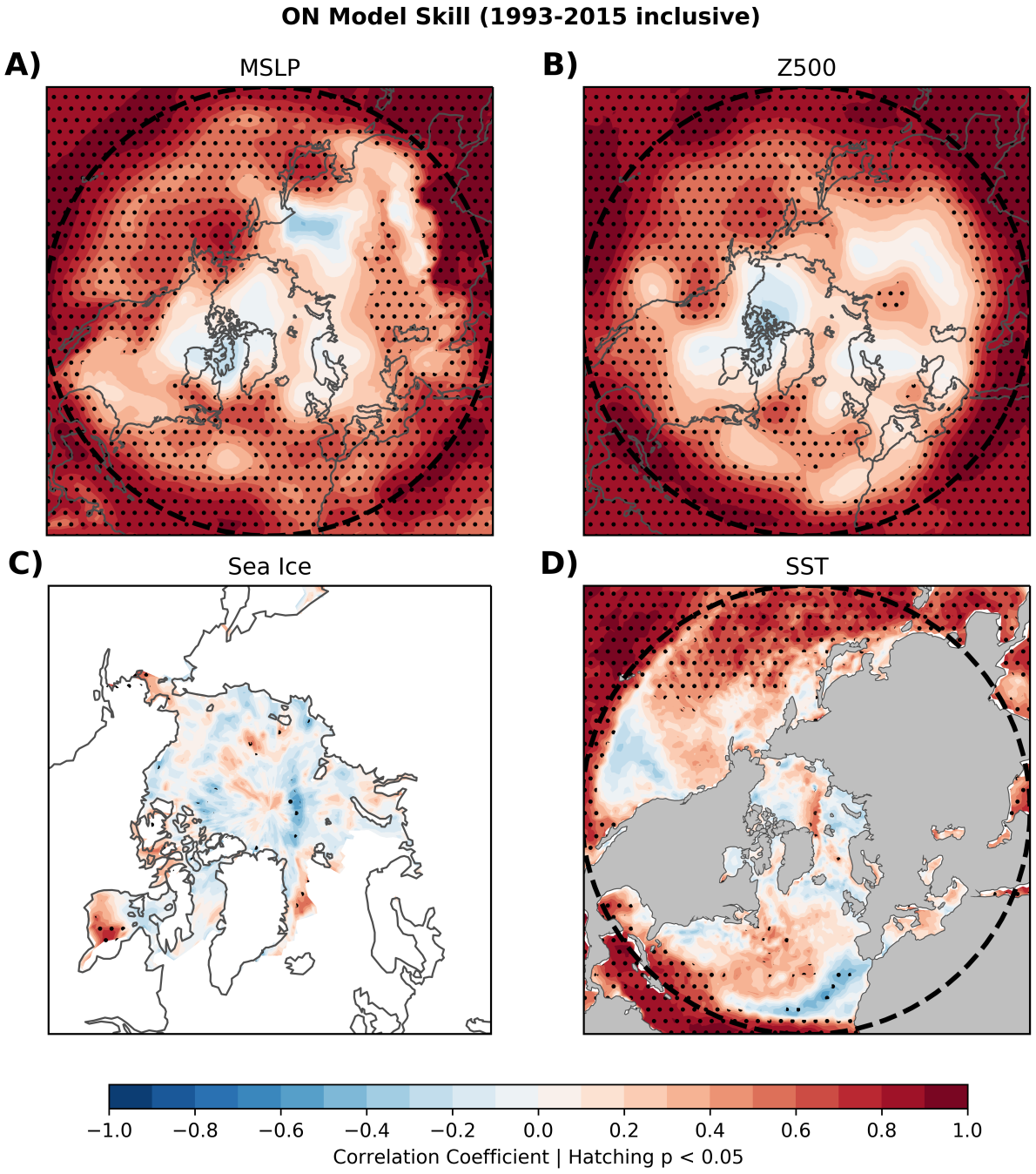

Figure 7.7: Skill across surface and tropospheric parameters. Interannual grid point correlation between October, November averaged **A)** mean sea level pressure, **B)** 500 hPa geopotential height, **C)** sea ice concentration and **D)** sea surface temperatures in reanalysis and the model ensemble mean. Hatching denotes regions where the correlation coefficient is significant at the 5% level. The tropical nudging boundary is shown by a dashed black line for reference.

Whilst the model cannot reproduce interannual variability in sea ice directly, it can reproduce aspects of the mid-latitude atmospheric circulation specifically over the storm tracks, as well as the polar stratospheric vortex in late autumn. Next, the relationship between BK sea ice and the NAO is investigated. If the NAO and sea ice is related, and given a large body of literature related polar stratosphere conditions to NAO variability in winter [*Hitchcock and Simpson,* 2014; *Scaife et al.,* 2016], and persistence in initial stratospheric conditions into winter [*Stockdale et al.,* 2015; *Nie et al.,* 2019], then it could be that tropical variability can influence key atmospheric regimes such as the NAO in autumn, but the link to sea ice involves two steps that contain too much atmospheric internal variability to isolate with an ensemble with 20 members; additionally due to the models erroneously weak signal (due to the signal, noise issues). Additionally, *Blanchard-Wrigglesworth and Ding* [2019] required the mid-latitudes to be additionally nudged to have a detectable impact on the Arctic, even in winter, suggesting the mid-latitudes may have an important role in mediating the strength of a tropospheric teleconnection between the tropics and the Arctic.

Through examining the signal-to-noise ratio and the ratio of predictable components in MSLP in figure 7.8, key regions are identified such as north east America and the Bering Sea. While the RPC is proportional to the correlation coefficient, which highlights these same regions in figure 7.7, the signal-to-noise ratio isolates the variance in the model ensemble mean compared to observations. This ratio decreases as a function of latitude; the ensemble becomes increasingly noisy and the ensemble mean signal becomes weak, demonstrating that this regions contain high internal variability (related to that found in figure 7.4).

7.5 Relationship between Sea Ice and the NAO

To further investigate the hypothesis developed in the previous section, the relationship between BK autumn sea ice and the atmospheric circulation is investigated in late autumn, using lead-lag regression and correlation. First, instantaneous interannual correlations between October-November averaged BK sea ice and the NAO are constructed within the ensemble, ensemble mean, and reanalysis, and the October-November lead-lag combinations are shown in figure 7.9. A strong instantaneous anti-correlation is revealed

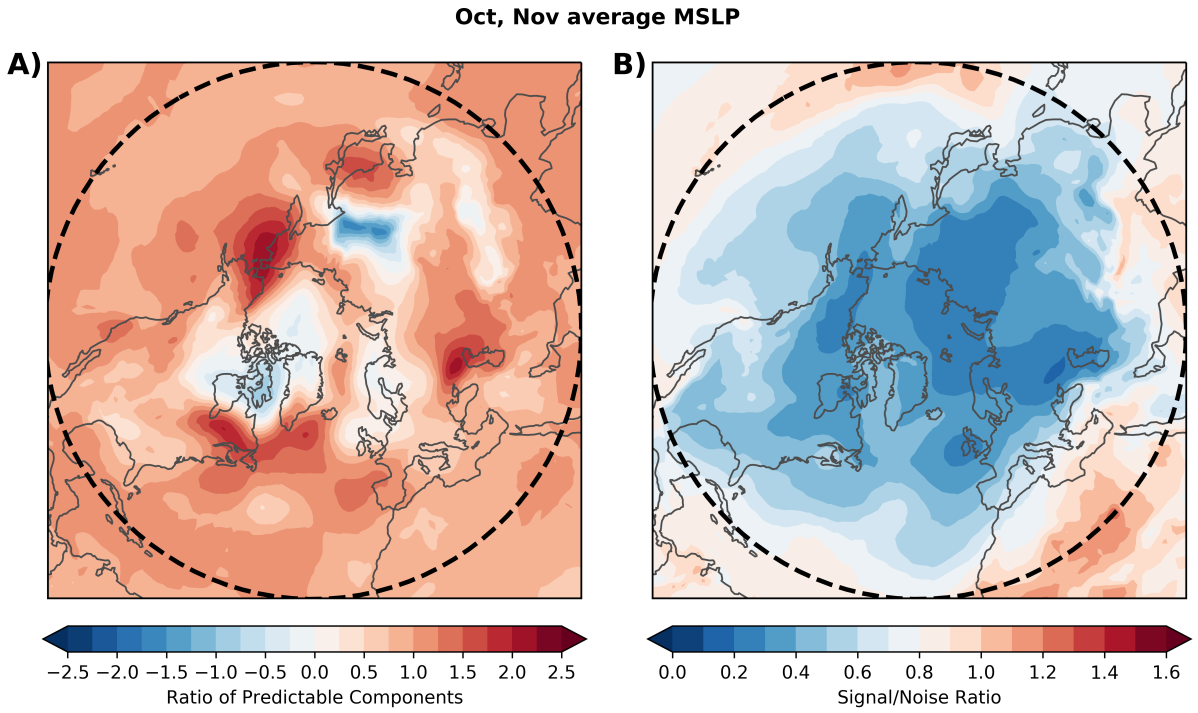

Figure 7.8: Spatial patterns of MSLP signal-to-noise ratio and RPC values. Gridpoint calculation of the signal-to-noise ratio and RPC value (equation 2.1), for October, November averaged mean sea level pressure. The boundary of tropical nudging is denoted by a dashed line.

between BK sea ice and the NAO in many members and the ensemble mean, but not in observations. Lead-lag correlation analysis shows this anti-correlation only manifests itself when the NAO leads BK sea ice. This is physically intuitive; a positive NAO indicates an enhanced storm track, and therefore enhanced heat and moisture fluxes into the high latitudes, which reduces sea ice concentration through melting and redistribution of sea ice.

A regression of November BK ice onto October 200hPa eddy streamfunction to identify wave like patterns and 700hPa temperature was performed using the model ensemble. A clear pattern is identified, revealing a wavenumber 1 pattern preceding high ice, with a dipole structure over Greenland and the Barents-Kara seas. In this configuration, anticyclonic eddy circulation over Greenland and cyclonic motion over the BK seas drives south-west motion of wind (not shown), preventing moisture and heat from lower latitudes in the Atlantic penetrating the Arctic leading to high BK sea ice concentration (reverse is true for low BK ice). The analysis is repeated for reanalysis, which shows a similar, but more noisy pattern. Given there is no trend in BK sea ice within the model, but there is

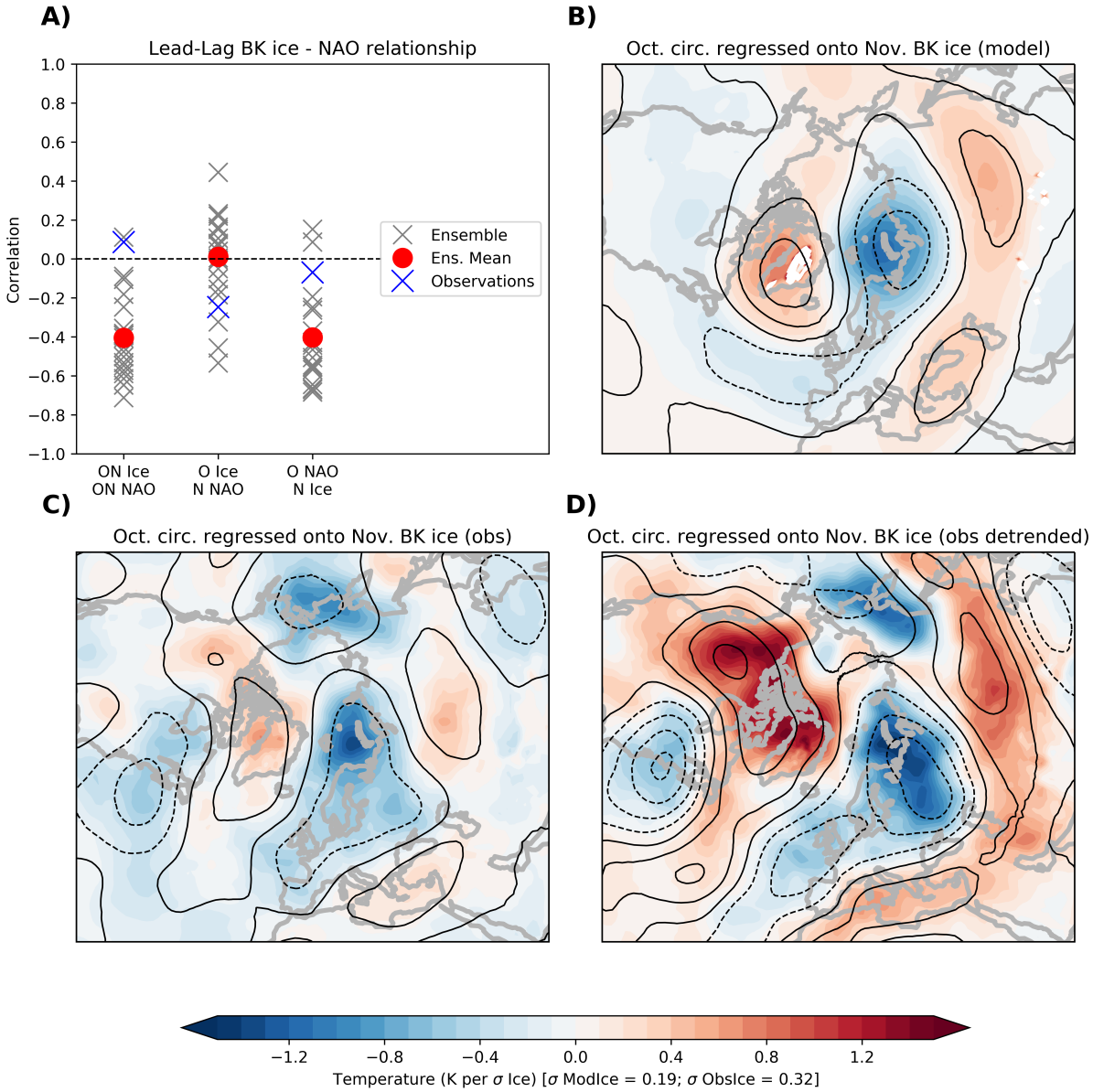

Figure 7.9: Lead-lag relationship between the NAO and BK sea ice in late autumn. A) Interannual correlation between the NAO and BK sea ice for each member; for instantaneous October, November averages, October BK ice, November NAO, and vice versa. The correlation after computing the ensemble mean is also shown as a red circle. The correlation in reanalysis is shown by a blue cross. **B)** October eddy streamfunction (contours) and 700hPa temperature (shading) in all ensemble members in the model are regressed onto standardised November BK sea ice. **C,D** Same as in the B, except for reanalysis (C) and linearly detrending all fields prior to analysis (D). In all cases, dashed contours indicate negative values of eddy streamfunction, with contour intervals of $1 \times 10^6 m^2 s^{-}1$

within reanalysis (figure 7.5A), this analysis is repeated for linearly detrended BK sea ice and circulation patterns in the figure 7.9D. This strengthens the pattern over the Arctic, and additionally reproduces features shown over lower latitudes of Asia found in the model regression. Note however, to draw this comparison, the respective model and observed ice is standardised prior to regression. Given the variance of model November BK ice is weaker than observed ice $\sigma_{MOD} = 0.19, \sigma_{OBS} = 0.32$ ($\times 10^6 km^2$) (as investigated in figure 7.4), if the sea ice was not standardised about its variance, then the model pattern would be weaker than reanalysis.

The source of the pattern related to ice variability in figure 7.9 is explored further to determine whether tropical sources can account for this. By again using 200hPa eddy streamfunction as a proxy for wave activity in the midlatitudes, sub-monthly model data is used. BK sea ice averaged over 20th-30th November is standardised about its mean and variance, and regressed onto the preceding circulation pattern up to 40 days prior. This analysis is shown in figure 7.10. Eddy anomalies are evident up to 20-40 days prior to BK sea ice variability in late autumn. Nearer to the period in question (0-10 days prior), circulation anomalies originating from the tropical Atlantic and Caribbean are found. These propagate over the Atlantic and arch over the storm track through to Eurasia and south-east China, supporting the idea that BK ice variability stems from tropical sources in autumn; particularly from variability within the tropical Atlantic and Caribbean. This begs the question; why doesn't tropical nudging reproduce sea ice variability if sea ice variability in late November can be related to tropical sources; is the wave source too far North?

7.6 Tropical Teleconnections

Tropical teleconnections into the mid-high latitudes are investigated to determine whether the model can reproduce observed teleconnections. Given the tropics in this model configuration are constrained to observations, the ENSO and QBO teleconnection in late autumn is explored. Firstly, the correlation between the September, October ENSO index and the September, October mid-latitude circulation is explored. Given the model tropical atmosphere is contrained to observations, the tropical SST's are also strongly constrained (ENSO 3.4 Index $r_{\mathrm{OBS,Model}} > 0.99$), therefore the observed ENSO index is

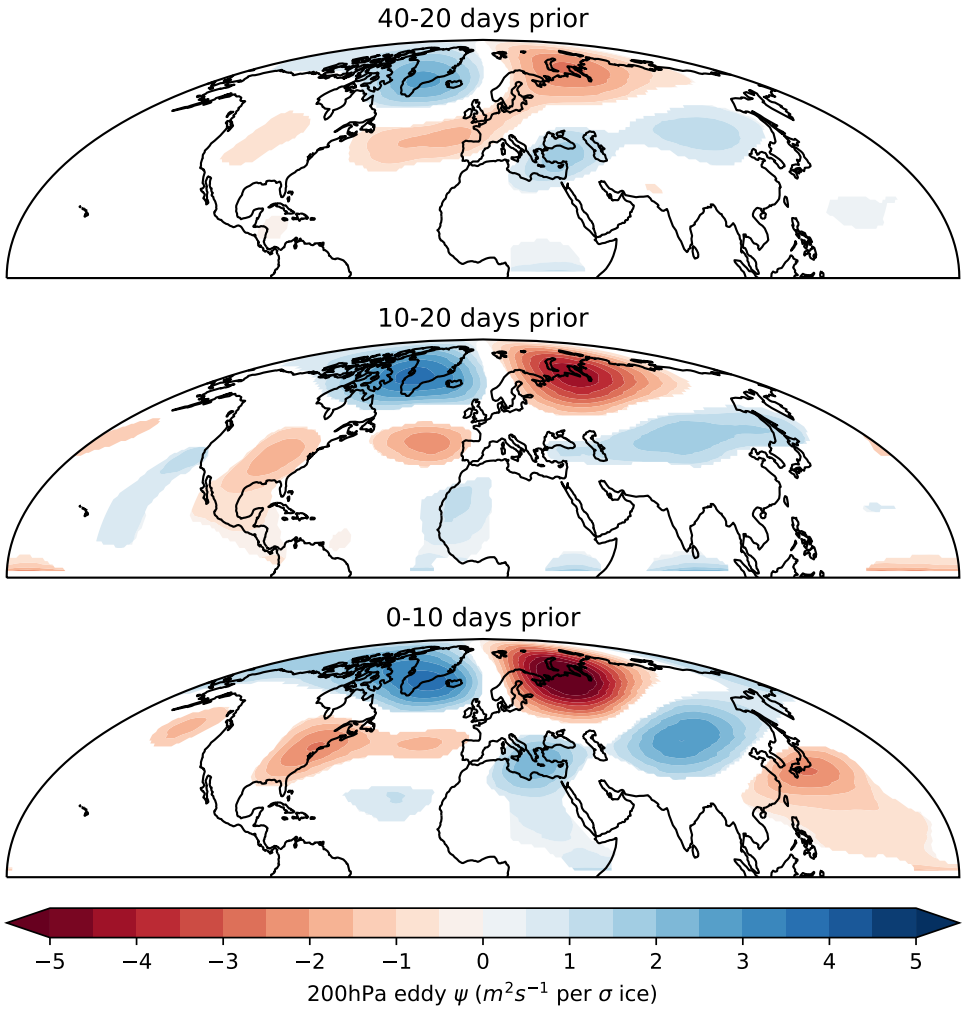

Figure 7.10: Relationship between BK sea ice and the preceding atmospheric circulation on sub-monthly timescales. BK sea ice is averaged between 20th and 30th November for every ensemble member for each year (total 460). This is regressed onto the 200hPa eddy streamfunction which is averaged over 0-10 days prior to the 20th November, 10-20 days prior and 40-20 days prior. Shading shows the regression coefficient; only regression coefficients significant at the 5% level are shown.

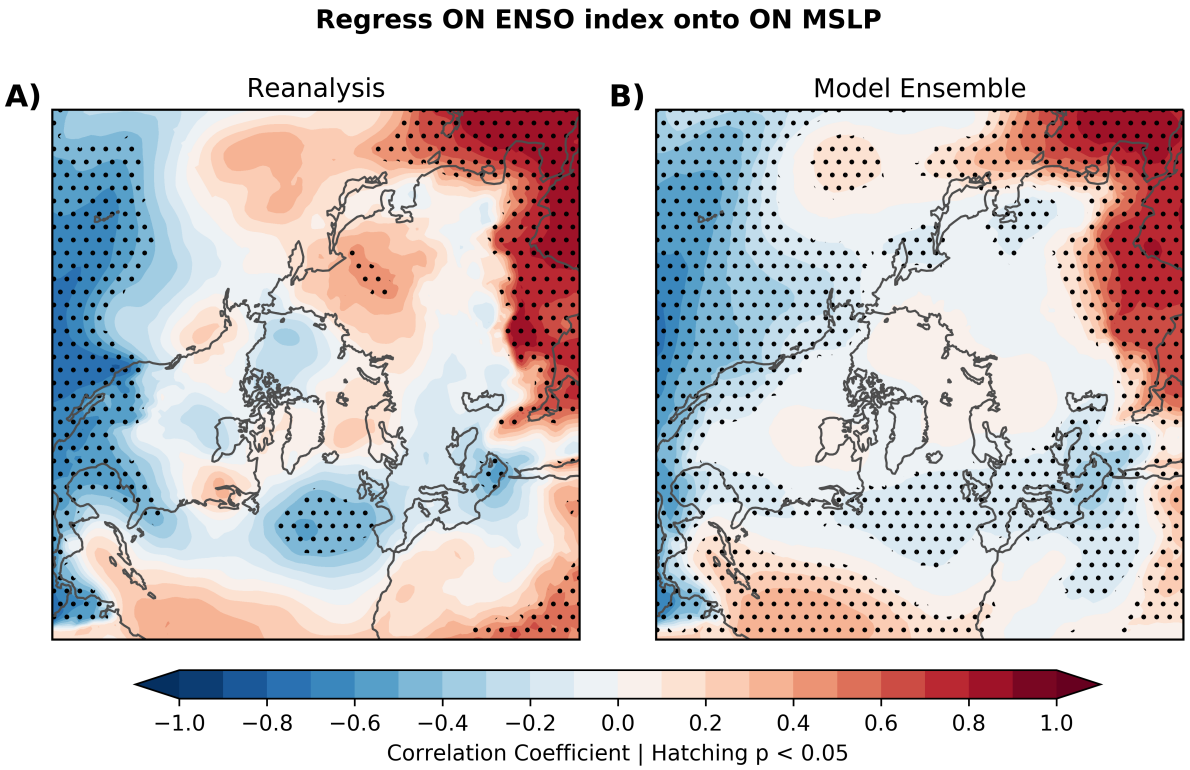

Figure 7.11: Correlation between late autumn ENSO and MSLP. Using October, November averaged data, the correlation coefficient of the ENSO 3.4 index with MSLP is shown for both reanalysis and the model ensemble across all members. Statistically significant correlation coefficients at the 5% level are indicated by stippling.

used to correlate with the observed and model ensemble mean circulation. These results are shown in figure 7.11.

Although tropical circulation patterns are trivially reproduced, the mid-latitude circulation is well reproduced by the model ensemble mean, particularly in the Atlantic sector (El Niño related to cyclonic conditions in the west Atlantic), though the relationship is weaker within the model. This pattern is the similar to the early winter pattern found in *Moron and Gouirand* [2003] and *Ayarzagüena et al.* [2018].

The QBO has been related to NAO variability via the polar vortex, and more recently to sea ice variability in early winter [*Labe et al.,* 2019]. This motivates analysis investigating the effect of the QBO on late autumn mid-latitude patterns within the model and reanalysis. In reanalysis, a strong anticyclonic pattern is found when compositing westerly and easterly QBO phase; a pattern which may affect BK sea ice given its proximity (figure 7.12A. No interannual correlation between QBO phase and BK ice variability is found; though given the QBO is non-normally distributed, conventional choices of corre-

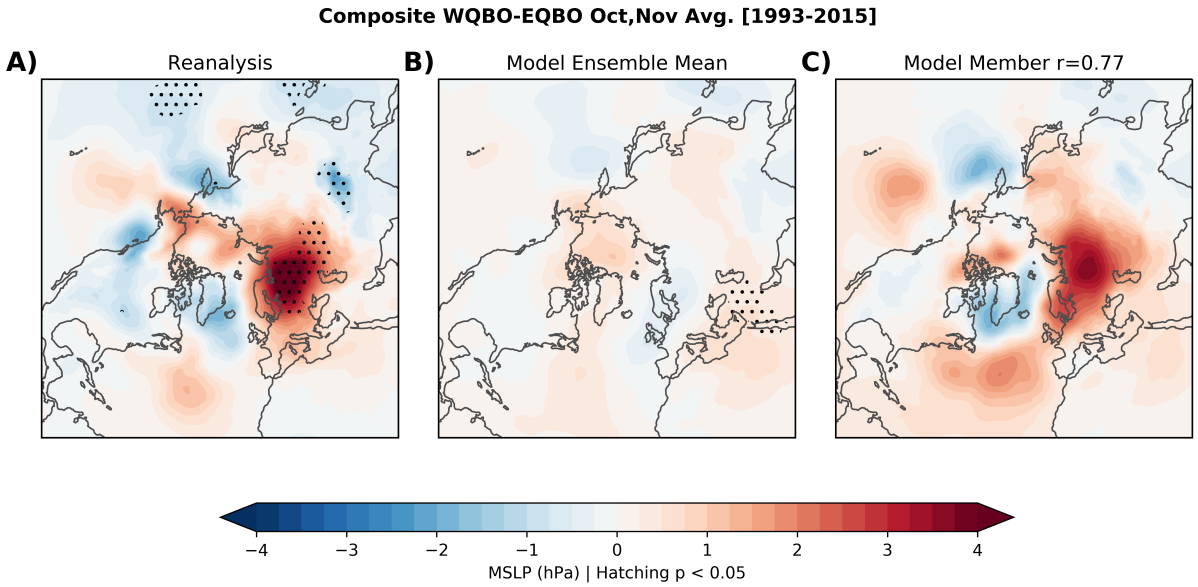

Figure 7.12: Compositing easterly and westerly QBO on the late autumn circulation. October-November averaged QBO index is calculated at 30hPa using reanalysis data for the period 1993-2015 inclusive. A composite is created based on whether the QBO is westerly or easterly on **A)** reanalysis and **B)** the model ensemble mean. Randomly sampling (10000 times) a member from each year, constructing the composite and performing a weighted pattern correlation north of 20N with the reanalysis composite pattern, a composite is found with the highest correlation and displayed on the right panel. For A and B, regions where the composite groups are significantly different at the 5% level using an independent t-test are hatched.

lation will not be strictly valid (see chapter 3). Each year, all members will have identical QBO as this is being nudged, so compositing the QBO on the ensemble mean (averaging members prior to analysis) or ensemble members will have the same result. This produces a very weak pattern with no resemblance to the pattern found in reanalysis, suggesting a forced pattern is weak (or not picked up by the model) during autumn (figure 7.12B). However, randomly sampling a member from each year to create a sample of 23 years like reanalysis, a combination can be found that has a high pattern correlation with reanalysis (figure 7.12C). Therefore, the pattern found in reanalysis may be due to internal variability.

7.7 Case Study: El Niño Autumn 1997

The autumn of 1997 is analysed, given the clear BK sea ice signal found in figure 7.5 (positive anomaly), which is found in the majority of ensemble members, and stands out from other years. This corresponds well with a simulated negative NAO (which, as found earlier, is associated with a weaker storm track and less poleward advection of heat and moisture). There is no suggestion of anomalously high BK ice during this year in observations; if tropical forcing is modifying sea ice in this year, why is this not found in observations, and is this due to internal variability? Here, the evolution of sea ice and tropospheric eddy streamfunction is investigated in the model ensemble mean and observations with each autumn month in 1997, and compared to reanalysis in figure 7.13.

Firstly, sea ice is explored in the model ensemble mean. Computing the ensemble mean first, prior to analysis, means internal variability can largely be averaged out, retaining the forced response to tropical variability. The year 1997 contains significantly more sea ice across the Atlantic sector, with some regions of reduced sea ice across the Pacific sector. BK sea ice appeared fairly typical in autumn 1997 according to figure 7.5. Sea ice appears highly variable with little consensus with the model ensemble mean composite; though by November, similarities occur, with some significance over the Pacific sector and parts of the Atlantic sector.

Examining the eddy streamfunction fields at 200hPa may reveal wave-like tropospheric patterns from tropical sources. Like sea ice, the atmosphere is highly variable so taking the ensemble mean isolates forced signals. The model shows pronounced signals in the

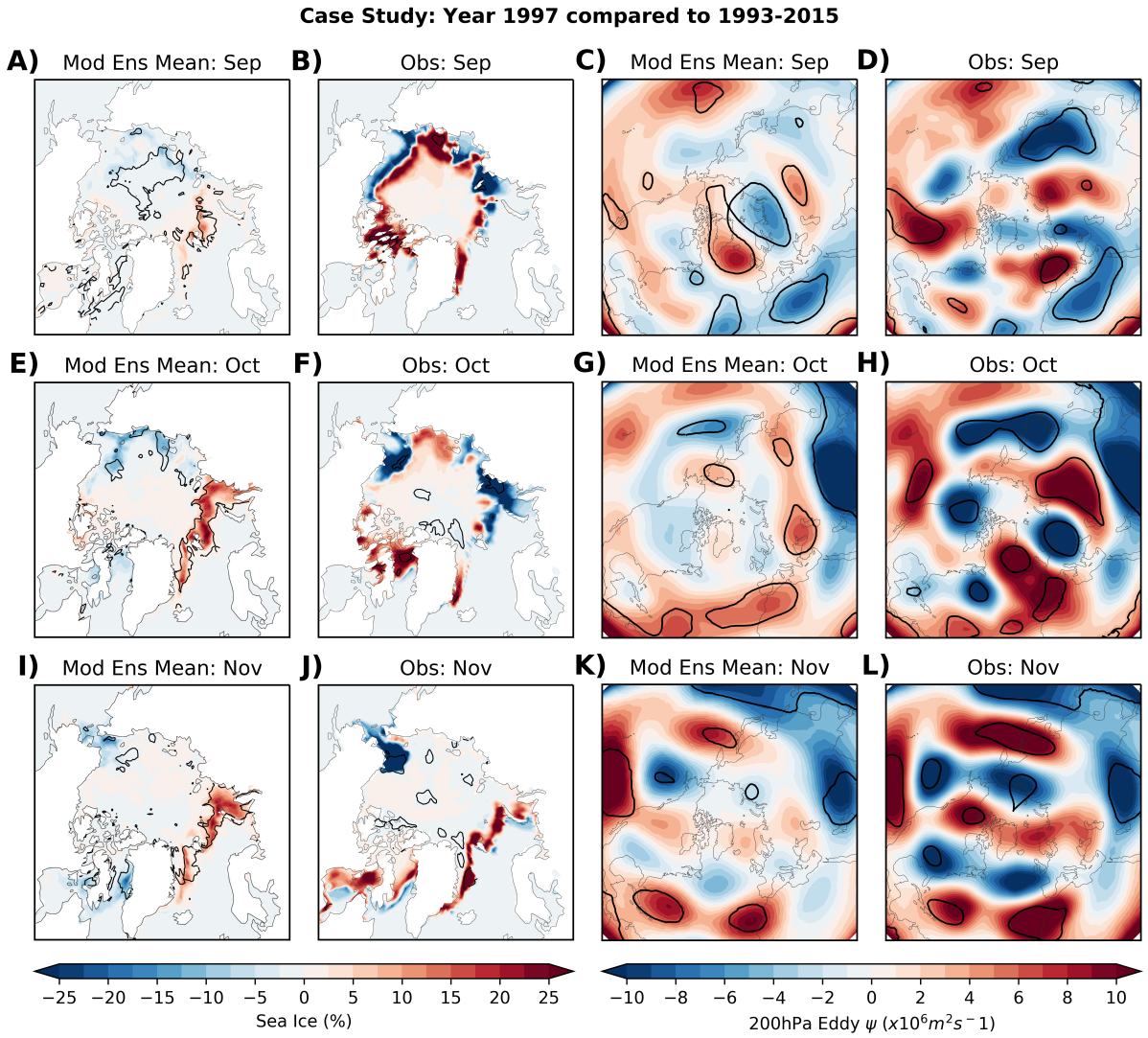

Figure 7.13: Comparing El Niño forced autumn 1997 to all other years in the model and obs. A,E,I) The difference between sea ice concentration in the year 1997 to 1993-2015 inclusive, excluding 1997, for each month in autumn respectively. At each gridpoint, contours indicate the enclosed regions where ice concentration in the year 1973 lies outside the 2σ spread in values from 1993-2015 inclusive, excluding 1997.The ensemble mean is taken first before any analysis. B,F,J) Same as in A,E,I, except using observations. At each gridpoint, sea ice is first linearly detrended, to remove the climate trend signal that would otherwise be picked up. C,G,K) Same as in A,E,I, except using 200hPa eddy streamfunction. D,H,L) Same as in C,G,K, excepting using reanalysis.

east Pacific towards the end of autumn, which extend into the Atlantic basin. While there are significant anomalies in early autumn in the Arctic (anticyclonic conditions over Iceland, cyclonic over the BK seas), signals are weak in mid and late autumn. With time, the pattern found in the ensemble mean becomes closer to that of observations; by November, the model can reproduce a large amount of the large scale circulation, albeit of weaker amplitude than observations at high latitudes. The similarity of panels K and L in figure 7.13 implies that much of the circulation pattern during late autumn can be reconstructed through knowledge of the tropics alone in this year. Additionally, similarity in the Pacific and Atlantic sectors (panels I and J) during this month indicate the model and observations had similar biases in sea ice in similar regions relative to 1993-2015, and thus it can be argued that in this specific case study there it tangible evidence linking tropical variability to Arctic sea ice variability.

7.8 Conclusions

This chapter isolated the impact of tropical variability on the mid to high latitudes during autumn, involving key months such as October which has previously been linked to winter NAO and mid-latitude variability (e.g. sea ice and Ural blocking [*Wang et al.,* 2017; *Kryjov*, 2015]). This involved running a coupled simulation of the Unified Model with initial conditions from the year 2000, a typical year within 1993-2015 for ice evolution through autumn and winter, and nudging the tropics to the years 1993-2015 inclusive. Through running an ensemble of 20 members for each year, taking into account internal variability, determining whether interannual variability in sea ice and the mid-latitude circulation could be reconstructed through knowledge of the tropics alone was a key research question:

- **Can tropical interannual variability be used to reproduce variability the wider atmospheric circulation and subsequently sea ice?**

Analysis showed that interannual variability in sea ice, both across the Arctic and the BK seas could not be reconstructed through nudging the tropics. However, this may be due to the model under-representing the strength of this teleconnection, an anomalously weak signal due to the signal-to-noise paradox, or a lack of teleconnection during autumn. Despite this, the model could reproduce some interannual variability of the NAO and polar

vortex. *Blanchard-Wrigglesworth and Ding* [2019] find similar results of limited ability of models to reproduce interannual variability within the Arctic region, due to strong internal variability, and require additional mid-latitude nudging to reconstruct variability at high latitudes.

- **Does the model replicate the observed relationship between sea ice and the wider atmospheric circulation?**

A strong relationship between BK sea ice variability in late autumn and preceding months NAO was found in the model simulations; not previously found in autumn observations. Additionally, regression maps onto eddy streamfunction and lower atmosphere temperatures suggests an important relationship between a dipole over Greenland and the BK seas in determining moisture and heat flux into the BK region, affecting sea ice variability. This pattern can also be found in observations, particularly when de-trending fields and isolating interannual variability. This relates back to the previous key research question; if there is a strong relationship between the NAO and BK sea ice, and the model can reconstruct interannual variability in the NAO, this two step teleconnection may be too weak in the model ensemble mean to isolate. Analysis of sub-monthly model data however revealed a wave train emanating from the tropical Atlantic and Caribbean preceding BK sea ice in late autumn, supporting a link between tropical variability and sea ice. While the model reproduces the ENSO teleconnection in midlatitudes, signals become weak at high latitudes, suggesting the model under-represents the amplitude of high-latitude ENSO teleconnections. Similarly, the model shows no overall impact of the QBO phase on the mid-high latitude circulation.

- **Case study: How do sea ice and atmospheric circulation patterns compare between the strong tropical forcing year of 1997 and other years?**

Finally, a case study of the year 1997 was investigated, due to the coincidental strong El Niño, and the model simulating anomalously high BK sea ice. A tropical to Arctic teleconnection is explored. Towards the end of autumn, the model does reproduce anomalously high sea ice in the Atlantic sector, and reduced sea ice in the Pacific sector. Additionally, large scale patterns characterised by 200hPa eddy streamfunction show the overall wave structure is well captured within the model ensemble, despite being weaker in amplitude at high latitudes.

Chapter 8

Conclusions

The work presented here confirms that the well-cited link between sea ice and the extratropical atmospheric circulation identified in observations is reproducible within model simulations, but that model ensembles suggest a large role for internal variability, and provide evidence that the link is partly incidental to common tropical drivers. The thesis provides new evidence that the tropics play a role in the Arctic-extratropical links, through use of large multi-model ensembles and nudging experiments. A summary of the key thesis results is presented below.

- **The strong relationship between autumn BK sea ice and the winter NAO found in observations is reproducible within climate models internal variability, but the mean relationship is weak in models.**

Using a large ensemble hindcast, ensemble members can be found that reproduce the link between autumn Barents-Kara sea ice and the wider extratropical circulation during winter. The average relationship across ensemble members, however, is weak, with a large component of internal variability. While it is hard to reject the null hypothesis that the strong observed link between BK sea ice and the NAO is due to internal variability, the forced model relationship (taking the ensemble mean prior to analysis) demonstrates a statistically significant correlation. The model may therefore be under-representing the sea ice-extratropical teleconnection due to a signal-to-noise issue in the extratropical circulation [*Scaife and Smith,* 2018], although note that a signal-to-noise problem is not found in the sea ice itself. It is important to note that the strong observed ice-NAO correlation depends on detrending. These results provide some evidence of a link between

sea ice and the extratropical circulation and build on single-model studies, or studies using only observations to create NAO predictions [e.g. *Wang et al.,* 2017; *Hall et al.,* 2017]. If the link between sea ice and the NAO is due to internal variability, statistical predictions of the NAO using sea ice may fail in the future.

- **Statistical analysis implies tropical variability mediates the observed relationship between BK sea ice and the NAO.**

Multiple linear regression, along with higher order analysis such as Causal Effect Network (CEN) analysis [*Runge et al.,* 2015], reveal that tropical rainfall in the Pacific may play a role in the link between Arctic sea ice and the winter NAO. Studies that have previously used CEN to conclude causal links between Arctic sea ice and the NAO, such as *Kretschmer et al.* 2016, do not include the tropics as a predictor. Given that one of the key limitations of CEN is that all important processes have to be included [*Runge et al.,* 2017]; thus requiring hindsight knowledge of key climate processes on these timescales, seasonal teleconnection work using CEN that omits tropical components may not be accurate. This is supported by the involvement of west Pacific tropical rainfall in the relationship between BK sea ice and the NAO found in this thesis.

- **Modelled links between BK sea ice and the extratropical atmospheric circulation can be explained by internal variability and tropical forcing.**

Multi-model atmosphere-only simulations can again reproduce a link between Barents-Kara sea ice and the NAO via internal variability, but suggest the forced response is minimal over the Atlantic sector. A stronger forced relationship with North Pacific MSLP is found. Model simulations which contain no sea ice variability produce the same pattern as time-varying sea ice experiments, implying that the forced response coincides with, but is not caused by, sea ice variability. Model simulations which only contain ENSO related variability also reproduce the same regression pattern of sea ice on the winter circulation, suggesting tropical origins. The use of large multi-model simulations builds on the limited use of single model experiments, which is particularly important given the large role of internal variability found earlier. This provides clear evidence that the link between Arctic sea ice and the extratropical circulation is at least partly symptomatic of tropical Pacific variability. These results have been published in the peer reviewed literature.

- **Autumn variability in the tropics has extratropical impacts, particularly during strong ENSO years.**

The proposed tropics to Arctic teleconnection, previously identified in *Yoo et al.* [2011] and *Henderson et al.* [2014], was explored using tropical nudging experiments. Here, the tropics were nudged to the years 1993-2015 during autumn, while the rest of the climate system was allowed to evolve freely, using the year 2000 as initial conditions. Similar studies have been used to identify the link between the tropics and the mid to high latitudes [*Jung et al.,* 2014; *Knight et al.,* 2017; *Maidens et al.,* 2019]. These experiments demonstrated that tropical nudging reproduce interannual variability of the autumn extratropical circulation, including the NAO. Additionally, interannual variability in the stratospheric polar vortex was reproduced, demonstrating a tropical-extratropical link previously found in other studies [*Greatbatch et al.,* 2015]. A strong link was also identified between the NAO and subsequent BK sea ice in late autumn, through control of poleward heat and moisture fluxes into the Arctic which are known to affect sea ice [*Lee,* 2012].

While interannual variability of Arctic sea ice was not well reproduced, these results suggests a two-step mechanism where the tropics exerts a causal influence on the extratropics, and the extratropics is linked to the Arctic climate, supported by an identifiable wave train originating from the tropics arching over the Atlantic and Eurasia. A direct link from the tropics to the Arctic sea ice may not be significant due to strong internal variability masking a forced signal, with larger ensembles needed possibly related to the erroneously weak mid-latitude signal due to the S/N paradox [*Scaife and Smith,* 2018]. Additionally, the model may not be representing the teleconnection from the tropics to the Arctic correctly; *Blanchard-Wrigglesworth and Ding* [2019] found the mid-latitudes also need to be nudged to find a response in the Arctic. However, in years where tropical forcing is strong, such as the strong El Niño of 1997, a measurable impact on the NAO and sea ice was found. Further analysis reveals this particular autumn is highly reproducible in the ensemble mean; suggesting that forced signals in the high latitudes stemming from tropical variability do appear in models when the tropical forcing is particularly strong.

The results presented in this thesis provide evidence of an incidental, non-causal relationship between BK sea ice and the winter extratropical circulation from tropical variability. The role of internal variability is better characterised using large ensembles and

multi-model experiments; which are essential to identify forced relationships between climate components. It is acknowledged that the presence of the signal-to-noise paradox in climate models may limit the interpretation of these results, by potentially underestimating the magnitude of the link between sea ice and the extratropical atmosphere. Through the use of very large ensembles (80 members) signals may still be extracted, but if the signal-to-noise problem applies here (e.g. *Scaife et al.,* 2019), then the models may not be representing larger-scale teleconnections correctly. To conclude, this thesis provides new evidence of a non-causal link between sea ice and the extratropical atmospheric circulation during winter, and better quantifies this relationship in observations and a variety of multi-model datasets. Furthermore it stems future work from this new perspective of non-causal and symptomatic climate relationships.

8.1 Future Work

The tropical nudging experiments here nudge the entire tropical band, including the stratosphere. However, there may be competing tropical influences in different basins that cancel out at high latitudes. Therefore, nudging tropical basins separately to isolate the differing roles of west and east Pacific rainfall could be useful in better attributing causality to a specific physical process (e.g. MJO, ENSO). Exploring the sensitivity to the season chosen may also be useful; *Henderson et al.* [2014] found the high latitude response to the MJO different in summer and winter. More widely, increased horizontal resolution [*Scaife et al.,* 2019] may also yield improved response.

The work presented in this thesis focuses on interannual variability within the recent observational period (1980-2016), therefore it does not contradict studies suggesting a causal impact of sea ice loss on the extratropical circulation in future decades, such as *McKenna et al.* 2018. Given the importance of the background atmospheric state in mediating Arctic-extratropical teleconnections [*Smith et al.,* 2017], a changing climate may lead to a different role of tropical processes in the incidental link between BK sea ice and the NAO. Recent studies have suggested an increase in the MJO in phases 5-6 due to a warming climate [*Roxy et al.,* 2019]. Given that MJO variability has detectable impact on Arctic sea ice [*Henderson et al.,* 2014], a trend in MJO phase may affect future relationships between the MJO and the Arctic climate, although in future decades

Arctic sea ice may be lost completely. Additionally, changes in ENSO under a warming climate may alter the MJO and Arctic sea ice. These questions could be addressed using techniques within this thesis and applying them to new datasets such as PAMIP [*Smith et al.,* 2019].

Chapter 9

Bibliography

Årthun, M., Eldevik, T., Smedsrud, L.H., Skagseth, Ø. and Ingvaldsen, R.B., 2012. Quantifying the influence of Atlantic heat on Barents Sea ice variability and retreat. *Journal of Climate*, **25(13)**, 4736-4743.

Adler, R.F., Huffman, G.J., Chang, A., Ferraro, R., Xie, P.P., Janowiak, J., Rudolf, B., Schneider, U., Curtis, S., Bolvin, D. and Gruber, A., 2003. The version-2 global precipitation climatology project (GPCP) monthly precipitation analysis (1979-present). *Journal of hydrometeorology*, **4(6)**, 1147-1167.

Allan, R. and Ansell, T., 2006. A new globally complete monthly historical gridded mean sea level pressure dataset (HadSLP2): 1850–2004. *Journal of Climate*, **19(22)**, 5816-5842.

Ambaum, M.H., Hoskins, B.J. and Stephenson, D.B., 2001. Arctic oscillation or North Atlantic oscillation?. *Journal of Climate*, **14(16)**, 3495-3507.

Andrews, D.G., 1987. On the interpretation of the Eliassen-Palm flux divergence. *Quarterly Journal of the Royal Meteorological Society*, **113(475)**, 323-338.

Andrews, M.B., Knight, J.R. and Gray, L.J., 2015. A simulated lagged response of the North Atlantic Oscillation to the solar cycle over the period 1960–2009. *Environmental Research Letters*, **10(5)**, 054022.

Anstey, J.A. and Shepherd, T.G., 2014. High-latitude influence of the quasi-biennial oscillation. *Quarterly Journal of the Royal Meteorological Society*, **140(678)**, 1-21.

Athanasiadis, P.J., Bellucci, A., Scaife, A.A., Hermanson, L., Materia, S., Sanna, A., Borrelli, A., MacLachlan, C. and Gualdi, S., 2017. A multisystem view of wintertime NAO seasonal predictions. *Journal of Climate*, **30(4)**, 1461-1475.

Austin, P.C. and Steyerberg, E.W., 2015. The number of subjects per variable required in linear regression analyses. *Journal of clinical epidemiology*, **68(6)**, 627-636.

Ayarzagüena, B., Ineson, S., Dunstone, N.J., Baldwin, M.P. and Scaife, A.A., 2018. Intraseasonal effects of el niño–southern oscillation on North Atlantic climate. *Journal of Climate*, **31(21)**, 8861-8873.

Babyak, M.A., 2004. What you see may not be what you get: a brief, nontechnical introduction to overfitting in regression-type models. *Psychosomatic medicine*, **66(3)**, 411-421.

Bader, J. and Latif, M., 2003. The impact of decadal-scale Indian Ocean sea surface temperature anomalies on Sahelian rainfall and the North Atlantic Oscillation. *Geophysical Research Letters*, **30(22)**, 2169.

Baggett, C. and Lee, S., 2015. Arctic warming induced by tropically forced tapping of available potential energy and the role of the planetary-scale waves. *Journal of the Atmospheric Sciences*, **72(4)**, 1562-1568.

Baker, L.H., Shaffrey, L.C., Sutton, R.T., Weisheimer, A. and Scaife, A.A., 2018. An intercomparison of skill and overconfidence/underconfidence of the wintertime North Atlantic Oscillation in multimodel seasonal forecasts. *Geophysical Research Letters*, **45(15)**, 7808-7817.

Baldwin, M.P. and Dunkerton, T.J., 2001. Stratospheric harbingers of anomalous weather regimes. *Science*, **294(5542)**, 581-584.

Baldwin, M.P., Gray, L.J., Dunkerton, T.J., Hamilton, K., Haynes, P.H., Randel, W.J., Holton, J.R., Alexander, M.J., Hirota, I., Horinouchi, T. and Jones, D.B.A., 2001. The quasi-biennial oscillation. *Reviews of Geophysics*, **39(2)**, 179-229.

Baldwin, M.P., Stephenson, D.B., Thompson, D.W., Dunkerton, T.J., Charlton, A.J. and O'neill, A., 2003. Stratospheric memory and skill of extended-range weather forecasts. *Science*, **301(5633)**, 636-640.

Balmaseda, M.A., Ferranti, L., Molteni, F. and Palmer, T.N., 2010. Impact of 2007 and 2008 Arctic ice anomalies on the atmospheric circulation: Implications for long-range predictions. *Quarterly Journal of the Royal Meteorological Society*, **136(652)**, 1655-1664.

Barnes, E.A. and Hartmann, D.L., 2010. Dynamical feedbacks and the persistence of the NAO. *Journal of the Atmospheric Sciences*, **67(3)**, 851-865.

Barnes, E.A. and Screen, J.A., 2015. The impact of Arctic warming on the midlatitude jet-stream: Can it? Has it? Will it?. *Wiley Interdisciplinary Reviews: Climate Change*, **6(3)**, 277-286.

Barnston, A.G. and Livezey, R.E., 1987. Classification, seasonality and persistence of low-frequency atmospheric circulation patterns. *Monthly weather review*, **115(6)**, 1083-1126.

Barnston, A.G., Tippett, M.K., L'Heureux, M.L., Li, S. and DeWitt, D.G., 2012. Skill of real-time seasonal ENSO model predictions during 2002–11: Is our capability increasing?. *Bulletin of the American Meteorological Society*, **93(5)**, 631-651.

Barrett, B.S., 2019. Connections between the Madden–Julian Oscillation and surface temperatures in winter 2018 over eastern North America. *Atmospheric Science Letters*, **20(1)**, p.e869.

Bell, C.J., Gray, L.J., Charlton-Perez, A.J., Joshi, M.M. and Scaife, A.A., 2009. Stratospheric communication of El Niño teleconnections to European winter. *Journal of Climate*, **22(15)**, 4083-4096.

Beynon, C., Wyke, S., Jarman, I., Robinson, M., Mason, J., Murphy, K., Bellis, M.A. and Perkins, C., 2011. The cost of emergency hospital admissions for falls on snow and ice in England during winter 2009/10: a cross sectional analysis. *Environmental health*, **10(1)**, 60.

Bhatt, U.S., Alexander, M.A., Battisti, D.S., Houghton, D.D. and Keller, L.M., 1998. Atmosphere–ocean interaction in the North Atlantic: Near-surface climate variability. *Journal of climate*, **11(7)**, 1615-1632.

Bjerknes, J., 1964. Atlantic air-sea interaction. *Advances in geophysics*, **10**, 1-82.

Bjerknes, J., 1969. Atmospheric teleconnections from the equatorial Pacific. *Monthly weather review*, **97(3)**, 163-172.

Black, J., Johnson, N.C., Baxter, S., Feldstein, S.B., Harnos, D.S. and L'Heureux, M.L., 2017. The predictors and forecast skill of Northern Hemisphere teleconnection patterns for lead times of 3–4 weeks. *Monthly Weather Review*, **145(7)**, 2855-2877.

Blackburn, M. and Hoskins, B.J., 2001. The UK record-breaking wet autumn 2000. *UGAMP newsletter*, **24**, 38-40.

Blackmon, M.L., Wallace, J.M., Lau, N.C. and Mullen, S.L., 1977. An observational study of the Northern Hemisphere wintertime circulation. *Journal of the Atmospheric*

Sciences, **34(7)**, 1040-1053.

Blackport, R. and Kushner, P.J., 2016. The transient and equilibrium climate response to rapid summertime sea ice loss in CCSM4. *Journal of Climate*, **29(2)**, 401-417.

Blackport, R. and Kushner, P.J., 2017. Isolating the atmospheric circulation response to Arctic sea ice loss in the coupled climate system. *Journal of Climate*, **30(6)**, 2163-2185.

Blackport, R. and Kushner, P.J., 2018. The role of extratropical ocean warming in the coupled climate response to Arctic sea ice loss. *Journal of Climate*, **31(22)**, 9193-9206.

Blackport, R., Screen, J.A., van der Wiel, K. and Bintanja, R., 2019. Minimal influence of reduced Arctic sea ice on coincident cold winters in mid-latitudes. *Nature Climate Change*, **9(9)**, 697-704.

Blanchard-Wrigglesworth, E., Armour, K.C., Bitz, C.M. and DeWeaver, E., 2011. Persistence and inherent predictability of Arctic sea ice in a GCM ensemble and observations. *Journal of Climate*, **24(1)**, 231-250.

Blanchard-Wrigglesworth, E. and Ding, Q., 2019. Tropical and Midlatitude Impact on Seasonal Polar Predictability in the Community Earth System Model. *Journal of Climate*, **32(18)**, 5997-6014.

Blüthgen, J., Gerdes, R. and Werner, M., 2012. Atmospheric response to the extreme Arctic sea ice conditions in 2007. *Geophysical Research Letters*, **39(2)**, 02707.

Boer, G.J., 2004. Long time-scale potential predictability in an ensemble of coupled climate models. *Climate dynamics*, **23(1)**, 29-44.

Boland, E.J., Bracegirdle, T.J. and Shuckburgh, E.F., 2017. Assessment of sea ice-atmosphere links in CMIP5 models. *Climate Dynamics*, **49(1-2)**, 683-702.

Brayshaw, D.J., Hoskins, B. and Blackburn, M., 2009. The basic ingredients of the North Atlantic storm track. Part I: Land–sea contrast and orography. *Journal of the Atmospheric Sciences*, **66(9)**, 2539-2558.

Buchan, J., Hirschi, J.J.M., Blaker, A.T. and Sinha, B., 2014. North Atlantic SST anomalies and the cold north European weather events of winter 2009/10 and December 2010. *Monthly Weather Review*, **142(2)**, 922-932.

Bunzel, F., Notz, D., Baehr, J., Müller, W.A. and Fröhlich, K., 2016. Seasonal climate forecasts significantly affected by observational uncertainty of Arctic sea ice concen-

tration. *Geophysical Research Letters*, **43(2)**, 852-859.

Bushuk, M., Msadek, R., Winton, M., Vecchi, G.A., Gudgel, R., Rosati, A. and Yang, X., 2017. Skillful regional prediction of Arctic sea ice on seasonal timescales. *Geophysical Research Letters*, **44(10)**, 4953-4964.

Bushuk, M., Msadek, R., Winton, M., Vecchi, G., Yang, X., Rosati, A. and Gudgel, R., 2019. Regional Arctic sea–ice prediction: potential versus operational seasonal forecast skill. *Climate dynamics*, **52(5-6)**, 2721-2743.

Butler, A.H., Thompson, D.W. and Heikes, R., 2010. The steady-state atmospheric circulation response to climate change–like thermal forcings in a simple general circulation model. *Journal of Climate*, **23(13)**, 3474-3496.

Butler, A.H., Arribas, A., Athanassiadou, M., Baehr, J., Calvo, N., Charlton-Perez, A., Déqué, M., Domeisen, D.I., Fröhlich, K., Hendon, H. and Imada, Y., 2016. The Climate-system Historical Forecast Project: do stratosphere-resolving models make better seasonal climate predictions in boreal winter?. *Quarterly Journal of the Royal Meteorological Society*, **142(696)**, 1413-1427.

Brönnimann, S., Xoplaki, E., Casty, C., Pauling, A. and Luterbacher, J., 2007. ENSO influence on Europe during the last centuries. *Climate Dynamics*, **28(2-3)**, 181-197.

Cassano, E.N., Cassano, J.J., Higgins, M.E. and Serreze, M.C., 2014. Atmospheric impacts of an Arctic sea ice minimum as seen in the Community Atmosphere Model. *International Journal of Climatology*, **34(3)**, 766-779.

Cassou, C., 2008. Intraseasonal interaction between the Madden–Julian oscillation and the North Atlantic Oscillation. *Nature*, **455(7212)**, 523.

Cattiaux, J., Vautard, R., Cassou, C., Yiou, P., Masson-Delmotte, V. and Codron, F., 2010. Winter 2010 in Europe: A cold extreme in a warming climate. *Geophysical Research Letters*, **37(20)**, 20704.

Cavalieri, D. J., C. L. Parkinson, P. Gloersen, and H. J. Zwally., 1996, updated yearly. Sea Ice Concentrations from Nimbus-7 SMMR and DMSP SSM/I-SSMIS Passive Microwave Data, Version 1. Boulder, Colorado USA. NASA *National Snow and Ice Data Center Distributed Active Archive Center*. [Accessed 24/07/2019].

Charlton-Perez, A.J., Ferranti, L. and Lee, R.W., 2018. The influence of the stratospheric state on North Atlantic weather regimes. *Quarterly Journal of the Royal Meteorological Society*, **144(713)**, 1140-1151.

Charney, J.G. and Drazin, P.G., 1961. Propagation of planetary-scale disturbances from the lower into the upper atmosphere. *Journal of Geophysical Research*, **66(1)**, 83-109.

Chen, D., Cane, M.A., Kaplan, A., Zebiak, S.E. and Huang, D., 2004. Predictability of El Niño over the past 148 years. *Nature*, **428(6984)**, 733.

Chen, D. and Cane, M.A., 2008. El Niño prediction and predictability. *Journal of Computational Physics*, **227(7)**, 3625-3640.

Chen, H.W., Zhang, F. and Alley, R.B., 2016. The robustness of midlatitude weather pattern changes due to Arctic sea ice loss. *Journal of Climate*, **29(21)**, 7831-7849.

Chen, M., Wang, W. and Kumar, A., 2013. Lagged ensembles, forecast configuration, and seasonal predictions. *Monthly Weather Review*, **141(10)**, 3477-3497.

Chevallier, M. and Salas-Mélia, D., 2012. The role of sea ice thickness distribution in the Arctic sea ice potential predictability: A diagnostic approach with a coupled GCM. *Journal of Climate*, **25(8)**, 3025-3038.

Chevallier, M., Salas y Mélia, D., Voldoire, A., Déqué, M. and Garric, G., 2013. Seasonal forecasts of the pan-Arctic sea ice extent using a GCM-based seasonal prediction system. *Journal of Climate*, **26(16)**, 6092-6104.

Chiodo, G., Oehrlein, J., Polvani, L.M., Fyfe, J.C. and Smith, A.K., 2019. Insignificant influence of the 11-year solar cycle on the North Atlantic Oscillation. *Nature Geoscience*, **12(2)**, 94.

Christiansen, B., 2001. Downward propagation of zonal mean zonal wind anomalies from the stratosphere to the troposphere: Model and reanalysis. *Journal of Geophysical Research: Atmospheres*, **106(D21)**, 27307-27322.

Clark, P.A. and Gray, S.L., 2018. Sting jets in extratropical cyclones: a review. *Quarterly Journal of the Royal Meteorological Society*, **144(713)**, 943-969.

Clark, R.T., Bett, P.E., Thornton, H.E. and Scaife, A.A., 2017. Skilful seasonal predictions for the European energy industry. *Environmental Research Letters*, **12(2)**, 024002.

Cohen, J. and Entekhabi, D., 1999. Eurasian snow cover variability and Northern Hemisphere climate predictability. *Geophysical Research Letters*, **26(3)**, 345-348.

Cohen, J., Foster, J., Barlow, M., Saito, K. and Jones, J., 2010. Winter 2009–2010: A case study of an extreme Arctic Oscillation event. *Geophysical Research Letters*,

37(17), 17707.

Cohen, J.L., Furtado, J.C., Barlow, M.A., Alexeev, V.A. and Cherry, J.E., 2012. Arctic warming, increasing snow cover and widespread boreal winter cooling. *Environmental Research Letters*, **7(1)**, 014007.

Cohen, J., Jones, J., Furtado, J.C. and Tziperman, E., 2013. Warm Arctic, cold continents: A common pattern related to Arctic sea ice melt, snow advance, and extreme winter weather. *Oceanography*, **26(4)**, 150-160.

Cohen, J., Furtado, J.C., Jones, J., Barlow, M., Whittleston, D. and Entekhabi, D., 2014. Linking Siberian snow cover to precursors of stratospheric variability. *Journal of Climate*, **27(14)**, 5422-5432.

Cohen, J., Screen, J.A., Furtado, J.C., Barlow, M., Whittleston, D., Coumou, D., Francis, J., Dethloff, K., Entekhabi, D., Overland, J. and Jones, J., 2014. Recent Arctic amplification and extreme mid-latitude weather. *Nature geoscience*, **7(9)**, 627.

Collins, M., 2002. Climate predictability on interannual to decadal time scales: The initial value problem. *Climate Dynamics*, **19(8)**, 671-692.

Collins, M., Chandler, R.E., Cox, P.M., Huthnance, J.M., Rougier, J. and Stephenson, D.B., 2012. Quantifying future climate change. *Nature Climate Change*, **2(6)**, 403.

Collow, T.W., Wang, W. and Kumar, A., 2019. Reduction in northern mid-latitude 2-m temperature variability due to Arctic sea ice loss. *Journal of Climate*, (2019).

D'Agostino, R.A.L.P.H. and Pearson, E.S., 1973. Tests for departure from normality. Empirical results for the distributions of b^2 and $\sqrt{b}$. *Biometrika*, **60(3)**, pp.613-622.

De, B. and Wu, Y., 2019. Robustness of the stratospheric pathway in linking the Barents-Kara Sea sea ice variability to the mid-latitude circulation in CMIP5 models. *Climate Dynamics*, **53(1-2)**, 193-207.

Decker, M., Brunke, M.A., Wang, Z., Sakaguchi, K., Zeng, X. and Bosilovich, M.G., 2012. Evaluation of the reanalysis products from GSFC, NCEP, and ECMWF using flux tower observations. *Journal of Climate*, **25(6)**, 1916-1944.

Dee, D.P., Uppala, S.M., Simmons, A.J., Berrisford, P., Poli, P., Kobayashi, S., Andrae, U., Balmaseda, M.A., Balsamo, G., Bauer, D.P. and Bechtold, P., 2011. The ERA?Interim reanalysis: Configuration and performance of the data assimilation system. *Quarterly Journal of the Royal Meteorological Society*, **137(656)**, 553-597.

Deser, C., Alexander, M.A. and Timlin, M.S., 2003. Understanding the persistence of sea

surface temperature anomalies in midlatitudes. *Journal of Climate*, **16(1)**, 57-72.

Deser, C., Tomas, R.A. and Sun, L., 2015. The role of ocean–atmosphere coupling in the zonal-mean atmospheric response to Arctic sea ice loss. *Journal of Climate*, **28(6)**, 2168-2186.

Deser, C., Sun, L., Tomas, R.A. and Screen, J., 2016. Does ocean coupling matter for the northern extratropical response to projected Arctic sea ice loss?. *Geophysical Research Letters*, **43(5)**, 2149-2157.

DeWeaver, E. and Bitz, C.M., 2006. Atmospheric circulation and its effect on Arctic sea ice in CCSM3 simulations at medium and high resolution. *Journal of Climate*, **19(11)**, 2415-2436.

Ding, Q., Wallace, J.M., Battisti, D.S., Steig, E.J., Gallant, A.J., Kim, H.J. and Geng, L., 2014. Tropical forcing of the recent rapid Arctic warming in northeastern Canada and Greenland. *Nature*, **509(7499)**, 209.

Ding, Q., Schweiger, A., L'Heureux, M., Steig, E.J., Battisti, D.S., Johnson, N.C., Blanchard-Wrigglesworth, E., Po-Chedley, S., Zhang, Q., Harnos, K. and Bushuk, M., 2019. Fingerprints of internal drivers of Arctic sea ice loss in observations and model simulations. *Nature Geoscience*, **12(1)**, 28.

Dirkson, A., Merryfield, W.J. and Monahan, A., 2017. Impacts of sea ice thickness initialization on seasonal Arctic sea ice predictions. *Journal of Climate*, **30(3)**, 1001-1017.

Dobrynin, M., Domeisen, D.I., Müller, W.A., Bell, L., Brune, S., Bunzel, F., Düsterhus, A., Fröhlich, K., Pohlmann, H. and Baehr, J., 2018. Improved teleconnection-based dynamical seasonal predictions of boreal winter. *Geophysical Research Letters*, **45(8)**, 3605-3614.

Domeisen, D.I., Badin, G. and Koszalka, I.M., 2018. How Predictable Are the Arctic and North Atlantic Oscillations? Exploring the Variability and Predictability of the Northern Hemisphere. *Journal of Climate*, **31(3)**, 997-1014.

Douville, H., Salas-Mélia, D. and Tyteca, S., 2006. On the tropical origin of uncertainties in the global land precipitation response to global warming. *Climate Dynamics*, **26(4)**, 367-385.

Drinkwater, K.F., Belgrano, A., Borja, A., Conversi, A., Edwards, M., Greene, C.H., Ottersen, G., Pershing, A.J. and Walker, H., 2003. The response of marine ecosystems

to climate variability associated with the North Atlantic Oscillation. *Geophysical Monograph-American Geophysical Union*, **134**, 211-234.

Dunstone, N., Smith, D., Scaife, A., Hermanson, L., Eade, R., Robinson, N., Andrews, M. and Knight, J., 2016. Skilful predictions of the winter North Atlantic Oscillation one year ahead. *Nature Geoscience*, **9(11)**, 809.

Eade, R., Smith, D., Scaife, A., Wallace, E., Dunstone, N., Hermanson, L. and Robinson, N., 2014. Do seasonal to decadal climate predictions underestimate the predictability of the real world?. *Geophysical research letters*, **41(15)**, 5620-5628.

Edmon Jr, H.J., Hoskins, B.J. and McIntyre, M.E., 1980. Eliassen-Palm cross sections for the troposphere. *Journal of the Atmospheric Sciences*, **37(12)**, 2600-2616.

Ebert-Uphoff, I. and Deng, Y., 2012. Causal discovery for climate research using graphical models. *Journal of Climate*, **25(17)**, 5648-5665.

England, M., Jahn, A. and Polvani, L., 2019. Nonuniform Contribution of Internal Variability to Recent Arctic Sea Ice Loss. *Journal of Climate*, **32(13)**, 4039-4053.

Fedorov, A.V., Harper, S.L., Philander, S.G., Winter, B. and Wittenberg, A., 2003. How predictable is El Niño?. *Bulletin of the American Meteorological Society*, **84(7)**, 911-920.

Feldstein, S.B., 2000. The timescale, power spectra, and climate noise properties of teleconnection patterns. *Journal of Climate*, **13(24)**, 4430-4440.

Fereday, D.R., Maidens, A., Arribas, A., Scaife, A.A. and Knight, J.R., 2012. Seasonal forecasts of northern hemisphere winter 2009/10. *Environmental Research Letters*, **7(3)**, 034031.

Ferranti, L., Palmer, T.N., Molteni, F. and Klinker, E., 1990. Tropical-extratropical interaction associated with the 30–60 day oscillation and its impact on medium and extended range prediction. *Journal of the Atmospheric Sciences*, **47(18)**, 2177-2199.

Fetterer, F., K. Knowles, W. Meier, M. Savoie, and A. K. Windnagel. 2017, updated daily. Sea Ice Index, Version 3. [Arctic sea ice extent]. Boulder, Colorado USA. NSIDC: National Snow and Ice Data Center. doi: https://doi.org/10.7265/N5K072F8. [05/09/2018].

Fisher, R.A., 1915. Frequency distribution of the values of the correlation coefficient in samples from an indefinitely large population. *Biometrika*, **10(4)**, 507-521.

Fletcher, C.G. and Saunders, M.A., 2006. Winter North Atlantic oscillation hindcast

skill: 1900–2001. *Journal of climate*, **19(22)**, 5762-5776.

Flournoy, M.D., Feldstein, S.B., Lee, S. and Clothiaux, E.E., 2016. Exploring the tropically excited Arctic warming mechanism with station data: Links between tropical convection and Arctic downward infrared radiation. *Journal of the Atmospheric Sciences*, **73(3)**, 1143-1158.

Folland, C.K., Scaife, A.A., Lindesay, J. and Stephenson, D.B., 2012. How potentially predictable is northern European winter climate a season ahead?. *International Journal of Climatology*, **32(6)**, 801-818.

Francis, J.A. and Vavrus, S.J., 2015. Evidence for a wavier jet stream in response to rapid Arctic warming. *Environmental Research Letters*, **10(1)**, 014005.

García-Serrano, J., Frankignoul, C., Gastineau, G. and De La Càmara, A., 2015. On the predictability of the winter Euro-Atlantic climate: lagged influence of autumn Arctic sea ice. *Journal of Climate*, **28(13)**, 5195-5216.

Garfinkel, C.I. and Hartmann, D.L., 2007. Effects of the El Niño–Southern Oscillation and the quasi-biennial oscillation on polar temperatures in the stratosphere. *Journal of Geophysical Research: Atmospheres*, **112**, D19112

Garfinkel, C.I. and Hartmann, D.L., 2008. Different ENSO teleconnections and their effects on the stratospheric polar vortex. *Journal of Geophysical Research: Atmospheres*, **113(D18)**, 18114.

Gastineau, G., García-Serrano, J. and Frankignoul, C., 2017. The influence of autumnal Eurasian snow cover on climate and its link with Arctic sea ice cover. *Journal of Climate*, **30(19)**, 7599-7619.

Gates, W.L., Boyle, J.S., Covey, C., Dease, C.G., Doutriaux, C.M., Drach, R.S., Fiorino, M., Gleckler, P.J., Hnilo, J.J., Marlais, S.M. and Phillips, T.J., 1999. An overview of the results of the Atmospheric Model Intercomparison Project (AMIP I). *Bulletin of the American Meteorological Society*, **80(1)**, 29-56.

Gerber, E.P. and Polvani, L.M., 2009. Stratosphere–troposphere coupling in a relatively simple AGCM: The importance of stratospheric variability. *Journal of Climate*, **22(8)**, 1920-1933.

Gerber, F., Sedláček, J. and Knutti, R., 2014. Influence of the western North Atlantic and the Barents Sea on European winter climate. *Geophysical Research Letters*, **41(2)**, 561-567.

Gillett, N.P. and Fyfe, J.C., 2013. Annular mode changes in the CMIP5 simulations. *Geophysical Research Letters*, **40(6)**, 1189-1193.

Gollan, G., Greatbatch, R.J. and Jung, T., 2015. Origin of variability in Northern Hemisphere winter blocking on interannual to decadal timescales. *Geophysical Research Letters*, **42(22)**, 10-037.

Gong, G., Cohen, J., Entekhabi, D. and Ge, Y., 2007. Hemispheric-scale climate response to Northern Eurasia land surface characteristics and snow anomalies. *Global and Planetary Change*, **56(3-4)**, 359-370.

Gong, T., Feldstein, S. and Lee, S., 2017. The role of downward infrared radiation in the recent Arctic winter warming trend. *Journal of Climate*, **30(13)**, 4937-4949.

Goswami, B.N. and Shukla, J., 1991. Predictability of a coupled ocean-atmosphere model. *Journal of Climate*, **4(1)**, 3-22.

Greatbatch, R.J., Gollan, G., Jung, T. and Kunz, T., 2012. Factors influencing Northern Hemisphere winter mean atmospheric circulation anomalies during the period 1960/1961 to 2001/2002. *Quarterly Journal of the Royal Meteorological Society*, **138(669)**, 1970-1982.

Greatbatch, R.J., Gollan, G., Jung, T. and Kunz, T., 2015. Tropical origin of the severe European winter of 1962/1963. *Quarterly Journal of the Royal Meteorological Society*, **141(686)**, 153-165.

Groeneveld, R.A. and Meeden, G., 1984. Measuring skewness and kurtosis. *Journal of the Royal Statistical Society: Series D (The Statistician)*, **33(4)**, 391-399.

Groisman, P.Y., 1992. Possible regional climate consequences of the Pinatubo eruption: An empirical approach. *Geophysical Research Letters*, **19(15)**, 1603-1606.

Guemas, V., Blanchard-Wrigglesworth, E., Chevallier, M., Day, J.J., Déqué, M., Doblas-Reyes, F.J., Fučkar, N.S., Germe, A., Hawkins, E., Keeley, S. and Koenigk, T., 2016. A review on Arctic sea-ice predictability and prediction on seasonal to decadal timescales. *Quarterly Journal of the Royal Meteorological Society*, **142(695)**, 546-561.

Hall, R.J., Scaife, A.A., Hanna, E., Jones, J.M. and Erdélyi, R., 2017. Simple statistical probabilistic forecasts of the winter NAO. *Weather and Forecasting*, **32(4)**, 1585-1601.

Hall, R.J. and Hanna, E., 2018. North Atlantic circulation indices: links with summer and winter UK temperature and precipitation and implications for seasonal forecasting.

International Journal of Climatology, **38**, 660-677.

Han, Z., Li, S., Liu, J., Gao, Y. and Zhao, P., 2016. Linear additive impacts of Arctic sea ice reduction and La Niña on the Northern Hemisphere winter climate. *Journal of Climate*, **29(15)**, 5513-5532.

Handorf, D., Jaiser, R., Dethloff, K., Rinke, A. and Cohen, J., 2015. Impacts of Arctic sea ice and continental snow cover changes on atmospheric winter teleconnections. *Geophysical Research Letters*, **42(7)**, 2367-2377.

Hannachi, A., Jolliffe, I.T. and Stephenson, D.B., 2007. Empirical orthogonal functions and related techniques in atmospheric science: A review. *International Journal of Climatology*, **27(9)**, 1119-1152.

Hardiman, S.C., Kushner, P.J. and Cohen, J., 2008. Investigating the ability of general circulation models to capture the effects of Eurasian snow cover on winter climate. *Journal of Geophysical Research: Atmospheres*, **113(D21)**, 21123.

Hawkins, D.M., 2004. The problem of overfitting. *Journal of chemical information and computer sciences*, **44(1)**, 1-12.

Held, I.M., Panetta, R.L. and Pierrehumbert, R.T., 1985. Stationary external Rossby waves in vertical shear. *Journal of the atmospheric sciences*, **42(9)**, 865-883.

Henderson, G.R., Barrett, B.S. and Lafleur, D.M., 2014. Arctic sea ice and the Madden–Julian oscillation (MJO). *Climate dynamics*, **43(7-8)**, 2185-2196.

Henderson, G.R., Peings, Y., Furtado, J.C. and Kushner, P.J., 2018. Snow–atmosphere coupling in the Northern Hemisphere. *Nature Climate Change*, **8(11)**, 954-963.

Hersbach, H. and Dee, D., 2016. ERA5 reanalysis is in production. *ECMWF newsletter*, **147(7)**.

Hitchcock, P. and Simpson, I.R., 2014. The downward influence of stratospheric sudden warmings. *Journal of the Atmospheric Sciences*, **71(10)**, 3856-3876.

Hoerling, M.P., Hurrell, J.W. and Xu, T., 2001. Tropical origins for recent North Atlantic climate change. *Science*, **292(5514)**, 90-92.

Holton, J.R. and Tan, H.C., 1980. The influence of the equatorial quasi-biennial oscillation on the global circulation at 50 mb. *Journal of the Atmospheric Sciences*, **37(10)**, 2200-2208.

Honda, M., Inoue, J. and Yamane, S., 2009. Influence of low Arctic sea-ice minima on anomalously cold Eurasian winters. *Geophysical Research Letters*, **36(8)**, 08707.

Hoskins, B.J. and Karoly, D.J., 1981. The steady linear response of a spherical atmosphere to thermal and orographic forcing. *Journal of the Atmospheric Sciences*, **38(6)**, 1179-1196.

Hoskins, B.J. and Valdes, P.J., 1990. On the existence of storm-tracks. *Journal of the atmospheric sciences*, **47(15)**, 1854-1864.

Hoskins, B., Fonseca, R., Blackburn, M. and Jung, T., 2012. Relaxing the tropics to an 'observed' state: Analysis using a simple baroclinic model. *Quarterly Journal of the Royal Meteorological Society*, **138(667)**, 1618-1626.

Howe, J. and White, I., 2002. The geography of the autumn 2000 floods in England and Wales: causes and solutions. *Geography*, 116-124.

Hu, D., Guan, Z., Tian, W. and Ren, R., 2018. Recent strengthening of the stratospheric Arctic vortex response to warming in the central North Pacific. *Nature communications*, **9(1)**, 1697.

Hunke, E.C., Lipscomb, W.H., Turner, A.K., Jeffery, N. and Elliott, S., 2010. CICE: the Los Alamos Sea Ice Model Documentation and Software User's Manual Version 4.1 LA-CC-06-012. T-3 Fluid Dynamics Group, Los Alamos National Laboratory, **675**, 500.

Huntingford, C., Marsh, T., Scaife, A.A., Kendon, E.J., Hannaford, J., Kay, A.L., Lockwood, M., Prudhomme, C., Reynard, N.S., Parry, S. and Lowe, J.A., 2014. Potential influences on the United Kingdom's floods of winter 2013/14. *Nature Climate Change*, **4(9)**, 769.

Hurrell, J.W., 1995a. Decadal trends in the North Atlantic Oscillation: regional temperatures and precipitation. *Science*, **269(5224)**, 676-679.

Hurrell, J.W., 1995b. Transient eddy forcing of the rotational flow during northern winter. *Journal of the atmospheric sciences*, **52(12)**, 2286-2301.

Hurrell, J.W., 2003. NAO Index Data provided by the Climate Analysis Section, NCAR, Boulder, USA. Updated regularly. Accessed 24/07/2019.

Hurrell, J.W., Hack, J.J., Shea, D., Caron, J.M. and Rosinski, J., 2008. A new sea surface temperature and sea ice boundary dataset for the Community Atmosphere Model. *Journal of Climate*, **21(19)**, 5145-5153.

Hurrell, J.W., and Deser, C., 2010. North Atlantic climate variability: the role of the North Atlantic Oscillation. *Journal of Marine Systems*, **79 (3-4)**, 231-244.

Hurrell, J.W., 2018. Hurrell North Atlantic Oscillation (NAO) Index (PC-based) — NCAR - Climate Data Guide. [online] Climatedataguide.ucar.edu. Available at: `https://climatedataguide.ucar.edu/climate-data/hurrell-north-atlantic-oscillation-nao-index-pc-based` [Accessed 26 Jul. 2018].

Ineson, S. and Scaife, A.A., 2009. The role of the stratosphere in the European climate response to El Niño. *Nature Geoscience*, **2(1)**, 32.

Ineson, S., Scaife, A.A., Knight, J.R., Manners, J.C., Dunstone, N.J., Gray, L.J. and Haigh, J.D., 2011. Solar forcing of winter climate variability in the Northern Hemisphere. *Nature Geoscience*, **4(11)**, 753.

Inoue, J., Hori, M.E. and Takaya, K., 2012. The role of Barents Sea ice in the wintertime cyclone track and emergence of a warm-Arctic cold-Siberian anomaly. *Journal of Climate*, **25(7)**, 2561-2568.

Iza, M., Calvo, N. and Manzini, E., 2016. The stratospheric pathway of La Niña. *Journal of Climate*, **29(24)**, 8899-8914.

Jaiser, R., Dethloff, K., Handorf, D., Rinke, A. and Cohen, J., 2012. Impact of sea ice cover changes on the Northern Hemisphere atmospheric winter circulation. *Tellus A: Dynamic Meteorology and Oceanography*, **64(1)**, p.11595.

Jaiser, R., Dethloff, K. and Handorf, D., 2013. Stratospheric response to Arctic sea ice retreat and associated planetary wave propagation changes. *Tellus A: Dynamic Meteorology and Oceanography*, **65(1)**, 19375.

Jia, L., Yang, X., Vecchi, G., Gudgel, R., Delworth, T., Fueglistaler, S., Lin, P., Scaife, A.A., Underwood, S. and Lin, S.J., 2017. Seasonal prediction skill of northern extratropical surface temperature driven by the stratosphere. *Journal of Climate*, **30(12)**, 4463-4475.

Johansson, Ã., 2007. Prediction skill of the NAO and PNA from daily to seasonal time scales. *Journal of climate*, **20(10)**, 1957-1975.

Jolliffe, I.T. and Cadima, J., 2016. Principal component analysis: a review and recent developments. *Phil. Trans. R. Soc. A*, **374(2065)**, 20150202.

Jung, T., Palmer, T., Rodwell, M. and Serrar, S., 2008. Diagnosing forecast error using relaxation experiments. *ECMWF newsletter*, **116**, 24-34.

Jung, T., Miller, M.J. and Palmer, T.N., 2010. Diagnosing the origin of extended-range

forecast errors. *Monthly Weather Review*, **138(6)**, 2434-2446.

Jung, T., Palmer, T.N., Rodwell, M.J. and Serrar, S., 2010. Understanding the anomalously cold European winter of 2005/06 using relaxation experiments. *Monthly Weather Review*, **138(8)**, 3157-3174.

Jung, T., Vitart, F., Ferranti, L. and Morcrette, J.J., 2011. Origin and predictability of the extreme negative NAO winter of 2009/10. *Geophysical Research Letters*, **38(7)**, 07701.

Jung, T., Kasper, M.A., Semmler, T. and Serrar, S., 2014. Arctic influence on subseasonal midlatitude prediction. *Geophysical Research Letters*, **41(10)**, 3676-3680.

Kang, D., Lee, M.I., Im, J., Kim, D., Kim, H.M., Kang, H.S., Schubert, S.D., Arribas, A. and MacLachlan, C., 2014. Prediction of the Arctic Oscillation in boreal winter by dynamical seasonal forecasting systems. *Geophysical Research Letters*, **41(10)**, 3577-3585.

Karoly, D.J., 1983. Rossby wave propagation in a barotropic atmosphere. *Dynamics of Atmospheres and Oceans*, **7(2)**, 111-125.

Karpechko, A.Y., Charlton-Perez, A., Balmaseda, M., Tyrrell, N. and Vitart, F., 2018. Predicting Sudden Stratospheric Warming 2018 and Its Climate Impacts With a Multimodel Ensemble. *Geophysical Research Letters*, **45(24)**, 13-538.

Kay, J.E., Deser, C., Phillips, A., Mai, A., Hannay, C., Strand, G., Arblaster, J.M., Bates, S.C., Danabasoglu, G., Edwards, J. and Holland, M., 2015. The Community Earth System Model (CESM) large ensemble project: A community resource for studying climate change in the presence of internal climate variability. *Bulletin of the American Meteorological Society*, **96(8)**, 1333-1349.

Keeley, S.P.E., Sutton, R.T. and Shaffrey, L.C., 2009. Does the North Atlantic Oscillation show unusual persistence on intraseasonal timescales?. *Geophysical Research Letters*, **36(22)**, 22706.

Kelleher, M. and Screen, J., 2018. Atmospheric precursors of and response to anomalous Arctic sea ice in CMIP5 models. *Advances in Atmospheric Sciences*, **35(1)**, 27-37.

Kendon, M. and McCarthy, M., 2015. The UK's wet and stormy winter of 2013/2014. *Weather*, **70(2)**, 40-47.

Kidston, J., Scaife, A.A., Hardiman, S.C., Mitchell, D.M., Butchart, N., Baldwin, M.P. and Gray, L.J., 2015. Stratospheric influence on tropospheric jet streams, storm

tracks and surface weather. *Nature Geoscience*, **8(6)**, 433.

Kim, B.M., Son, S.W., Min, S.K., Jeong, J.H., Kim, S.J., Zhang, X., Shim, T. and Yoon, J.H., 2014. Weakening of the stratospheric polar vortex by Arctic sea-ice loss. *Nature communications*, **4**, 4646.

King, M.P., Herceg-Bulić, I., Bladé, I., García-Serrano, J., Keenlyside, N., Kucharski, F., Li, C. and Sobolowski, S., 2018. Importance of late fall ENSO teleconnection in the Euro-Atlantic sector. *Bulletin of the American Meteorological Society*, **99(7)**, 1337-1343.

Kirchner, I., Stenchikov, G.L., Graf, H.F., Robock, A. and Antuña, J.C., 1999. Climate model simulation of winter warming and summer cooling following the 1991 Mount Pinatubo volcanic eruption. *Journal of Geophysical Research: Atmospheres*, **104(D16)**, 19039-19055.

Knight, J.R., Maidens, A., Watson, P.A., Andrews, M., Belcher, S., Brunet, G., Fereday, D., Folland, C.K., Scaife, A.A. and Slingo, J., 2017. Global meteorological influences on the record UK rainfall of winter 2013–14. *Environmental Research Letters*, **12(7)**, 074001.

Kodera, K., 1995. On the origin and nature of the interannual variability of the winter stratospheric circulation in the northern hemisphere. *Journal of Geophysical Research: Atmospheres*, **100(D7)**, 14077-14087.

Kodera, K., 2002. Solar cycle modulation of the North Atlantic Oscillation: Implication in the spatial structure of the NAO. *Geophysical Research Letters*, **29(8)**, 59-1.

Kodera, K. and Kuroda, Y., 2002. Dynamical response to the solar cycle. *Journal of Geophysical Research: Atmospheres*, **107**, 4749.

Koenigk, T., Caian, M., Nikulin, G. and Schimanke, S., 2016. Regional Arctic sea ice variations as predictor for winter climate conditions. *Climate Dynamics*, **46(1-2)**, 317-337.

Koenigk, T., Gao, Y., Gastineau, G., Keenlyside, N., Nakamura, T., Ogawa, F., Orsolini, Y., Semenov, V., Suo, L., Tian, T. and Wang, T., 2019. Impact of Arctic sea ice variations on winter temperature anomalies in northern hemispheric land areas. *Climate Dynamics*, **52(5-6)**, 3111-3137.

Kohout, A.L., Williams, M.J.M., Dean, S.M. and Meylan, M.H., 2014. Storm-induced sea-ice breakup and the implications for ice extent. *Nature*, **509(7502)**, 604.

Kolstad, E.W. and Screen, J.A., 2019. Non-Stationary Relationship between Autumn Arctic Sea Ice and the Winter North Atlantic Oscillation. *Geophysical Research Letters*, in press.

Krahmann, G. and Visbeck, M., 2003. Arctic Ocean sea ice response to Northern Annular Mode-like wind forcing. *Geophysical research letters*, **30**, 1793.

Kretschmer, M., Coumou, D., Donges, J.F. and Runge, J., 2016. Using causal effect networks to analyze different Arctic drivers of midlatitude winter circulation. *Journal of Climate*, **29(11)**, 4069-4081.

Krinner, G., Rinke, A., Dethloff, K. and Gorodetskaya, I.V., 2010. Impact of prescribed Arctic sea ice thickness in simulations of the present and future climate. *Climate dynamics*, **35(4)**, 619-633.

Kryjov, V.N., 2015. October circulation precursors of the wintertime Arctic Oscillation. *International Journal of Climatology*, **35(2)**, 161-171.

Kryjov, V.N. and Min, Y.M., 2016. Predictability of the wintertime Arctic Oscillation based on autumn circulation. *International Journal of Climatology*, **36(12)**, 4181-4186.

Kumar, A., 2009. Finite samples and uncertainty estimates for skill measures for seasonal prediction. *Monthly Weather Review*, **137(8)**, 2622-2631.

Kushner, P.J. and Polvani, L.M., 2006. Stratosphere–troposphere coupling in a relatively simple AGCM: Impact of the seasonal cycle. *Journal of climate*, **19(21)**, 5721-5727.

Kwok, R., 2000. Recent changes in Arctic Ocean sea ice motion associated with the North Atlantic Oscillation. *Geophysical Research Letters*, **27(6)**, 775-778.

Kwok, R. and Rothrock, D.A., 2009. Decline in Arctic sea ice thickness from submarine and ICESat records: 1958–2008. *Geophysical Research Letters*, **36(15)**, 15501.

Kumar, A. and Chen, M., 2018. Causes of skill in seasonal predictions of the Arctic Oscillation. *Climate Dynamics*, **51(5-6)**, 2397-2411.

L'Heureux, M. and Higgins, R.W., 2008. Boreal winter links between the Madden–Julian oscillation and the Arctic Oscillation. *Journal of Climate*, **21(12)**, pp.3040-3050.

L'Heureux, M., Butler, A., Jha, B., Kumar, A. and Wang, W., 2010. Unusual extremes in the negative phase of the Arctic Oscillation during 2009. *Geophysical Research Letters*, **37(10)**, 10704.

L'Heureux, M.L., Tippett, M.K., Kumar, A., Butler, A.H., Ciasto, L.M., Ding, Q.,

Harnos, K.J. and Johnson, N.C., 2017. Strong Relations Between ENSO and the Arctic Oscillation in the North American Multimodel Ensemble. *Geophysical Research Letters*, **44(22)**, 11654-11662.

Labe, Z., Peings, Y. and Magnusdottir, G., 2019. The effect of QBO phase on the atmospheric response to projected Arctic sea-ice loss in early winter. *Geophysical Research Letters*, in press.

Labitzke, K., Naujokat, B. and McCormick, M.P., 1983. Temperature effects on the stratosphere of the April 4, 1982 eruption of El Chichon, Mexico. *Geophysical Research Letters*, **10(1)**, 24-26.

Labitzke, K., 1987. Sunspots, the QBO, and the stratospheric temperature in the north polar region. *Geophysical Research Letters*, **14(5)**, 535-537.

Lamarque, J.F., Bond, T.C., Eyring, V., Granier, C., Heil, A., Klimont, Z., Lee, D., Liousse, C., Mieville, A., Owen, B. and Schultz, M.G., 2010. Historical (1850–2000) gridded anthropogenic and biomass burning emissions of reactive gases and aerosols: methodology and application. *Atmospheric Chemistry and Physics*, **10(15)**, 7017-7039.

Latif, M., Anderson, D., Barnett, T., Cane, M., Kleeman, R., Leetmaa, A., O'Brien, J., Rosati, A. and Schneider, E., 1998. A review of the predictability and prediction of ENSO. *Journal of Geophysical Research: Oceans*, **103**, 14375-14393.

Latif, M., Arpe, K. and Roeckner, E., 2000. Oceanic control of decadal North Atlantic sea level pressure variability in winter. *Geophysical Research Letters*, **27(5)**, 727-730.

Lee, S., 1999. Why Are the Climatological Zonal Winds Easterly in the Equatorial Upper Troposphere?. *Journal of the atmospheric sciences*, **56(10)**, 1353-1363.

Lee, S., Gong, T., Johnson, N., Feldstein, S.B. and Pollard, D., 2011. On the possible link between tropical convection and the Northern Hemisphere Arctic surface air temperature change between 1958 and 2001. *Journal of Climate*, **24(16)**, 4350-4367.

Lee, S., 2012. Testing of the tropically excited Arctic warming mechanism (TEAM) with traditional El Nino and La Nina. *Journal of Climate*, **25(12)**, 4015-4022.

Lee, S., 2014. A theory for polar amplification from a general circulation perspective. *Asia-Pacific Journal of Atmospheric Sciences*, **50(1)**, 31-43.

Li, F. and Wang, H., 2012. Autumn sea ice cover, winter Northern Hemisphere annular

mode, and winter precipitation in Eurasia. *Journal of Climate*, **26(11)**, 3968-3981.

Lim, Y.K., Ham, Y.G., Jeong, J.H. and Kug, J.S., 2012. Improvement in simulation of Eurasian winter climate variability with a realistic Arctic sea ice condition in an atmospheric GCM. *Environmental Research Letters*, **7(4)**, 044041.

Lin, H., Brunet, G. and Derome, J., 2009. An observed connection between the North Atlantic Oscillation and the Madden–Julian oscillation. *Journal of Climate*, **22(2)**, 364-380.

Lindsay, R.W., Zhang, J., Schweiger, A.J. and Steele, M.A., 2008. Seasonal predictions of ice extent in the Arctic Ocean. *Journal of Geophysical Research: Oceans*, **113**, 02023.

Lindsay, R., Wensnahan, M., Schweiger, A. and Zhang, J., 2014. Evaluation of seven different atmospheric reanalysis products in the Arctic. *Journal of Climate*, **27(7)**, 2588-2606.

Lindsay, R. and Schweiger, A., 2015. Arctic sea ice thickness loss determined using subsurface, aircraft, and satellite observations. *The Cryosphere*, **9(1)**, 269-283.

Liptak, J. and Strong, C., 2014. The winter atmospheric response to sea ice anomalies in the Barents Sea. *Journal of Climate*, **27(2)**, 914-924.

Liu, J., Curry, J.A. and Hu, Y., 2004. Recent Arctic sea ice variability: Connections to the Arctic Oscillation and the ENSO. *Geophysical Research Letters*, **31(9)**, 09211.

Liu, J., Curry, J.A., Wang, H., Song, M. and Horton, R.M., 2012. Impact of declining Arctic sea ice on winter snowfall. *Proceedings of the National Academy of Sciences*, **109**, 4074-4079.

Luo, B., Wu, L., Luo, D., Dai, A. and Simmonds, I., 2019. The winter midlatitude-Arctic interaction: effects of North Atlantic SST and high-latitude blocking on Arctic Sea ice and Eurasian cooling. *Climate Dynamics*, **52(5-6)**, 2981-3004.

MacDonald, G.M. and Case, R.A., 2005. Variations in the Pacific Decadal Oscillation over the past millennium. *Geophysical Research Letters*, **32**, L08703.

MacLachlan, C., Arribas, A., Peterson, K.A., Maidens, A., Fereday, D., Scaife, A.A., Gordon, M., Vellinga, M., Williams, A., Comer, R.E. and Camp, J., 2015. Global Seasonal forecast system version 5 (GloSea5): a high-resolution seasonal forecast system. *Quarterly Journal of the Royal Meteorological Society*, **141(689)**, 1072-1084.

Madden, R.A. and Julian, P.R., 1972. Description of global-scale circulation cells in the tropics with a 40–50 day period. *Journal of the atmospheric sciences*, **29(6)**, 1109-1123.

Maidens, A., Arribas, A., Scaife, A.A., MacLachlan, C., Peterson, D. and Knight, J., 2013. The influence of surface forcings on prediction of the North Atlantic Oscillation regime of winter 2010/11. *Monthly Weather Review*, **141(11)**, 3801-3813.

Maidens, A., Knight, J., Martin, N. and Andrews, M., 2019. Contrasting Conditions in the UK Winter of 2015/16 as a Result of Remote Tropical Influences. *Journal of Climate*, **32(11)**, 3227-3243.

Mantua, N.J. and Hare, S.R., 2002. The Pacific decadal oscillation. *Journal of oceanography*, **58(1)**, 35-44.

Marshall, A.G. and Scaife, A.A., 2009. Impact of the QBO on surface winter climate. *Journal of Geophysical Research: Atmospheres*, **114(D18)**.

Marshall, A.G., Scaife, A.A. and Ineson, S., 2009. Enhanced seasonal prediction of European winter warming following volcanic eruptions. *Journal of climate*, **22(23)**, 6168-6180.

Massey Jr, F.J., 1951. The Kolmogorov-Smirnov test for goodness of fit. *Journal of the American statistical Association*, **46(253)**, 68-78.

Matsuno, T., 1971. A dynamical model of the stratospheric sudden warming. *Journal of the Atmospheric Sciences*, **28(8)**, 1479-1494.

Matthews, A.J., Hoskins, B.J. and Masutani, M., 2004. The global response to tropical heating in the Madden–Julian oscillation during the northern winter. *Quarterly Journal of the Royal Meteorological Society: A journal of the atmospheric sciences, applied meteorology and physical oceanography*, **130(601)**, 1991-2011.

Matthes, K., Kuroda, Y., Kodera, K. and Langematz, U., 2006. Transfer of the solar signal from the stratosphere to the troposphere: Northern winter. *Journal of Geophysical Research: Atmospheres*, **111**, 06108.

McCusker, K.E., Fyfe, J.C. and Sigmond, M., 2016. Twenty-five winters of unexpected Eurasian cooling unlikely due to Arctic sea-ice loss. *Nature Geoscience*, **9(11)**, 838.

McKenna, C.M., Bracegirdle, T.J., Shuckburgh, E.F., Haynes, P.H. and Joshi, M.M., 2018. Arctic Sea Ice Loss in Different Regions Leads to Contrasting Northern Hemisphere Impacts. *Geophysical Research Letters*, **45(2)**, 945-954.

Mesquita, M.D., Hodges, K.I., Atkinson, D.E. and Bader, J.R., 2011. Sea-ice anomalies in the Sea of Okhotsk and the relationship with storm tracks in the Northern Hemisphere during winter. *Tellus A: Dynamic Meteorology and Oceanography*, **63(2)**, 312-323.

Minobe, S., Kuwano-Yoshida, A., Komori, N., Xie, S.P. and Small, R.J., 2008. Influence of the Gulf Stream on the troposphere. *Nature*, **452(7184)**, 206.

Mitchell, D.M., Gray, L.J., Anstey, J., Baldwin, M.P. and Charlton-Perez, A.J., 2013. The influence of stratospheric vortex displacements and splits on surface climate. *Journal of Climate*, **26(8)**, 2668-2682.

Mitchell, J.M., 1961. Recent secular changes of global temperature. *Annals of the New York Academy of Sciences*, **95(1)**, 235-250.

Mokhov, I.I., Smirnov, D.A., Nakonechny, P.I., Kozlenko, S.S., Seleznev, E.P. and Kurths, J., 2011. Alternating mutual influence of El-Niño/Southern Oscillation and Indian monsoon. *Geophysical Research Letters*, **38(8)**.

Monahan, A.H., Fyfe, J.C., Ambaum, M.H., Stephenson, D.B. and North, G.R., 2009. Empirical orthogonal functions: The medium is the message. *Journal of Climate*, **22(24)**, 6501-6514.

Moon, J.Y., Wang, B. and Ha, K.J., 2011. ENSO regulation of MJO teleconnection. *Climate dynamics*, **37(5-6)**, 1133-1149.

Mori, M., Watanabe, M., Shiogama, H., Inoue, J. and Kimoto, M., 2014. Robust Arctic sea-ice influence on the frequent Eurasian cold winters in past decades. *Nature Geoscience*, **7(12)**, 869.

Moron, V. and Gouirand, I., 2003. Seasonal modulation of the El Niño–Southern Oscillation relationship with sea level pressure anomalies over the North Atlantic in October–March 1873–1996. *International Journal of Climatology*, **23(2)**, 143-155.

Murphy, J.M., 1988. The impact of ensemble forecasts on predictability. *Quarterly Journal of the Royal Meteorological Society*, **114(480)**, 463-493.

Murphy, J.M., 1990. Assessment of the practical utility of extended range ensemble forecasts. *Quarterly Journal of the Royal Meteorological Society*, **116(491)**, 89-125.

Msadek, R., Vecchi, G.A., Winton, M. and Gudgel, R.G., 2014. Importance of initial conditions in seasonal predictions of Arctic sea ice extent. *Geophysical Research Letters*, **41(14)**, 5208-5215.

Mysak, L.A. and Venegas, S.A., 1998. Decadal climate oscillations in the Arctic: A new feedback loop for atmosphere-ice-ocean interactions. *Geophysical Research Letters*, **25(19)**, 3607-3610.

Nakamura, T., Yamazaki, K., Iwamoto, K., Honda, M., Miyoshi, Y., Ogawa, Y. and Ukita, J., 2015. A negative phase shift of the winter AO/NAO due to the recent Arctic sea-ice reduction in late autumn. *Journal of Geophysical Research: Atmospheres*, **120(8)**, 3209-3227.

Neale, R. B., et al., 2010. Description of the NCAR Community Atmosphere Model (CAM 4.0), *NCAR Tech. Note NCAR/TN-XXX+STR*, 206 pp., Natl. Cent. for Atmos. Res, Boulder, Colo.

Neale, R. B., et al., 2012. Description of the NCAR Community Atmosphere Model (CAM 5.0), *NCAR Tech. Note NCAR/TN-486+STR*, 289 pp., Natl. Cent. for Atmos. Res, Boulder, Colo.

Newson, R.L., 1973. Response of a general circulation model of the atmosphere to removal of the Arctic ice-cap. *Nature*, **241(5384)**, 39.

Nie, Y., Scaife, A.A., Ren, H.L., Comer, R.E., Andrews, M.B., Davis, P. and Martin, N., 2019. Stratospheric initial conditions provide seasonal predictability of the North Atlantic and Arctic Oscillations. *Environmental Research Letters*, **14(3)**, 034006.

O'Reilly, C.H., Weisheimer, A., Woollings, T., Gray, L.J. and MacLeod, D., 2019. The importance of stratospheric initial conditions for winter North Atlantic Oscillation predictability and implications for the signal-to-noise paradox. *Quarterly Journal of the Royal Meteorological Society*, **145(718)**, 131-146.

Ogawa, F., Keenlyside, N., Gao, Y., Koenigk, T., Yang, S., Suo, L., Wang, T., Gastineau, G., Nakamura, T., Cheung, H.N. and Omrani, N.E., 2018. Evaluating impacts of recent Arctic sea ice loss on the northern hemisphere winter climate change. *Geophysical Research Letters*, **45(7)**, 3255-3263.

Onarheim, I.H., Eldevik, T., Årthun, M., Ingvaldsen, R.B. and Smedsrud, L.H., 2015. Skillful prediction of Barents Sea ice cover. *Geophysical Research Letters*, **42(13)**, 5364-5371.

Orsolini, Y.J., Senan, R., Benestad, R.E. and Melsom, A., 2012. Autumn atmospheric response to the 2007 low Arctic sea ice extent in coupled ocean–atmosphere hindcasts. *Climate dynamics*, **38(11-12)**, 2437-2448.

Overland, J.E., Wood, K.R. and Wang, M., 2011. Warm Arctic—cold continents: climate impacts of the newly open Arctic Sea. *Polar Research*, **30(1)**, 15787.

Overland, J.E., 2016. A difficult Arctic science issue: Midlatitude weather linkages. *Polar Science*, **10(3)**, 210-216.

Overland, J.E., Dethloff, K., Francis, J.A., Hall, R.J., Hanna, E., Kim, S.J., Screen, J.A., Shepherd, T.G. and Vihma, T., 2016. Nonlinear response of mid-latitude weather to the changing Arctic. *Nature Climate Change*, **6(11)**, 992.

Palin, E.J., Scaife, A.A., Wallace, E., Pope, E.C., Arribas, A. and Brookshaw, A., 2016. Skillful seasonal forecasts of winter disruption to the UK transport system. *Journal of Applied Meteorology and Climatology*, **55(2)**, 325-344.

Pall, P., Aina, T., Stone, D.A., Stott, P.A., Nozawa, T., Hilberts, A.G., Lohmann, D. and Allen, M.R., 2011. Anthropogenic greenhouse gas contribution to flood risk in England and Wales in autumn 2000. *Nature*, **470(7334)**, 382.

Park, D.S.R., Lee, S. and Feldstein, S.B., 2015. Attribution of the recent winter sea ice decline over the Atlantic sector of the Arctic Ocean. *Journal of climate*, **28(10)**, 4027-4033.

Park, H.S., Lee, S., Son, S.W., Feldstein, S.B. and Kosaka, Y., 2015. The impact of poleward moisture and sensible heat flux on Arctic winter sea ice variability. *Journal of Climate*, **28(13)**, 5030-5040.

Pasini, A., Lorè, M. and Ameli, F., 2006. Neural network modelling for the analysis of forcings/temperatures relationships at different scales in the climate system. *Ecological Modelling*, **191(1)**, 58-67.

Peings, Y. and Magnusdottir, G., 2014. Response of the wintertime Northern Hemisphere atmospheric circulation to current and projected Arctic sea ice decline: A numerical study with CAM5. *Journal of Climate*, **27(1)**, 244-264.

Peings, Y., Douville, H., Colin, J., Martin, D.S. and Magnusdottir, G., 2017. Snow–(N) AO teleconnection and its modulation by the Quasi-Biennial Oscillation. *Journal of Climate*, **30(24)**, 10211-10235.

Peings, Y., 2019. Ural Blocking as a Driver of Early-Winter Stratospheric Warmings. *Geophysical Research Letters*, **46(10)**, 5460-5468.

Peng, S., Robinson, W.A. and Li, S., 2003. Mechanisms for the NAO responses to the North Atlantic SST tripole. *Journal of Climate*, *16(12)*, 1987-2004.

Petoukhov, V., Semenov, V. A., 2009. A link between reduced Barents-Kara sea ice and cold winter extremes over northern continents. *Journal of Geophysical Research Atmospheres*, **115**, 21111.

Petrie, R.E., Shaffrey, L.C. and Sutton, R.T., 2015. Atmospheric impact of Arctic sea ice loss in a coupled ocean–atmosphere simulation. *Journal of Climate*, **28(24)**, 9606-9622.

Pinto, J.G., Zacharias, S., Fink, A.H., Leckebusch, G.C. and Ulbrich, U., 2009. Factors contributing to the development of extreme North Atlantic cyclones and their relationship with the NAO. *Climate dynamics*, **32(5)**, 711-737.

Pinto, J.G., Karremann, M.K., Born, K., Della-Marta, P.M. and Klawa, M., 2012. Loss potentials associated with European windstorms under future climate conditions. *Climate Research*, **54(1)**, 1-20.

Pozo-Vázquez, D., Esteban-Parra, M.J., Rodrigo, F.S. and Castro-Diez, Y., 2001a. A study of NAO variability and its possible non-linear influences on European surface temperature. *Climate Dynamics*, **17(9)**, 701-715.

Pozo-Vázquez, D., Esteban-Parra, M.J., Rodrigo, F.S. and Castro-Diez, Y., 2001b. The association between ENSO and winter atmospheric circulation and temperature in the North Atlantic region. *Journal of Climate*, **14(16)**, 3408-3420.

Rajagopalan, B., Kushnir, Y. and Tourre, Y.M., 1998. Observed decadal midlatitude and tropical Atlantic climate variability. *Geophysical Research Letters*, **25(21)**, 3967-3970.

Rayner, N.A., Parker, D.E., Horton, E.B., Folland, C.K., Alexander, L.V., Rowell, D.P., Kent, E.C. and Kaplan, A., 2003. Global analyses of sea surface temperature, sea ice, and night marine air temperature since the late nineteenth century. *Journal of Geophysical Research: Atmospheres*, **108**, 4407.

Rennert, K.J. and Wallace, J.M., 2009. Cross-frequency coupling, skewness, and blocking in the Northern Hemisphere winter circulation. *Journal of Climate*, **22(21)**, 5650-5666.

Riddle, E.E., Butler, A.H., Furtado, J.C., Cohen, J.L. and Kumar, A., 2013. CFSv2 ensemble prediction of the wintertime Arctic Oscillation. *Climate dynamics*, **41(3-4)**, 1099-1116.

Rigor, I.G., Wallace, J.M. and Colony, R.L., 2002. Response of sea ice to the Arctic

Oscillation. *Journal of Climate*, **15(18)**, 2648-2663.

Rinke, A., Maslowski, W., Dethloff, K. and Clement, J., 2006. Influence of sea ice on the atmosphere: A study with an Arctic atmospheric regional climate model. *Journal of Geophysical Research: Atmospheres*, **111(D16)**.

Rinke, A., Dethloff, K., Dorn, W., Handorf, D. and Moore, J.C., 2013. Simulated Arctic atmospheric feedbacks associated with late summer sea ice anomalies. *Journal of Geophysical Research: Atmospheres*, **118(14)**, 7698-7714.

Robertson, A.W., Mechoso, C.R. and Kim, Y.J., 2000. The influence of Atlantic sea surface temperature anomalies on the North Atlantic Oscillation. *Journal of Climate*, **13(1)**, 122-138.

Robock, A. and Mao, J., 1992. Winter warming from large volcanic eruptions. *Geophysical Research Letters*, **19(24)**, 2405-2408.

Rodwell, M.J., Rowell, D.P. and Folland, C.K., 1999. Oceanic forcing of the wintertime North Atlantic Oscillation and European climate. *Nature*, **398(6725)**, 320.

Roeckner, E., Bäuml, G., Bonaventura, L., Brokopf, R., Esch, M., Giorgetta, M., Hagemann, S., Kirchner, I., Kornblueh, L., Manzini, E. and Rhodin, A., 2003. The atmospheric general circulation model ECHAM 5. PART I: Model description. *Max Planck Institute for Meteorology Rep*, **349**, 127.

Romanowsky, E., Handorf, D., Jaiser, R., Wohltmann, I., Dorn, W., Ukita, J., Cohen, J., Dethloff, K. and Rex, M., 2019. The role of stratospheric ozone for Arctic-midlatitude linkages. *Scientific reports*, **9(1)**, 7962.

Roxy, M.K., Dasgupta, P., McPhaden, M.J., Suematsu, T., Zhang, C. and Kim, D., 2019. Twofold expansion of the Indo-Pacific warm pool warps the MJO life cycle. *Nature*, **575(7784)**, 647-651.

Ruggieri, P., Buizza, R. and Visconti, G., 2016. On the link between Barents-Kara sea ice variability and European blocking. *Journal of Geophysical Research: Atmospheres*, **121(10)**, 5664-5679.

Runge, J., Petoukhov, V. and Kurths, J., 2014. Quantifying the strength and delay of climatic interactions: The ambiguities of cross correlation and a novel measure based on graphical models. *Journal of Climate*, **27(2)**, 720-739.

Runge, J., Petoukhov, V., Donges, J.F., Hlinka, J., Jajcay, N., Vejmelka, M., Hartman, D., Marwan, N., Paluš, M. and Kurths, J., 2015. Identifying causal gateways and

mediators in complex spatio-temporal systems. *Nature communications*, **6**, 8502.

Runge, J., Nowack, P., Kretschmer, M., Flaxman, S. and Sejdinovic, D., 2017. Detecting causal associations in large nonlinear time series datasets. *arXiv preprint arXiv:1702.07007*

Saha, S., Moorthi, S., Pan, H.L., Wu, X., Wang, J., Nadiga, S., Tripp, P., Kistler, R., Woollen, J., Behringer, D. and Liu, H., 2010. The NCEP climate forecast system reanalysis. *Bulletin of the American Meteorological Society*, **91(8)**, 1015-1058.

Saha, S., Moorthi, S., Wu, X., Wang, J., Nadiga, S., Tripp, P., Behringer, D., Hou, Y.T., Chuang, H.Y., Iredell, M. and Ek, M., 2014. The NCEP climate forecast system version 2. *Journal of Climate*, **27(6)**, 2185-2208.

Saito, K., Cohen, J. and Entekhabi, D., 2001. Evolution of atmospheric response to early-season Eurasian snow cover anomalies. *Monthly Weather Review*, **129(11)**, 2746-2760.

Saito, N., Maeda, S., Nakaegawa, T., Takaya, Y., Imada, Y. and Matsukawa, C., 2017. Seasonal Predictability of the North Atlantic Oscillation and Zonal Mean Fields Associated with Stratospheric Influence in JMA/MRI-CPS2. *SOLA*, **13**, 209-213.

Sansom, P.G., Stephenson, D.B. and Williamson, D.B., 2018. State-space modeling of intra-seasonal persistence in daily climate indices: a data-driven approach for seasonal forecasting. *arXiv preprint arXiv* 1807.02671.

Sardeshmukh, P.D. and Hoskins, B.J., 1988. The generation of global rotational flow by steady idealized tropical divergence. *Journal of the Atmospheric Sciences*, **45(7)**, 1228-1251.

Scaife, A.A., Knight, J.R., Vallis, G.K. and Folland, C.K., 2005. A stratospheric influence on the winter NAO and North Atlantic surface climate. *Geophysical Research Letters*, **32(18)**.

Scaife, A.A. and Knight, J.R., 2008. Ensemble simulations of the cold European winter of 2005-2006. *Quarterly Journal of the Royal Meteorological Society*, **134(636)**, 1647-1659.

Scaife, A.A., Copsey, D., Gordon, C., Harris, C., Hinton, T., Keeley, S., O'Neill, A., Roberts, M. and Williams, K., 2011. Improved Atlantic winter blocking in a climate model. *Geophysical Research Letters*, **38(23)**, 23703.

Scaife, A.A., Arribas, A., Blockley, E., Brookshaw, A., Clark, R.T., Dunstone, N., Eade,

R., Fereday, D., Folland, C.K., Gordon, M. and Hermanson, L., 2014. Skillful long range prediction of European and North American winters. *Geophysical Research Letters*, **41(7)**, 2514-2519.

Scaife, A.A., Athanassiadou, M., Andrews, M., Arribas, A., Baldwin, M., Dunstone, N., Knight, J., MacLachlan, C., Manzini, E., Müller, W.A. and Pohlmann, H., 2014. Predictability of the quasi-biennial oscillation and its northern winter teleconnection on seasonal to decadal timescales. *Geophysical Research Letters*, **41(5)**, 1752-1758.

Scaife, A.A., Karpechko, A.Y., Baldwin, M.P., Brookshaw, A., Butler, A.H., Eade, R., Gordon, M., MacLachlan, C., Martin, N., Dunstone, N. and Smith, D., 2016. Seasonal winter forecasts and the stratosphere. *Atmospheric Science Letters*, **17(1)**, 51-56.

Scaife, A.A., Comer, R., Dunstone, N., Fereday, D., Folland, C., Good, E., Gordon, M., Hermanson, L., Ineson, S., Karpechko, A. and Knight, J., 2017. Predictability of European winter 2015/2016. *Atmospheric Science Letters*, **18(2)**, 38-44.

Scaife, A.A., Comer, R.E., Dunstone, N.J., Knight, J.R., Smith, D.M., MacLachlan, C., Martin, N., Peterson, K.A., Rowlands, D., Carroll, E.B. and Belcher, S., 2017. Tropical rainfall, Rossby waves and regional winter climate predictions. *Quarterly Journal of the Royal Meteorological Society*, **143(702)**, 1-11.

Scaife, A.A. and Smith, D., 2018. A signal-to-noise paradox in climate science. *npj Climate and Atmospheric Science*, **1(1)**, 28.

Scaife, A.A., Camp, J., Comer, R., Davis, P., Dunstone, N., Gordon, M., MacLachlan, C., Martin, N., Nie, Y., Ren, H.L. and Roberts, M., 2019. Does increased atmospheric resolution improve seasonal climate predictions?. *Atmospheric Science Letters*, p.e922.

Schenzinger, V., 2016. Tropical stratosphere variability and extratropical teleconnections (Doctoral dissertation, University of Oxford).

Schenzinger et al., 2019. HTE or no HTE? Investigating the QBO-Northern Hemisphere teleconnection with causal effect networks. *EGU*, Vienna, April 2019.

Schmidt, H., Brasseur, G.P. and Giorgetta, M.A., 2010. Solar cycle signal in a general circulation and chemistry model with internally generated quasi-biennial oscillation. *Journal of Geophysical Research: Atmospheres*, **115**, 00I14.

Schwartz, C. and Garfinkel, C.I., 2017. Relative roles of the MJO and stratospheric

variability in North Atlantic and European winter climate. *Journal of Geophysical Research: Atmospheres*, **122(8)**, 4184-4201.

Screen, J.A. and Simmonds, I., 2010. The central role of diminishing sea ice in recent Arctic temperature amplification. *Nature*, **464(7293)**, 1334.

Screen, J.A., Deser, C. and Simmonds, I., 2012. Local and remote controls on observed Arctic warming. *Geophysical Research Letters*, **39(10)**, 10709.

Screen, J.A., Simmonds, I., Deser, C. and Tomas, R., 2013. The atmospheric response to three decades of observed Arctic sea ice loss. *Journal of Climate*, **26(4)**, 1230-1248.

Screen, J.A., Deser, C., Simmonds, I. and Tomas, R., 2014. Atmospheric impacts of Arctic sea-ice loss, 1979–2009: Separating forced change from atmospheric internal variability. *Climate dynamics*, **43(1-2)**, 333-344.

Screen, J.A., 2017a. Simulated atmospheric response to regional and pan-Arctic sea ice loss. *Journal of Climate*, **30(11)**, 3945-3962.

Screen, J.A., 2017b. The missing Northern European winter cooling response to Arctic sea ice loss. *Nature communications*, **8**, 14603.

Screen, J.A., Deser, C., Smith, D.M., Zhang, X., Blackport, R., Kushner, P.J., Oudar, T., McCusker, K.E. and Sun, L., 2018. Consistency and discrepancy in the atmospheric response to Arctic sea-ice loss across climate models. *Nature Geoscience*, **11(3)**, 155-163.

Seierstad, I.A. and Bader, J., 2009. Impact of a projected future Arctic sea ice reduction on extratropical storminess and the NAO. *Climate dynamics*, **33(7-8)**, 937.

Semmler, T., Jung, T., Kasper, M.A. and Serrar, S., 2018. Using NWP to assess the influence of the Arctic atmosphere on midlatitude weather and climate. *Advances in Atmospheric Sciences*, **35(1)**, 5-13.

Shi, W., Schaller, N., MacLeod, D., Palmer, T.N. and Weisheimer, A., 2015. Impact of hindcast length on estimates of seasonal climate predictability. *Geophysical research letters*, **42(5)**, 1554-1559.

Siegert, S., Stephenson, D.B., Sansom, P.G., Scaife, A.A., Eade, R. and Arribas, A., 2016. A Bayesian framework for verification and recalibration of ensemble forecasts: How uncertain is NAO predictability?. *Journal of Climate*, **29(3)**, 995-1012.

Sigmond, M., Fyfe, J.C., Flato, G.M., Kharin, V.V. and Merryfield, W.J., 2013. Seasonal forecast skill of Arctic sea ice area in a dynamical forecast system. *Geophysical*

Research Letters, **40(3)**, 529-534.

Sillmann, J., Croci-Maspoli, M., Kallache, M. and Katz, R.W., 2011. Extreme cold winter temperatures in Europe under the influence of North Atlantic atmospheric blocking. *Journal of Climate*, **24(22)**, 5899-5913.

Silver, N.C. and Dunlap, W.P., 1987. Averaging correlation coefficients: should Fisher's z transformation be used?. *Journal of Applied Psychology*, **72(1)**, 146.

Singarayer, J.S., Bamber, J.L. and Valdes, P.J., 2006. Twenty-first-century climate impacts from a declining Arctic sea ice cover. *Journal of Climate*, **19(7)**, 1109-1125.

Smith, D.M., Scaife, A.A., Eade, R. and Knight, J.R., 2016. Seasonal to decadal prediction of the winter North Atlantic Oscillation: emerging capability and future prospects. *Quarterly Journal of the Royal Meteorological Society*, **142(695)**, 611-617.

Smith, D.M., Dunstone, N.J., Scaife, A.A., Fiedler, E.K., Copsey, D. and Hardiman, S.C., 2017. Atmospheric response to Arctic and Antarctic sea ice: the importance of ocean–atmosphere coupling and the background state. *Journal of Climate*, **30(12)**, 4547-4565.

Smith, D.M., Eade, R., Scaife, A.A., Caron, L.P., Danabasoglu, G., DelSole, T.M., Delworth, T., Doblas-Reyes, F.J., Dunstone, N.J., Hermanson, L. and Kharin, V., 2019. Robust skill of decadal climate predictions. *npj Climate and Atmospheric Science*, **2(1)**, 1-10.

Smith, D.M., Screen, J.A., Deser, C., Cohen, J., Fyfe, J.C., García-Serrano, J., Jung, T., Kattsov, V., Matei, D., Msadek, R. and Peings, Y., 2019. The Polar Amplification Model Intercomparison Project (PAMIP) contribution to CMIP6: investigating the causes and consequences of polar amplification. *Geoscientific Model Development*, **12(3)**, 1139-1164.

Sokolova, E., Dethloff, K., Rinke, A. and Benkel, A., 2007. Planetary and synoptic scale adjustment of the Arctic atmosphere to sea ice cover changes. *Geophysical Research Letters*, **34**, 17816.

Song, J., 2019. The Long-and Short-Lived North Atlantic Oscillation Events in a Simplified Atmospheric Model. *Journal of the Atmospheric Sciences*, **76(9)**, pp.2673-2700.

Sorokina, S.A., Li, C., Wettstein, J.J. and Kvamstø, N.G., 2016. Observed atmospheric coupling between Barents Sea ice and the warm-Arctic cold-Siberian anomaly pat-

tern. *Journal of Climate*, **29(2)**, 495-511.

Stenchikov, G.L., Kirchner, I., Robock, A., Graf, H.F., Antuña, J.C., Grainger, R.G., Lambert, A. and Thomason, L., 1998. Radiative forcing from the 1991 Mount Pinatubo volcanic eruption. *Journal of Geophysical Research: Atmospheres*, **103 (D12)**, 13837-13857.

Stenchikov, G., Hamilton, K., Stouffer, R.J., Robock, A., Ramaswamy, V., Santer, B. and Graf, H.F., 2006. Arctic Oscillation response to volcanic eruptions in the IPCC AR4 climate models. *Journal of Geophysical Research: Atmospheres*, **111**, 07107.

Stephenson, D.B., Pavan, V. and Bojariu, R., 2000. Is the North Atlantic Oscillation a random walk?. *International Journal of Climatology*, **20(1)**, 1-18.

Stockdale, T.N., Molteni, F. and Ferranti, L., 2015. Atmospheric initial conditions and the predictability of the Arctic Oscillation. *Geophysical Research Letters*, **42(4)**, 1173-1179.

Strey, S.T., Chapman, W.L. and Walsh, J.E., 2010. The 2007 sea ice minimum: Impacts on the Northern Hemisphere atmosphere in late autumn and early winter. *Journal of Geophysical Research: Atmospheres*, **115**, 23103.

Stroeve, J., Holland, M.M., Meier, W., Scambos, T. and Serreze, M., 2007. Arctic sea ice decline: Faster than forecast. *Geophysical research letters*, **34(9)**.

Strommen, K. and Palmer, T.N., 2019. Signal and noise in regime systems: A hypothesis on the predictability of the North Atlantic Oscillation. *Quarterly Journal of the Royal Meteorological Society*, **145(718)**, 147-163.

Sun, J. and Ahn, J.B., 2015. Dynamical seasonal predictability of the Arctic Oscillation using a CGCM. *International Journal of Climatology*, **35(7)**, 1342-1353.

Sun, L., Deser, C. and Tomas, R.A., 2015. Mechanisms of stratospheric and tropospheric circulation response to projected Arctic sea ice loss. *Journal of Climate*, **28(19)**, 7824-7845.

Sun, L., Perlwitz, J. and Hoerling, M., 2016. What caused the recent "Warm Arctic, Cold Continents" trend pattern in winter temperatures?. *Geophysical Research Letters*, **43(10)**, 5345-5352.

Svensson, C., Brookshaw, A., Scaife, A.A., Bell, V.A., Mackay, J.D., Jackson, C.R., Hannaford, J., Davies, H.N., Arribas, A. and Stanley, S., 2015. Long-range forecasts of UK winter hydrology. *Environmental Research Letters*, **10(6)**, 064006.

Taws, S.L., Marsh, R., Wells, N.C. and Hirschi, J., 2011. Re-emerging ocean temperature anomalies in late-2010 associated with a repeat negative NAO. *Geophysical Research Letters*, **38(20)**, 20601.

Thompson, D.W. and Wallace, J.M., 1998. The Arctic Oscillation signature in the wintertime geopotential height and temperature fields. *Geophysical research letters*, **25(9)**, 1297-1300.

Titchner, H.A. and Rayner, N.A., 2014. The Met Office Hadley Centre sea ice and sea surface temperature data set, version 2: 1. Sea ice concentrations. *Journal of Geophysical Research: Atmospheres*, **119(6)**, 2864-2889.

Toniazzo, T. and Scaife, A.A., 2006. The influence of ENSO on winter North Atlantic climate. *Geophysical research letters*, **33(24)**, 24704.

Trenberth, K.E., Branstator, G.W., Karoly, D., Kumar, A., Lau, N.C. and Ropelewski, C., 1998. Progress during TOGA in understanding and modeling global teleconnections associated with tropical sea surface temperatures. *Journal of Geophysical Research: Oceans*, **103**, 14291-14324.

Trenberth, K.E., Fasullo, J.T., Branstator, G. and Phillips, A.S., 2014. Seasonal aspects of the recent pause in surface warming. *Nature Climate Change*, **4(10)**, 911.

Tsutsui, J., Nishizawa, K. and Sassi, F., 2009. Response of the middle atmosphere to the 11-year solar cycle simulated with the Whole Atmosphere Community Climate Model. *Journal of Geophysical Research: Atmospheres*, **114(D2)**, 02111.

Tyrrell et al., 2019. Analysing Northern Hemisphere teleconnections in the SPARC-QBOi dataset using Causal Effect Networks. *EGU*, Vienna, April 2019.

Ulbrich, U. and Christoph, M., 1999. A shift of the NAO and increasing storm track activity over Europe due to anthropogenic greenhouse gas forcing. *Climate dynamics*, **15(7)**, 551-559.

Vallis, G.K., Gerber, E.P., Kushner, P.J. and Cash, B.A., 2004. A mechanism and simple dynamical model of the North Atlantic Oscillation and annular modes. *Journal of the atmospheric sciences*, **61(3)**, 264-280.

Vallis, G.K. and Gerber, E.P., 2008. Local and hemispheric dynamics of the North Atlantic Oscillation, annular patterns and the zonal index. *Dynamics of atmospheres and oceans*, **44**, 184-212.

Vihma, T., 2014. Effects of Arctic sea ice decline on weather and climate: A review.

Surveys in Geophysics, **35(5)**, 1175-1214.

Vimont, D.J., Wallace, J.M. and Battisti, D.S., 2003. The seasonal footprinting mechanism in the Pacific: Implications for ENSO. *Journal of Climate*, **16(16)**, 2668-2675.

Visbeck, M.H., Hurrell, J.W., Polvani, L. and Cullen, H.M., 2001. The North Atlantic Oscillation: past, present, and future. *Proceedings of the National Academy of Sciences*, **98(23)**, 12876-12877.

Wallace, J.M. and Gutzler, D.S., 1981. Teleconnections in the geopotential height field during the Northern Hemisphere winter. *Monthly Weather Review*, **109(4)**, 784-812.

Wang, C., 2002. Atmospheric circulation cells associated with the El Niño–Southern Oscillation. *Journal of Climate*, **15(4)**, 399-419.

Wang, C. and Fiedler, P.C., 2006. ENSO variability and the eastern tropical Pacific: A review. *Progress in Oceanography*, **69(2-4)**, 239-266.

Wang, C., Kucharski, F., Barimalala, R. and Bracco, A., 2009. Teleconnections of the tropical Atlantic to the tropical Indian and Pacific Oceans: A review of recent findings. *Meteorologische Zeitschrift*, **18(4)**, 445-454.

Wang, L. and Chen, W., 2010. Downward Arctic Oscillation signal associated with moderate weak stratospheric polar vortex and the cold December 2009. *Geophysical Research Letters*, **37(9)**, 09707.

Wang, L., Ting, M. and Kushner, P.J., 2017. A robust empirical seasonal prediction of winter NAO and surface climate. *Scientific reports*, **7(1)**, 279.

Wang, Y.H., Magnusdottir, G., Stern, H., Tian, X. and Yu, Y., 2014. Uncertainty estimates of the EOF-derived North Atlantic Oscillation. *Journal of Climate*, **27(3)**, 1290-1301.

Watanabe, M. and Kimoto, M., 1999. Tropical-extratropical connection in the Atlantic atmosphere-ocean variability. *Geophysical research letters*, **26(15)**, 2247-2250.

Watanabe, M. and Nitta, T., 1999. Decadal changes in the atmospheric circulation and associated surface climate variations in the Northern Hemisphere winter. *Journal of Climate*, **12(2)**, 494-510.

Watson, P.A. and Gray, L.J., 2014. How does the quasi-biennial oscillation affect the stratospheric polar vortex?. *Journal of the Atmospheric Sciences*, **71(1)**, 391-409.

Watson, P.A., Weisheimer, A., Knight, J.R. and Palmer, T.N., 2016. The role of the tropical West Pacific in the extreme Northern Hemisphere winter of 2013/2014.

Journal of Geophysical Research: Atmospheres, **121(4)**, 1698-1714.

Wayand, N.E., Bitz, C.M. and Blanchard-Wrigglesworth, E., 2019. A Year-Round Subseasonal-to-Seasonal Sea Ice Prediction Portal. *Geophysical Research Letters*, **46(6)**, 3298-3307.

Weisheimer, A., Schaller, N., O'Reilly, C., MacLeod, D.A. and Palmer, T., 2017. Atmospheric seasonal forecasts of the twentieth century: multi-decadal variability in predictive skill of the winter North Atlantic Oscillation (NAO) and their potential value for extreme event attribution. *Quarterly Journal of the Royal Meteorological Society*, **143(703)**, 917-926.

Welch, B.L., 1947. The generalization of student's' problem when several different population variances are involved. *Biometrika*, **34(1/2)**, 28-35.

Wheeler, M.C. and Hendon, H.H., 2004. An all-season real-time multivariate MJO index: Development of an index for monitoring and prediction. *Monthly Weather Review*, **132(8)**, 1917-1932.

Williams, K.D., Harris, C.M., Bodas-Salcedo, A., Camp, J., Comer, R.E., Copsey, D., Fereday, D., Graham, T., Hill, R., Hinton, T. and Hyder, P., 2015. The met office global coupled model 2.0 (GC2) configuration. *Geoscientific Model Development*, **8(5)**, 1509-1524.

Wolter, K. and Timlin, M.S., 1998. Measuring the strength of ENSO events: How does 1997/98 rank?. *Weather*, **53(9)**, 315-324.

Woods, C., Caballero, R. and Svensson, G., 2013. Large-scale circulation associated with moisture intrusions into the Arctic during winter. *Geophysical Research Letters*, **40(17)**, 4717-4721.

Woods, C. and Caballero, R., 2016. The role of moist intrusions in winter Arctic warming and sea ice decline. *Journal of Climate*, **29(12)**, 4473-4485.

Woollings, T., Hannachi, A. and Hoskins, B., 2010. Variability of the North Atlantic eddy-driven jet stream. *Quarterly Journal of the Royal Meteorological Society*, **136(649)**, 856-868.

Woollings, T., Lockwood, M., Masato, G., Bell, C. and Gray, L., 2010. Enhanced signature of solar variability in Eurasian winter climate. *Geophysical Research Letters*, **37(20)**.

Woollings, T. and Blackburn, M., 2012. The North Atlantic jet stream under climate

change and its relation to the NAO and EA patterns. *Journal of Climate*, **25(3)**, 886-902.

Woollings, T., Franzke, C., Hodson, D.L.R., Dong, B., Barnes, E.A., Raible, C.C. and Pinto, J.G., 2015. Contrasting interannual and multidecadal NAO variability. *Climate dynamics*, **45(1-2)**, 539-556.

Wu, Q. and Zhang, X., 2010. Observed forcing-feedback processes between Northern Hemisphere atmospheric circulation and Arctic sea ice coverage. *Journal of Geophysical Research: Atmospheres*, **115**, 14119.

Xue, D., Lu, J., Sun, L., Chen, G. and Zhang, Y., 2017. Local increase of anticyclonic wave activity over northern Eurasia under amplified Arctic warming. *Geophysical Research Letters*, **44(7)**, 3299-3308.

Yamamoto, K., Tachibana, Y., Honda, M. and Ukita, J., 2006. Intra-seasonal relationship between the Northern Hemisphere sea ice variability and the North Atlantic Oscillation. *Geophysical research letters*, **33(14)**.

Yang, G.Y. and Hoskins, B.J., 1996. Propagation of Rossby waves of nonzero frequency. *Journal of the atmospheric sciences*, **53(16)**, 2365-2378.

Yang, S. and Christensen, J.H., 2012. Arctic sea ice reduction and European cold winters in CMIP5 climate change experiments. *Geophysical Research Letters*, **39(20)**, 20707.

Yang, X.Y., Yuan, X. and Ting, M., 2016. Dynamical link between the Barents–Kara sea ice and the Arctic Oscillation. *Journal of Climate*, **29(14)**, 5103-5122.

Ye, K., T. Jung, and T. Semmler, 2018: The influences of the Arctic troposphere on the midlatitude climate variability and the recent Eurasian cooling. *J. Geophys. Res. Atmos.*, **123**, 10162–10184

Yoo, C., Feldstein, S. and Lee, S., 2011. The impact of the Madden-Julian Oscillation trend on the Arctic amplification of surface air temperature during the 1979–2008 boreal winter. *Geophysical Research Letters*, **38(24)**, 24804.

Yu, J.Y. and Kim, S.T., 2011. Relationships between extratropical sea level pressure variations and the central Pacific and eastern Pacific types of ENSO. *Journal of Climate*, **24(3)**, 708-720.

Yukimoto, S., Kodera, K. and Thiéblemont, R., 2017. Delayed North Atlantic Response to Solar Forcing of the Stratospheric Polar Vortex. *SOLA*, **13**, 53-58.

Zhang, C., 2005. Madden-Julian oscillation. *Reviews of Geophysics*, **43(2).**, 2003.

Zhang, J., Steele, M., Rothrock, D.A. and Lindsay, R.W., 2004. Increasing exchanges at Greenland-Scotland Ridge and their links with the North Atlantic Oscillation and Arctic sea ice. *Geophysical research letters*, **31(9)**, 09307.

Zhang, P., Wu, Y. and Smith, K.L., 2017. Prolonged effect of the stratospheric pathway in linking Barents–Kara Sea sea ice variability to the midlatitude circulation in a simplified model. *Climate Dynamics*, **50(1-2)**, 527-539.

Zhang, P., Wu, Y., Simpson, I.R., Smith, K.L., Zhang, X., De, B. and Callaghan, P., 2018. A stratospheric pathway linking a colder Siberia to Barents-Kara Sea sea ice loss. *Science advances*, **4(7)**, 6025.

Zheng, F. and Zhu, J., 2010. Spring predictability barrier of ENSO events from the perspective of an ensemble prediction system. *Global and Planetary Change*, **72(3)**, 108-117.

Zhou, S. and Miller, A.J., 2005. The interaction of the Madden–Julian oscillation and the Arctic Oscillation. *Journal of climate*, **18(1)**, 143-159.

Zhou, X., Li, J., Xie, F., Chen, Q., Ding, R., Zhang, W. and Li, Y., 2018. Does extreme El Niño have a different effect on the stratosphere in boreal winter than its moderate counterpart?. *Journal of Geophysical Research: Atmospheres*, **123(6)**, 3071-3086.

Chapter 10

Appendix

Propagating error in quadrature using the equation in *Murphy* [1990]:

$$X = C_{om}, \qquad \Delta X = E_{om}, \qquad Y = \sqrt{C_{mm}}, \qquad \Delta Y = Y \cdot \frac{1}{2} \cdot \frac{E_{mm}}{C_{mm}} \tag{10.1}$$

$$\Delta r = r\sqrt{\left(\frac{\Delta X}{X}\right)^2 + \left(\frac{\Delta Y}{Y}\right)^2} \tag{10.2}$$

Using the Fisher-Z transform to construct confidence intervals:

Suppose there is a coefficient R_{om} (correlations between members and observations, 20 values) and R_{mm} (correlations between members, 190 unique combinations). In the current example, averaging these groups is performed to find the coefficients to use in the Murphy 1990 equation. However, correlation coefficients are not additive, therefore they cannot be added (raw r values) to compute an arithmetic average. So z Fisher transform can be employed to make these additive.

1) Transform correlation coefficients in each group to z values

$$Z = \frac{1}{2}\left[\ln\left(1+r\right) - \ln\left(1-r\right)\right] \qquad Z = \operatorname{arctanh}\left(Z\right) \tag{10.3}$$

2) Calculate average $\bar{Z}$ and transform back to get Fisher mean weighted r

$$\bar{r} = \tanh\left(\bar{Z}\right) \tag{10.4}$$

3) Confidence intervals at 95% ($Z_{table} = 1.96$)

$$CI = \pm Z_{table} * SE_z \qquad SE_z = \frac{1}{\sqrt{n-3}} \tag{10.5}$$

4) Therefore,

$$Z_{lower} = \bar{Z} - \frac{Z_{table}}{\sqrt{n-3}} \qquad Z_{upper} = \bar{Z} + \frac{Z_{table}}{\sqrt{n-3}} \tag{10.6}$$

5) Finally, convert these lower and upper bounds to correlation values by applying hyperbolic tangent function $tanh(x)$.

For this method, this produces $C_{om} = 0.139\,[0.548, -0.324]$ and

$C_{mm} = 0.080\,[0.219, -0.063]$, where [Upper confidence interval, Lower confidence interval]. The upper and lower confidence intervals are not equidistant from the mean; methods to propagate these errors forward in quadrature are not trivial.